Environmental Effects Monitoring Program
2023 Annual Report

December 31, 2023

What's New?

FALL 2021 LOBSTER BASELINE SURVEY REPORT
FORCE implemented a fall lobster survey in 2021 in partnership with the Fishermen and Scientists Research Society and with the help of a local lobster fisher. The survey revealed a 'high' catchability rate (i.e., CPUE ≥ 2.4 kg/trap haul) – consistent with a prior baseline survey at the FORCE site in 2017 and comparable to available commercial landings. read more

RAP – FISH TAGGING; OTN AND FORCE MERGE LINES OF ACOUSTIC RECEIVERS
Fish tagging for 2023 was completed under the Risk Assessment Program in partnership with Acadia University and the Mi'kmaw Conservation Group and focused on alewife, American shad and Inner Bay of Fundy Atlantic salmon smolts. Further, FORCE and the Ocean Tracking Network merged their lines of acoustic receivers into a single array of 24 stations that span the vast majority of Minas Passage; increasing the chances of detecting tagged fish as they navigate through the area. read more

PUBLICATIONS
FORCE and its collaborators published three new peer-reviewed papers on the use of acoustic telemetry for estimating probability of fish encountering a tidal turbine installed at the FORCE tidal demonstration site in Minas Passage. These three 'companion' manuscripts were published as 'open-access' articles in a special issue of the *Journal of Marine Science and Engineering* entitled 'Interface between offshore renewable energy and the environment'. read more

FORCE worked with staff from Ocean Energy Systems-Environmental (OES-E) and collaborated with a suite of international experts to publish a new peer-reviewed 'open-access' paper in *Science of the Total Environment* to understand how the environmental effects of marine renewable energy development might 'scale up' from single devices to large-scale commercial array. read more

FORCE collaborated with the tidal stream industry and staff from OES-E to publish a new peer-reviewed 'open-access' paper in the *Journal of Marine Science and Engineering* that describes a probabilistic assessment framework for helping to determine collision risk for marine animals with tidal stream turbines, and explores the process using a case study from Minas Passage. read more

NEW INITIATIVES
FORCE is collaborating with Innovasea to test the capabilities of innovative new acoustic receiver technologies in high flow environments. Five different acoustic receivers were mounted on a subsea platform and deployed at the FORCE test site. A series of passive drifts were then

conducted over the platform using acoustic tags of various frequencies deployed at differing depths. [read more](#)

FORCE has partnered with Innovasea and a series of other collaborators on an Ocean Supercluster funded project to advance the application of artificial intelligence for monitoring fish around hydroelectric and tidal stream energy projects. [read more](#)

Executive Summary

Tidal stream energy devices are an emerging renewable energy technology that use the ebb and flow of the tides to generate electricity. These devices are in various stages of research, development, operation and testing in countries around the world.

FORCE was established in 2009 after undergoing a joint federal-provincial environmental assessment with the mandate to enable the testing and demonstration of tidal stream devices. Since that time, more than 100 related research studies have been completed or are underway with funding from FORCE, the Offshore Energy Research Association (OERA), and others. These studies have considered physical, biological, socioeconomic, and other research areas.

The current suite of monitoring programs implemented by FORCE build off those initiated during 2016-2020 that were conducted in anticipation of tidal stream energy device deployments at FORCE's tidal demonstration site. These efforts are divided into two components: FORCE 'site-level' monitoring activities (>100 metres from a device), and developer or 'device-specific' monitoring led by project developers (≤100 metres from a device) at the FORCE site. All monitoring plans are reviewed by FORCE's independent Environmental Monitoring Advisory Committee (EMAC) and federal and provincial regulators prior to implementation.

FORCE monitoring presently consists of monitoring for fish, marine mammals, seabirds, lobster, and marine sound. During monitoring from 2016 through 2020, FORCE completed:

- ~564 hours of hydroacoustic fish surveys;
- more than 5,083'C-POD' marine mammal monitoring days;
- bi-weekly shoreline observations;
- 49 observational seabird surveys;
- four drifting marine sound surveys and additional sound monitoring; and
- 11 days of lobster surveys

The 2021-2023 EEMP is designed to prepare for effects testing with the deployment of operational tidal stream energy devices and adheres to the principles of adaptive management by evaluating existing datasets to ensure appropriate monitoring approaches are being implemented. Moreover, the plan adopts internationally accepted standards for monitoring where possible, including feasibility assessments for new monitoring approaches that are planned to be implemented. The 2021-2023 EEMP has been implemented as designed and reviewed by FORCE's environmental monitoring advisory committee (EMAC). Device deployments are pending and there has not been an opportunity for effects testing under the 2021-2023 proposed EEMP.

Since the beginning of the 2021-2023 EEMP, FORCE has completed;

- 8 days of lobster surveys;
- a preliminary radar feasibility study to monitor for seabirds; and
- bi-weekly shoreline observations

FORCE is working with academic and Indigenous partner organizations to advance the Risk Assessment Program (RAP) for tidal stream energy. This program seeks to develop credible and statistically robust encounter rate models for migratory and resident fish species in Minas Passage with tidal stream energy devices. This will be accomplished by combining physical oceanographic data related to flow and turbulence in the Minas Passage with acoustic tagging information for various fish species in the region curated by the Ocean Tracking Network at Dalhousie University. Since the start of the project, FORCE has established a high-resolution

radar network in Minas Passage and has started to quantify hydrodynamic features in the region and build the tidal flow atlas required for the program. FORCE has also started modelling the spatiotemporal distributions for the nine species for which sufficient acoustic tracking data is available and is developing species distribution maps for each species. In partnership with FORCE, the Mi'kmaw Conservation Group (MCG), local fishers and Acadia University have completed the fish tagging component of the program that is required for species distribution model development and encounter rate model validation. The results of this work are expected to be shared through the development of a user-friendly graphical-user interface for non-technical stakeholders, and an R-package (or similar) for regulators and academic stakeholders. Fish tagging continued in 2023 as part of FORCE's fish monitoring program, and is anticipated to continue in 2024 and beyond. Ultimately, this work will contribute towards understanding the risk of tidal stream energy development for fishes in the Bay of Fundy and will assist in the development of future environmental effects monitoring programs.

This report provides a summary of monitoring activities and data analyses completed by FORCE up to the end of 2023. In addition, it also highlights findings from international research efforts, previous data collection periods at the FORCE site, and additional research work that is being conducted by FORCE and its partners. This includes supporting fish tagging efforts with Acadia University and the Ocean Tracking Network, radar research projects, and subsea instrumentation platform deployments through the Fundy Advanced Sensor Technology (FAST) Program. Finally, the report presents details regarding future research and monitoring efforts at the FORCE test site. This includes work in support of the adaptive nature of the EEMP and the RAP program.

All reports, including quarterly monitoring summaries, are available online at www.fundyforce.ca/document-collection.

Contents

Appendices

Appendix I   Acronyms

Appendix II   Petrichencko, J., E. Blacklock, S. Thompson, S. Scott-Tibbetts, and A. Whitney. 2023. FORCE lobster survey in Minas Passage Fall 2021. Fishermen and Scientists Research Society. 48 pp.

Appendix III Sanderson, B.G., C.W. Bangley, L.P. McGarry, and D.J. Hasselman. 2023. Measuring detection efficiency of high-residency acoustic signals for estimating probability of fish-turbine encounter in a fast-flowing tidal passage. *Journal of Marine Science and Engineering* 11(6): 1172.

Appendix IV   Sanderson, B.G., R.H. Karsten, and D.J. Hasselman. *2023.* Towards estimating probability of fish-turbine encounter: Using drifters equipped with acoustic tags to verify the efficacy of an array of acoustic receivers. *Journal of Marine Science and Engineering 11(8): 1592.*

Appendix V   Sanderson, B.G., R.H. Karsten, C.C. Solda, D.C. Hardie, and D.J. Hasselman. 2023. Probability of Atlantic salmon post-smolts encountering a tidal turbine installation in Minas Passage, Bay of Fundy. Journal of Marine Science and Engineering 11(5): 1095.

Appendix VI   Hasselman, D.J., L.G. Hemery, A.E. Copping, E.A. Fulton, J. Fox, A.B. Gill, and B. Polagye. 2023. 'Scaling up' our understanding of environmental effects of marine renewable energy development from single devices to large-scale commercial arrays. *Science of the Total Environment* 904: 166801.

Appendix VII Copping, A.E., D.J. Hasselman, C.W. Bangley, J. Culina, and M. Carcas. 2023. A probabilistic methodology for determining collision risk of marine animals with tidal energy turbines. *Journal of Marine Science and Engineering* 11(11): 2151.

Introduction

This report outlines monitoring activities and results of data analyses conducted at the Fundy Ocean Research Centre for Energy test site in the Minas Passage, Bay of Fundy during 2023. Specifically, this report highlights results of environmental monitoring activities conducted by FORCE and other research and development activities conducted at the FORCE site. This report also provides a summary of international research activities around tidal stream energy devices.

About FORCE

FORCE was created in 2009 to lead research, demonstration, and testing for high flow, industrial-scale tidal stream energy devices. FORCE is a not-for-profit entity that has received funding support from the Government of Canada, the Province of Nova Scotia, Encana Corporation, and participating developers.

FORCE has two central roles in relation to the demonstration of tidal stream energy converters in the Minas Passage:

1. Host: providing the technical infrastructure to allow demonstration devices to connect to the transmission grid; and
2. Steward: research and monitoring to better understand the interaction between devices and the environment.

The FORCE project currently consists of five undersea berths for subsea tidal stream energy device generators, four subsea power cables to connect the devices to land-based infrastructure, an onshore substation and power lines connected to the Nova Scotia Power transmission system, and a Visitor Centre that is free and open to the public from May to November annually. These onshore facilities are located approximately 10 km west of Parrsboro, Nova Scotia.

The marine portion of the project is located in a 1.6 km x 1.0 km tidal demonstration area in the Minas Passage. It is also identified as a Marine Renewable-electricity Area under the Province's Marine Renewable-energy Act. This area consists of five subsea berths that are leased to tidal energy companies[1] selected by the Nova Scotia Department of Natural Resources and Renewables. Current berth holders at FORCE are:

Berth A: Eauclaire Tidal Limited Partnership[2]
Berth B: Rio Fundo Operations Canada Limited[3]
Berth C: Sustainable Marine Energy (Canada)[4]
Berth D: Big Moon Power Canada
Berth E: Halagonia Tidal Energy Limited[5]

---

[1] Further information about each company may be found at: fundyforce.ca/partners

[2] On January 16, 2023 the Department of Natural Resources and Renewables approved the transfer of the Project Agreement and FIT approvals from Minas Tidal Limited Partnership to Eauclaire Tidal Limited Partnership.

[3] On April 30, 2019 the Department of Energy and Mines approved the transfer of the Project Agreement and FIT approvals from Atlantis Operations (Canada) Ltd. to Rio Fundo Operations Canada Ltd.

[4] On May 15, 2019 the Department of Energy and Mines issued an approval for Black Rock Tidal Power to change its name to Sustainable Marine Energy (Canada) Ltd. with the transfer of assets from SCHOTTEL to Sustainable Marine Energy.

[5] Berth E does not have a subsea electrical cable provided to it.

Research, monitoring, and associated reporting is central to FORCE's steward role, to assess whether tidal stream energy devices can operate in the Minas Passage without causing significant adverse effects on the environment, electricity rates, and other users of the Bay.

As part of this mandate, FORCE has a role to play in supporting informed, evidence-based decisions by regulators, industry, rightsholders, the scientific community, and the public. As deployments of different technologies are expected to be phased in over the next several years, FORCE and regulators will have the opportunity to learn and adapt environmental monitoring approaches as lessons are learned.

Background

The FORCE demonstration project received its environmental assessment (EA) approval on September 15, 2009, from the Nova Scotia Minister of Environment. The conditions of its EA approval[6] provide for comprehensive, ongoing, and adaptive environmental management. The EA approval has been amended since it was issued to accommodate changes in technologies and inclusion of more berths to facilitate provincial demonstration goals.

In accordance with this EA approval, FORCE has been conducting an Environmental Effects Monitoring Program (EEMP) to better understand the natural environment of the Minas Passage and the potential effects of tidal stream energy devices as related to fish, seabirds, marine mammals, lobster, marine sound, benthic habitat, and other environmental variables. All reports on site monitoring are available online at: www.fundyforce.ca/document-collection.

Since 2009, more than 100 related research studies have been completed or are underway with funding from FORCE, the Offshore Energy Research Association (OERA) and others. These studies have considered socioeconomics, biological, and other research areas.[7]

Monitoring at the FORCE site is currently focused on lobster, fish, marine mammals, seabirds, and marine sound and is divided into developer led 'device-specific' (≤ 100 m from a device) monitoring and FORCE led site-specific (> 100 m from a device) monitoring. As approved by regulators, individual berth holders complete monitoring in direct vicinity of their device(s), in recognition of the unique design and operational requirements of different technologies. FORCE completes site level monitoring activities as well as supporting integration of data analysis between these monitoring zones, where applicable.

All developer and FORCE led monitoring programs are reviewed by FORCE's Environmental Monitoring Advisory Committee (EMAC), which includes representatives from scientific, First Nations, and local fishing communities.[8] These programs are also reviewed by federal and provincial regulators prior to device installation. In addition, FORCE and berth holders also submit an Environmental Management Plan (EMP) to regulators for review prior to device installation. EMP's include environmental management roles and responsibilities and commitments, environmental protection plans, maintenance and inspection requirements, training and education requirements, reporting protocols, and more.

---

[6] FORCE's Environmental Assessment Registration Document and conditions of approval are found online at: www.fundyforce.ca/document-collection.
[7] Net Zero Atlantic Research (formerly Offshore Energy Research Association) Portal (https://netzeroatlantic.ca/research) includes studies pertaining to infrastructure, marine life, seabed characteristics, socio-economics and traditional use, technology, and site characterization.
[8] Information about EMAC may be found online at: www.fundyforce.ca/about-us

Tidal Stream Energy Device Deployments

Since FORCE's establishment in 2009, tidal stream energy devices have been installed at the FORCE site three times: once in 2009/2010, November 2016 – June 2017, and July 2018 – present. Given the limited timescales in which a device has been present and operating at the FORCE site, environmental studies to-date have largely focused on the collection of baseline data and developing an understanding of the capabilities of monitoring instruments in high flow tidal environments.

On July 22, 2018, CSTV installed a two-megawatt OpenHydro turbine at Berth D of the FORCE site and successfully connected the subsea cable to the turbine. CSTV confirmed establishment of communication with the turbine systems on July 24. On July 26, 2018, Naval Energies unexpectedly filed a petition with the High Court of Ireland for the liquidation of OpenHydro Group Limited and OpenHydro Technologies Limited.[9] For safety purposes, the turbine was isolated from the power grid that same day. On September 4, 2018, work began to re-energize the turbine, but soon afterwards it was confirmed that the turbine's rotor was not turning. It is believed that an internal component failure in the generator caused sufficient damage to the rotor to prevent its operation. Environmental sensors located on the turbine and subsea base continued to function at that time except for one hydrophone.

As a result of the status of the turbine, the monitoring requirements and reporting timelines set out in CSTV's environmental effects monitoring program were subsequently modified under CSTV's Authorization from Fisheries and Oceans Canada. The modification required that CSTV provide written confirmation to regulators monthly that the turbine was not spinning by monitoring its status during the peak tidal flow of each month. This began October 1, 2018, and was expected to continue until the removal of the turbine; however, as a result of the insolvency of OpenHydro Technology Ltd., all developer reporting activities by CSTV ceased as of March 1, 2019. FORCE subsequently provided monthly reports to regulators confirming the continued non-operational status of the CSTV turbine from March 2019 – May 2020 and received authorization from the Nova Scotia Department of Environment on June 2, 2020, to conclude these monthly reports.

In September 2020, Big Moon Canada Corporation (Big Moon) was announced as the successful applicant to fill berth D at the FORCE test site following a procurement procedure administered by Power Advisory LLC. As part of the agreement, Big Moon provided a $4.5 million security deposit to remove the non-operational CSTV turbine currently deployed at berth D, and has until December 31, 2024, to raise the turbine. The project start date for BigMoon is not known at this time, but is anticipated to commence in 2024.

On December 5, 2023, Eauclaire Tidal Limited Partnership announced that Orbital Marine Power would provide the tidal stream technology for berth A at the FORCE test site. The technology (i.e., 'O2X') is a 2.4 megawatt floating device with two horizontal axis turbines. The project start date for Eauclaire and Orbital is not known at this time, and the project description is currently undergoing a review with regulators.

Additional devices are expected to be deployed at the FORCE site in the coming years. In 2018, Sustainable Marine Energy (formerly Black Rock Tidal Power) installed a PLAT-I system in Grand Passage, Nova Scotia under a Demonstration Permit.[10] This permit allows for a demonstration of the 280 kW system to help SME and its partners learn about how the device operates in the marine environment of the Bay of Fundy. On May 11, 2022, SME announced it had successfully

---

[9] See original news report: https://www.irishexaminer.com/breakingnews/business/renewable-energy-firms-with-more-than-100-employees-to-be-wound-up-857995.html.

[10] To learn more about this project, see: https://novascotia.ca/news/release/?id=20180919002.

delivered the first floating tidal stream energy to Nova Scotia's power grid. However, on March 20, 2023, SME announced that it was withdrawing its application to Fisheries and Oceans Canada (DFO) for a Fisheries Act Authorization to deploy a PLAT-I system at FORCE, citing an unclear regulatory pathway for project build-out. Consequently, on May 12, 2023, SME was placed into voluntary bankruptcy and their Pempa'q project at the FORCE site will not proceed. FORCE is working with various governmental departments at both the federal and provincial level to define a regulatory path for tidal stream energy demonstration in Minas Passage that considers effective environmental monitoring approaches, includes proportionality with respect to environmental risks of tidal project development, and account for the needs of the tidal energy sector. Fisheries and Oceans Canada and Natural Resources Canada recently announced the formation of a task force to address regulatory uncertainty surrounding tidal project development in Minas Passage, and the terms of reference that will guide the mission and objectives of the task force are currently being developed. An interim report on the progress of the task force was released on September 29, 2023, and can be found here. The final report is anticipated to be released in January 2024, and will also be made publicly available at that time.

In 2018, Natural Resources Canada announced a $29.8 million contribution to Halagonia Tidal Energy's project at the FORCE site through its Emerging Renewable Power Program.[11] The project consists of submerged turbines for a total of nine megawatts – enough capacity to provide electricity to an estimated 2,500 homes.

Each berth holder project will be required to develop a device-specific monitoring program, which will be reviewed by FORCE's EMAC and federal and provincial regulators including Fisheries and Oceans Canada, the Nova Scotia Department of Environment and Climate Change, and the Nova Scotia Department of Natural Resources and Renewables prior to device installation.

Overall, the risks associated with single device or small array projects are anticipated to be low given the relative size/scale of devices (Copping 2018). For example, at the FORCE site a single two-megawatt OpenHydro turbine occupies ~ 1/1,000th of the cross-sectional area in the Minas Passage (Figure 1). A full evaluation of the risks of tidal stream energy devices, however, will not be possible until more are tested over a longer-term period with monitoring that documents local impacts, considers far-field and cumulative effects, and adds to the growing global knowledge base.

Figure 1: The scale of a single turbine (based on the dimensions of the OpenHydro turbine deployed by CSTV, indicated by the red dot and above the blue arrow) in relation to the cross-sectional area of the Minas Passage. The Passage reaches a width of ~ 5.4 km and a depth of 130 m.

---

[11] To learn more about this announcement, see: https://www.canada.ca/en/natural-resources-canada/news/2018/09/minister-sohi-announces-major-investment-in-renewable-tidal-energy-that-will-power-2500-homes-in-nova-scotia.html.

International Experience & Cooperation

The research and monitoring being conducted at the FORCE test site is part of an international effort to evaluate the risks tidal energy poses to marine life (Copping 2018; Copping and Hemery 2020). Presently, countries such as China, France, Italy, the Netherlands, South Korea, the United Kingdom, and the United States (Marine Renewables Canada 2018) are exploring tidal energy, supporting environmental monitoring and innovative R&D projects. Tidal energy and other marine renewable energy (MRE) technologies such as tidal range, tidal current, wave, and ocean thermal energy offer significant opportunities to replace carbon fuel sources in a meaningful and sustainable manner. Some estimates place MRE's potential as exceeding current human energy needs (Lewis et al. 2011; Gattuso et al. 2018). Recent research includes assessments of operational sounds on marine fauna (Schramm et al. 2017; Lossent et al. 2018; Robertson et al. 2018; Pine et al. 2019), the utility of PAM sensors for monitoring marine mammal interactions with turbines (Malinka et al. 2018) and collision risk (Joy et al. 2018b), demonstrated avoidance behavior by harbour porpoise around tidal turbines (Gillespie et al. 2021), a synthesis of known effects of marine renewable energy devices on fish (Copping et al. 2021), and the influence of tidal turbines on fish behavior (Fraser et al. 2018).

Through connections to groups supporting tidal energy demonstration and R&D, FORCE is working to inform the global body of knowledge pertaining to environmental effects associated with tidal power projects. This includes participation in the Bay of Fundy Ecosystem Partnership[12], TC114[13], the Atlantic Canadian-based Ocean Supercluster[14], and OES-Environmental[15].

FORCE will continue to work closely with OES-Environmental and its members to document and improve the state of knowledge about the interactions of MRE devices interactions with the marine environment. For instance, OES-Environmental is pursuing the development of new research topics for the 2024 State of the Science Report related to i) knowledge of environmental effects as the tidal energy industry scales up from single devices to arrays, ii) understanding the cumulative impacts of marine renewable energy with other anthropogenic effects, and iii) an ecosystem approach for understanding environmental effects, including interactions between trophic levels, between ecosystems and between ecosystem services. Dr. Daniel J. Hasselman, FORCE Science Director, is involved in the development of all three of these topics and lead the effort to understand the 'scaling up' of environmental effects of devices as the tidal energy sector transitions towards the development of commercial arrays. The manuscript focused on this topic was recently published in *Science of the Total Environment* and can be found here. A synopsis of this publication and the other topics outlined above will be included in a chapter of the OES-E 2024 State of the Science Report that is scheduled for release in the fall of 2024.

The 'scaling up' paper (Appendix VI) expands our understanding of the environmental effects of MRE arrays through the adaptation and application of cumulative environmental effects terminology (i.e., dominance, additive, antagonistic, synergistic) to key stressor-receptor interactions (e.g., collision risk, underwater noise, electromagnetic fields, changes to habitats and oceanographic systems, etc.). This approach facilitates the development of generalized concepts

---

[12] BoFEP is a 'virtual institute' interested in the well-being of the Bay of Fundy. To learn more, see www.bofep.org.

[13] TC114 is the Canadian Subcommittee created by the International Electrotechnical Commission (IEC) to prepare international standards for marine energy conversion systems. Learn more: tc114.oreg.ca.

[14] The OSC was established with a mandate to "better leverage science and technology in Canada's ocean sectors and to build a digitally-powered, knowledge-based ocean economy." Learn more: www.oceansupercluster.ca.

[15] OES Environmental was established by the International Energy Agency (IEA) Ocean Energy Systems (OES) in January 2010 to examine environmental effects of marine renewable energy development. Member nations include: Australia, China, Canada, Denmark, France, India, Ireland, Japan, Norway, Portugal, South Africa, Spain, Sweden, United Kingdom, and United States. Further information is available at https://tethys.pnnl.gov.

for the scaling of environmental effects for these stressor-receptors, allowing the identification of high priority risks and revealing knowledge gaps that require investigation to support expansion of the marine renewable energy sector to large-scale commercial arrays.

FORCE recently collaborated with industry members from the tidal stream energy sector and staff from OES-E to publish a new peer-reviewed paper in the *Journal of Marine Science and Engineering* that describes a probabilistic assessment framework that may help determine collision risk for marine animals with tidal stream turbines (Figure 2). The framework outlines a series of sequential steps that must take place, each with an associated probability, for a marine animal to approach an operational turbine, be struck by a turbine blade and be harmed (i.e., suffer a critical injury or mortality). The paper explores the process using striped bass in Minas Passage as a case study (to the extent currently possible) and can be found here.

1. Animal in water near turbine
2. Animal at turbine depth
3. Animal near turbine during fast flows
4. Animal not avoiding or evading turbine
5. Animal not deflected from turbine face
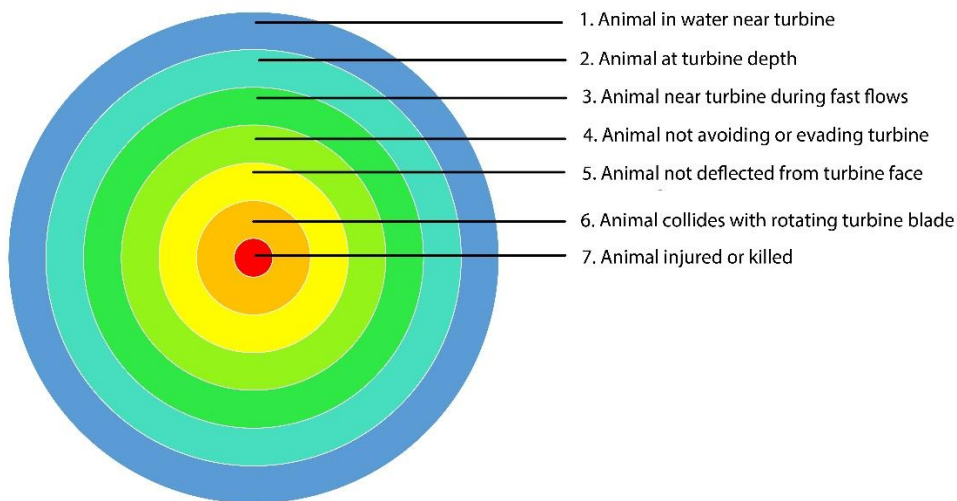6. Animal collides with rotating turbine blade
7. Animal injured or killed

Figure 2: Conceptual probabilistic framework for quantifying the likelihood of collision risk for marine animals and operational tidal energy turbines. (Reproduced from Copping et al. 2023; Figure 1).

FORCE Monitoring Activities

FORCE has been leading site-level monitoring for several years, focusing on a variety of valued ecosystem components. FORCE's previous environmental effects monitoring program (2016-2020) was developed in consultation with SLR Consulting (Canada)[16] and was strengthened by review and contributions by national and international experts and scientists, DFO, NSECC, and FORCE's EMAC. The most recent version of the EEMP (2021-2023) was developed in consultation with Atlantis Watershed Consultants Ltd. with input from national and international experts, including FORCE's EMAC, and was submitted to regulators for approval. The 2021-2023 EEMP was modified from the 2016-2020 EEMP based on results of previous monitoring activities, experience and lessons learned. This is consistent with the adaptive management approach

---

[16] This document is available online at: www.fundyforce.ca/document-collection.

inherent to the FORCE EEMP – the process of monitoring, evaluating and learning, and adapting (AECOM 2009) that has been used at the FORCE site since its establishment in 2009.[17] A similar process will be used for the development of the next iteration of the EEMP (i.e., 2024-2027).

FORCE's EEMP currently focuses on the impacts of operational tidal stream energy devices on lobster, fish, marine mammals, and seabirds as well as the impact of device-produced sound. Overall, these research and monitoring efforts, detailed below, were designed to test the predictions made in the FORCE EA. Over the course of the 2016-2020 EEMP, FORCE completed approximately:

- 564 hours of hydroacoustic fish surveys;
- more than 5,083'C-POD' (marine mammal monitoring) days;
- bi-weekly shoreline observations;
- 49 observational seabird surveys;
- four drifting marine sound surveys and additional bottom-mounted instrument sound data collection; and
- 11 days of lobster surveys.

Since the beginning of the 2021-2023 EEMP, FORCE has undertaken:

- 8 days of lobster surveys;
- a preliminary radar feasibility study to monitor for seabirds; and
- bi-weekly shoreline observations

The following pages provide a summary of the site-level monitoring activities conducted at the FORCE site during 2023, including data collection, data analyses performed, initial results, and lessons learned, that builds on activities and analyses from previous years. Where applicable, this report also presents analyses that have integrated data collected through developer and FORCE monitoring programs to provide a more complete understanding of device-marine life interactions.

Monitoring Objectives

The overarching purpose of environmental monitoring is to test the accuracy of the environmental effect predictions made in the original EA. These predictions were generated through an evaluation of existing physical, biological, and socioeconomic conditions of the study area, and an assessment of the risks the tidal energy demonstration project poses to components of the ecosystem.

A comprehensive understanding of device-marine life interactions will not be possible until device-specific and site-level monitoring efforts are integrated, and additional data is collected in relation to operating tidal stream energy devices. Further, multi-year data collection will be required to consider seasonal variability at the FORCE test site and appropriate statistical analyses of this data will help to obtain a more complete understanding of device-marine life interactions.

Table 1 outlines the objectives of the site-level monitoring activities conducted at the FORCE demonstration site. FORCE led site-level monitoring summaries will be updated as devices are

---

[17] The adaptive management approach is necessary due to the unknowns and difficulties inherent with gathering data in tidal environments such as the Minas Passage and allows for adjustments and constant improvements to be made as knowledge about the system and environmental interactions become known. This approach has been accepted by scientists and regulators.

scheduled for deployment at FORCE. At this time, and considering the scale of device deployments in the near-term at FORCE, it is unlikely that significant effects in the far-field will be measurable (SLR Consulting 2015). Far-field studies such as sediment dynamics will be deferred until such time they are required. However, recent discussions with scientists serving on FORCE's EMAC suggests that the natural variability inherent to the upper Bay of Fundy ecosystem far exceeds what could be measured by far-field monitoring efforts. Moreover, the scale of tidal power development would need to surpass what is possible at the FORCE tidal demonstration site to extract sufficient energy from the system to have any measurable effects (Whiting et al. *in press)*. In short, far-field monitoring would be futile unless tidal power development transitions from demonstration scale to commercial arrays. As more devices are scheduled for deployment at the FORCE site and as monitoring techniques are improved, monitoring protocols will be revised in keeping with the adaptive management approach. These studies will be developed in consultation with FORCE's EMAC, regulators, and key stakeholders.

Table 1: The objectives of each of the environmental effects monitoring activities, which consider various Valued Ecosystem Components (VECs), led by FORCE.

FORCE Environmental Effects Monitoring VEC	*Objectives*
Lobster	● to determine if the presence of a tidal stream energy device affects commercial lobster catches
Fish	● to test for indirect effects of tidal stream energy devices on water column fish density and fish vertical distribution ● to estimate probability of fish encountering a device based on fish density proportions in the water column relative to device depth in the water column
Marine Mammals	● to determine if there is permanent avoidance of the study area during device operations ● to determine if there is a change in the distribution of a portion of the population across the study area
Marine Sound (Acoustics)	● to conduct ambient sound measurements to characterize the soundscape prior to and following deployment of the tidal stream energy device
Seabirds	● to understand the occurrence and movement of bird species in the vicinity of tidal stream energy devices ● to confirm FORCE's Environmental Assessment predictions relating to the avoidance and/or attraction of birds to tidal stream energy devices

Lobster

FORCE conducted a baseline lobster catchability survey in fall 2021 (Fishermen and Scientists Research Society (FSRS), 2023) following the study design developed by TriNav Fisheries Consultants Ltd. in 2019. This study design was implemented in partnership with the FSRS (Figure 3) and with the assistance of a local lobster fisher. The catch-and-release survey included the deployment of experimental lobster traps at 18 locations distributed over three sites (i.e., 'Near-Control site', 'Far-Control site', and 'Impact site') in the vicinity of the FORCE tidal demonstration area. The baseline survey occurred prior to the fall 2021 commercial lobster fishery in Minas Passage, was conducted over two phases that coincided with neap tidal conditions, and quantified the number of lobsters captured and Catch Per Unit Effort (CPUE) for each site.

The survey captured 582 lobsters, and a subset of these (n=477) were tagged with conventional t-bar tags prior to being released to understand the extent of lobster movement in Minas Passage. Results indicated a 'high' catchability rate (i.e., CPUE ≥ 2.4 kg/trap haul) during the fall survey – consistent with a prior baseline survey at the FORCE site in 2017 (NEXUS Coastal Resource Management Ltd. 2017), and comparable to available commercial landings data provided by Fisheries and Oceans Canada (DFO). Statistical analyses revealed a marginally significant (p=0.052) difference in the number of lobsters captured among sites, with the Impact site (i.e., the intended deployment location for proposed tidal projects at FORCE) having on average fewer lobsters (6.2 lobster/trap haul) than either the Near Control site (8.46 lobster/trap haul) or Far Control site (8.92 lobster/trap haul). These differences were not reflected in the CPUE data, as non-significant differences were observed among these sites. Tagged lobsters that were recaptured during the fall commercial lobster fishery and reported to FORCE suggest wide variation in the movement of individuals over relatively short periods of time.

Commercial landings data provided by DFO revealed a marked increase in Lobster Fishing Area 35 (including grid 17 where the FORCE site is located) (Figure 4). This could be associated with a northward shift in the species distribution as a consequence of increasing water temperature in the Gulf of Maine, and its effects on lobster movement, survival and recruitment to the fishery. A repeat of this study design in the presence of an operational turbine deployed at the FORCE site is required to test whether it has an effect on lobster catchability. The 2021 baseline lobster report is provided in Appendix II.

Figure 3: Lobster scientist from the Fishermen and Scientist Research Society showing a tagged lobster prior to release.
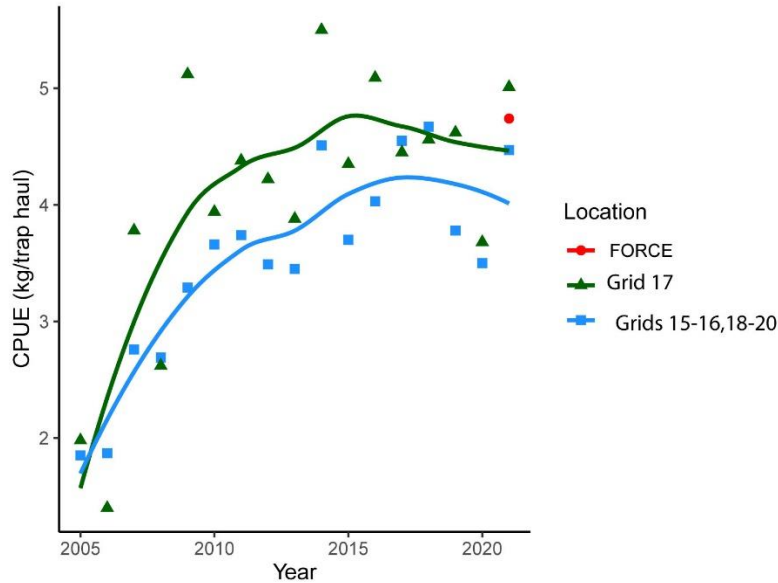
Figure 4: Scatterplot and loess (locally weighted smoothing) regression of CPUE (kg/trap haul) for the fall commercial lobster fishery (2005-2021) from LFA 35. The CPUE data from the FORCE 2021 lobster survey is consistent with existing commercial landings data collected from Grid 17 and other grids within LFA 35.

Fish

FORCE has been conducting mobile fish surveys since May 2016 to test the EA prediction that tidal stream energy devices are unlikely to cause substantial impacts to fishes at the test site (AECOM 2009). To that end, the surveys are designed to:

- test for indirect effects of tidal stream energy devices on water column fish density and fish vertical distribution; and
- estimate the probability of fish encountering a device based on any 'co-occurrence' relative to device depth in the water column.

Moreover, these surveys follow a 'BACI' (Before/After, Control/Impact) design to permit a comparison of data collected before a device is installed with data collected while a device is operational at the FORCE site, and in relation to a reference site along the south side of the Minas Passage. These 24-hour mobile surveys encompass two tidal cycles and day/night periods using a scientific echosounder, the Simrad EK80, mounted on a vessel, the Nova Endeavor (Huntley's Sub-Aqua Construction, Wolfville, NS). This instrument is an active acoustic monitoring device and uses sonar technology to detect fish by recording reflections of a fish's swim bladder.

Analyses of hydroacoustic fish surveys completed during baseline studies in 2011 and 2012 (Melvin and Cochrane 2014) and surveys during May 2016 – August 2017 (Daroux and Zydlewski 2017) evaluated changes in fish densities in association with diel stage (day/night), tidal stage (ebb/flood), and device presence or absence (an OpenHydro turbine was present November 2016 – June 2017). Results support the EA prediction that tidal stream devices have minimal impact on marine fishes. However, additional surveys in relation to an operating device are required to fully test this prediction.

In 2019, the University of Maine conducted a thorough analysis for 15 fish surveys conducted by FORCE from 2011-2017. The hydroacoustic data set included six 'historical' surveys conducted between August 2011 and May 2012, and nine 'contemporary' surveys conducted between May 2016 and August 2017. The analyses included comparisons of fish presence/absence and relative fish density with respect to a series of temporal (historical vs. contemporary, or by survey), spatial (CLA vs. reference study area, or by transect) and environmental (tide phase, diel state, or with/against predicted tidal flow) explanatory variables. The report identified a statistically significant difference in fish presence/absence and relative fish density between the historical and contemporary data sets that may be attributable to differences in the survey design/execution between the time periods, or could reflect changes in fish usage of the site. As such, remaining analyses were restricted to the contemporary data sets. The results revealed that: i) data collection during the ebb tide and at night are important for understanding fish presence in the CLA, ii) various explanatory variables and their additive effects should be explored further, and iii) increasing the frequency of surveys during migratory periods (consecutive days in spring/fall) may be required to understand patterns and variability of fish presence and density in Minas Passage. Importantly, the report suggested a statistically significant difference in fish presence/absence and relative density between the CL and reference site, suggesting that the reference site may not be sufficiently representative to serve as a control for the CLA, and for testing the effects of an operational device on fish density and distribution in Minas Passage. Additional work is underway using data from eight additional contemporary fish surveys (2017-2018) to determine whether this finding is biologically meaningful, or whether it is simply a statistical artefact of how the data was aggregated in the original analysis.

Because complex hydrodynamic features of the Minas Passage introduce turbulence and bubbles into the water column that interfere with the use of hydroacoustics, FORCE's mobile fish surveys have been optimized for collecting data during the best neap tidal cycle per month when turbulence is greatly reduced. However, this approach limits the number of surveys that can be conducted, and regulators have suggested that the scope of the program be expanded so that survey results are more representative of how fish use the Minas Passage. To that end, FORCE conducted multiple fish surveys during each of three neap tidal cycles in fall 2020 (i.e., September 25, 27, 29; October 7, 9, 13; and October 24, 26, 29) to determine whether variation in fish density and distribution for any given survey within a neap cycle was representative of the other surveys conducted during that same time frame. Previous work comparing stationary and mobile hydroacoustic surveys in Minas Passage found that the temporal representative range of a 24-hr mobile was approximately three days (Viehman et al. 2019).

A recent study (Viehman et al. (2022)) examined entrained air contamination in echosounder data collected at the FORCE test site. It found that fish abundance estimates in the lower 70% of the water column and current speeds less than 3 m/s were well represented in that there was little contamination of the data set from entrained air. However, undersampling of the upper water column and faster speeds strongly affected fish abundance estimates especially during strong spring tides. This means that data collected during neap tides are more likely to yield a more accurate picture of fish abundance and distribution than those collected during spring tides. The study also highlighted how estimates of fish abundance may be affected differently depending on where fish are in the water column. For example, (hypothetical) fish located at mid-depths were omitted from the data more often as current speeds increased. These findings indicate a complex and dynamic ecosystem where the interactions of water movement and fish distribution affect our ability to infer how fish populations may interact with tidal power devices in the Minas Passage. The use of acoustic telemetry being studied under the RAP program could be used to fill gaps in datasets and optimize what can be learned about fish abundance and distribution at tidal energy sites.

Another issue with the entrained air found in high flow environments is the need to remove the contaminated data prior to analysis which is often a tedious and time-consuming process. Existing algorithms used to identify the depth-of-penetration of entrained air are insufficient for a boundary that is discontinuous, depth-dynamic, porous, and varies with tidal flow speed. Using a case study from data obtained at the FORCE test site a recent study (Lowe et al. (2022)) described the development and application of a deep machine learning model called Echofilter. Echofilter was found to be highly responsive to dynamic range of turbulence conditions in the data and produced an entrained-air boundary line with an average error of less than half that of the existing algorithms. The model had a high level of agreement with human data trimming. This resulted in 50% reduction in the time required for manual edits to the data set when using currently available algorithms to trim the data.

FORCE is currently working towards the development of a comprehensive fish synthesis that will bring together existing knowledge of fish distribution, abundance, and use of the Minas Passage using existing literature from stock assessments, prior hydroacoustic surveys, acoustic telemetry-based surveys, as well as other relevant sources of information. This synthesis will focus on species of conservations concern, cultural relevance, and commercial and recreational value. The results of this synthesis project will be available in 2024 and will help to determine the extent to which questions regarding fish and tidal energy project permitting have been answered and identifying remaining knowledge gaps. Dr. Graham Daborn at Acadia University is leading this work and a final report is expected in 2024.

Marine Mammals

Since 2016, FORCE has been conducting two main activities to test the EA prediction that project activities are not likely to cause significant adverse residual effects on marine mammals within the FORCE test site (AECOM 2009):

- passive acoustic monitoring (PAM) using 'click recorders' known as C-PODs; and
- an observation program that includes shoreline, stationary, and vessel-based observations.

Passive Acoustic Monitoring

The first component of FORCE's marine mammal monitoring program involves the use of PAM mammal detectors known as C-PODs, which record the vocalizations of toothed whales, porpoises, and dolphins.[18] The program focuses mainly on harbour porpoise – the key marine mammal species in the Minas Passage that is known to have a small population that inhabits the inner Bay of Fundy (Gaskin 1992). The goal of this program is to understand if there is a change in marine mammal presence in proximity to a deployed tidal stream energy device and builds upon baseline C-POD data collection within the Minas Passage since 2011.

From 2011 to early 2018, more than 4,845 'C-POD days'[19] of data were collected in the Minas Passage. Over the study period, it was found that harbour porpoise use and movement varies

---

[18] The C-PODs, purchased from Chelonia Limited, are designed to passively detect marine mammal 'clicks' from toothed whales, dolphins, and porpoises.

[19] A 'C-POD day' refers to the number of total days each C-POD was deployed times the number of C-PODs deployed.

over long (i.e., seasonal peaks and lunar cycles) and short (i.e., nocturnal preference and tide stage) timescales. This analysis, completed by Sea Mammal Research Unit (Canada) (Vancouver, BC), showed some evidence to suggest marine mammal exclusion within the vicinity of CSTV turbine when it was operational (November 2016 – June 2017) (Joy et al. 2018a). This analysis revealed that the C-PODs in closest proximity to the turbine (230 m and 210 m distance) had reduced frequency of detections, but no evidence of site avoidance with a device present and operating. These findings also revealed a decrease in detections during turbine installation activities, consistent with previous findings (Joy et al. 2017), but requiring additional data during an operational device to permit a full assessment of the EA predictions.

This monitoring program demonstrates the prevalence of harbour porpoise at FORCE, with the species being detected on 98.8% of the 1,888 calendar days since monitoring with C-PODs commenced in 2011. Harbour porpoise detections at FORCE varies seasonally, with peak activity occurring during May – August, and lowest detections during December – March. Harbour porpoise detections also vary spatially, with C-PODs deployed at locations W2 and S2 recording the greatest detection rates, and D1 values typically low. Mean lost time across C-PODs, due to ambient flow noise saturating the detection buffer on the C-POD, averaged 22.6%. Interestingly, an analysis against past datasets that controlled for time of year, indicated that the effects of the non-operational CSTV turbine structure had no detectable effect on the rate of harbour porpoise detection.

SMRU provided their 4th year final report of harbour porpoise monitoring using C-PODs at the FORCE test site (Palmer et al. 2021). The report describes the results of C-POD deployments #11-12 (i.e., 1,043 days of monitoring from August 2019 – September 2020), and places the results in the broader context of the overall marine mammal monitoring program at FORCE. The final report includes summary data that revealed that harbour porpoise was detected on a least one C-POD every day, with a median value of 11 and 17 minutes of porpoise detections per day during deployments 11 and 12, respectively. The mean percent lost time due to ambient flow and sediment noise was 19.5% and 23.8%, respectively, comparable to previous deployments. Overall, the final report supports previous findings of monitoring activities that harbour porpoise are prevalent at the FORCE test site.

The final report also reiterates that sufficient baseline data has been collected to meet the goals of the EEMP. As such, FORCE has recommended in its 2021-2023 EEMP proposal that the collection of additional baseline harbour porpoise data using C-PODs be suspended until an operational device is deployed at the FORCE site. Upon receiving confirmation that a device will be deployed at the tidal demonstration area, FORCE will deploy C-PODs prior to the construction phase to begin collecting data and assessing any changes to harbour porpoise detections in the presence of an operational device. FORCE is currently working with SMRU to continue with this monitoring program when operational devices are present.

Harbor porpoise (Phocoena phocoena) monitoring at the FORCE Test Site, Canada featured on Tethys (by FORCE and SMRU): https://tethys.pnnl.gov/stories/harbor-porpoise-phocoena-phocoena-monitoring-force-test-site-canada

Observation Program

FORCE's marine mammal observation program in 2023 includes observations made during bi-weekly shoreline surveys, stationary observations at the FORCE Visitor Centre, and marine-based observations during marine operations. All observations and sightings are recorded, along with weather data, tide state, and other environmental data. Any marine mammal observations will be shared with SMRU Consulting to support validation efforts of PAM activities when C-PODs are deployed.

FORCE uses an Unmanned Aerial Vehicle (UAV) for collecting observational data along the shoreline and over the FORCE site using transects by programming GPS waypoints in the UAV to standardize flight paths. FORCE staff received training to operate FORCE's UAV and have acquired UAV pilot certification by successfully passing the 2019 Canadian Drone Pilot Basic Operations Examination, administered by Transport Canada. These staff are now licensed to safely operate the UAV at the FORCE site. FORCE also hosts a public reporting tool that allows members of the public to report observations of marine life: mmo.fundyforce.ca. On April 13, 2023, the UAV observed a harbour seal hauled out on the west side of Black Rock. This is the first time FORCE has observed this, but seals are known to be present on occasion.

Marine Sound (Acoustics)

Marine sound – often referred to as 'acoustics' or 'noise' – monitoring efforts are designed to characterize the soundscape of the FORCE test site. Data collected from these monitoring efforts will be used to test the EA predictions that operational sounds produced from functioning tidal stream energy devices are unlikely to cause mortality, physical injury or hearing impairment to marine animals (AECOM 2009).

Results from previous acoustic analyses completed at the FORCE site indicate that the CSTV turbine was audible to marine life at varying distances from the turbine, but only exceeded the threshold for behavioural disturbance at very short ranges and during particular tide conditions (Martin et al. 2018). This is consistent with findings at the Paimpol-Bréhat site in France where an OpenHydro turbine was also deployed – data suggests that physiological trauma associated with a device is improbable, but that behavioural disturbance may occur within 400 m of a device for marine mammals and at closer distances for some fish species (Lossent et al. 2018).

In previous years, regulators have encouraged FORCE to pursue integration of results from multiple PAM instruments deployed in and around the FORCE test site. To that end, FORCE, and its partner JASCO Applied Sciences (Canada) Ltd. pursued a comparative integrated analysis of sound data collected by various hydrophones (i.e., underwater sound recorders) deployed autonomously and mounted on the CSTV turbine. That work revealed that flow noise increased with the height of the hydrophone off the seabed but had little effect on hydrophones deployed closer to the sea floor. The comparative integrated analysis provided valuable information about future marine sound monitoring technologies and protocols while building on previous acoustics analyses at the FORCE site.

In its 2021-2023 EEMP proposal, FORCE has recommended conducting a test survey in the presence of an operational device using an internationally recognized standard methodology for monitoring sound (International Electrotechnical Commission 2019). This would permit the feasibility of the approach to be tested in the Minas Passage to ensure the method can be implemented as described. This work is pending an operational device being deployed at the

FORCE tidal demonstration area. FORCE will work with JASCO to collect and analyze marine sound data once a device is deployed.

Seabirds

FORCE's seabird monitoring program is designed to test the EA prediction that project activities are not likely to cause adverse residual effects on marine birds within the FORCE test area (AECOM 2009). However, there has been limited opportunity to determine potential effects of an operational device on seabirds at the FORCE test site and to test the EA predictions.

Since 2011, FORCE and Envirosphere Consultants Ltd. (Windsor, NS) have collected observational data from the deck of the FORCE Visitor Centre, documenting seabird species presence, distribution, behaviour, and seasonality throughout the FORCE site (Envirosphere Consultants Ltd. 2017). Envirosphere Consultants Ltd. recently published the results of their monitoring from 2010-2012 and demonstrated that the species and seasonal cycles of seabirds in Minas Passage reflect patterns that are typical of the inner Bay of Fundy and the northeast Atlantic coast of North American. The report also highlights the importance of the Minas Passage as a migratory pathway for black scoter (*Melanitta americana*) and Red-throated loon (*Gavia stellata*).

In 2019, FORCE commissioned Envirosphere Consultants Ltd. and Dr. Phil Taylor (Acadia University) to synthesize the results of its observational seabird surveys (2011-2018) at the FORCE test site, and to evaluate advanced statistical techniques for analysing seabird count data in relation to environmental predictor variables. The seabird count data were examined using Generalized Additive Models (GAMs) to characterize seabird abundance and to better understand the potential impacts of tidal stream energy devices on seabirds at the FORCE test site. The results of the analyses revealed that overall model fit is suitable to characterize count data for some species, and that there are clear patterns of effects of time of year, wind speed and direction, tide height and time of day on the number of seabirds observed. However, the analyses also revealed that not all species reported at FORCE have been observed frequently enough to be modelled effectively using the GAM approach. This is due in part to the variability in count data that is particularly relevant for modelling abundance of migratory species that are only present at the FORCE site for brief periods during annual migrations. This is consistent with observational data collected over the course of these surveys that have demonstrated that the FORCE site has a lower abundance of seabirds in relation to other areas of the Bay of Fundy, and even other regions of Atlantic Canada. Given these results, the report recommends that future monitoring and analyses focus on locally resident species (i.e., great black-backed gull, herring gull, black guillemot, and common eider) so that the EA predictions can be tested most effectively. This work contributes to the development of appropriate analytical methods for assessing the impacts of tidal power development in the Minas Passage on relevant seabird populations and supports the continued responsible development of tidal energy at FORCE.

In 2022 FORCE began working with Strum Consulting to test radar-based seabird monitoring capabilities and to adapt existing data processing algorithms and statistical analysis tools for quantifying seabird use of the FORCE site. Strum provided a technical report which highlighted challenges and options to move forward with this approach. Challenges with the quality of the radar data limited the assessment and the full study could not be completed. The feasibility study continued in 2023 with FORCE providing a new radar data set to Strum, but the challenges in locating avian targets from the radar data could not be resolved using current methods. A commercially available software option may resolve these issues, but requires further examination.

Developer Monitoring Activities

While FORCE completes site-level monitoring activities at the FORCE site, device specific monitoring is led by individual berth holders. Like the FORCE monitoring programs, the developer monitoring plans and reports undergo review by FORCE's EMAC and regulators.

In September 2018, it was confirmed that that CSTV turbine rotor was not spinning. Since that time, CSTV had been providing written confirmation to regulators monthly that the turbine is not operational by monitoring its status during the peak tidal flow of each month. However, because of the insolvency of OpenHydro Technology Ltd., all reporting activities by CSTV ceased as of March 1, 2019. Data collection from the turbine-mounted ADCPs to confirm the turbine is no longer spinning was managed and reported by FORCE to regulators monthly from March 2019 – May 2020 but was discontinued following an amendment to this requirement.

As additional developer, device-specific environmental effects monitoring programs are required and implemented for deployed tidal stream devices, berth holder updates will be included as appendices to future reports.

Other FORCE Research Activities

Risk Assessment Program

The Risk Assessment Program (RAP) for tidal stream energy is a collaborative effort between FORCE, academic partners, First Nations, and industry to advance our understanding of the environmental risks of tidal stream energy development in Minas Passage. The greatest potential risk of tidal stream energy device operations is believed to be from collisions between marine animals and turbine blades (Copping and Hemery 2020). However, these types of interactions are difficult to observe directly due to the environmental conditions under which they would occur (i.e., fast flowing, turbulent waters) and using the suite of environmental monitoring instrumentation currently available (i.e., standard oceanographic and remote sensing instruments intended for use in more benign marine conditions) (Hasselman et al. 2020), but can be modeled using appropriate baseline data. The objective of the RAP program is to develop statistically robust encounter rate models for migratory and resident fishes with tidal stream energy devices in the Bay of Fundy using a combination of physical oceanographic data related to flow and turbulence in the Minas Passage and acoustic tag detection data for various fish species curated by the Ocean Tracking Network (OTN) at Dalhousie University.

Recent research has revealed how hydrodynamics (flow and turbulence-related features) in tidal stream environments can influence the distribution of marine animals, including fish (Lieber et al. 2018, 2019; McInturf et al. 2019). The Minas Passage is characterized by a series of turbulent hydrodynamics features (i.e., vortices, eddies, whirlpools, wakes, and shear currents) that could impact the spatiotemporal distribution of various fishes. The RAP uses ADCP data combined with data from a high-resolution radar network to create the first spatiotemporal flow atlas of the Minas Passage to understand these hydrodynamic features. Concurrently, acoustic tag detection data for various migratory and resident fish species in the Bay of Fundy that is curated by OTN was compiled and is being analysed to understand their spatiotemporal distributions. The hydrodynamic and acoustic tag detection data will be combined with information about device specific parameters (e.g., turbine blade length, swept area, turbine height off the seabed) to develop encounter rate models for various fish species. These models will then be refined and validated through a series of acoustic tagging efforts, ultimately leading to the development of a user-friendly Graphical User Interface (GUI) similar to what is available for the offshore wind

energy industry in the United Kingdom (McGregor et al. 2018). Ultimately, the RAP will contribute towards improving our understanding of the risks of tidal stream energy development for fishes of commercial, cultural, and conservation importance in the Bay of Fundy, and will assist in the development of future environmental effects monitoring programs.

Since the program commenced in April 2020, OTN has facilitated access to acoustic tag detection data from 22 contributors (17 projects), covering nine fish species in the Bay of Fundy (i.e., alewife (*Alosa pseudoharengus*), American shad (*A. sapidissima*), American eel (*Anguilla rostrata*), Inner Bay of Fundy Atlantic salmon (*Salmo salar*), Atlantic sturgeon (*Acipenser oxyrhinchus oxyrhinchus*), Atlantic tomcod (*Microgadus tomcod*), spiny dogfish (*Squalus acanthias*), striped bass (*Morone saxatilis*), and white shark (*Carcharodon carcharias*)). FORCE has also established a high-resolution radar network in Minas Passage and has begun quantifying hydrodynamic features (turbulence, flow etc.) of Minas passage (Figure 5). The integration of physical habitat variables with acoustic tag detection data commenced in 2021, including the development of species distribution models for each species and species distribution maps. Fish tagging was undertaken in 2021 and 2022 in collaboration with the Mi'kmaw Conservation Group (MCG), Acadia University, and DFO Science to validate predictions of the species distribution models (Figure 6). Fish tagging efforts focused on alewife, American shad, Atlantic sturgeon, spiny dogfish, and Inner Bay of Fundy Atlantic salmon smolts. Additional tagging was conducted in 2023 and focused on alewife (n=30; Gaspereau River), American shad (n=20; Kennetcook River) and Inner Bay of Fundy Atlantic salmon smolts (n=25; Gaspereau River).

In 2021 and 2022, the FORCE array of acoustic receivers consisted of 12 stations set approximately 150 metres apart, and extended from the FORCE site out towards the middle of Minas Passage. However, this resulted in incomplete coverage of Minas Passage for detecting tagged fish. For 2023, FORCE and OTN collaborated to establish more complete coverage of the area by merging their respective lines of acoustic receivers into a 24-station array that spans the vast majority of Minas Passage (Figure 7), thereby increasing the probability of detecting tagged fish as they navigate through the area. This array was established in May 2023 and while the original intent was to recover the array in the fall, discussions between FORCE, Acadia and OTN extended the coverage until spring 2024 to increase the temporal scale of monitoring.

Figure 5: One of two high-resolution radars constructed near the FORCE site to be used for the Risk Assessment Program.

Figure 6: Acoustic tagging of spiny dogfish from the Minas Basin by RAP partner organization Mi'kmaw Conservation Group in 2022.
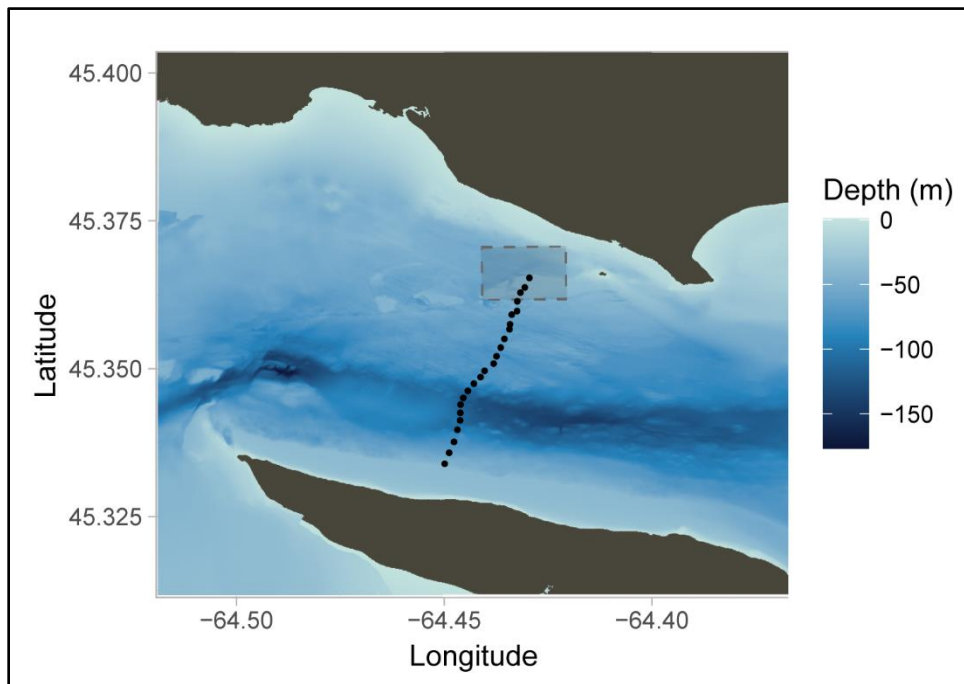

Figure 7: Acoustic receiver array deployment configuration (24 stations) in Minas Passage in 2023. This more thorough coverage of Minas Passage for detecting tagged fish is made possible through collaboration between FORCE and OTN.

The RAP program has generated cutting-edge research on the application of acoustic telemetry for understanding the risk of tidal stream projects to fish in Minas Passage. Specifically, three manuscripts led by Dr. Brian Sanderson (Acadia University) were submitted for publication in a

special issue of the *Journal of Marine Engineering and Science* entitled 'Interface between offshore renewable energy and the environment', and collectively highlight the efficacy of acoustic telemetry for estimating probability of fish-turbine encounter at the FORCE tidal demonstration site. All three of these papers are now published are publicly available.

The first paper (Sanderson et al., 2023a; Appendix III) measures the detection efficiency of acoustic tags in Minas Passage – a prerequisite for estimating fish-turbine encounter using these technologies. Acoustic tags are commonly programmed to emit a pulse position modulation (PPM; 69 kHz, 180 kHz) signal or high-residency (HR; 170 kHz) signal. Although a useful technology under many conditions, the PPM signal is spaced over an extended period of time (usually > 30 seconds) and could remain undetected by an acoustic receiver in Minas Passage if the PPM tag is swept by at high current speeds. This could lead to the incorrect conclusion that a tagged fish was not present when in fact it was, but simply remained undetected. Alternatively, HR technology emits signals much more frequently and may be better suited for detecting tagged fish across the range of tidal current speeds experienced at the FORCE site. Sanderson et al. (2023a) conducted a detection range experiment using tags moored near the seafloor at the FORCE site to determine how efficiently 170 kHz HR acoustic transmissions were detected as a function of range (distance between signal source and receiver) and tidal current speed. The study revealed that the detection density (efficiency) of these signals is high (> 90%) for ranges out to 150 m and current speeds up to 3 m/sec, but drops off quickly for higher current speeds (Figure 8).
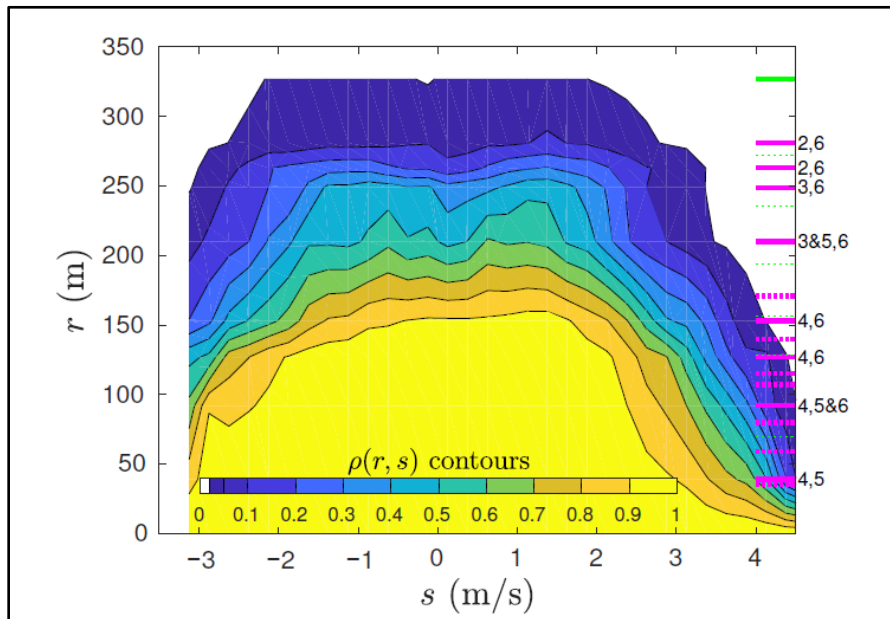

Figure 8: Contours of the detection efficiency for 170 kHz HR signals that best applies to detecting tagged fish that swim well clear of the seafloor (reproduced from Sanderson et al. 2023a; Figure 12).

The second paper (Sanderson et al., 2023b; Appendix IV) examines how reliably a tagged fish can be detected as it passes by an array of receivers in Minas Passage. When combined with detection efficiency estimates, this information can help determine the probability of fish-turbine encounter at the FORCE site. Prior tag detection efficiency estimates (Sanderson et al., 2023a)

relied on tags and receivers deployed at fixed locations on the seafloor and revealed that signal paths are sometimes blocked by variable bathymetry. However, many fish swim well clear of the seafloor in Minas Passage, and their movements are similar to those of drifters that move passively with tidal currents (Sanderson et al. 2021). As such, deploying acoustic tags on GPS-tracked drifters permits verification of prior detection efficiency estimates using tags positioned higher in the water column, and also enables demonstration of a method for obtaining probability of detecting a tagged fish as it passes by a receiver array. Sanderson et al. (2023b) suspended multiple 170 kHz HR acoustic tags and a 69 kHz PPM at varying depths (as surrogates for fish swimming at varying depths) below GPS-tracked drifters and released them in Minas Passage for varying lengths of time. Results confirm the findings of Sanderson et al. (2023a) that 69 kHz PPM signals are poorly detected by acoustic receivers when tidal current speeds are high (> 3.5 m/sec), and is due to the extended period of time required to transmit the entire PPM signal. However, 170 kHz HR signals were usually detected by the receiver array even in fast currents (>3.5 m/sec) during spring tides, and short signal transmission intervals (≤ 2 seconds) are needed to ensure detection across tidal current speeds. Indeed, there is a high likelihood (≥0.90) that frequently transmitted HR signals will be detected across current speeds ≥ 3.5 m/sec at the FORCE tidal demonstration site if acoustic receivers in an array are spaced ≤ 150 m apart (Figure 9).

Interestingly, drifters that were deployed for extended periods of time become 'caught' in quasi-steady trajectories by tidal currents and typically pass through the center of Minas Passage to the south of the FORCE tidal demonstration site (Figure 10). These results are consistent with Sanderson et al. (2021), and given that the movements of drifters and some fish species are similar, it is reasonable to expect that the majority of individual fish tracks also pass through the center of Minas Passage to the south of the FORCE tidal demonstration site.
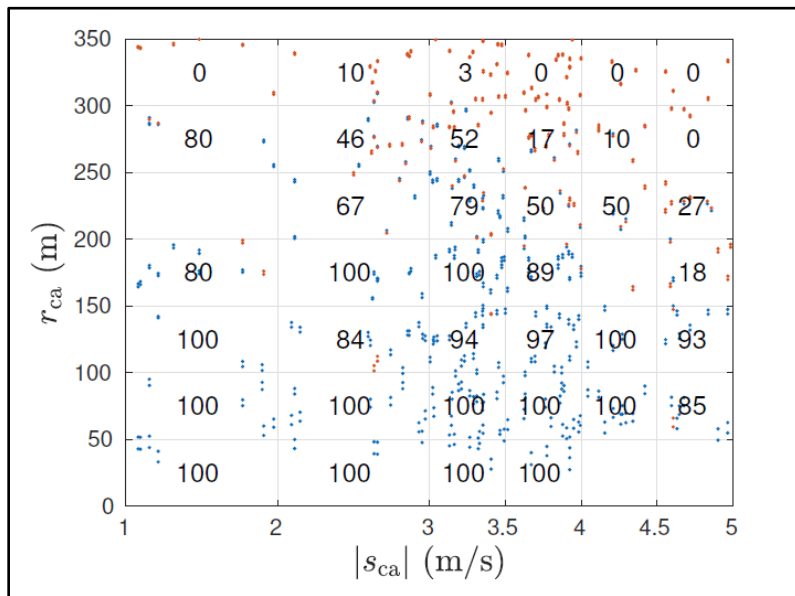

Figure 9: Percentage of tag passing events that are detected by moored HR2 acoustic receivers as a function of current speed $|s_{ca}|$ and range r_{ca} at closest approach, based on HR tags deployed 19 m and 28 m below a GPS-tracked drifter transmitting every 2 seconds (reproduced from Sanderson et al. 2023b; Figure 12).
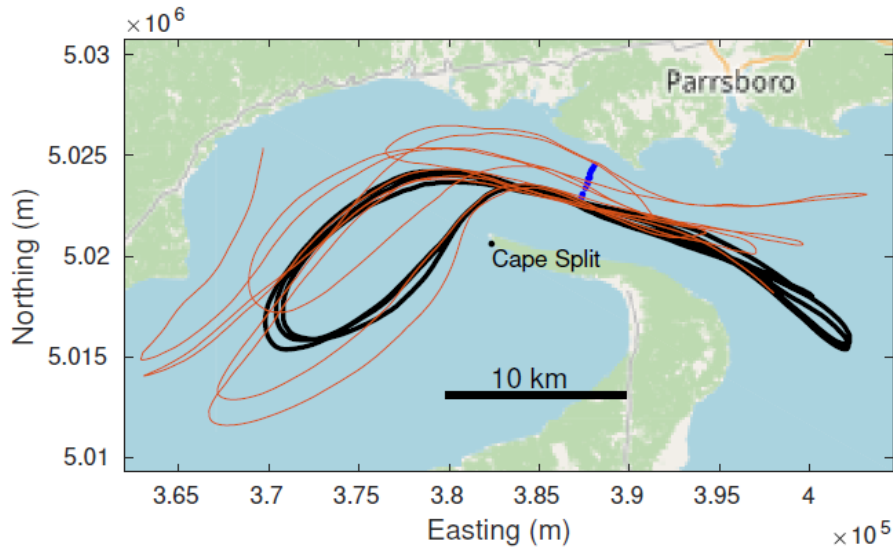
Figure 10: Drifter tracks through Minas Passage. A quasi-steady track (black) frequently passes near the southern end of an acoustic receiver array (blue) in the center of Minas Passage, whereas a highly variable track (orange) sometimes passes through the northern end of the receiver array (reproduced from Sanderson et al. 2023b; Figure 8).

The first two papers (Sanderson et al. 2023a,b) serve as building blocks for the third paper (Sanderson et al., 2023c; Appendix V). Specifically, having demonstrated the detection efficiency of HR acoustic tags and shown that drifters carrying these tags will be reliably detected as they pass an array of acoustic receivers in Minas Passage, this paper develops and applies a method by which acoustic tag detections by the HR2 acoustic receiver array can be used to estimate the expected number of times an Inner Bay of Fundy (IBoF) Atlantic salmon post-smolt would encounter a single near-surface tidal energy device at the FORCE site during its seaward migration. IBoF Atlantic salmon are a federally endangered species protected by Canada's *Species at Rick Act*; they are known to occupy the upper water column during various life history stages, and there is concern about harm from encounters with floating tidal energy technologies deployed at FORCE. The method developed in Sanderson et al. (2023c) uses acoustic detections of tagged IBoF Atlantic salmon post-smolts from the Gaspereau River (2019, 2022) and Stewiacke River (2021) by HR2 acoustic receivers in Minas Passage and builds upon the approach used by Sanderson et al. (2021) to calculate the probability that drifters would collide with a tidal turbine installed in Minas Passage. Specifically, the method calculates the probability of encounter from an ensemble averaged estimate of detection efficiency, with a small empirical correction for fluctuations about the typical value at a given range and modelled tidal current speed.

Here, probability of encounter is defined as the probability that a tagged fish passes within the width of a floating tidal energy device (e.g., PLAT-I; 38 m) of a receiver location. Estimation of probability of encounter in the absence of a turbine was deliberate as turbine presence has been shown to elicit behavioural responses in fish in both laboratory and field conditions (e.g., Müller et al. 2023; Bender et al. 2023). As such, probability of encounter in this paper can only be considered as an *upper limit* on the probability of harm, because it does not consider fish

behavioural responses like avoidance or evasion that have been demonstrated elsewhere and that could reduce the probability of encounter in Minas Passage.

Results indicate that IBoF Atlantic salmon post-smolts are substantially displaced by tidal currents and can be swept through Minas Passage multiple times during their seaward migration. However, most of these passes are on quasi-steady trajectories that would carry fish through the center of Minas Passage to the south of the FORCE tidal demonstration site (Sanderson et al. 2023b). Indeed, the expected number of encounters with a near-surface deployed tidal device at FORCE is relatively low (Figure 11), but higher for post-smolts from the Stewiacke River compared to the Gaspereau River. The expected number of encounters at the FORCE site is also low across tidal current speeds, and consistently lower than if a tidal device was installed in the middle of Minas Passage (Table 2), suggesting that the FORCE tidal demonstration area is positioned in a geographic location in Minas Passage that does not expose IBoF Atlantic post-smolts to increased risk of encounter with tidal devices. Moreover, Sanderson et al. (2023c) show that if every encounter of a post-smolt with a near-surface turbine at FORCE was fatal, then this would be projected to result in a loss of 0.9% and 3% of the Gaspereau River and Stewiacke River post-smolts, respectively. However, these estimates represent an *upper limit* on mortality, and do not consider demonstrated avoidance and evasion behavior exhibited by fish, including salmonids in turbulent and turbid conditions (Müller et al. 2023; Bender et al. 2023; Courtney et al. 2022). Putting this into broader context, the average at-sea mortality for immature Atlantic salmon was 97% for the period 1990-2003 (DFO, 2008), so outmigration losses caused by a near-surface turbine at FORCE would add, at most, 0.027% and 0.09% to the estimated 97% marine mortality that Atlantic salmon already experience.
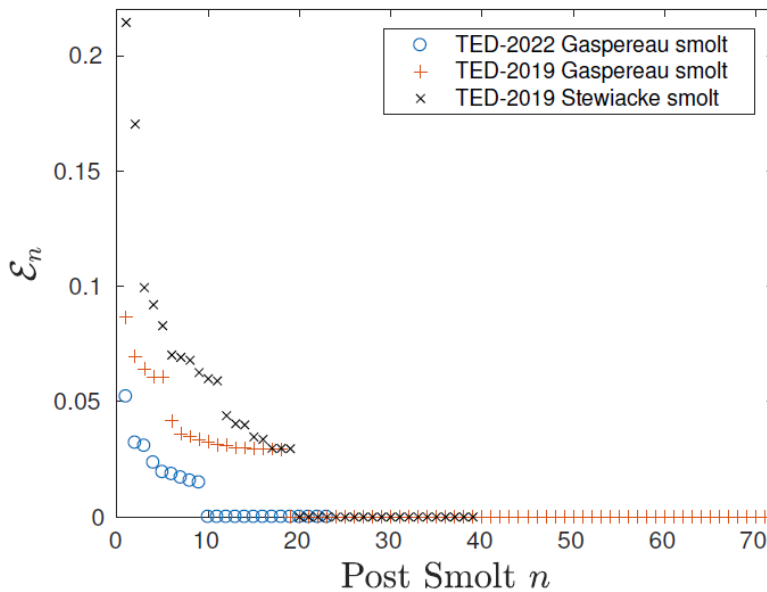

Figure 11: Expected number of encounters that each tagged Inner Bay of Fundy Atlantic salmon post-smolt would make with a single near-surface tidal turbine installed at the FORCE tidal demonstration site (reproduced from Sanderson et al. 2023c; Figure 8).

Table 2: Expected number of times that a smolt would encounter a single turbine installation at the FORCE tidal energy demonstration (ε_{TED}) site or the middle of Minas Passage ($\varepsilon_{mid\text{-}passage}$, ε_{S2}) during its seaward migration from the Gaspereau and Stewiacke Rivers at different current speeds (reproduced from Sanderson et al. 2023c; Table 3).

2022 Gaspereau River		2019 Gaspereau River		2019 Stewiacke River		$\lvert s_d \rvert$
$\overline{\varepsilon}_{TED}$	$\overline{\varepsilon}_{mid-passage}$	$\overline{\varepsilon}_{TED}$	$\overline{\varepsilon}_{S2}$	$\overline{\varepsilon}_{TED}$	$\overline{\varepsilon}_{S2}$	(ms^{-1})
0.0098 ± 0.0030	0.075 ± 0.031	0.0110 ± 0.0024	0.014 ± 0.004	0.034 ± 0.0078	0.075 ± 0.017	≥ 0
0.0091 ± 0.0028	0.073 ± 0.031	0.0087 ± 0.0022	0.014 ± 0.004	0.032 ± 0.0078	0.072 ± 0.017	≥ 1
0.0091 ± 0.0028	0.072 ± 0.031	0.0082 ± 0.0022	0.013 ± 0.004	0.03 ± 0.0079	0.063 ± 0.016	≥ 1.5
0.0085 ± 0.0029	0.069 ± 0.032	0.0074 ± 0.0021	0.011 ± 0.004	0.026 ± 0.0071	0.058 ± 0.015	≥ 2
0.0078 ± 0.0029	0.067 ± 0.031	0.0070 ± 0.0020	0.008 ± 0.004	0.024 ± 0.0064	0.044 ± 0.013	≥ 2.5

Fundy Advanced Sensor Technology (FAST) Activities

FORCE's Fundy Advanced Sensor Technology Program is designed to advance capabilities to monitor and characterize the FORCE site. Specifically, the FAST Program was designed to achieve the following objectives:

  1) To advance capabilities of site characterization;
  2) To develop and refine environmental monitoring standards and technologies; and
  3) To enhance marine operating methodologies.

FAST combines both onshore and offshore monitoring assets. Onshore assets include a meteorological station, video cameras, an X-band radar system, and tide gauge. Offshore assets include modular subsea platforms for both autonomous and cabled data collection and a suite of instrumentation for a variety of research purposes. Real-time data collected through FAST assets will be broadcasted through the Canadian Integrated Ocean Observing System (CIOOS) later this year. Static ADCP data is currently available on the CIOOS website.[20]

Platform Projects

The first and largest of the FAST platforms houses an instrument called the Vectron. Developed in partnership with Nortek Scientific (Halifax, NS), Memorial University (St. John's, NL), and Dalhousie University (Halifax, NS), the Vectron is the world's first stand-alone instrument to remotely measure, in high resolution, turbulence in the mid-water column. Measurements and analysis from the Vectron will help tidal energy companies to better design devices, plan marine operations, and characterize the tidal energy resource.

A smaller platform called FAST-3 was equipped with an upward looking echosounder and deployed during 2017-2018 to monitor fish densities at the FORCE site. FORCE and its partners, including Echoview Software completed data processing and analysis in 2019. This data was integrated with the mobile hydroacoustic surveys that FORCE conducts as part of its EEMP to evaluate the temporal and spatial representativeness of each method and to determine the

---

[20] This is available online at: https://catalogue.cioosatlantic.ca/dataset/ca-cioos_db15458d-df2c-4efb-b5a0-791e7561a0cb

degree to which results were corroborative (Figure 12). Although the spatial representative range of the stationary results could not be determined from the mobile data, it did reveal strong tidal and diel periods in fish density estimates at the site, with greater variation over shorter time frames than over the course of a year. These findings reinforce the importance of 24-hr data collection periods in ongoing monitoring efforts. The report reveals that collecting 24 hours of data allows the tidal and diel variability to be quantified and isolated from the longer-term trends in fish density and distribution that need to be monitored for testing the EA predictions. This project was funded by Natural Resources Canada (NRCan), the NSNRR, and the Offshore Energy Research Association (now Net Zero Atlantic).
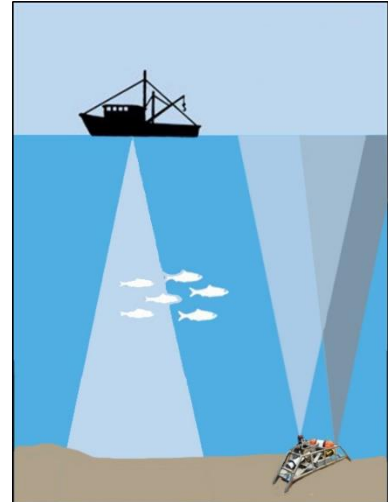
Figure 12: A representation of the data collection methods of the FORCE site-level fish EEMP and the FAST-3 platform.

FORCE is currently collaborating with Innovasea to test innovative new acoustic receiver technology in Minas Passage to assess instrument capabilities in high flow environments. Five different acoustic receiver technologies (with duplicates for redundancy) were mounted on the FAST-2 platform and deployed at the FORCE site in September (Figure 13). A Nortek Signature 500 Acoustic Doppler Current Profiler (ADCP) was deployed alongside the acoustic receivers to record flow speed, along with an OceanSonics icListen HF hydrophone to record underwater noise that can impact the detection of acoustic signals. A series of passive drifts were then conducted over the platform using acoustic tags of various frequencies deployed at differing depths. The drifts were conducted on the flood tide during the strong spring tides of late September and early October. The platform was recovered in mid-October and the acoustic detection data downloaded from the receivers for analyses.

Figure 13: FAST-2 platform equipped with five Innovasea acoustic receiver technologies (with duplicates for redundancy), an ADCP and hydrophone for recording flow speed and underwater noise.

FORCE is also collaborating on an Ocean Supercluster funded project lead by Innovasea, and in partnership with DeepSense (Dalhousie University), BigMoon Power, Nova Scotia Power Incorporated, and New Brunswick Power Corporation to advance the capabilities of artificial intelligence (AI) for monitoring fish around hydroelectric facilities and tidal stream energy devices. The HydroAware project will build off recent advances in the application of AI for detecting, identifying and tracking fish by Innovasea and DeepSense (Kandimalla et al. 2022), and shows promise for the renewable energy community, as improved fish monitoring capabilities may help address some of the challenges facing tidal stream energy projects in Canada.

Fish Tracking

To enhance fish monitoring and to expand its data collection capacity, FORCE partnered with the Ocean Tracking Network (OTN)[21] and attached one Innovasea (formerly VEMCO)[22] fish tag receiver (a VR2W receiver) to each C-POD mooring/SUBS (Streamlined Underwater Buoyancy System) package (see above). These receivers are used to supplement OTN's ongoing data collection program within the Minas Passage and are referred to as 'Buoys of Opportunity.' Upon retrieval of the C-PODs and receivers, instruments are shared with OTN where data is offloaded prior to redeployment. This effort will support increased knowledge of fish movement within the Minas Passage, which has applicability beyond tidal energy demonstration, as well as complement FORCE's hydroacoustic data collection efforts that do not allow for species identification. No C-POD mooring/SUBS have been deployed since 2020, however ongoing data collection for fish monitoring is occurring through the RAP acoustic receiver line.

OTN data managers are in the process of acquiring information, including species identification, and sharing this with FORCE. Initial results show that the OTN receivers deployed by FORCE have detected tags from the following projects:

- Maritimes Region Atlantic salmon marine survival and migration (Hardie, D.C., 2017);
- Quebec MDDEFP Atlantic Sturgeon Tagging (Verreault, G., Dussureault, J., 2013);
- Gulf of Maine Sturgeon (Zydlewski, G., Wippelhauser, G. Sulikowski, J., Kieffer, M., Kinnison, M., 2006);
- OTN Canada Atlantic Sturgeon Tracking (Dadswell, M., Litvak, M., Stokesbury, M., Bradford, R., Karsten, R., Redden, A., Sheng, J., Smith, P.C., 2010);
- Darren Porter Bay of Fundy Weir Fishing (Porter, D., Whoriskey, F., 2017);
- Movement patterns of American lobsters in the Minas Basin, Minas Passage, and Bay of Fundy Canada (2017);
- Shubenacadie River Monitoring Project: Tomcod (Marshall, J., Fleming, C., Hunt, A., and Beland, J., 2017);
- MA Marine Fisheries Shark Research Program (Skomal, G.B., Chisholm, J., 2009);
- UNB Atlantic Sturgeon and Striped Bass tracking (Curry, A., Linnansaari, T., Gautreau, M., 2010);
- Inner Bay of Fundy Striped Bass (Bradford, R., LeBlanc, P., 2012);
- Minas Basin Salmon Kelt (McLean, M., Hardie, D., Reader, J., Stokesbury, M.J.W., 2019);
- New York Juvenile White Shark Study (Tobey Curtis)

---

[21] Ocean Tracking Network's website: www.oceantrackingnetwork.org.
[22] Innovasea is "the world leader in the design and manufacture of acoustic telemetry equipment used by researchers worldwide to study behaviour and migration patterns of a wide variety of aquatic animals." Learn more: www.innovasea.com.

- Massachusetts White Shark Research Program (Greg Skomal); and
- St. Lawrence River Fish Monitoring (Valiquette, E., Légaré, J., Soulard, Y. 2020)

Further information about these Buoys of Opportunity, and the projects listed above, can be found on OTN's website: https://members.oceantrack.org/project?ccode=BOOFORCE

Starting in 2018, FORCE has worked in collaboration with Dr. Mike Stokesbury at Acadia University to install additional Innovasea receivers of a new design on FORCE's C-POD moorings/SUBS packages. These new receivers are expected to be even more effective in picking up acoustic detections in high flow environments, where tag signals can be obscured by noise. This partnership will contribute additional information regarding movement patterns of Atlantic salmon, sturgeon, striped bass, and alewife in Minas Passage and Basin. This work is sponsored by the OERA, NRCan, NSNRR, the Natural Sciences and Engineering Research Council of Canada (NSERC), and the Canadian Foundation for Innovation (CFI).[23]

Discussion

The 2021-2023 EEMP represents a strategic opportunity for FORCE and its partners to learn from previous experiences, incorporate regulatory advice, and to re-evaluate approaches to research and monitoring in the high flows of the Minas Passage. The EEMP is designed to prepare for effects testing with the deployment of operational devices, and adheres to the principles of adaptive management by evaluating existing datasets to ensure appropriate monitoring approaches are being implemented. Moreover, the plan adopts internationally accepted standards for monitoring where possible, including feasibility assessments for new monitoring approaches that are planned to be implemented.

Advances in monitoring capabilities made possible through programs like FORCE's Risk Assessment Program enhance our ability to understand how animals use Minas Passage, and contribute towards a better understanding of risk from the development of tidal stream power in the Upper Bay of Fundy. Ongoing research and the development of peer-reviewed publications add credibility to the innovative science activities that FORCE continues to undertake in support of its role as environmental steward. FORCE and its partners continue conducting monitoring, engaging in meaningful assessments of monitoring technology capabilities, and providing data analyses and interpretation that advance our ability to effectively monitor the effects of tidal stream energy devices in high flow environments, and specifically at the FORCE test site. Reports from FORCE's partners and updates are routinely subjected to review by FORCE's EMAC and regulators, along with continued results from FORCE's ongoing monitoring efforts.

FORCE continues to implement lessons learned from the experiences of local and international partners, build local capacity, and enhance skills development, test new sensor capabilities, and integrate results from various instruments. Cumulatively, these efforts provide an opportunity for adaptive management and the advancement and refinement of scientific approaches, tools, and

---

[23] Information about this project, and others funded through this program, is available online at:
https://netzeroatlantic.ca/sites/default/files/2020-04/2020-04-09%20NRCan%20Public%20Report%20Final%20-%20Resize.pdf

techniques required for effectively monitoring the device and site-level areas of tidal stream energy devices in dynamic, high-flow marine environments.

Ongoing monitoring efforts will continue to build on the present body of knowledge of marine life-device interactions. While it is still early to draw conclusions, initial findings internationally and at the FORCE test site have documented some disturbance of marine mammals primarily during marine operations associated with device installation/removal activities, but otherwise have not observed significant effects.

FORCE will continue to conduct environmental research and monitoring to increase our understanding of the natural conditions within the Minas Passage and, when the next device(s) are deployed and operating, test the EA prediction that tidal energy is unlikely to cause significant harm to marine life. In the longer-term, monitoring will need to be conducted over the full seasonal cycle and in association with multiple different device technologies to understand if tidal energy can be a safe and responsibly produced energy source. FORCE will continue to report on progress and release results and lessons learned in keeping with its mandate to inform decisions regarding future tidal energy projects.

References

AECOM. 2009. Environmental Assessment Registration Document - Fundy Tidal Energy Demonstration Project Volume I: Environmental Assessment. Available from Available at www.fundyforce.ca.

Bangley, C.W., Hasselman, D.J., Flemming, J.M., Whoriskey, F.G., Culina, J., Enders, L., and Bradford, R.G. 2022. Modeling the probability of overlap between marine fish distributions and marine renewable energy infrastructure using acoustic telemetry data. Front. Mar. Sci. **9**: 851757. doi:10.3389/fmars.2022.851757.

Bender, A., Langhamer, O., Francisco, F., Forslund, F., Hammar, L., Sundberg, J., and Molander, S. 2023. Imaging-sonar observations of salmonid interactions with a vertical axis instream turbine. River Research and Applications 1: 1-12. doi: 10.1002/rra.4171.

Copping, A.E. 2018. The State of knowledge for environmental effects - driving consenting/permitting for the marine renewable energy industry. Available from https://tethys.pnnl.gov/sites/default/files/publications/The State of Knowledge Driving Consenting Permiting for the MRE.pdf.

Copping, A.E., and Hemery, L.G. 2020. OES-Environmental 2020 State of the Science Report: Environmental Effects of Marine Renewable Energy Development Around the World. Report for Ocean Energy Systems (OES). *In* State Sci. Rep. doi:10.2172/1632878.

Copping, A.E., Hemery, L.G., Viehman, H., Seitz, A.C., Staines, G.J., and Hasselman, D.J. 2021. Are fish in danger? A review of environmental effects of marine renewable energy on fishes. Biol. Conserv. **262**: 109297. Elsevier Ltd. doi:10.1016/j.biocon.2021.109297.

Copping, A.E., D.J. Hasselman, C.W. Bangley, J. Culina, and M. Carcas. 2023. A probabilistic methodology for determining collision risk of marine animals with tidal energy turbines. *Journal of Marine Science and Engineering* 11(11): 2151

Courtney, M., Flanigan, A.J., Hostetter, M. and Seitz, A.C. 2022. Characterizing sockeye salmon smolt interactions with a hydrokinetic turbine in the Kvichak River, Alasks. NOrth American Journal of Fisheries Management 42: 1054-1065. doi: 10.1002/nafm.10806.

Daroux, A., and Zydlewski, G. 2017. Marine fish monitoring program tidal energy demonstration site – Minas Passage. : 34. Orono, ME.

DFO. Recovery Potential Assessment for Inner Bay of Fundy Atlantic Salmon. DFO Canadian Science Advisory Secretariat Science Advisory Report 2008/050. 2008. Available online: https://waves-vagues.dfo-mpo.gc.ca/library-bibliotheque/335147.pdf

Envirosphere Consultants Ltd. 2017. Marine seabirds monitoring program – tidal energy demonstration site – Minas Passage, 2016-2017.

Fraser, S., Williamson, B.J., Nikora, V., and Scott, B.E. 2018. Fish distributions in a tidal channel indicate the behavioural impact of a marine renewable energy installation. Energy Reports **4**: 65–69. Elsevier Ltd. doi:10.1016/j.egyr.2018.01.008.

Gaskin, D.E. 1992. Status of the harbour porpoise, Phocoena phocoena, in Canada. Can. F. Nat. **106**(1): 36–54.

Gattuso, J.P., Magnan, A.K., Bopp, L., Cheung, W.W.L., Duarte, C.M., Hinkel, J., Mcleod, E., Micheli, F., Oschlies, A., Williamson, P., Billé, R., Chalastani, V.I., Gates, R.D., Irisson, J.O., Middelburg, J.J., Pörtner, H.O., and Rau, G.H. 2018. Ocean solutions to address climate change and its effects on marine ecosystems. Front. Mar. Sci. **5**(OCT). doi:10.3389/fmars.2018.00337.

Gillespie, D., Hastie, G., Palmer, L., Macaulay, J., and Sparling, C. 2021. Harbour porpoises exhibit localized evasion of a tidal turbine. Aquat. Conserv. Freshw. Ecosyst.: 1–10. doi:10.1002/aqc.3660.

Hasselman, D.J., Barclay, D.R., Cavagnaro, R., Chandler, C., Cotter, E., Gillespie, D.M., Hastie, G.D., Horne, J.K., Joslin, J., Long, C., McGarry, L.P., Mueller, R.P., Sparling, C.E.,

Williamson, B.J., and Staines, G.J. 2020. Environmental monitoring technologies and techniques for detecting interactions of marine animals with turbines. *In* Report for Ocean Energy Systems (OES).

Hasselman, D.J., Li, H., Cotter, E., and Joslin, J. 2022. Editorial: Novel technologies for assessing the environmental and ecological impacts of marine renewable energy systems. Front. Mar. Sci. **9**: 990327. doi:10.3389/fmars.2022.990327.

Hasselman, D.J., Hemery, L.G., Copping, A.E., Fulton, E.A., Fox, J., Gill, A.B., and Polagye, B. 2023. 'Scaling up ' our understanding of environmental effects of marine renewable energy development from single devices to large-scale commercial arrays. Sci. Total Environ. **904**: 166801. Elsevier B.V. doi:10.1016/j.scitotenv.2023.166801.

International Electrotechnical Commission. 2019. Marine Energy - Wave, tidal and other water current converters - Part 40: Acoustic characterization of marine energy converter.

Joy, R., Robertson, F., and Tollit, D. 2017. FORCE Marine Mammal Environmental Effects Monitoing Program - 1st Year (2017) Monitoring Report.

Joy, R., Wood, J., and Tollit, D. 2018a. FORCE echolocating marine mammal environmental effects monitoring program - 2nd year (2018) monitoring report.

Joy, R., Wood, J.D., Sparling, C.E., Tollit, D.J., Copping, A.E., and McConnell, B.J. 2018b. Empirical measures of harbor seal behavior and avoidance of an operational tidal turbine. Mar. Pollut. Bull. **136**: 92–106. Elsevier. doi:10.1016/j.marpolbul.2018.08.052.

Kandimalla, V., Richard, M., Smith, F., Quirion, J., Torgo, L., and Whidden, C. 2022. Automated Detection, Classification and Counting of Fish in Fish Passages With Deep Learning. Front. Mar. Sci. **8**: 1–15. doi:10.3389/fmars.2021.823173

Lewis, A., Estefen, S., Huckerby, J., Musial, W., Pontes, T., and Torres-Martinez, J. 2011. Ocean Energy. *In* Renewable Energy Sources and Climate Change Mitigation: Special Report of the Intergovernmental Panel on Climate Change. *Edited by* O. Edenhofer, R. Pichs-Madruga, Y. Sokona, K. Seyboth, P. Matschoss, and S. Kadner. Cambridge University Press, Cambridge, Massachusetts. pp. 497–534.

Lieber, L., Nimmo-Smith, W.A.M., Waggitt, J.J., and Kregting, L. 2018. Fine-scale hydrodynamic metrics underlying predator occupancy patterns in tidal stream environments. Ecol. Indic. **94**: 397–408. Elsevier. doi:10.1016/j.ecolind.2018.06.071.

Lieber, L., Nimmo-Smith, W.A.M., Waggitt, J.J., and Kregting, L. 2019. Localised anthropogenic wake generates a predictable foraging hotspot for top predators. Commun. Biol. **2**(1): 1–8. Springer US. doi:10.1038/s42003-019-0364-z.

Lossent, J., Lejart, M., Folegot, T., Clorennec, D., Di Iorio, L., and Gervaise, C. 2018. Underwater operational noise level emitted by a tidal current turbine and its potential impact on marine fauna. Mar. Pollut. Bull. **131**(May 2017): 323–334. Elsevier. doi:10.1016/j.marpolbul.2018.03.024.

Lowe, S.C., McGarry, L.P., Douglas, J., Newport, J., Oore, S., Whidden, C., and Hasselman, D.J. 2022. Echofilter: A deep learning segmentation model improves the automation, standardization, and timeliness for post-processing echosounder data in tidal energy streams. Front. Mar. Sci. **9**: 867857. doi:10.3389/fmars.2022.867857.

Malinka, C.E., Gillespie, D.M., Macaulay, J.D.J., Joy, R., and Sparling, C.E. 2018. First in situ passive acoustic monitoring for marine mammals during operation of a tidal turbine in Ramsey Sound, Wales. Mar. Ecol. Prog. Ser. **590**: 247–266. doi:10.3354/meps12467.

Marine Renewables Canada. 2018. State of the Sector Report: Marine Renewable Energy in Canada.

Martin, B., Whitt, C., and Horwich, L. 2018. Acoustic data analysis of the OpenHydro opencentre turbine at FORCE: final report.

McGregor, R.M., King, S., Donovan, C.R., Caneco, B., and Webb, A. 2018. A Stochastic

Collision Risk Model for Seabirds in Flight. Available from https://www2.gov.scot/Resource/0053/00536606.pdf.

McInturf, A.G., Steel, A.E., Buckhorn, M., Sandstrom, P., Slager, C.J., Fangue, N.A., Klimley, A.P., and Caillaud, D. 2019. Use of a hydrodynamic model to examine behavioral response of broadnose sevengill sharks (Notorynchus cepedianus) to estuarine tidal flow. Environ. Biol. Fishes **102**(9): 1149–1159. Environmental Biology of Fishes. doi:10.1007/s10641-019-00894-3.

Melvin, G.D., and Cochrane, N.A. 2014. Investigation of the vertical distribution, movement and abundance of fish in the vicinity of proposed tidal power energy conversion devices. Final Report for the Offshore Energy Research Association. Research Project 300-170-09-12.

Müller, S., Muhawenimana, V., Sonnino-Sorisio, G., Wilson, C.A.M.E., Cable, J., and Ouro, P. 2023. Fish response to the presence of hydrokinetic turbines as a sustainable energy solution. Scientific Reports 13: 7459. doi: 10.1038/s41598-023-33000-w.

NEXUS Coastal Resource Management Ltd. 2017. Lobster Catchability Study Report.

Palmer, K.J., Wood, J., and Tollit, D.J. 2021. FORCE Marine Mammal EEMP - Year 4 Final Report.

Pine, M.K., Schmitt, P., Culloch, R.M., Lieber, L., and Kregting, L.T. 2019. Providing ecological context to anthropogenic subsea noise: Assessing listening space reductions of marine mammals from tidal energy devices. Renew. Sustain. Energy Rev. **103**(July 2018): 49–57. Elsevier Ltd. doi:10.1016/j.rser.2018.12.024.

Robertson, F., Wood, J., Joslin, J., Joy, R., and Polagye, B. 2018. Marine Mammal Behavioral Response to Tidal Turbine Sound. (206). doi:10.2172/1458457.

Sanderson, B.G., Stokesbury, M.J.W., and Redden, A.M. 2021. Using trajectories through a tidal energy development site in the Bay of Fundy to study interaction of renewable energy with fish. Journal of Ocean Technology 16(1): 50-70.

Sanderson, B.G., C.W. Bangley, L.P. McGarry, and D.J. Hasselman. 2023a. Measuring detection efficiency of high-residency acoustic signals for estimating probability of fish-turbine encounter in a fast-flowing tidal passage. *Journal of Marine Science and Engineering* 11(6): 1172.

Sanderson, B.G., R.H. Karsten, and D.J. Hasselman. *2023b. In review.* Towards estimating probability of fish-turbine encounter: using drifters equipped with acoustic tags to verify efficacy of an array of acoustic receivers. *Journal of Marine Science and Engineering.*

Sanderson, B.G., R.H. Karsten, C.C. Solda, D.C. Hardie, and D.J. Hasselman. 2023c. Probability of Atlantic salmon post-smolts encountering a tidal turbine installation in Minas Passage, Bay of Fundy. Journal of Marine Science and Engineering 11(5): 1095.

Schramm, M.P., Bevelhimer, M., and Scherelis, C. 2017. Effects of hydrokinetic turbine sound on the behavior of four species of fish within an experimental mesocosm. Fish. Res. **190**: 1–14. Elsevier B.V. doi:10.1016/j.fishres.2017.01.012.

SLR Consulting. 2015. Proposed Environmental Effects Monitoring Programs 2015-2020 for Fundy Ocean Research Center for Energy (FORCE).

Viehman, H., Hasselman, D., Boucher, T., Douglas, J., and Bennett, L. 2019. Integrating hydroacoustic approaches to predict fish interactions with in-stream tidal turbines. Available from https://netzeroatlantic.ca/sites/default/files/2020-04/FISH FINDER Final Report 31-03-2020_0.pdf.

Viehman, H.A., Hasselman, D.J., Douglas, J., and Boucher, T. 2022. The ups and downs of using active acoustic technologies to study fish at tidal energy sites. Front. Mar. Sci. **9**: 851400. doi:10.3389/fmars.2022.851400.

Whiting J., Garavelli, L, Farr, H. and Copping, A.E. *In press.* Effects of small marine energy deployments on oceanographic systems. International Journal of Marine Energy.
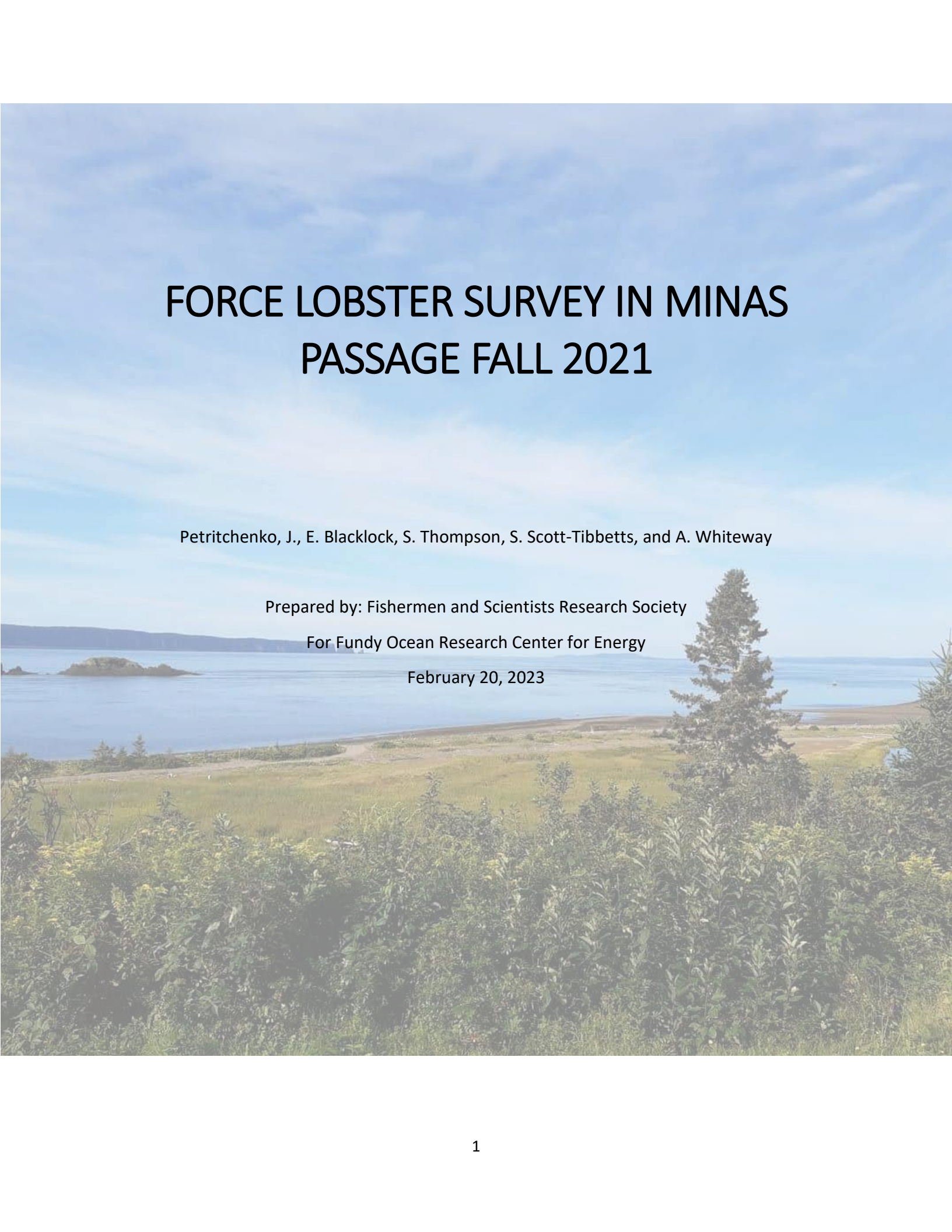
Appendix I

Acronyms

AAM	Active Acoustic Monitoring
ADCP	Acoustic Doppler Current Profiler
AMAR	Autonomous Multichannel Acoustic Recorder
BACI	Before/After, Control/Impact
BC	British Columbia
BoFEP	Bay of Fundy Ecosystem Partnership
CFI	Canadian Foundation for Innovation
CIOOS	Canadian Integrated Ocean Observing System
CLA	Crown Lease Area
cm	Centimetre(s)
CPUE	Catch Per Unit Effort
CSTV	Cape Sharp Tidal Venture
DFO	Department of Fisheries and Oceans (Canada)
DEM	Department of Energy and Mines (Nova Scotia)
EA	Environmental Assessment
EEMP	Environmental Effects Monitoring Program
EMAC	Environmental Monitoring Advisory Committee
EMP	Environmental Management Plan
FAD	Fish Aggregation Device
FAST	Fundy Advanced Sensor Technology
FAST-EMS	Fundy Advanced Sensor Technology – Environmental Monitoring System
FERN	Fundy Energy Research Network
FORCE	Fundy Ocean Research Center for Energy
GPS	Global Positioning System
hr	Hour(s)
IEA	International Energy Agency
kg	Kilogram(s)
km	Kilometre(s)
kW	Kilowatt(s)
m	Metre(s)
MET	Meteorological
MRE	Marine Renewable Energy
MREA	Marine Renewable-electricity Area
NL	Newfoundland and Labrador
NRCan	Natural Resources Canada
NS	Nova Scotia
NSDEM	Nova Scotia Department of Energy and Mines
NSE	Nova Scotia Department of Environment
NSERC	Natural Sciences and Engineering Research Council
NSPI	Nova Scotia Power Inc.
OERA	Offshore Energy Research Association of Nova Scotia
OES	Ocean Energy Systems
ONC	Ocean Networks Canada
ORJIP	Offshore Renewables Joint Industry Programme
OSC	Ocean Supercluster
OTN	Ocean Tracking Network
PAM	Passive Acoustic Monitoring
Q1/2/3	Quarter (1, 2, 3), based on a quarterly reporting schedule

R&D	Research and Development
TC114	Technical Committee 114
SUBS	Streamlined Underwater Buoyancy System
SME	Sustainable Marine Energy (Canada)
UAV	Unmanned Aerial Vehicle
UK	United Kingdom
VEC(s)	Valuable Ecosystem Component(s)

Appendix II

FORCE LOBSTER SURVEY IN MINAS PASSAGE FALL 2021

Petritchenko, J., E. Blacklock, S. Thompson, S. Scott-Tibbetts, and A. Whiteway

Prepared by: Fishermen and Scientists Research Society

For Fundy Ocean Research Center for Energy

February 20, 2023

Executive Summary

As part of its Environmental Effects Monitoring Program (EEMP), the Fundy Ocean Research Centre for Energy (FORCE) commissioned a lobster survey in fall 2021 to establish baseline data on lobster catchability by quantifying the number of lobsters captured and Catch Per Unit Effort (CPUE) in the vicinity of the FORCE tidal demonstration site. The survey design followed that developed by TriNav Fisheries Consultants Ltd. in 2019, and included the deployment of experimental lobster traps at 18 locations distributed over three sites ('Near-Control site', 'Far-Control site', and 'Impact site'). The survey occurred prior to the commencement of the fall 2021 commercial lobster fishery in Minas Passage and was conducted over two sampling phases that coincided with neap tidal conditions (Phase I: August 29 – September 3, and Phase II: September 27 – October 1). Prior to their release, biological data collected from captured lobsters included carapace length, sex, shell hardness, and reproductive stage (females). Lobster weight was estimated from a previously documented polynomial length-weight regression for lobster in the region, and was used for estimating CPUE (kg/trap haul). A subset of individuals were tagged with conventional t-bar tags prior to being released. A total of 582 lobsters were caught and released over the course of the survey, with 477 being tagged. Approximately 5% of tagged lobsters were recaptured and reported by local fishers during the fall 2021 commercial lobster fishing season; providing important information about the short term (approximately 1-2 months) movements of lobster in Minas Passage. Statistical analyses were conducted to determine if there was a significant ($p < 0.05$) difference in the abundance of lobster and CPUE between survey phases and sample sites, and if water temperature influenced the abundance of lobster captured and CPUE.

We detected no significant difference in lobster abundance or CPUE between Phases I and II of the survey. However, we observed marginally significant ($p=0.052$) differences in the abundance of lobster captured among sites, with the Impact Site having on average fewer lobster (6.2 lobster/trap haul) than either the Near Control Site (8.46 lobster/trap haul) or Far Control Site (8.92 lobster/trap haul). These differences were not reflected in the CPUE data, as non-significant differences in CPUE were observed among the sites. We observed a significant decrease in water temperature over the course of the survey, and observed a statistically significant, but weak negative correlation between water temperature and lobster abundance and CPUE during Phase II of the survey. However, we cannot draw any conclusions about the influence of water temperature on lobster catchability due to the protracted time frame over which data was collected during Phase II of the survey (i.e., limited sample sizes and reduced statistical power).

Commercial landings data provided by Fisheries and Oceans Canada (2005-2021) revealed a marked increase in lobster CPUE in LFA 35, including grid 17 where the FORCE tidal demonstration site is located. This may be associated with a northward shift in the distribution of lobster associated with increasing water temperatures in the Gulf of Maine and it effects on lobster movement, survival and recruitment to the fishery. These data provide important context for the interpretation of the results from the 2021 fall lobster survey.

Contents

Introduction

Objectives

The primary objective of FORCE's American lobster (*Homarus americanus*) monitoring program is to determine whether the presence of a tidal stream energy turbine affects commercial lobster catches ('catchability') (AECOM 2009). This objective is intended to be met by determining whether turbine operations result in a statistical change in commercial lobster catchability. There is a need for statistically robust baseline data about lobster presence and movement in the vicinity of the FORCE tidal demonstration site to quantify any changes after tidal energy devices have been deployed. Therefore, the objective of the Fall 2021 FORCE lobster survey was to improve the quality of baseline catchability data for lobster at the FORCE tidal demonstration site so that a meaningful comparison could be made once operational turbines are deployed.

Background

In fall 2017, FORCE commissioned a baseline lobster catchability survey (NEXUS Coastal Resource Management Ltd., 2017) that involved a catch-and-release BACI (Before-After-Control-impact) survey design conducted over 11 days and consisting of commercial traps deployed in two concentric rings around the future location of the Cape Sharp Tidal Venture (CSTV) turbine deployment planned for 2018. Captured lobsters were measured (carapace length (mm)), had their sex and reproductive stage determined (male, female, and berried female), and shell condition evaluated. This baseline survey captured 351 lobsters and reported a 'high' Catch Per Unit Effort (CPUE) (> 2.7 kg/trap) following established criteria (Serdynska and Coffen-Smout, 2017) (Table 1). Preliminary analyses indicated that catch rates declined during the survey and was associated with increasing tidal velocities (i.e., a statistically significant negative correlation between catch rates and maximum tidal range was reported). No significant differences in catch rates were observed between trap deployment locations (either within or between concentric rings or quadrants of that survey design), suggesting a uniformly high density of lobster in the survey area. A repeat of the survey in the presence of an operational turbine is required to determine whether turbine operations have an impact on lobster catchability. Although a repeat of the catchability survey was planned for fall 2018 following the deployment of the CSTV turbine, that device ceased working shortly after installation, and its non-operational status necessitated a postponement of the survey until an operational device could be installed. Additionally, Fisheries and Oceans Canada (DFO) provided feedback on the design of the lobster survey, advocating for the incorporation of a tagging component to account for variability in lobster behavior and its influence on catchability (DFO, 2016); something that was not included in the 2017 survey design.

In 2019, FORCE commissioned TriNav Fisheries Consultants Ltd. ('TriNav Fisheries') to redesign the lobster monitoring program based on the feedback from regulators to include a more statistically robust survey design. TriNav Fisheries evaluated the efficacy of a variety of methods and identified the combination of a modified catchability survey design with a mark-recapture

component using conventional tags as the best approach. This new survey design included the use of an impact site (i.e., where turbines are intended to be deployed), and a near-, and far-control site for lobster trap deployment, and was implemented in fall 2021 in partnership with the Fishermen and Scientists Research Society (FSRS) and with the assistance of a local lobster fisher. The survey design also included comparisons of lobster abundance and CPUE to water temperature to determine whether this environmental variable influenced lobster catchability. Historical commercial catch (landings) data from Minas Passage and the surrounding region (Lobster Fishing Area (LFA) 35) was made available by DFO and provides additional information to help contextualize baseline lobster catchability over time, and is considered herein.

Table 1. An index of lobster catchability indicators in terms of Catch Per Unit Effort (CPUE) (kg/trap haul) (modified from Serdynska and Coffen-Smout, 2017).

CPUE (kg/trap haul)	Lobster Catchability
0-0.7	Low
0.8-1.1	Moderately low
1.2-1.7	Moderate
1.8-2.3	Moderately high
2.4-10.7	High

The Minas Basin lobster fishery and the value of local ecological knowledge

The FORCE tidal demonstration site is located in LFA 35 (Figure 1). Based on the 2021 Science Advisory Report (DFO 2021) for LFAs 35-38, the abundance of lobster and the CPUE trend indicate an increase in lobster stock biomass in LFA 35. The lobster fishery in LFA 35 is an effort-controlled fishery, with effort limited by season, minimum legal size, number of licenses, and number of traps per license. LFA 35 has two fishing seasons annually: i) spring (March 31st to July 31st) and ii) fall (Oct 15th to December 31st). The FORCE fall lobster survey (late August to early October) precedes the fall lobster fishing season and does not interfere with the commercial fishery, but does permit tagged lobster to be capture during the fall fishing season and reported to FORCE.

The inclusion of local stakeholders in fisheries research is imperative for assisting with positive perceptions of projects related to marine industries (Bundy et al., 2017; Cooke et al., 2017; Fujitani et al., 2017). Engaging community members in scientific monitoring activities promotes a willingness to share information and increased support for marine science and conservation (Martin et al., 2016; Fujitani et al., 2017; Dean et al., 2018). In LFA 35, fishers actively participate in scientific data collection through participating in scientific sampling of lobster at sea and maintaining catch logbooks and field notebooks (This Fish, 2021). For the purposes of the FORCE fall lobster survey, lobster traps were rented from a local fisher and a fishing vessel was used for trap deployment/retrieval and the collection of biological data. Beyond this, the

incorporation of local and traditional ecological knowledge acquired from extensive experience is invaluable for assisting with the planning and execution of fisheries related research (Childress et al., 2010; Farr et al., 2018). To that end, a local fisher was employed during the 2021 fall lobster survey to share insights about sampling locations and how to deploy and retrieve lobster traps in the Minas Passage safely and efficiently (Figure 2). Following completion of trap deployments, retrievals and tagging activities, the survey also partially relied on fishers notifying FORCE of any tagged lobsters that were captured during the fall 2021 commercial fishery including the date of capture and approximate coordinates (i.e., latitude and longitude).
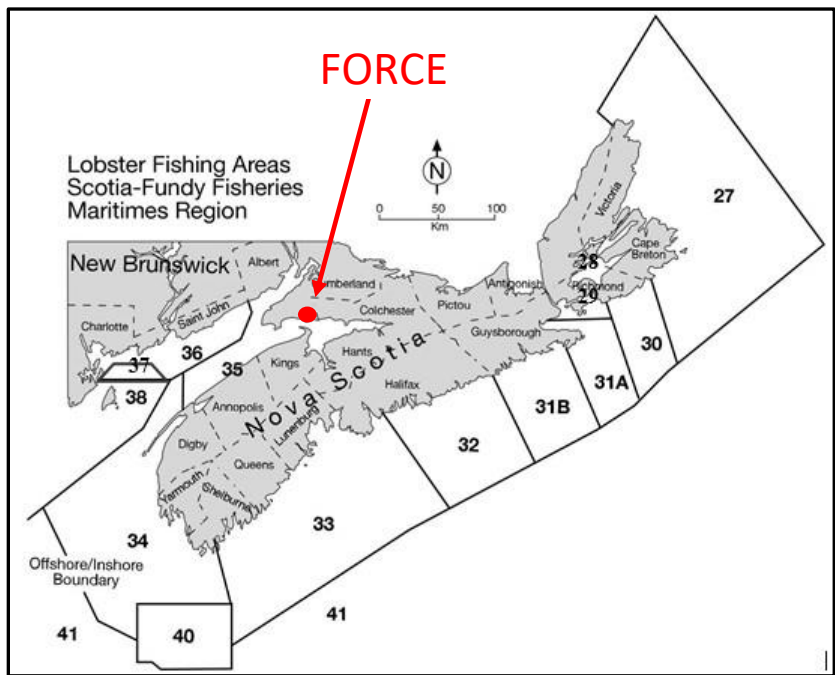

Figure 1: Map of lobster fishing areas in the DFO 'Maritimes Region'. (Source: https://www.dfo-mpo.gc.ca/fisheries-peches/ifmp-gmp/maritimes/2019/inshore-lobster-eng.html)

Figure 2: A local lobster fisher (right) oversees the deployment and retrieval of lobster traps during the FORCE fall lobster survey 2021.

American Lobster biology and distribution

Lobster life history and habitat

The life history of the American lobster is divided into pelagic and benthic stages (Cobb and Wahle, 1994; Lillis and Snelgrove, 2010). The larvae first exists as pelagic zoea, and the post-larval stage settles to a benthic environment, where the juvenile lobster matures in sheltered nursery habitat (Cobb and Wahle, 1994; Wahle and Incze, 1997; Barret et al., 2017). FORCE's monitoring objective focuses on assessing the effects of operational turbines on lobster that have already undergone this transition and are susceptible to capture in commercial lobster fishing gear. Temperature influences the moult cycle and size at maturity of lobster (Watson et al., 2013). In this survey, sex was recorded for each lobster, and moult stage was recorded for two lobsters from each trap haul. Clutch maturity and percent coverage were noted for egg-bearing (i.e., 'berried') female lobsters.

Lobster spatial distribution is largely habitat dependent. Juvenile lobsters are more at risk of predation and are largely restricted to habitats that provide shelter. Shelter-restricted juveniles depend on cobble and eelgrass meadow habitats where there are plenty of spaces to escape from predators (Factor, 1995). However, all lobster life stages can be found on mud or clay where they can form depressions or burrows, or on a more heterogenous substrate of sand and rock where lobster can make shallow burrows under rock (Factor, 1995). Scoured bedrock habitat, which is characteristic of the FORCE tidal demonstration site, tends to have reduced habitat complexity for burrowing, but lobster can be found where boulders or other complex habitat features are present (Factor, 1995). Figure 3 provides a heatmap of bathymetry around

the FORCE tidal demonstration site. The impact site has scoured bedrock as a substrate, with more heterogenous benthic habitats in the near and far control sites (Figure 4).
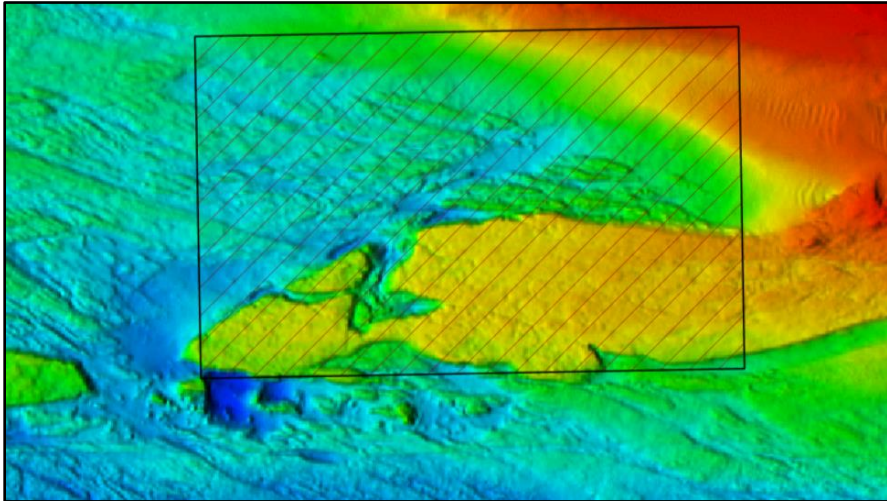

Figure 3: Heat map of bathymetry of the FORCE tidal demonstration site (shaded black square). 'Warmer' colours indicate more shallow locations, and the impact site (future site of tidal turbine deployments) shown in Figure 4 is located on the relatively shallow volcanic plateau.

Figure 4: Map showing the 18 deployment locations for lobster traps in the Impact Site (IMP1-6), Near Control Site (NC1-6), and Far Control Site (FC1-6) in the Minas Passage. Note: the Near Control Site and Impact Site are located within the FORCE tidal demonstration site.

Lobster moult stage and tagging

Observations made from lobster hemolymph (blood) and pleopods can be used to predict the likelihood that a lobster will moult; information that is relevant to tag retention (i.e., a lobster close to moulting may lose its tag). Therefore, pleopod and hemolymph samples were taken to predict moult stage and to assess the likelihood that t-bar tags would be retained by sampled lobster (Haakonsen & Anoruo, 1994). From the hemolymph, degree's brix (°Bx) is a metric that is used as an indicator of pre-moult, inter-moult, and post-moult stages (Battison, 2018). Pleopod samples can be taken and examined at 40x magnification with a compound light microscope to also determine moulting stage (Aiken, 1973). When used in combination, these metrics can account for confounding variables (e.g., scarring which alters the edge of the pleopod, injury or illness that lower degrees brix). For more information see Appendix A.

Lobsters were tagged with individually numbered Hallprint t-bar tags that are inserted in the soft tissue of the lobster where the carapace meets the first somite. Tagged lobster with moult stage 'D0' were susceptible to recapture in the Fall 2021 commercial lobster season, while intermoult lobster were expected to retain their tags until the spring 2022 commercial season. T-bar tags are cost-effective, easy to insert and have a low risk of mortality (Comeau et al., 2003). While mortality associated with tagging occurs most often in lobster that are two weeks pre- or post-moult, little mortality is associated with tagging intermoult lobster (Comeau et al., 2003). Injury during the tagging process can occur using t-bar tags, but can be mitigated by tagging intermoult lobster, tagging larger lobster, and tagging to the lateral portion of the carapace to avoid piercing organs (Comeau et al., 2003).

Influence of water temperature on lobster physiology, behaviour, and epidemiology

Water temperature influences many physiological and behavioural parameters in marine animals (Nielson and McGaw, 2016) and can influence the seasonal distribution of lobster (Jury and Watson (2013). Lobster have different optimal temperature ranges at different life history stages (Annis, 2005; Quinn 2016); juveniles avoid water temperatures below 8°C and above 20°C (Nielson and McGaw, 2016). Water temperature at the sea floor stimulates lobster egg development, hatching and larval settlement (Cobb and Wahle, 1994; Annis, 2005). Water temperature also determines the duration of the pelagic larval phase, affecting settlement and distribution, which are relevant to fisheries management (Cobb and Wahle, 1994; Annis, 2005). Water temperature at the sea floor was collected at each trap deployment site using a temperature logger deployed in each trap and was used to better understand lobster distribution and catch data.

Elevated water temperatures can result in shell disease (Wahle et al., 2013; Nielson and McGaw, 2016; Quinn, 2016) that can influence the distribution of larval settlement and recruitment to the commercial fishery (Wahle et al., 2015; Le Bris et al., 2017). Lobster shell disease is an 'catch-all' term for a variety of pathogens and parasites, including bacteria, protozoans and nematodes, that create lesions on lobster shells (NOAA, 2018). An increase in water temperature in southern New England led to increased prevalence of shell disease and recruitment failure that culminated in the collapse of the lobster fishery in that region (Wahle et al., 2015; Le Bris et al., 2017). Instances of shell disease were noted during the FORCE Fall 2021 lobster survey.

Water temperature at the seafloor also influences lobster growth and moult cycles (Annis, 2005; Wahle et al., 2013). Lobster require four to nine years of growth before being recruited to the fishery (Wahle et al., 2004), and the collection of life history data over multiple years is important for understanding lobster population dynamics (Phillips, 1986; Li et al., 2015). Many research projects last only three to five years, but in the context of long-lived crustaceans, longer time series data are required (Phillips, 1986; Caputi et al., 1995; Wahle et al., 2004; Star, 2010). To that end, the results of the 2021 fall lobster survey were compared to historic CPUE data for lobster in the Minas Passage area to provide added context on lobster population dynamics in the region.

Quantifying lobster catchability

CPUE is a standardized unit of measurement for assessing lobster catchability and is commonly used to measure relative population abundance (Appleman, 2015). The unit of measurement for catch and the effort indicated in CPUE are fishery-dependent; catch can be measured by weight or number of individuals (Appleman, 2015). Effort must be measured in a way that is relevant to the fishery, and the number of trap hauls is the standard unit of effort for the lobster fishery (Tremblay et al., 2009). CPUE is often overestimated for migratory species (Appleman, 2015) and can be different for lobster populations during spring and fall due to lobster migration (Tremblay et al., 2009; Haakonsen and Anoruo, 1994). For the purposes of this survey, CPUE is expressed as the number of lobster caught per trap haul, and weight of lobster caught per trap haul. A scale for lobster CPUE (kg/ trap haul) for the Minas Passage is provided in Table 1 (Serdynska and Coffen-Smout, 2017).

Materials and Methods

Sampling schedule

Consultations with local lobster fishers suggested that tidal flow conditions in Minas Passage would place logistical constraints on the survey design due to the influence of strong currents on vessel mobility, timing of buoy resurfacing, and the operational window for successfully recovering and re-deploying 18 traps during low water slack conditions. To optimize the survey design within these operational constraints, the survey was scheduled around two neap tide phases (Phase I: August 29 – September 3; Phase II: September 27 – October 1) so that nine traps could be recovered and deployed during each survey phase around the low water slack portion of the tidal cycle. This required 10 marine operational days (five days for each phase of the survey) to ensure a minimum 24-hour soak period for each trap between deployment and recovery.

This survey was conducted under DFO Scientific Licence #347451. A total of six traps were deployed in each of the Impact Site, Near Control Site and Far Control Site over the course of the survey; three traps within each site in Phase I and Phase II (Figure 4; Table 2). Trap deployment locations within each of these sites was selected using a random number generator assigned to unique combinations of latitude and longitude within the geographic boundaries of each site; these locations were maintained throughout the duration of the survey phase (Table 2). Traps were deployed at each location and retrieved four times on subsequent days throughout each survey phase for a total of 72 trap hauls over the course of the survey.

Captured lobster were measured (i.e., carapace length (mm)), assessed (i.e., sex, reproductive stage for females, moult staging – hemolymph and pleopod assessment) and tagged before being released back to the area from which they were captured.

During Phase I, traps were deployed on August 29 and hauled daily from August 30 through September 1, with the final haul delayed to September 3 due to inclement weather that prevented marine operations on September 2. During Phase II, trap deployment was delayed by one day due to inclement weather, and traps were deployed on September 27, with trap hauls occurring daily from September 28 through October 1.

During Phase II of the survey, the trap that was intended to be deployed at site IMP4 was deployed at incorrect coordinates due to a data entry error in the vessel GPS. Given that the traps were deployed outside of the Impact Site, the data collected from these traps were excluded from analyses. Trap deployment locations during Phase I and Phase II of the survey, including incorrect deployment location for IMP4 are shown in Figure 5.

Sampling equipment and trap deployment

Due to the elevated tidal current speeds in Minas Passage (up to 5 m/s), the commercial wire lobster traps (dimensions: 1.21m x .038m x 0.61m) used in this survey were modified to include 150 kg of ballast (concrete) to ensure traps remained in place following deployment; this is common practice among commercial lobster fishers in Minas Passage. Each trap was affixed with a DFO-approved identification tag and was connected to a 100 m buoy line with a corresponding marked buoy. The traps also had their escape vents blocked to permit full enumeration of lobster and the collection of size distribution data for Minas Passage. Traps were baited using 1.5 kg of redfish (*Sebastes spp.*) heads impaled on a bait spike and were deployed from a commercial vessel (the Nova Endeavor) using the planned deployment coordinates (Figure 6).

Table 2: Lobster trap deployment coordinates during the 2021 fall lobster survey.

| Survey phase	Near Control Site			Impact Site			Far Control Site		
	Site	Latitude	Longitude	Site	Latitude	Longitude	Site	Latitude	Longitude
Phase I	NC1	45°21.599	-64°26.240	IMP1	45°21.540	-64°26.214	FC1	45°22.008	-64°24.144
Phase I	NC2	45°22.120	-64°26.258	IMP2	45°21.543	-64°25.307	FC2	45°21.518	-64°24.162
Phase I	NC3	45°22.089	-64°25.510	IMP3	45°21.441	-64°26.441	FC3	45°21.540	-64°24.036
Phase II	NC4	45°22.075	-64°25.415	IMP4	45°21.542	-64°25.379	FC4	45°21.432	-64°23.564
Phase II	NC5	45°21.599	-64°25.219	IMP5	45°21.432	-64°26.240	FC5	45°21.504	-64°23.528
Phase II	NC6	45°22.074	-64°26.027	IMP6	45°21.448	-64°25.336	FC6	45°21.468	-64°24.072
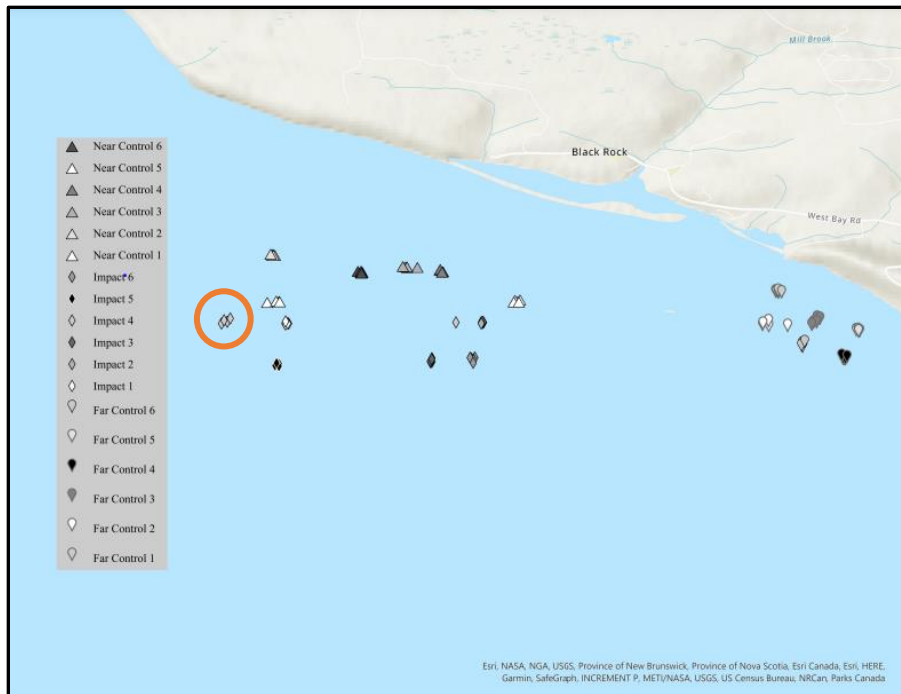
Figure 5: Map of the trap deployment locations during Phases I and II of the lobster survey. The incorrect deployment location for IMP4 are marked with an orange circle.

Figure 6: Photo of trap retrieval (left) and deployment (right) aboard the Nova Endeavor.

Data collection

The biological sampling procedure followed the standardized protocol for lobster assessment developed by DFO (2019a) and applied broadly across the DFO Maritimes Region (LFA 27-38; Figure 1). Following trap recovery, lobsters were removed from the trap and placed in individually labelled totes so they could be processed (Figure 7). Carapace length for each lobster was measured using 8" vernier calipers held parallel to the carapace from the eye socket to the posterior edge of the carapace (Figure 8) and rounded down to the nearest millimetre. Sex was determined by inspection of secondary sexual characteristics (i.e., pleopods). While males have rigid modified pleopods where the tail meets the body, females have soft reduced pleopods (Figure 9). Sex was recorded as 1-males, 2-females, and 3-egg bearing (berried) females. For berried females, the egg maturity stage (Table 3) and the density of their clutch (%) (Table 4) was recorded. Lobster condition as a result of the fishing activity was recorded on a scale from 0-no damage to 4-dead or dying (Table 5). Shell hardness and moult stage was recorded on a scale from (1) to (7) (Table 6) and was assessed by gently pressing on three regions of the carapace. When a lobster moults, the shell hardens sequentially from the anterior region of the carapace to the ventral region of the carapace (Figure 10). The presence of a v-notch in one of the uropods (a conservation measure used to mark reproductive females to prevent them from being retained in the fishery) was recorded as present or absent (Figure 11).

Moult stage determination

To understand the likelihood that tagged lobster would retain their tags, we assessed their molt stage through a combination of hemolymph examination and pleopod inspection. Hemolymph was extracted from two lobster per trap per day from a sinus in the underside of the tail using a syringe. A brix refractometer was used to quantify the amount of protein in the hemolymph and was used to determine degrees brix (°Bx) – an indicator of lobster moult stage (Battison 2018). Values of °Bx < 7 typically indicate that a lobster is post-moult or is suffering from disease or injury, °Bx between 8-16 indicate an intermoult stage, and °Bx values > 16 are indicative of lobster that are actively preparing to moult (Battison 2018). In addition to determining °Bx, the anterior right pleopod was excised and subsequently examined using a compound light microscope under 40x and 100x magnification to help determine moult stage (Appendix A). When a lobster is in active pre-moult a separation can be observed at the edge of the pleopod.

Figure 7: Following trap recovery, lobsters were placed in individually labelled totes until they could be processed.

Figure 8: Measurement of lobster carapace length.

Figure 9: Female (left) and male (right) secondary sexual characteristics (i.e., modified pleopods) used to determine lobster sex. Source: DFO (2019a).

Table 3: Egg stage codes adapted from DFO (2019a).

Egg stage	Description
0	No eggs
1	Newly deposited eggs, which are shiny and dark green or black.
2	Older eggs lose their luster and may be larger and brown or orange.
3	Mature eggs are bulky, orange and less loosely packed. You will see eyespots of the larval lobster. These eggs are partially hatched or hatching soon.
4	Eggs hatching or hatched (mossy), empty egg casings become opaque, the "glue" that adheres eggs to the tail becomes visible as well as the long hairs on the egg-bearing pleopods.

Table 4: Percent clutch coverage codes adapted from DFO (2019a).

Percent Clutch Coverage	Description
0	No clutch
1	Full clutch, 100% coverage
2	Partial clutch, 10%- 50% coverage
3	Small clutch, >10% coverage

Table 5. Lobster condition adapted from DFO (2019a).

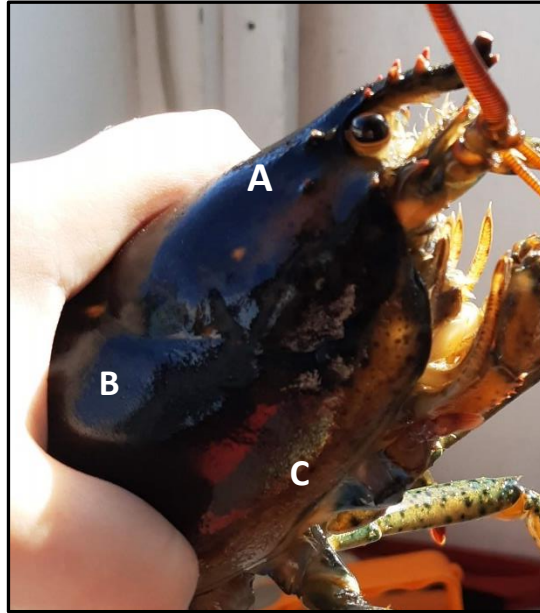| Lobster condition	Description
0	No injury
1	Minor damage, such as a broken rostrum or missing leg
2	Multiple minor damages
3	Severe damage, such as crushed carapace or tail
4	Dead or dying

Figure 10: Lobster carapace hardens sequentially from the anterior portion of the carapace (A) to the posterior portion of the carapace (B), and to the lateral portion of the carapace (C).

Table 6: Descriptions of moult stages adapted from DFO (2019a).

Moult Stage	Description
1	Recent moult, firm gelatin texture
2	Soft shell compressible
3	Hardened in the anterior portion of carapace only
4	Dorsal anterior and posterior portions of carapace hardened
5	Dorsal anterior, posterior, and lateral portions of the carapace are hardened
6	Hard shell with epiphytic growth
7	Hard carapace split bilaterally, a lobster actively moulting

Figure 11: A V-notched female lobster. The v-notch is cut in the tail on the uropod to the right of the telson when observing the dorsal side of the lobster (indicated by a circle).

Lobster tagging

Lobsters with a minimum carapace length of 80 mm were tagged with uniquely numbered t-bar tags inserted under the posterior portion of the carapace using a tagging gun (Figure 12). Lobster with a carapace length < 80 mm, those with moult condition 3 or 4 (Table 5) and berried females were not tagged due to the increased risk of injury, reduced probability of tag retention, and out of conservation concern for the local commercial fishery, respectively. Tags were also labelled 'FORCE' and 'REWARD' with an associated phone number to increase the chances that tagged lobster captured during the fall commercial fishery would be reported. The duration of time between release and recapture and the distance between the release and recapture location were calculated in R (R Development Core Team 2021) using the 'geosphere' package.
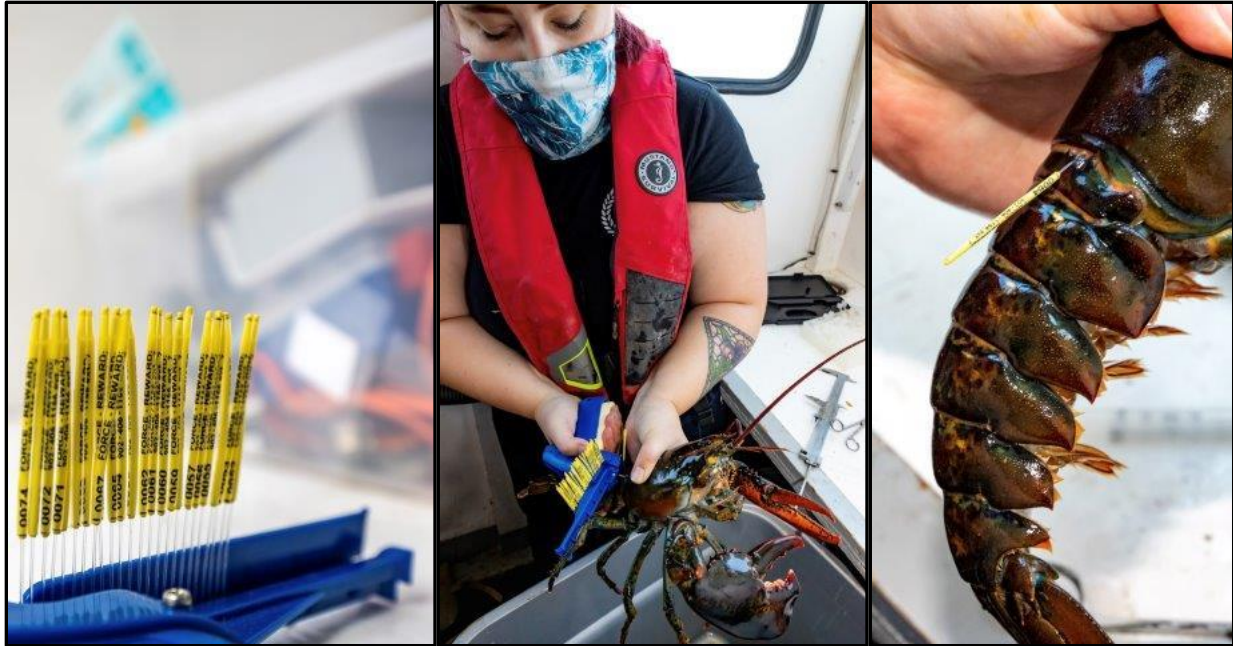
Figure 12: Photographs of lobster tagging during the lobster survey. Individually numbered Hallprint t-bar tags (left), tagging process (center), position of inserted tag (right).

Water temperature data

Water temperature near the sea floor was recorded using HOBO tidbit V2 temperature loggers (Figure 13) attached to each trap. Following each phase of the survey, the data from the temperature loggers were downloaded using the HOBO Optic USB Base Station. Lobster CPUE data was compared with these abiotic variables to identify whether any correlations could be detected that might shed light on environmental factors that could influence lobster catchability.

Figure 13: HOBO tidbit V2 temperature logger and Optic base station.

Data analyses

Raw data was recorded in the field on a standardized data sheet developed for lobster (Appendix B) and was transferred to an electronic format (Microsoft Excel) at the end of each field day. Data analyses were conducted in R (R Development Core Team 2021) to determine the extent to which lobster abundance and CPUE (kg/trap haul) varied among survey phases, among sites (i.e., Impact Site, Near-Control Site and Far-Control Site), and to understand correlations with water temperature. Statistical analyses included standard tests for data normality and equal variance, correlations, and univariate statistics (detailed below).

CPUE calculation

To estimate CPUE (kg/trap haul), lobster weight (Wt) (lbs) was estimated from carapace length (CL) (mm) using a documented polynomial length-weight regression for female American lobster in the region (MacDonald and Scott, 2000) (Figure 14):

Wt (lbs) = 1.492 − 0.04037(CL) + 0.000444(CL)^2

Estimated weight was then converted to kilograms prior to statistical analyses. Individuals below the legal commercial harvest size (i.e., < 82.5 mm CL), berried females and v-notched individuals were omitted from CPUE calculation for making comparisons with historical commercial landings data from LFA 35 provided by DFO (see below).
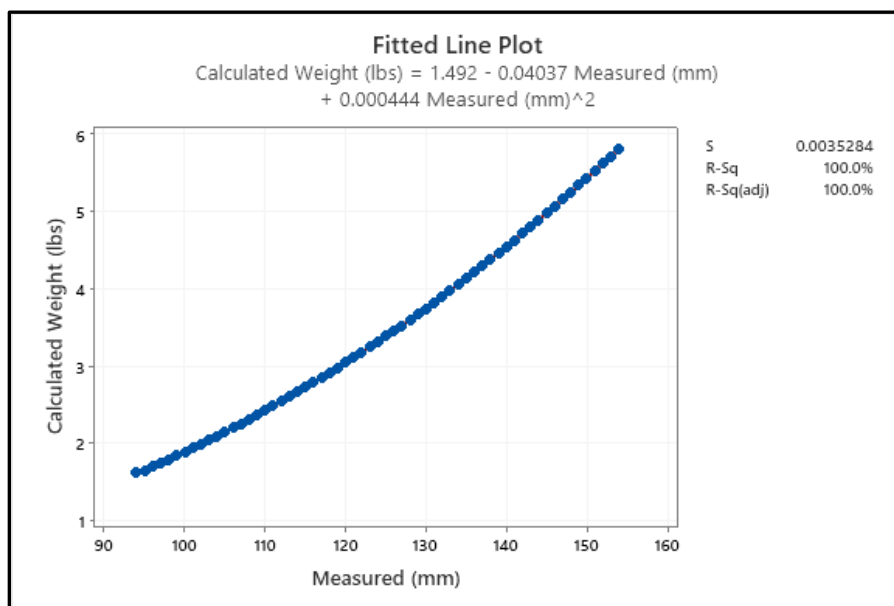

Figure 14: A fitted line plot of the measured carapace length (mm) to the calculated weight (lbs) based on a polynomial regression (MacDonald and Scott, 2000).

Comparison among survey phases

Lobster abundance and CPUE data were compared between the two phases of the survey to determine whether the data from each phase could be combined for analyses. A Shapiro-Wilks test was conducted in R to determine if the data collected in Phase I and Phase II of the survey were normally distributed. If the data from the two survey phases approximated normality and had equal variance, a two-sample t-test was conducted to determine if there was a statistically significant difference (i.e., $p < 0.05$) in lobster abundance and CPUE between the phases of the survey. If the data was non-normal, a two-sample Wilcoxon rank test was conducted (suitable for non-parametric data).

Comparison among sites

A Shapiro-Wilks test was conducted in R to determine if the data collected among the sites were normally distributed. A one-way Analysis of Variance (ANOVA) and a Tukey Honest Significant Differences (HSD) test was conducted in R to determine if there was a statistically significant difference between the Impact Site, Near Control Site and Far Control Site for i) the abundance of lobster and, ii) CPUE.

Influence of water temperature on lobster abundance and CPUE

Water temperature data collected during both survey phases was checked for normality (Shapiro-Wilks test) and then subjected to a two-sample Wilcoxon rank test to determine if there was a statistically significant differences in water temperature between survey phases. Correlations between water temperature and lobster abundance and CPUE were then investigated.

Historical Commercial Landings Data

Commercial landings data (i.e., lobster weight and trap haul data for 2005-2021) was requested from DFO for LFA 35 (grids 15-20) as part of a data sharing agreement established in August 2021 (Appendix C). The FORCE tidal demonstration site is located in grid 17 (Figure 15), and commercial landings data from all grids in LFA 35 were examined for temporal trends in CPUE, including comparisons with CPUE from grid 17. The commercial landings data (Appendix C) only includes lobster that were recruited to the fishery and eligible for commercial harvest (i.e., does not include individuals <82.5 mm carapace length, berried females, of v-notched individuals).
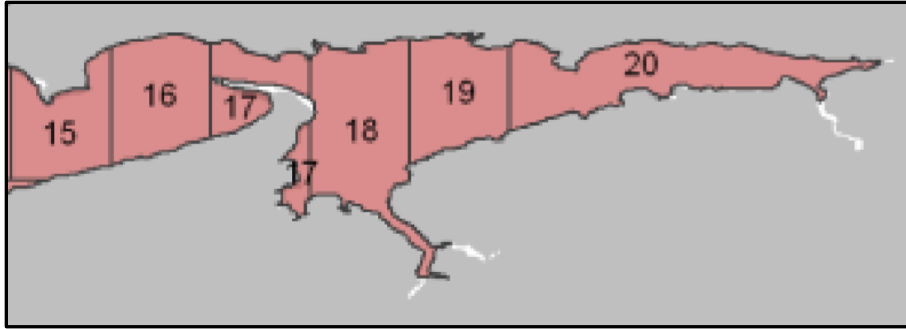
Figure 15: Grids 15-20 for LFA 35; adapted from Coffen-Smout et al. (2013).

Results

Lobster abundance and sex distribution

Over the course of the fall 2021 survey, 582 lobster were captured across all sites; Phase I (n=277), Phase II (n=305) (Table 7). This total includes 40 individuals that were captured from traps deployed at the incorrect deployment coordinates for IMP4 during Phase II of the survey, and that are excluded from analyses below. Males and females comprised 57% and 43% of the total catch, respectively (Table 7; Figure 16). The number of male and female lobster captured for each site is provided in Table 8. Across the survey, one lobster exhibit no external secondary sexual characteristics and could not be assigned to sex, 17 females (~6%) were berried, and 30 females exhibited signs of having recently released their eggs (i.e., 'mossy' condition).

Table 7: Number of lobsters caught over the course of the fall 2021 lobster survey.

	Male	Female	Total
Phase I	165	112	277
Phase II	166	138	305*
Total	331	250	582*

* Includes one lobster that did not display secondary sex characteristics

Table 8: Number of lobsters caught at each site during the fall 2021 lobster survey.

	Male	Female	Total
Impact Site	85	79	165*
Far Control	131	83	214
Near Control	115	88	203

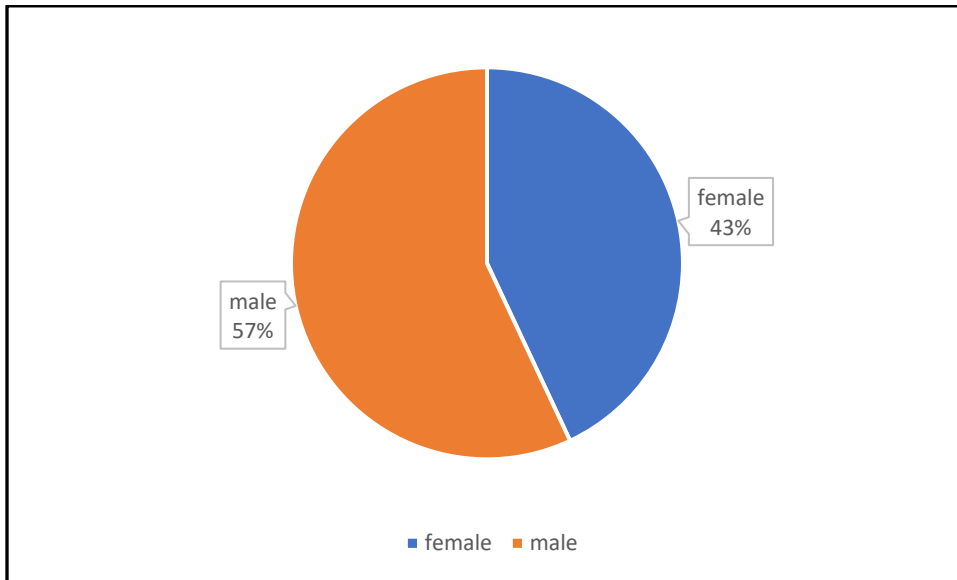* Includes one lobster that showed no secondary sex characteristics

Figure 16: Percent male and female lobster captured during the fall 2021 lobster survey (N=582).

Shell hardness, moult stage and presence of shell disease

Over the course of the fall 2021 lobster survey, 15 individuals had shell hardness stage 3 (i.e., soft, but hardening shells), 65 were in stage 4 (i.e., medium hard shells), and 502 were in stage 5 (i.e., hard shells) (Figure 17). During the survey, pleopods and hemolymph were taken from 145 lobster. The distribution of pleopod stages observed during the survey are shown in Figure 18, and indicated that most of the sampled lobster had experienced a recent moult. The mean °Bx value for sampled lobster was 8.4 (range: 5.6 – 15.4) and supported results of pleopod inspection (Figure 19). Severe shell disease was observed for ~3% (n=18) of the lobsters captured during the fall 2021 survey (Figure 20).
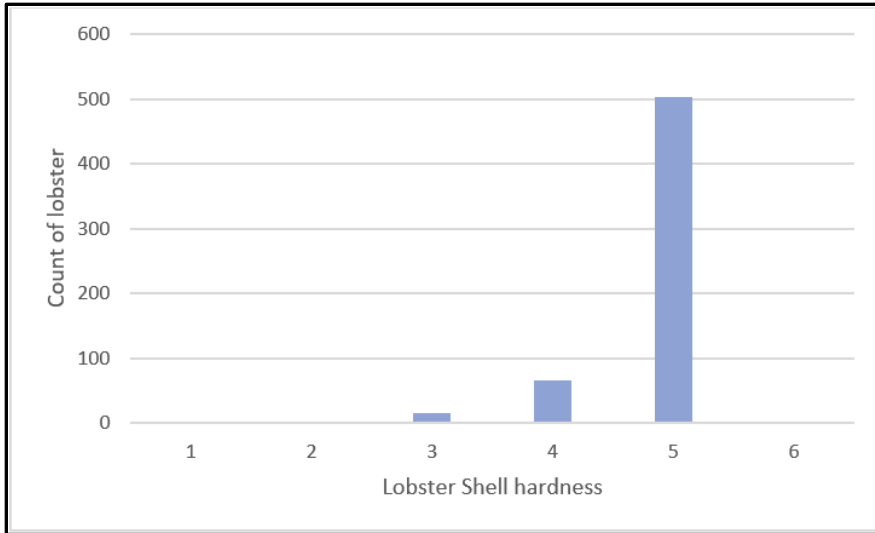
Figure 17: Shell hardness for lobster sampled during the fall 2021 survey (N = 582). See Table 6 for descriptions of shell hardness.
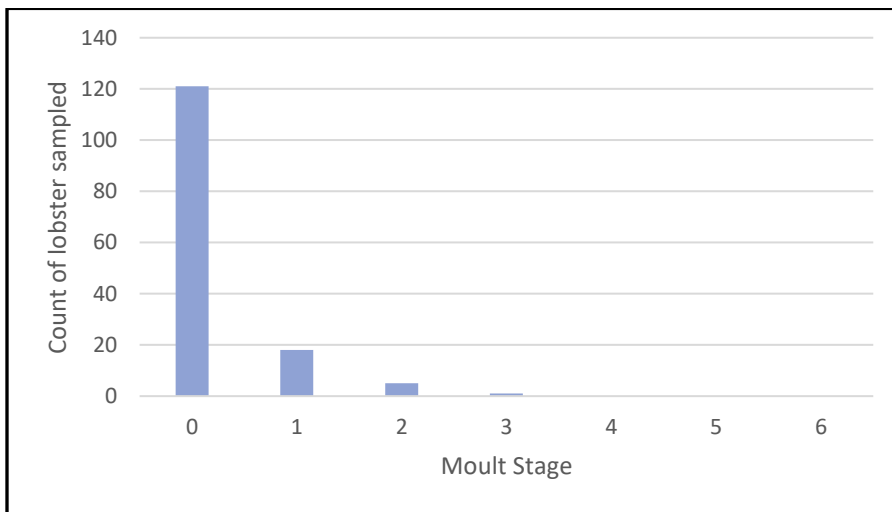

Figure 18: Moult stage determined by pleopod samples for lobster sampled during the fall 2021 survey (n=145) (see Appendix A).
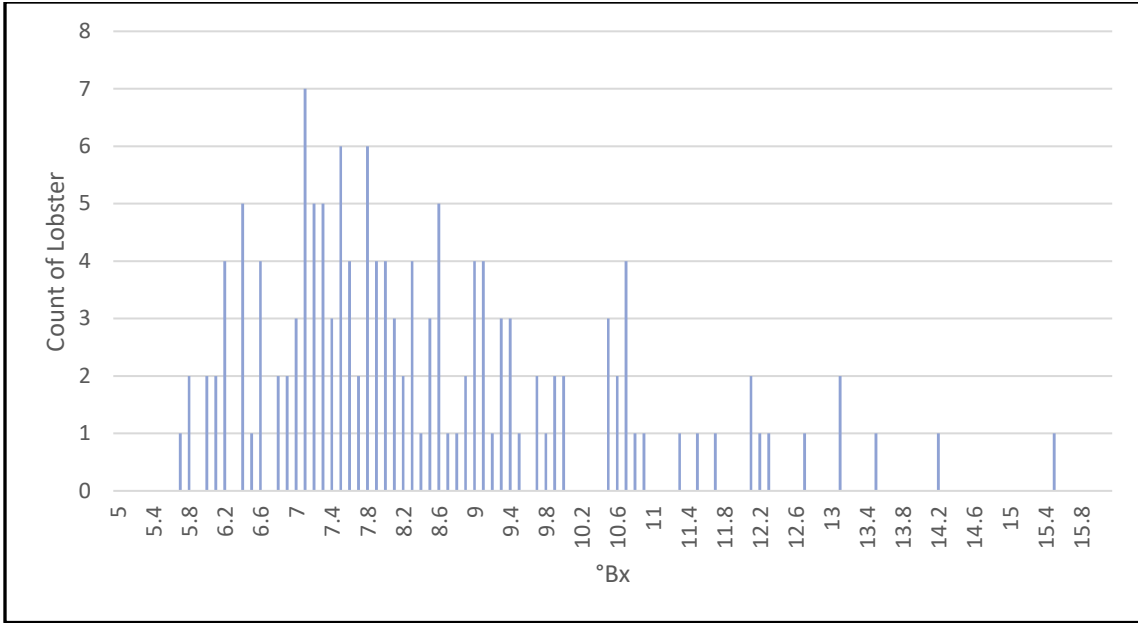
Figure 19: Distribution of °Bx from hemolymph samples taken during the fall 2021 lobster survey (n=145).

Figure 20: Examples of shell disease observed during the fall 2021 lobster survey.

Lobster size distribution and CPUE estimation

Over the course of the fall 2021 lobster survey, the carapace length of lobster ranged from 52mm – 136 mm (Figure 21). The average carapace length during Phase I and Phase II of the survey was 88.28 mm and 94.48 mm, respectively. Across all sites, 68 trap hauls were conducted and the average number of lobsters captured per trap haul during Phase I and Phase II of the survey was 7.69 and 8.25, respectively. On average, fewer lobster were captured at the Impact site (6.20) than either the Near Control site (8.46) or Far control site (8.92) (Table 9). Across all sites, CPUE was 5.72 kg/trap haul. However, this includes all lobster captured during the survey, including those that were < 82.5 mm CL that could not be legally harvested. When undersized lobster, berried females, and v-notched individuals were omitted, CPUE across all sites was 4.74 kg/trap haul. CPUE was lower at the Impact site (4.58 kg/trap haul) than either the Near Control site (6.07 kg/trap haul) or Far Control site (6.02 kg/trap haul) (Table 10).
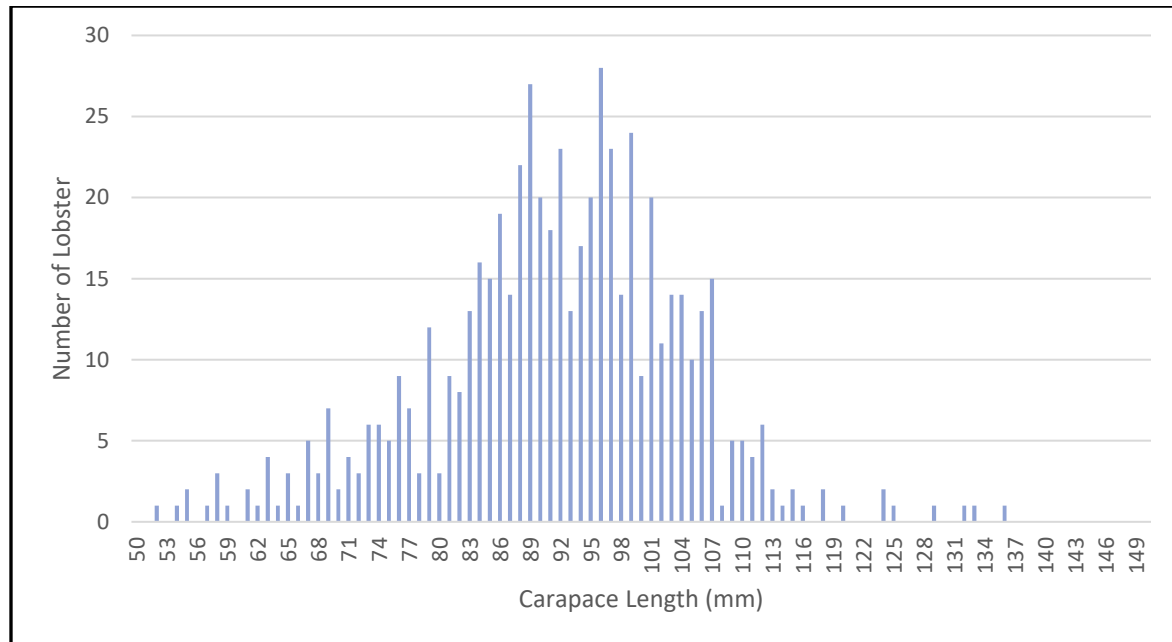

Figure 21: Size distribution of lobster during the fall 2021 lobster survey (N=582).

Table 9: Summary statistics for number of lobsters captured by site during the fall 2021 survey.

Site	Traps Hauled	# Lobster Caught	Mean lobsters/trap haul	SD lobsters/trap haul
Impact	20*	125	6.20	3.69
Far Control	24	214	8.92	4.55
Near Control	24	203	8.46	2.99
All sites	68	542	7.97	3.92

*Excludes data collected from IMP4 deployed at incorrect coordinates during Phase II

Table 10: Summary statistics for weight and CPUE of lobsters captured by site during the fall 2021 survey.

Site	Traps Hauled	Total Weight (lbs)	Total Weight (kg)	Mean CPUE (kg/trap haul)	SD CPUE (kg/trap haul)
Impact	20*	201.72	91.55	4.58	2.74
Far Control	24	318.26	144.36	6.02	2.97
Near Control	24	320.95	145.58	6.07	2.30
All sites	68	841.04	381.49	5.66	2.73

*Excludes data collected from IMP4 deployed at incorrect coordinates during Phase II

Comparison of lobster catchability among survey phases

A Shapiro-Wilks test indicated that lobster abundance during Phase I of the survey was not normally distributed (p=0.017), whereas lobster abundance during Phase II was normally distributed (p=0.528). A two-sample Wilcoxon rank test indicated that the median lobster catch between Phase I and II was not significantly different (p=0.427) (Table 11), and catch data from each phase was subsequently combined for further analyses.

A Shapiro-Wilks test confirmed that lobster CPUE data collected during Phases I and II of the survey were both normally distributed (p > 0.05), and an F-test confirmed equal variance in CPUE between both survey phases (p=0.637). A two-sample t-test confirmed no significant difference in CPUE (Table 12) between Phase I and II (p=0.081) (Table 12), and CPUE data from both survey phases were combined for further analysis.

Table 11: Summary statistics and results of two-sample Wilcoxon rank test for lobster catch data (abundance) collected during the fall 2021 lobster survey excluding data collected at IMP4 during Phase II (deployed outside of Impact Site).

Sample	N	Median	IQR	p-value
Phase I	36	7.00	6.50	0.427
Phase II	32	8.50	4.25	

Table 12: Summary statistics and results of a two-sample t-test for lobster CPUE data collected during the fall 2021 lobster survey excluding data collected at IMP4 during Phase II (deployed outside of Impact Site).

Sample	N	Mean	SD	T-value	DF	p-value
Phase I	36	5.07	2.79	-1.77	66	0.081
Phase II	32	6.22	2.56			

Comparisons of lobster catchability among sites

A one-way ANOVA revealed a marginally significant difference (p=0.052) in the abundance of lobster captured between the sites (Table 13). A Tukey HSD test revealed that this was attributable to more lobster being captured at the Far Control Site relative to the Impact Site; however, this result was also only marginally significant (p=0.055) (Figure 22).

Table 13: Summary statistics from ANOVA and a Tukey HSD test for abundance data between the Impact site, Near Control site and Far Control site.

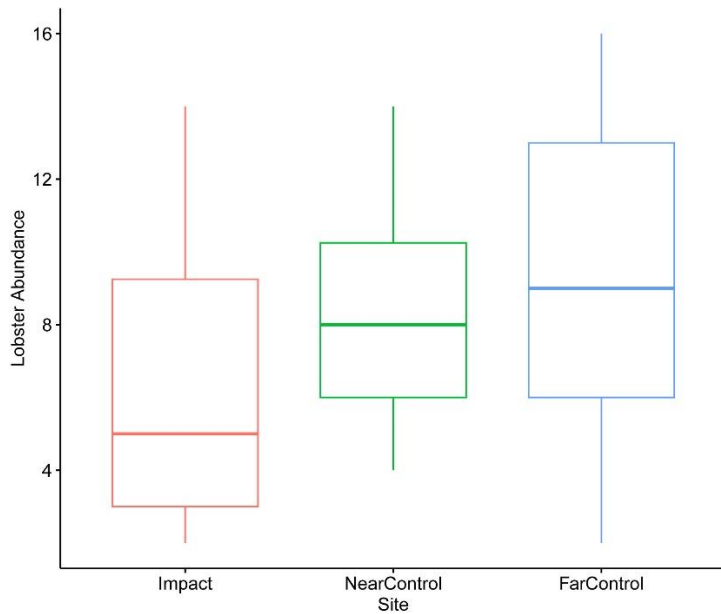| Source	DF	Sum Sq	Mean Sq	F-value	p-value
Site	2	89.9	44.94	3.104	0.052
Residuals	65	941	14.48		

Figure 22: Boxplot displaying the abundance of lobster captured at each site over the course of the fall 2021 lobster survey. A marginally significant difference was observed in the number of lobster captured across sites and was attributed to a greater number of lobster captured at the Far Control site relative to the Impact site.

Although greater CPUE was observed for both the Near Control site and Far Control site relative to the Impact Site (Table 10), a one-way ANOVA revealed this difference to be statistically non-significant (p=0.13) (Table 14). The similarities in CPUE by site are shown in Figure 23.

Table 14: Summary statistics from ANOVA and a Tukey HSD test for CPUE data between the Impact site, Near Control site and Far Control site.

Source	DF	Sum Sq	Mean Sq	F-value	p-value
Site	2	30.3	15.152	2.107	0.13
Residuals	65	467.4	7.191		
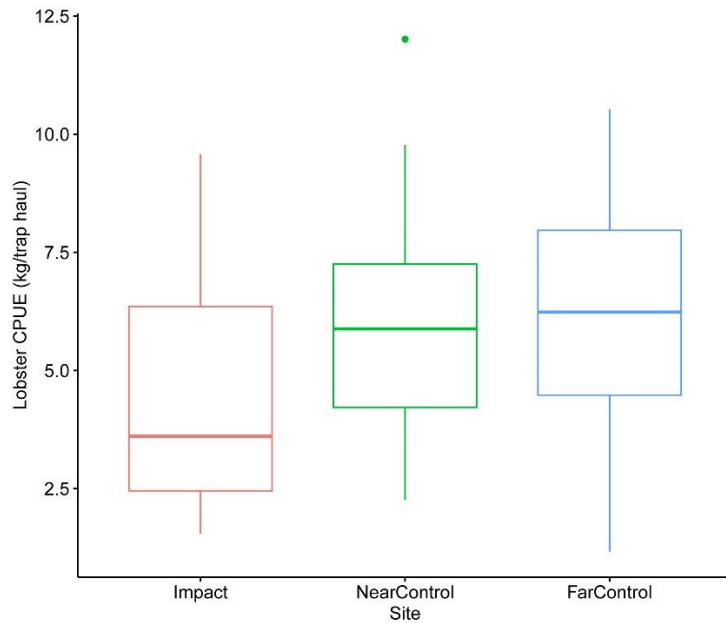
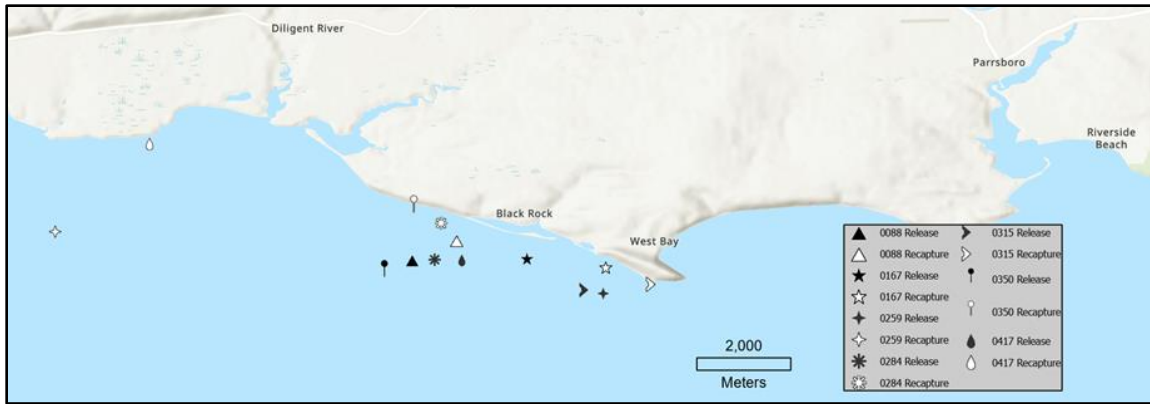Figure 23: Boxplot displaying lobster CPUE at each site over the course of the fall 2021 lobster survey.

Lobster tagging

Over the course of the fall 2021 survey, 477 lobster were tagged and released (Phase I: n=203; Phase II: n=274). Of those tagged lobster, n=24 (i.e., 5% of those tagged) were subsequently captured during the fall 2021 commercial lobster fishery and had their tags returned to FORCE; 20 with accompanying data on coordinates and date of capture. Based on moult stage assessment for tagged individuals it is unlikely that many lobsters lost their tags. However, there is no way to know how many tagged lobsters may have been captured during the fall 2021 commercial fishery but not reported.

The original release and subsequent recapture location for tagged lobster are visualized in Figures 24-26 and data summarized in Table 15. The greatest distance traversed between release and recapture was approximately 10.8 KM during 63 days at large (tag# 0214), while the shortest was 0.42 KM during 30 days at large (tag# 0374) (Table 16). There was no correlation between the amount of time between release and recapture (i.e., 'days at large') and distance between these locations (Pearson correlation = -0.003) (data not shown) and may be due to the relatively small sample size included in the analysis (n=20).

Figure 24: Release and recapture locations for lobsters with tag IDs 0010, 0038, 0060, 0214, 0267, 0374, 0378, and 0502 sampled during 2021 fall survey.

Figure 25: Release and recapture locations for lobsters with tag IDs 0088, 0167, 0259, 0284, 0315, 0350, and 0417 sampled during 2021 fall survey.
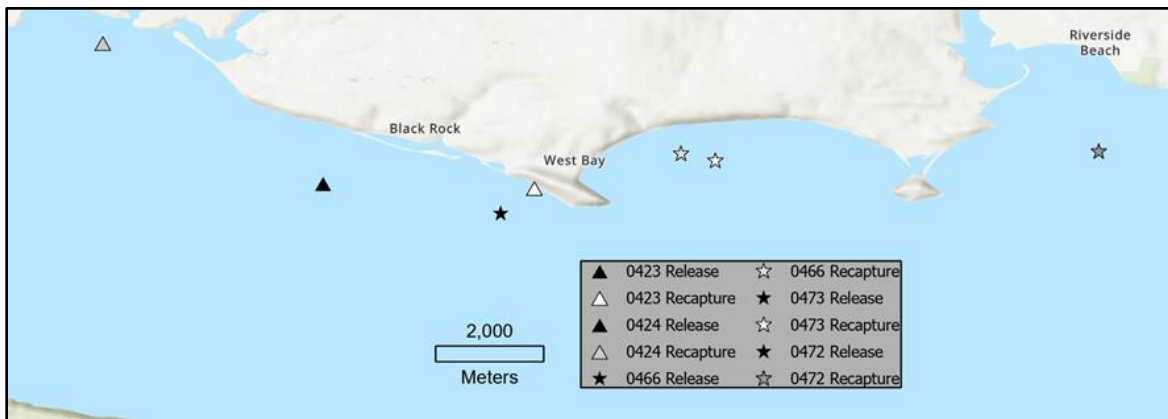

Figure 26: Release and recapture locations for lobsters with tag IDs 0423, 0424, 0466, 0473, and 0472 sampled during 2021 fall survey. Note: the release location for tag IDs 0423 and 0424 are the same, as are those with tag IDs 466, 472, 473.

Table 15: Summary information for tagged lobster (n=20) including date and coordinates for release and recapture during the fall 2021 commercial lobster fishery in LFA 35.

Tag ID	Release Location		Recapture Location		Release Date	Recapture Date	Linear Distance Travelled (m)	Days at Large
	Latitude	Longitude	Latitude	Longitude				
0010	45°21.848	-64°24.276	45°21.766	-64°17.131	08-30-2021	10-29-2021	9,316	60
0038	45°22.192	-64°25.868	45°22.084	-64°22.956	08-30-2021	11-01-2021	3,798	63
0060	45°22.147	-64°25.892	45°21.832	-64°23.507	08-31-2021	10-21-2021	3,158	51
0088	45°22.111	-64°26.288	45°22.334	-64°25.778	08-31-2021	11-24-2021	782	85
0167	45°22.123	-64°26.971	45°22.024	-64°24.067	09-03-2021	10-21-2021	3,789	48
0214	45°21.704	-64°25.673	45°22.194	-64°17.406	09-03-2021	11-05-2021	10,816	63
0259	45°21.728	-64°24.097	45°22.433	-64°30.384	09-28-2021	11-01-2021	8,301	34
0267	45°22.074	-64°25.049	45°21.985	-64°20.589	09-28-2021	10-15-2021	5,821	17
0284	45°22.114	-64°26.031	45°22.530	-64°25.957	09-28-2021	11-01-2021	774	34
0315	45°21.768	-64°24.267	45°21.832	-64°23.499	09-29-2021	10-15-2021	1,009	16
0350	45°21.913	-64°26.607	45°22.650	-64°26.270	09-29-2021	11-28-2021	1,438	61
0374	45°22.053	-64°24.712	45°22.266	-64°24.838	09-29-2021	10-29-2021	423	30
0378	45°21.813	-64°24.219	45°22.172	-64°19.198	09-30-2021	11-01-2021	6,571	33
0417	45°22.108	-64°25.719	45°23.433	-64°29.302	09-30-2021	11-12-2021	5,284	45
0423	45°22.100	-64°26.017	45°22.054	-64°23.910	09-30-2021	11-11-2021	2,746	43
0424	45°22.100	-64°26.017	45°23.498	-64°28.214	09-30-2021	10-16-2021	3,862	16
0466	45°21.801	-64°24.245	45°22.396	-64°22.446	10-01-2021	10-29-2021	2,592	28
0472	45°21.801	-64°24.245	45°22.418	-64°18.279	10-01-2021	10-21-2021	7,864	20
0473	45°21.801	-64°24.245	45°22.326	-64°22.104	10-01-2021	11-11-2021	2,955	42
0502	45°22.118	-64°25.982	45°25.982	-64°25.381	10-01-2021	11-01-2021	7,211	31

Water temperature and associations with lobster abundance and CPUE

We observed a subtle, but statistically significant (p <0.001), decrease in water temperature at the sea floor over the course of the survey (Table 16; Figure 27). During Phase I, the mean water temperature at the sea floor was 17.2°C (range: 16.6°C – 19.6°C); whereas, during Phase II, the mean water temperature at the sea floor was 16.7°C (range: 16.3°C – 17.8°C). This was not unexpected given the time frames for the different phases of the survey (i.e., early vs. late September).

Table 16: Summary statistics for bottom temperature (C°) during both phases of the survey for the Far Control (FC), Near Control (NC) and Impact (IMP) sites.

Water Temperature (°C)	Phase I			Phase II		
	Far Control	Near Control	Impact	Far Control	Near Control	Impact
Mean	17.15	17.18	17.35	16.65	16.73	16.75
Min	16.61	16.63	17.03	16.32	16.39	16.39
Max	19.58	17.77	17.92	17.03	17.15	17.18
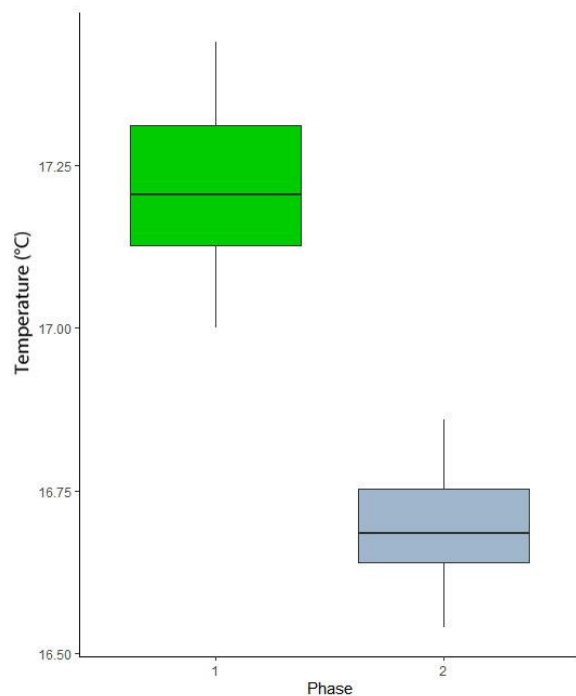
Figure 27: Boxplot displaying water temperature data collected during Phase I and II of the survey. Water temperature was significantly (p < 0.001) lower during Phase II of the survey.

A Shapiro-Wilks test confirmed that water temperature data collected within each phase of the survey was normally distributed. However, when combined these data significantly departed from normality ($p < 0.001$) and had significantly different variance ($p = 0.044$). As such, examination of the influence of temperature on lobster abundance and CPUE was conducted separately for each phase of the survey. During Phase I, we detected a non-significant ($p < 0.05$) and weak negative correlations between water temperature and lobster abundance ($r = -0.193$; $p = 0.259$) and CPUE (kg/haul) ($r = -0.170$; $p = 0.321$). However, during Phase II, we observed a statistically significant but weak negative relationship between water temperature and lobster abundance ($r = -0.362$; $p = 0.042$) and CPUE (kg/haul) ($r = -0.403$; $p = 0.022$).

Historical Commercial Landings Data

We observed a marked increase in commercial landings data (CPUE) for the fall lobster fishery from LFA 35 since at least 2005 (Figure 28). This pattern was observed for commercial landings reported from Grids 15-16 and 18-20, and from Grid 17 where the FORCE tidal demonstration site is located. Interestingly, CPUE from Grid 17 is generally higher than that reported from the remaining grids in LFA 35 (Appendix C). The CPUE data generated from the fall 2021 lobster survey is consistent with the CPUE reported from the other grids in LFA 35.
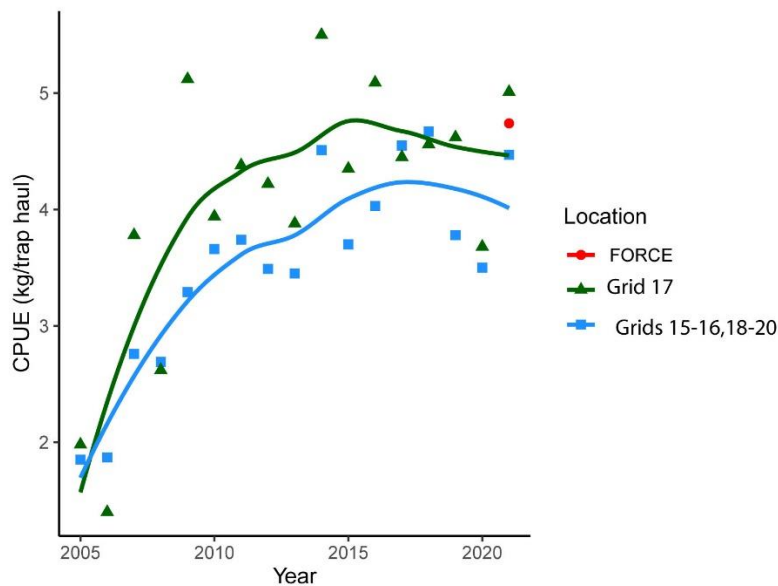
Figure 28: Scatterplot and loess regression of CPUE (kg/trap haul) for the fall commercial lobster fishery (2005-2021) from LFA 35. The CPUE data from the FORCE 2021 lobster survey is consistent with existing commercial landings data collected from Grid 17 and other grids within LFA 35.

Discussion

The objective of FORCE's lobster monitoring program is to determine whether operational tidal stream turbines have an effect on the catchability of lobster at the tidal demonstration site. The fall 2021 lobster survey followed the survey design developed by TriNav Fisheries to provide a statistically robust baseline dataset on lobster catchability in the vicinity of the FORCE tidal demonstration site, and incorporated a tagging component to understand the extent of lobster movement over relatively short time frames (approximately 1-2 months). A total of 582 lobsters were captured, assessed and released over the course of the survey, with 477 being tagged with conventional t-bar tags prior to release. We observed a nearly 1:1 sex ratio and few instances of shell disease (~3%), with 97.4% of assessed lobsters exhibiting moult stages 4 or 5 (i.e., 'hard shells'). Moult stage determination was supported by hemolymph and pleopod assessment which indicated that the majority of lobster were at the intermoult stage and had a high likelihood of retaining their tags. Over the course of the survey, carapace length ranged from 52-136 mm (mean: 92 mm CL), with average size during Phase I (88.28 mm CL) being slightly smaller than that during Phase II (94.48 mm CL). The minimum legal harvest size for lobster in LFA 35 is 82.5 mm CL.

Statistical analyses revealed non-significant differences in lobster abundance (lobster/trap haul) or CPUE (kg/trap haul) between Phase I (early September) and Phase II (late September) of the survey. However, we detected a marginally significant (p=0.052) difference in the abundance of lobster captured among sites, with the Impact Site having on average fewer lobster (6.2 lobster/trap haul) than either the Near Control Site (8.46 lobster/trap haul) or Far Control Site (8.92 lobster/trap haul) (Table 13; Figure 22). While we also observed lower CPUE at the Impact Site (4.58 kg/trap haul) relative to the Near Control site (6.07 kg/trap haul) or Far Control Site (6.02 kg/trap haul), this difference was non-significant (Table 14; Figure 23). Nonetheless, results of this survey reveal a 'high' catchability (i.e., 2.4 – 10.7 kg/trap haul; Table 1) of lobster in the vicinity of the FORCE tidal demonstration site, and is consistent with the findings of the 2017 lobster survey (Nexus Coastal Resource Management Ltd., 2017). Although the exclusion of data from Impact Site 4 (i.e., due to trap deployment at incorrect coordinates) reduced the sample size for comparison among sites, this was mitigated through examination of lobster abundance and CPUE through scaling the data by the number of trap hauls. The Impact Site constitutes the southern portion of the FORCE tidal demonstration site, and is located on an elevated volcanic plateau that is relatively flat with benthic habitat comprised of scoured bedrock (Figure 3, 4) (AECOM, 2009). These conditions may not provide optimal habitat for lobster (preferring habitats with boulders and rocks that provide shelter; Cobb, 1976) and may explain why catch rates and CPUE were lower relative to the control sites.

A slight (~0.5 °C) but statistically significant decrease in water temperature was detected at the seafloor over the course of the survey (Figure 27); consistent with survey time frame (Phase I: early September; Phase II: late September). We detected statistically significant, albeit weak negative correlations between water temperature and both lobster abundance and CPUE

during Phase II of the survey. However, we cannot draw any conclusions about the influence of water temperature on lobster catchability due to the protracted time frame over which data was collected during Phase II of the survey (September 27 – October 1). A considerably longer time series, including continuous data collection to increase sample sizes and improve statistical power, would be required to conduct a more meaningful analysis. Unfortunately, the high tidal flow rates and turbulent conditions of the Minas Passage impose operational limitations on the implementation of the lobster survey that necessitate trap deployments and recoveries around neap tides to increase operational windows around 'slack water' conditions (i.e., the period of transition from flood to ebb tidal phase). In a more benign marine environment, it would be possible to extend the duration of the survey, deploy all 18 trap simultaneously, maintain 24-hour soak periods for data collection, and complete the survey in a single phase. This is simply not feasible in Minas Passage, and the advice of local lobster fishers proved invaluable in fine-tuning the approach to be taken during this survey. While the 2017 lobster survey was able to recover and deploy eight lobster traps per day (Nexus Coastal Resource Management Ltd., 2017), this survey was only able to increase that to nine traps per day.

Approximately 5% of tagged lobsters were recaptured and reported by local fishers during the fall 2021 commercial lobster fishing season and provided important information about the short term (approximately 1-2 months) movements of lobster in Minas Passage. Lobster movement was highly variable (0.42-10.8 KM; Table 15), and there was no correlation between the number of days an individual was at large and the distance travelled, and may be due to the relatively small sample size (n=20).

The marked increase in commercial landings data provided by Fisheries and Oceans Canada for the fall lobster fishery in LFA 35 for 2005-2021, including for grid 17 where the FORCE tidal demonstration site is located (Figure 28), is consistent with a northward shift in the distribution of lobster associated with climate change. Sea surface temperatures in the Gulf of Maine have increased faster than 99% of the global ocean, and is related to a northward shift in the Gulf Stream and changes to the global ocean circulation patterns (Pershing et al. 2015). Increasing water temperature can impact lobster movement, susceptibility to disease, survival and recruitment to the fishery (Wahle et al. 2009; Mills et al. 2013). It is possible that a combination of these and other factors are contributing to the increased abundance of lobster being captured by the fall commercial lobster fishery in LFA 35.

Acknowledgements

FORCE is located in Mi'kma'ki, the ancestral and unceded territory of the Mi'kmaq, covered by the "Treaties of Peace and Friendship" which Mi'kmaq and Wolastoqiyik (Maliseet) People first signed with the British Crown in 1725. Mi'kmaw Peoples have lived on and cared for this land for over 13,500 years.

We would also like to acknowledge Bliss Walton, a local lobster harvester who devoted his time and local ecological knowledge to this project. Local ecological knowledge includes perceptions about an environment formed by consistent interaction with an environment, and cultural knowledge about an environment passed down generations. Fish harvesters like Mr. Walton are stewards of their resource, and their contributions to surveys like this provide a perspective that is invaluable to research. We would like to thank Mr. Walton for making marine operations a safe and efficient experience, and for bringing a positive outlook onboard the vessel each day.

We would also like to thank Mike Huntley and the crew of the Nova Endeavor for their assistance in executing the survey, Jason Clarkson for assistance with operation planning and survey execution, and FORCE staff for survey coordination.

References

AECOM. 2009. Environmental assessment registration document – Fundy tidal energy demonstration project. Volume 1: environmental assessment. Fundy Ocean Research Centre for Energy Pro. # 107405.

Aiken, D. E. (1973). Proecdysis, Setal Development, and Molt Prediction in the American Lobster *Homarus americanus.* Journal of the Fisheries Research Board of Canada, 30(9), 1337–1344. Doi:10.1139/f73-214

Ainsworth, C.H. (2011) Quantifying species abundance trends in the Northern Gulf of California using local ecological knowledge. *Marine and Coastal Fisheries*, 3(1), 190-218. Doi: 10.1080/19425120.2010.549047

Annis, E. R. (2005). Temperature effects on the vertical distribution of lobster postlarvae *(Homarus americanus*). *Limnology and Oceanography*, 50, 1972–1982.

Appelman, M. (2015). A Catch Per Unit Effort (CPUE) Spatial Metric with Respect to the Western North Atlantic Pelagic Longline Fishery. Master's thesis. Nova Southeastern University. Retrieved from NSUWorks, Oceanographic Center.

Barret, L., Miron, G., Ouellet, P., & Tremblay R. (2017). Settlement behaviour of American lobster (*Homarus Americanus)*: effect of female origin and developmental temperature. *Fisheries Oceanography*, 26(1), 69-82.

Battison, A. L. (2018). Use of the Brix value with cuticle indices to describe haemolymph biochemistry parameters in Homarus americanus H. Milne Edwards, 1837 (Decapoda: Malacostraca: Nephropidae). Journal of Crustacean Biology, Volume 38, Issue 5, September 2018, Pages 625–634, https://academic.oup.com/jcb/article/38/5/625/5087934

Boudreau, S. A., & Worm, B. (2010). Top-down control of lobster in the Gulf of Maine: insights from local ecological knowledge and research surveys. *Marine Ecology Progress Series,* 403, 181-191.

Brennan, C. E., Blanchard, H. & Fennel, K. (2016). Putting Temperature and Oxygen Thresholds of Marine Animals in Context of Environmental Change: A Regional Perspective for the Scotian Shelf and Gulf of St. Lawrence*. PLOS ONE,* 11(12), 1-27 https://journals.plos.org/plosone/article?id=10.1371/journal.pone.0167411

Brewin, R. J. W., Smale, D. A., Moore, P. J., Dall'Olmo, G., Miller, P. I., Taylor, B. H., Smyth, T. J., 38tlantic, J. R., & Yang, M. (2018). Evaluating operational AVHRR sea surface temperature data at the coastline using benthic temperature loggers. *Remote Sensing,* 10, 1-23. https://www.mdpi.com/2072-4292/10/6/925

Bundy, A., Chuenpagdee, R., Boldt, J. L., de Fatima Borges, M., Camara, M. L. Coll, M., Diallo, I., Fox, C., Fulton, E. A., Gazihan, A., Jarre, A., Jouffre, D., Kneisner, K., M., Knight, B., Link, J., Matiku, P. P., Masski, H., Moutopoulos, D. K., Piroddi, C., Raid, T., Sobrino, I., Tam, J., Thiao, D., Torres, M. A., Tsagarakis, K., van der Meeren, G.I, & Shin, Y. (2017). Strong fisheries management and governance positively impact ecosystem status. *Fish and Fisheries,* 18, 412-439.

Caputi, N., Brown, R. S., & Chubb, C.F. (1995). Regional prediction of the western rock lobster, *Panulirus Cygnus*, commercial catch in Western Australia. *Crustaceana,* 68(2), 245-256.

CEF Consultants Ltd. (2010). Fundy Tidal Energy Demonstration Project Lobster Catch Monitoring. FORCE.

CEF Consultants (2011) Fundy Tidal Energy Demonstration Project Lobster Catch Monitoring: Summary of Results from Three Surveys with Recommendations for a Revised Survey Design. FORCE.

Chang, Y., Sun, C., Chen, Y., Zhang, Y., & Yeh S. (2011). Incorporating climate changes into population modelling: an individual-based modelling approach for lobster. *Canadian Journal of Fisheries and Aquatic Sciences,* 68, 122-136. https://cdnsciencepub.com/doi/abs/10.1139/F10-148

Childress, J. L., Shearman, R. K., & Harte, M. (2010). Evaluation of 39tlantic39 crab pots as platforms of opportunity for ocean-observing research. Presented at Oceans 2010, Seattle, WA, USA. Doi: 10.1109/OCEANS.2010.5664269

Cigliano, J. A., Meyer, R., Ballard, H. L. Frietag, A., Phillips, T. B., & Wasser, A. (2015). Making marine and coastal citizen science matter. *Ocean and Coastal Management*, 115, 77-87.

Cobb, J.S. 1976. The American lobster: the biology of Homarus americanus. University of Rhode Island, Marine Technical Report 49.

Cobb, J. S., & Wahle, R. A. (1994). Early Life History and Recruitment Processes of Clawed Lobsters. *Crustaceana,* 67(1), 1-25.

Coffen-Smout, C., D. Shervill, D. Sam, C. Denton, and J. Tremblay. 2013. Mapping Inshore Lobster Landings and Fishing Effort on a Maritimes Region Modified Grid System. Can. Tech. Rep. Fish. Aquat. Sci. 3024; 33 pp.

Comeau, Michel; Mallet, Manon. (2003). The effect of timing of tagging on streamer-tag recapture rates for American lobster (Homarus americanus). The Free Library (July, 1), https://www.thefreelibrary.com/The%20effect%20of%20timing%20of%20tagging%20on%20streamer-tag%20recapture%20rates%20for...-a0107524523

Cooke, S. J., Wesch, S., Donaldson, L. A., Wilson, A. D. M., & Haddaway, N. R. (2017). A call for evidence-based conservation and management of fisheries and aquatic resources. *Fisheries,*42(3), 143-149.

DFO (Fisheries and Oceans Canada). 2016. Review of Environmental Effects Monitoring Program for the Fundy Tidal Energy Project. DFO Can. Sci. Advis. Sec. Sci. Resp. 2016/022.

DFO. 2019a. At-sea sampling protocol for American Lobster. Lobster Unit, Population Ecology Division Department of Fisheries and Oceans.

DFO. 2019b. Assessment of Lobster (*Homarus Americanus*) in Lobster Fishing Areas 27-32. DFO Canadian Science Advisory Secretariat Science Advisory Report 2019

DFO. 2021. Science Advisory Report 2021/020 Assessment of American Lobster (Homarus americanus) in Lobster Fishing Areas 35–38. Retrieved January 2 from dfo-mpo.gc.ca/csas-sccs/Publications/SAR-AS/2021/2021_020-eng.html

Factor, J. R. (Ed). (1995). Biology of the Lobster *Homarus americanus.* Academic Press Inc.

Farr, E. R., Stoll, J. S., & Beitl, C. M. (2018). Effects of fisheries management on local ecological knowledge. *Ecology and Society,* 23(3), 1-9.

FORCE. (2021) Operational safety plan: Lobster survey Minas Basin

FORCE. (2019). Renewable and predictable: Our purpose. Retrieved January 17, 2022 from fundyforce.ca/about-us

Freer, J. J., Partridge, J. C., Tarling, G. A., Collincs, M. J. (2018). Predicting ecological responses in a changing ocean: the effects of cimate uncertainty. *Marine Biology,* 165(7), 1-19.

FSRS (2022). About the FSRS. Retrieved January 17, 2022 from https://fsrsns.ca/objectives//

Fujitani, M., McFall, A., Randler, C., & Arlinghaus, R. (2017). Participatory adaptive management leads to environmental learning outcomes extending beyond the sphere of science. *Science Advances,* 3, 1-11.

Haakonsen, H. O.; Anoruo, A. O. (1994). Tagging and migration of the American lobster Homarus americanus. Reviews in Fisheries Science, 2(1), 79–93. https://www.tandfonline.com/doi/abs/10.1080/10641269409388553

Jury, S. H., & Watson, W. H. (2013). Seasonal and sexual differences in the thermal preferences and movements of American lobsters. *Journal of Fisheries and Aquatic Sciences,* 70(11), 1650-1657. https://doi-org.qe2a-proxy.mun.ca/10.1139/cjfas-2013-0061

Lavalli, K.L., & Lawton P. (1996). Historical Review of Lobster Life History Terminology and Proposed Modifications to Current Schemes. *Crustaceana,* 69, 594-609.

Le Bris, A., Mills, K. E., Wahle, R. A., Chen, Y., Alexander, M. A., Allyn, A. J., Shuetz, J.G., Scott, J.D. & Pershing, A. J. (2017). Climate vulnerability and resilience in the most valuable North American fishery. *PNAS,* 115(8), 1831-1836.

Li, B., Cao, J., Chang, J., Wilson, C., & Chen, Y. (2015). Evaluation of effectiveness of fixed-station sampling for monitoring American lobster settlement. *North American Journal of Fisheries Management,* 35, 942–957.
https://www.tandfonline.com/doi/abs/10.1080/02755947.2015.1074961

Li, B., Tanaka, K.R., Chen, Y., Brady, D. C., & Thomas, A.C. (2017). Assessing the quality of bottom water temperatures from the Finite-Volume Community Ocean Model (FVCOM) in the Northwest Atlantic Shelf region. *Journal of Marine Systems,* 173, 21–30.

Lillis, A., & Snelgrove, P. V. R. (2010). Near-bottom hydrodynamic effects on postlarval settlement in the American lobster *Homarus americanus. Marine Ecology Progress Series,* 401, 161-172.

MacDonald, C. and Scott, S. 2000. Lobster v-notch conservation program for LFA 32 and 31B, Fishermen and Scientists Research Society, 19 p.

Medeiros, M. C., Barboza, R. R. D., Martel, G. & da Silva Mourao, J (2018). Combining local fishers' and scientific ecological knowledge: Implications for comanagement. Ocean and Coastal Management, 158, 1-10.

Medley, A. H., & Ninnes, C. H. (1997). A recruitment index and population model for spiny lobster (*Panulirus argus)* using catch and effort data. *Canadian Journal of Fisheries and Aquatic Sciences,* 54, 1414-1421.

Mills, K.E., A.J. Pershing, C.J. Brown, Y. Chen, F.-S. Chiang, D.S. Holland, S. Lehuta, J.A. Nye, J.C. Sun, A.C. Thomas, and R.A. Wahle. 2013. Fisheries management in a changing climate: Lessons from the 2012 ocean heat wave in the Northwest Atlantic. Oceanography 26(2):191–195, http://dx.doi.org/10.5670/oceanog.2013.27.

Morrison, K., Broome, J., and Redden, A.M. (2014). Minas Passage Lobster Tracking Study. Acadia University. FORCE.

NEXUS Coastal Resource Management Ltd. (2017). Lobster Catchability Study Report. FORCE

Nielsen, T. V., & McGaw, I. J. (2016). Behavioural thermoregulation and trade-offs in juvenile

NOAA (2018). Lobster shell disease. Retrieved January 19, 2022, from
https://www.fisheries.noaa.gov/science-blog/lobster-shell-disease

Pershing, A. J., Alexander, M. A., Christina, M., Kerr, L. A., Bris, A. Le, Mills, K. E., Nye, J. A., Record, N. R., Scannell, H. A., Scott, D., Sherwood, G. D., & Thomas, A. C. (2015). Slow

adaptation in the face of rapid warming leads to collapse of the Gulf of Maine cod fishery. *Science*, *October*, 1–8.

Phillips, B. F. (1986). Prediction of commercial catches of the western rock lobster *Panulirus Cygnus. Canadian Journal of Fisheries and Aquatic Sciences,* 43, 2126-2130.

Quackenbush, L. S. (1994). Lobster reproduction: a review. *Crustaceana,* 67(1), 82-94.

Quinn, B. K. (20167). Threshold temperatures for performance and survival of American lobster larvae : A review of current knowledge and implications to modeling impacts of climate change. *Fisheries Research*, 186, 383-396. http://dx.doi.org/10.1016/j.fishres.2016.09.022.

R Development Core Team (2021) R: A Language and Environment for Statistical Computing. R Foundation for Statistical Computing, Vienna, Austria, ISBN 3-9000051-07-0, URL http://www.R-project.org.

Roman, S., Jacobson, N., & Cadrin, S. X. (2011). Assessing the Reliability of Fisher Self-Sampling Programs. *North American Journal of Fisheries Management,* 31, 165–175., 2011. https://www.tandfonline.com/doi/abs/10.1080/02755947.2011.562798

Serdynska, A., and Coffen-Smout, S. (2014). Mapping Inshore Lobster Landings and Fishing Effort on a Maritimes Region Statistical Grid. Fisheries and Oceans Canada Maritimes Region.

Serdynska, A., & Coffen-Smout, S. (2017). Mapping inshore lobster landings and fishing effort on a Maritimes Regional statistical grid (2012-2014). Dartmouth, NS: Fisheries and Oceans Canada.

Shearman, R. K., & Childress, J. L. (2012). Deploying dissolved oxygen sensors on crab pots for ocean observations. *Sea Technology*, 53(6), 25-30.

Sobral, A., La Torre-Cuadros, M., Alves, R. R. N. & Albuquerque, U. P. (2017). Conservation efforts based on local ecological 42tlantic42 : The role of social variables in identifying environmental indicators. *Ecological Indicators,* 81, 171-181

Starr, P. J., & Vignaux, M. (1997). Comparison of data from voluntary logbook and research catch-sampling programmes in the New Zealand lobster fishery. *Marine and Freshwater Research*, 48, 1075-1080

Starr, P. (2010). Fisher-Collected Sampling Data: Lessons from the New Zealand Experience. *Marine and Coastal Fisheries*, 2(1), 47-59, DOI: 10.1577/C08-030.1

Tremblay, M. J., Macdonald C., and Claytor, R. R. (2009) Indicators of abundance and spatial distribution of lobsters (Homarus americanus) from standard traps, New Zealand Journal of Marine and Freshwater Research, 43:1, 387-399, DOI: 10.1080/00288330909510008

This Fish (2021). Fishery Profile: Bay of Fundy Nova Scotia Lobster Fishing Area 35. Retrieved Jan 2 from https://thisfish.info/fishery/43tlantic-lobster-canada-lfa35

Van-Sander, S., Clifton, J., & Harvey, E. (2016). Can citizen science work? Perceptions of the role and utility of citizen science in a marine policy and management context. *Marine Policy,* 72, 82-93.

Waddy, S. L., Feindel, N. Hamilton-Gibson, N., Aiken, D. E., Merrit, V., & Leavitt, N. (2017). Reproductive cycles and mating capacity in male American Lobsters (*Homarus americanus). Fisheries Research,* 186, 358-366. https://www.sciencedirect.com/science/article/abs/pii/S0165783616303277?via%3Dihub

Wahle, R. A., Battison, A., Bernatchez, L., Boudreau, S., Castro, K., Grabowski, J. H., Greenwood, C. G., Rochette, R., & Wilson, J. (2013). The American lobster in a changing ecosystem: a US-Canada Science Symposium. *Canadian Journal of Fisheries and Aquatic Science,* 70, 1571-1575. https://cdnsciencepub.com/doi/10.1139/cjfas-2013-0465

Wahle, R. A., Cobb, J. S., Incze, L. S., Lawton, P. Gibson, M., Glenn, R., Wilson, C., & Tremblay, J. (2010). The American lobster settlement index at 20 years: looking back – looking ahead. *Journal of the Marine Biological Association of India,* 52, 180-188.

Wahle, R. A., Dellinger, L., Olszewski, S., & Jekielek, P. (2015). American lobster nurseries of southern New England receding in the face of climate change. *ICES Journal of Marine Science*, 72(Supplement 1), i69-i78. https://academic.oup.com/icesjms/article/72/suppl_1/i69/622623

Wahle, R. A., & Incze, L. S. (1997). Pre- and post-settlement processes in recruitment of the American Lobster. *Journal of Experimental Marine Biology and Ecology,* 217, 179-207.

Wahle, R. A., Incze, L. S., & Fogarty, M. J. (2004). First projections of American lobster fishery recruitment using a settlement index and variable growth. *Bulletin of Marine Science,* 74(1), 101–114.

Watson, F. L., Miller, R. J., & Stewart, S. A. Spatial and temporal variation in size at maturity for female American lobster in Nova Scotia. *Canadian Journal of Fisheries and Aquatic Sciences,* 70, 1240–1251. Dxdoi.org/10.1139/cjfas-2012-0480

Xu C., & Scneider, D. C. (2012). Efficacy of conservation measures for the A,erican lobster: reproduction value as a criterion. *ICES Journal of Marine Science,* 69(10), 1831-1839. https://academic.oup.com/icesjms/article/69/10/1831/622515

Zhang, Y., Chen, Y., & Wilson, C. (2011). Developing and evaluating harvest control rules with different biological reference points for the American lobster (*Homarus americanus*) fishery in the Gulf of Maine. *ICES Journal of Marine Science,* 68(7): 1511-1524. https://academic.oup.com/icesjms/article/68/7/1511/656815

Appendices

Appendix A: Moult Staging in American Lobster

A brix refractometer is used to quantify solute in liquids, which is primarily protein in lobster hemolymph (Battison 2018). Degrees brix (°Bx) can be used as an indicator of pre-moult, inter-moult and post-moult stages of the lobster moult cycle (Battison 2018). Less than 7 °Bx could indicate a lobster is recovering from moult or is suffering from disease or injury (Battison 2018). An intermoult lobster provides hemolymph with greater than 8 °Bx (Battison 2018). A lobster with near 16 °Bx is actively preparing to moult (Battison 2018).

Pleopod samples can be taken and examined at 40x magnification using a compound light microscope to determine whether a lobster is preparing to moult or is in the intermoult stage (Aiken 1973). The figure below shows indicators a technician would observe to establish whether a lobster is preparing to moult. The table describes moult and pleopod stages shown in the figure. Pleopod stage 0 is seen in intermoult lobster that are not preparing to moult (Aiken 1973). Pleopod stages 1 through 2.5 are described as moult stage D0, where it will still be several months before the lobster moults (Aiken 1973). Lobster with pleopods stages 4.5 to 5 are in moult stage D2 and will moult in under two weeks (Aiken 1973). Lobster with pleopods in stage 5.5 or moult stage D3 will moult within several days (Aiken 1973).
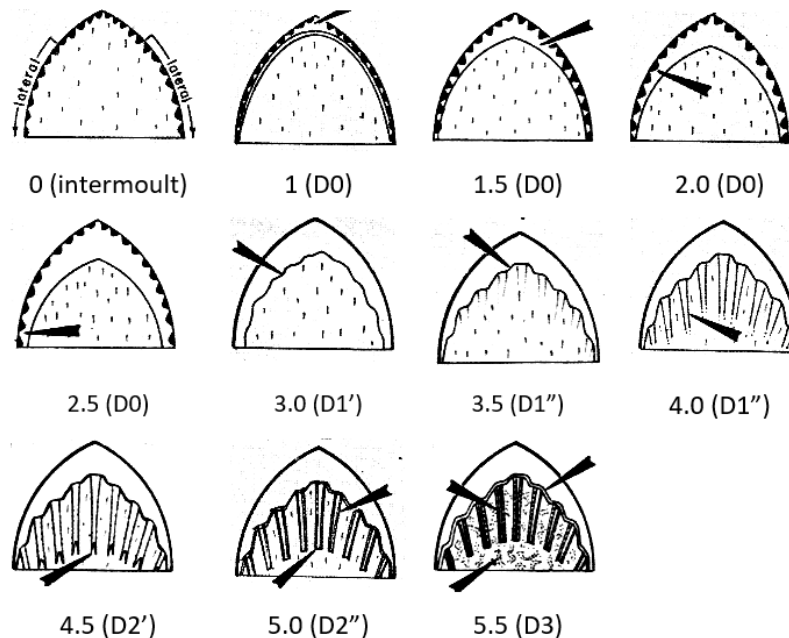
Pleopod moult stages as observed through a compound light microscope. Modified from Aiken (1973).

Moult and pleopod staging in American lobster. Modified from Aiken (1973).

Moult Stage	Pleopod Stage	Description
C4	0	Epidermis closely applied to cuticular nodes at tip of pleopod; no amber zone or epidermal retraction at pleopod tip
D0	1	First indication of apolysis - amber or double-bordered region forms at the pleopod tip. Chromatophores often show signs of reorganization but there is no epidermal retraction from the cuticle
D0	1.5	Epidermis retracting from terminal cuticular nodes; may have double-bordered appearance
D0	2.0	Epidermal line clearly formed and retracting from lateral cuticular nodes
D0	2.5	5 Maximum epidermal retraction - not touching any lateral cuticular nodes
D1'	3.0	Invagination papillae form at site of future setae; epidermis becomes scalloped
D1"	3.5	Invagination papillae clearly formed but shafts of new setae not well defined
D1"'	4.0	Shafts of developing setae visible but proximal ends not clearly defined. Shafts now invaginated to maximum length.
D2'	4.5	Shafts visible full length but proximal ends are bifurcate instead of blunt (Fig. 4N, O). Barbules becoming visible on setal shafts.
D2"	5.0	0 Shafts of developing setae thick, proximal ends blunt
D3	5.5	Shafts of setae very thick and dark, proximal ends blunt. Classify as Ds" if folds or ripples are visible in cuticle on upper surface of pleopod

Appendix B: Sample Data Sheet

FORCE FALL LOBSTER SURVEY 2021

Date	
Lat	
Long	
Trap ID	
Temp logger	
Sampler	
Release coordinates	

Length	Sex	Clutch stage	Clutch %	Shell Hardness	Condition	V-notch	Tag no.	Moult Stage	Blood Protein	Comments

Appendix C: DFO Historic Landings Data

CPUE calculated as weight (lbs) per trap haul and weight (kg) per trap haul for LFA 35 grids 15, 16, 18, 19, and 20 in the Minas Basin during the fall fishing season from 2005 to 2021. N is the number of trips sampled each year used to calculate CPUE.

Year	N	Weight (kg)	Number of trap hauls	CPUE (kg/trap haul)
2005	192	35,122.00	18,970	1.85
2006	316	59,510.88	31,891	1.87
2007	469	134,628.80	48,851	2.76
2008	476	154,862.81	57,661	2.69
2009	530	165,584.13	50,310	3.29
2010	557	191,163.27	52,222	3.66
2011	642	195,429.93	52,314	3.74
2012	575	192,284.35	55,069	3.49
2013	430	144,655.78	41,986	3.45
2014	488	216,613.15	48,016	4.51
2015	300	143,446.71	38,728	3.70
2016	418	176,088.62	43,693	4.03
2017	315	167,320.18	36,810	4.55
2018	228	116,031.97	24,854	4.67
2019	265	104,219.50	27,572	3.78
2020	252	99,543.31	28,412	3.50
2021	151	82,956.92	18,579	4.47

CPUE calculated as weight (lbs) per trap haul and weight (kg) per trap haul for LFA 35 grid 17 in the Minas Basin during the fall fishing season from 2005 to 2021. N is the number of trips sampled each year used to calculate CPUE.

Year	N	Weight (kg)	Number of Trap hauls	CPUE (kg/trap haul)
2005	5	467.12	236	1.98
2006	49	4,150.11	2,965	1.40
2007	42	16,217.69	4,294	3.78
2008	108	25,643.99	9,789	2.62
2009	99	49,231.29	9,617	5.12
2010	85	23,793.65	6,044	3.94
2011	139	50,917.91	11,627	4.38
2012	164	75,192.74	17,810	4.22
2013	112	42,834.47	11,027	3.88
2014	149	76,883.90	13,972	5.50
2015	72	46,877.10	10,776	4.35
2016	120	58,564.63	11,507	5.09
2017	73	25,013.61	5,623	4.45
2018	67	30,226.76	6,623	4.56
2019	88	44,154.20	9,552	4.62
2020	82	38,272.56	10,388	3.68
2021	49	36,947.85	7,377	5.01

Appendix III

Brian Gavin Sanderson [1,*] , **Charles William Bangley** [2] , **Louise Patricia McGarry** [3] and **Daniel James Hasselman** [3,*]

1   Acadia Centre for Estuarine Research, Acadia University, Wolfville, NS B4P 2R6, Canada
2   Department of Biology, Dalhousie University, Halifax, NS B3H 4R2, Canada; charles.bangley@dal.ca
3   Fundy Ocean Research Center for Energy, Halifax, NS B3J 3N5, Canada; louise.p.mcgarry@gmail.com
*   Correspondence: bxs@bellaliant.net (B.G.S.); dan.hasselman@fundyforce.ca (D.J.H.);
     Tel.: +1-902-697-2592 (B.G.S.); +1-902-406-1166 (ext. 7) (D.J.H.)

Abstract: Semidiurnal tidal currents can exceed 5 ms^{-1} in Minas Passage, Bay of Fundy, where a tidal energy demonstration area has been designated to generate electricity using marine hydrokinetic turbines. The risk of harmful fish–turbine interaction cannot be dismissed for either migratory or local fish populations. Individuals belonging to several fish populations were acoustically tagged and monitored by using acoustic receivers moored within the Minas Passage. Detection efficiency ρ is required as the first step to estimate the probability of fish–turbine encounter. Moored Innovasea HR2 receivers and high-residency (HR) tags were used to obtain detection efficiency ρ as a function of range and current speed, for near-seafloor signal paths within the tidal energy development area. Strong tidal currents moved moorings, so HR tag signals and their reflections from the sea surface were used to measure ranges from tags to receivers. HR2 self-signals that reflected off the sea surface showed which moorings were displaced to lower and higher levels on the seafloor. Some of the range testing paths had anomalously low ρ, which might be attributed to variable bathymetry blocking the line-of-sight signal path. Clear and blocked signal paths accord with mooring levels. The application of ρ is demonstrated for the calculation of abundance, effective detection range, and detection-positive intervals. High-residency signals were better detected than pulse position modulation (PPM) signals. Providing that the presently obtained ρ applies to tagged fish that swim higher in the water column, there is a reasonable prospect that probability of fish–turbine encounter can be estimated by monitoring fish that carry HR tags.

Keywords: detection efficiency; effective detection range; abundance; tidal energy; MHK turbine; fish–turbine encounter

1. Introduction

The ocean is vast and largely opaque to human senses. Acoustic telemetry tags have been used in many ways to study the ecology and behavior of fish. Strategically placed arrays of acoustic receivers can be used to observe and quantify migration [1–3] or demonstrate seasonal presence [4] and indicate species' residency patterns [5,6]. With a sufficient density of acoustic receivers, localization can be achieved so that fish can be tracked with high resolution and their behavior studied within a small area [7–9]. Detection range experiments [10–12] quantify how efficiently acoustic tag transmissions are detected as a function of range and environmental conditions, and such knowledge is fundamental for designing experiments to achieve all of the above.

The detection of an acoustic signal from a tagged fish indicates presence in some sense but has restricted value as an ecological variable. Ecology is usually measured and modeled in terms of variables such as abundance, sometimes quantified in terms of the number of individuals per unit area at some location [13]. The probability of detecting known signal

transmissions as a function of range enables the effective detection area to be defined, and so detection range experiments are, therefore, fundamental for converting detected signals from acoustically tagged fish into metrics for ecological interpretation.

Our motivation for undertaking detection range measurements is closely related to the quantification of abundance. Specifically, our ultimate goal is to quantify the probability that a fish belonging to some local population will encounter marine hydrokinetic (MHK) turbines [14,15] that are to be deployed at the Fundy Ocean Research Center for Energy tidal energy demonstration (TED) area in the Minas Passage, Bay of Fundy, Canada (Figure 1).

Vertically averaged tidal current can be in excess of 5 ms^{-1} in the TED area and the associated power density is enticing for the deployment of MHK turbines that convert tidal kinetic energy to electricity [16,17]. Large tidal range can result in about 60% of the water in the Minas Basin flowing in and out through the Minas Passage in a semidiurnal tidal cycle [18], so some fish that are commonly found in the Minas Basin also pass through the TED area in the Minas Passage [19]. The Minas Passage is also the sole corridor for migratory diadromous fish populations that utilize the Minas Basin and its associated freshwater tributaries for reproduction and rearing. Of the species of fish commonly found in the Minas Basin [20], acoustic telemetry measurements made in the Minas Passage are reported for striped bass *Morone saxatilis* [4], Atlantic sturgeon *Acipenser oxyrinchus* [2], alewife *Alosa pseudoharengus* [3], Atlantic salmon *Salmo salar* and American eel *Anguilla rostrata* [21]. Acoustic telemetry work continues on the above species as well as tomcod *Microgadus tomcod*, spiny dogfish *Squalus acanthias* and American shad *A. sapidissima*.
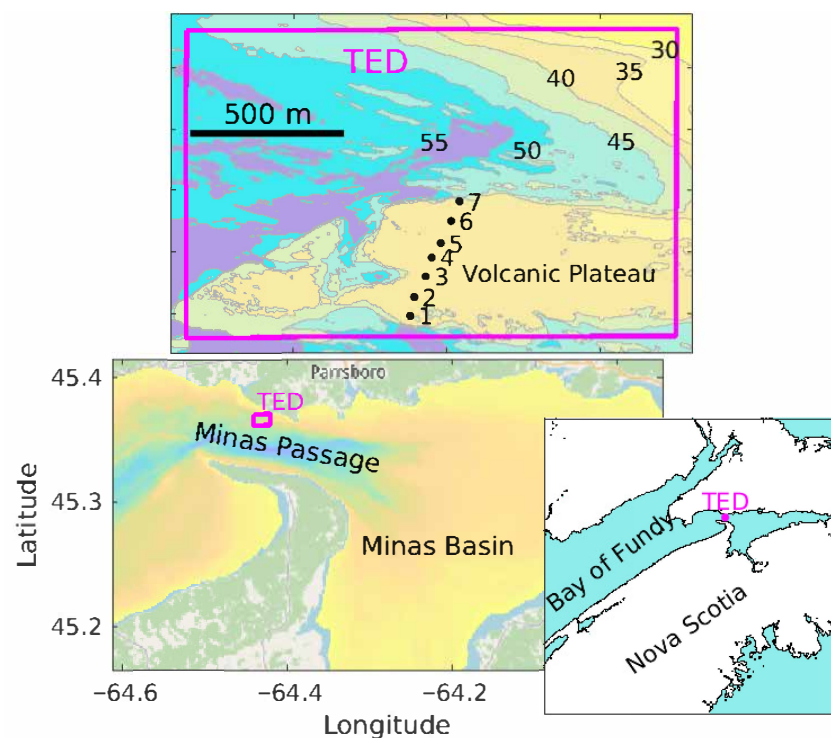
Figure 1. Location of the mooring array on a flat volcanic plateau within the TED area on the northern side of Minas Passage, Bay of Fundy, Nova Scotia. The present study used seven moorings that are numbered from south to north. Depth contours are labeled in 5 m intervals.

Fast current makes the TED area a difficult place to deploy scientific instruments and adversely affects acoustic telemetry [12,22,23]. Active acoustic measurements (echosounders) are also difficult to utilize [24] and have the added disadvantage of not being able to identify the species of a target. Since 2010, Innovasea VR2W receivers have been used in the Minas Passage to monitor Atlantic sturgeon, striped bass and American eel that carry Innovasea acoustic tags that use pulse position modulation (PPM) of a 69 kHz carrier

frequency [21]. At 69 kHz, the ambient sound level is greatly increased when the current is fast and PPM tags can only be detected at close range [12]. Furthermore, at small range, close proximity detection interference (CPDI) [11] causes further uncertainty for signal detection [12]. A 69 kHz PPM tag signal encodes information according to the gaps between eight 10 ms pulses that are spaced over a few seconds (Figure A1a), so signals are transmitted infrequently because of the energy cost and the need to avoid interference by pulses originating from another tag. Few 69 kHz PPM signals can be transmitted before fast currents sweep a tagged fish beyond the detection range of a VR2W receiver, so few tagged fish are detected. This presents an impediment for estimating fish–turbine encounter probability because it is the encounters at high current speeds that are of the most interest.

Given the lower ambient sound level at higher frequencies [12], some of the tagging effort has shifted to using Innovasea 170 kHz high-residency (HR) tags in recent years. HR tags can transmit both 180 kHz PPM signals (eight pulses that each have 5 ms duration) and 170 kHz HR signals. HR signals encode information by abrupt phase changes within a 6 ms pulse (Figure A2), so HR signals can be transmitted much more frequently than PPM signals and many signals can reach a moored HR2 receiver before the current sweeps a tagged fish out of range. Alewives carrying HR tags that transmitted signals every 1–2 s were detected making many passes through the Minas Passage on flood and ebb tides [3], even though the HR2 receiver array monitored only a small portion of the width of the passage. The apparent advantages of HR tags motivates the present measurements of their detection efficiency as a function of range and current speed.

HR technology has additional capabilities that were judged to be of potential use at our study site. The ability of HR2 receivers to separately identify a HR signal and its reflection allows the calculation of range between a receiver and a transmitting tag that is at a known depth. HR signals reflected from the sea surface can also be used to monitor the depth of a HR2 receiver. These capabilities turned out to be crucial for measuring detection efficiency, and the ability of the HR2 receiver to detect both 170 kHz HR and 180 kHz PPM signals enables a clear comparison of detection efficiency for those two signal types.

2. Materials and Methods

2.1. Moorings Design and Instrument Layout

Seven moorings were deployed for 32 d (9 April to 11 May 2021) on the volcanic plateau within the TED area (Figure 1). The line of moorings was orthogonal to the flood–tide current velocity. Each mooring consisted of a 240 kg anchor (a steel chain link) that was tethered by a 3 m riser chain to an acoustic release that was housed within the streamlined hull of a SUBS-Model A2 (Open Seas Instrumentation Inc., Musquodoboit Harbour, NS, Canada). Ideally, the moorings would hold HR2 receivers well clear of the seafloor to prevent the blocking of transmission paths but strong, turbulent currents make severe mooring tilt inevitable using the available buoyancy-based, mooring technology [12]. The location was selected for its relatively flat and regular seafloor, which was anticipated to minimize the blocking of sound signals traveling between moored HR2 receivers.

Mooring deployment was during low tide with the intent of separating moorings by 50 m. Currents are never really slack in the TED area, so navigation is difficult. Table 1 documents the research vessel position at the time each mooring was released overboard from the stern. The research vessel's GPS was about 10 m forward of the drop position, so acoustic methods must be used to check and refine estimates of the mooring separation. HR tags were attached to the top of the SUBS tail fin at sites 1 and 7. HR tags transmitted 143 dB signals with 170 kHz HR signals set to a random delay interval of 1.8–2.2 s and 180 kHz PPM signals set to 15–25 s delay. Due to a miscommunication with the manufacturer, both of the HR tags turned off at about 1832 UTC on 23 Apr 2021, a little short of halfway through the experiment. It was intended that all HR2 receivers be set to transmit 143 dB HR signals within a random delay interval of 4–6 s, but the delay interval was mistakenly set to 25–35 s for site 3.

Table 1. Mooring locations and depths at low tide.

Site	Latitude	Longitude	Depth (m)	Device	HR TX-Interval (s)
1	45.3623	−64.4316	34	Tag	1.8–2.2
2	45.3628	−64.4314	33	HR2	4–6
3	45.3634	−64.4310	32	HR2	25–35
4	45.3640	−64.4308	34	HR2	4–6
5	45.3644	−64.4304	34	HR2	4–6
6	45.3650	−64.4300	34	HR2	4–6
7	45.3656	−64.4296	33	Tag	1.8–2.2

Every 10 min, the HR2 receivers recorded water temperature and the tilt angle of the HR2 from vertical. When using water temperature to estimate sound speed, 10 min sampling is adequate but underresolves fluctuations in SUBS orientation. Nevertheless, in a statistical sense, the tilt measurements indicate whether or not a SUBS maintains a streamlined orientation relative to the current.

2.2. Types of HR Signals That Are Detected by a HR2 Receiver

A HR2 receiver records detected signals according to the time they are detected and their identity. Presently, we define five types of HR signals that are detected by HR2 receivers. For a given purpose, detected signals may be useful or a hindrance, depending upon their type.

Type HR_{1d} are signals that travel along a direct path from some other source to the detecting HR2 receiver. The other source might be a tag or a different HR2. Type HR_{1r} are signals that are transmitted from some other source but are reflected off the sea surface before reaching the detecting HR2.

Type HR_{SELF} is classified by Innovasea as a "SELF DET" and is a HR signal that a HR2 both transmits and records at the time of transmission. Type HR_{SELFr} is when a HR2 receiver detects a reflection of its own HR_{SELF} transmission. HR_{SELFr} signals are usually reflected from the sea surface but sometimes they are reflected from deeper objects nearby the mooring.

Rarely, the HR_{SELF} transmission can interact with a very nearby object in such a way as to create a signal with a fake identity. Remarkably, the transmitting HR2 will correctly record the identity and time at which the HR_{SELF} was transmitted and fractionally later will also record the time of arrival of the fake signal along with its fake identity. This will be called a HR_{FAKE} signal. Very infrequently, the transmitting HR2 will detect such fake signals after they have been reflected from the sea surface. Sometimes, the fake signal is detected by an HR2 that is different from that from which it originated.

2.3. Removal of Some HR_{1r} for Estimating Detection Efficiency

Acoustic impedance is much greater in water than air, so the sea surface reflects sound very well [25]. A HR signal that is detected by a HR2 receiver (but was not transmitted by that receiver) might have traveled a direct path from the transmitter to the receiver, or it might have traveled a path corresponding to reflection from the sea surface. Sometimes, the same transmitted signal will be detected twice; first, the HR_{1d} signal, and a fraction of a second later, the HR_{1r}. In such circumstances, the HR_{1r} signals are easy to identify because the time lapse from the HR_{1d} is very much less than the time lapse between successive transmissions (Table 1).

Let $N_{d \wedge r}$ be the number of transmissions that were detected after traveling both a direct (*d*) and ($\wedge$) reflected (*r*) path, corresponding to $2N_{d \wedge r}$ detected signals. For estimating detection efficiency, we must remove the $N_{d \wedge r}$ reflected signals that closely follow signals that traveled a direct path.

2.4. Removal of HR_{1r} for HR2 Synchronization and Separation

HR_{1r} signals (received after reflection from the sea surface) are troublesome if included in the data set used for synchronizing clocks on two HR2 receivers and measuring the distance between those receivers. Usually, HR_{1r} are also a hindrance when using an array of receivers to localize the position of a tagged fish, although they can also be valuable for such calculations providing special care is taken [26].

The total number of detected signals N_{total}, from X transmissions, can be written in a form that is relevant for calculating mooring separation:

$$N_{total} = N_{d \wedge \sim r} + N_{\sim d \wedge r} + 2N_{d \wedge r} \tag{1}$$

where $N_{d \wedge \sim r}$ is the number of transmissions that were detected after traveling a direct (d) path and ($\wedge$) were not ($\sim$) detected after traveling a reflected (r) path. $N_{\sim d \wedge r}$ is the number of transmissions that were not detected after traveling a direct path but were detected after traveling a reflected path. $N_{d \wedge r}$ transmissions were detected for both direct and reflected paths. As before, it is easy to remove the $N_{d \wedge r}$ reflections that immediately follow the detection of a direct-path signal, so the the number of detected transmissions is

$$X_{det} = N_{d \wedge \sim r} + N_{\sim d \wedge r} + N_{d \wedge r}. \tag{2}$$

The number of undetected transmissions can be written $X_{\sim det} = N_{\sim d \wedge \sim r}$, so the total number of transmissions is

$$X = X_{det} + X_{\sim det}. \tag{3}$$

That leaves $N_{\sim d \wedge r}$ troublesome reflected signals within the detected signals X_{det}, which cannot be identified and removed before synchronizing clocks and calculating mooring separation. Let us, therefore, evaluate the extent to which those $N_{\sim d \wedge r}$ reflected signals are present.

HR2 synchonization and separation first requires matching a short sequence of transmissions to a sequence of detections. Such matching is best achieved when the proportion of transmissions that are detected following a direct path, β, approaches 1 from below, i.e., $\beta \to 1^-$.

Signals traveling both reflected and direct paths suffer signal attenuation and distortion as they travel through the turbulent water volume and both must rise above the same ambient noise level to be detected. These things affect the probability of detecting a transmission in a way that is similar for both direct and reflected paths and they scale as β. Reflected signals suffer additional distortion and scattering from a roughened sea surface, which introduces a probability P_s that an incident signal will be reflected sufficiently cleanly for the possibility of detection. This suggests that $N_{d \wedge \sim r}$ scales as $\beta(1 - P_s)$, $N_{d \wedge r}$ scales as βP_s, $N_{\sim d \wedge \sim r}$ scales as $(1 - \beta)(1 - P_s)$, and $N_{\sim d \wedge r}$ scales as $(1 - \beta)P_s$.

When P_s and $1 - \beta$ are similarly small,

$$N_{d \wedge \sim r} \gg N_{d \wedge r} \approx N_{\sim d \wedge \sim r} \gg N_{\sim d \wedge r} \tag{4}$$

and the troublesome reflections are rare. More generally, the physical scaling above gives

$$\frac{N_{d \wedge r}}{N_{d \wedge \sim r}} \approx \frac{N_{\sim d \wedge r}}{N_{\sim d \wedge \sim r}} \approx \frac{P_s}{1 - P_s}. \tag{5}$$

Using (2) to substitute $X_{det} - N_{\sim d \wedge r} - N_{d \wedge r}$ for $N_{d \wedge \sim r}$ and remembering that $N_{\sim d \wedge \sim r} = X_{\sim det}$, we see that (5) cross multiplies to give the following quadratic equation:

$$N_{\sim d \wedge r}^2 + (N_{d \wedge r} - X_{det})N_{\sim d \wedge r} + N_{d \wedge r}X_{\sim det} \approx 0 \tag{6}$$

which can be solved for $N_{\sim d \wedge r}$. $N_{\sim d \wedge r}$ can then be substituted into (2) to evaluate $N_{d \wedge \sim r}$.

2.5. HR2 Depth Relative to the Sea Surface

When a HR2 receiver detects a reflection HR_{SELFr} of its own transmission HR_{SELF}, then there is a high probability that that reflection was from the sea surface. In such circumstances, the vertical distance is the speed of sound c multiplied by half the time lapse between when the HR signal was transmitted and when it was detected. The speed of sound was calculated following [27] by using the temperature measured by the HR2, using hydrostatic pressure at half the mooring depth in Table 1, and by assuming 31.5 ppt salinity. Previous measurements in the Minas Passage indicated salinities in the range of 30.5 to 32 ppt [28–30] with tidal excursion causing salinity to sometimes vary by as much as 1 ppt [29]. Current also influences sound wave propagation, but signal paths are approximately orthogonal to the current, so the effect is minimal.

Reflections from the sea surface give a gappy time series for the height of the water column above the HR2. For each day, at each site, a regression fit to tidal harmonics (M2, S2, N2, and M4) was then used to obtain a daily averaged estimate of depth along with its 95% confidence interval.

2.6. HR2 Synchronization and Site Separation

By taking care to reference the HR2 to UTC soon before/after mooring deployment/recovery, much of the clock skew could be removed. It is then less computationally difficult to pattern match a time sequence of HR_{SELF} transmissions from one HR2 to a corresponding (possibly gappy) time sequence of HR_{1d} signals detected by a neighboring HR2. Times at which signals are detected and transmitted enable more accurate synchronization and calculation of the separation between receivers.

Consider that HR2 receivers $\Re_1$ and $\Re_2$ are separated by some unknown range r and that there is an unknown clock offset so that at an instant when receiver $\Re_1$ records time t_1, the receiver $\Re_2$ records time $t_2 = t_1 + t_{offset}$. In order to calculate separation range r and the time offset, we write the travel-time equations for two signals. Receiver $\Re_1$ transmits signal i at time t_{1Xi} and $\Re_2$ receives signal i at time

$$t_{2Ri} = t_{1Xi} + \frac{r}{c} + t_{offset} \tag{7}$$

where c is the speed of sound. Receiver $\Re_2$ transmits signal j at time t_{2Xj} and $\Re_1$ receives that signal at time

$$t_{1Rj} = t_{2Xj} + \frac{r}{c} - t_{offset} \tag{8}$$

It is now trivial to solve the above equations for r

$$r = \frac{c}{2}\left(t_{2Ri} - t_{1Xi} + t_{1Rj} - t_{2Xj}\right) \tag{9}$$

and t_{offset}

$$t_{offset} = \frac{1}{2}\left(t_{2Ri} - t_{1Xi} - t_{1Rj} + t_{2Xj}\right) \tag{10}$$

as functions of the transmission and reception times that the two receivers recorded for signals i and j. The current has minimal influence on the calculation of r because moorings are aligned across the current (Figure 1).

2.7. Separation between Tags and HR2 Receivers

A first estimate of separations between moorings can be obtained from latitudes and longitudes in Table 1. Separations between HR tags and HR2 receivers were also calculated from the time lag τ_{lag} between the reception of a tag transmission traveling a direct path and a path that reflected from the sea surface. In order to make this calculation, we assume that the HR2 receiver and the tag are at the same depth D below the seasurface. This amounts to synchronous signals being sent from two sources separated by $2D$ in the vertical. For

sufficiently large D, this amounts to a large aperture. Using the Pythagorean identity, separation range r is then calculated as

$$r = \frac{4D^2 - c^2\tau_{\text{lag}}^2}{2c\tau_{\text{lag}}}. \tag{11}$$

This equation is a simplification of a calculation [26] for obtaining the range and depth of a harbor porpoise (*Phocoena phocoena*). Lag distance $c\tau_{\text{lag}}$ also varies with tidal elevation. Before applying (11), linear regression was used to remove tidal constituents (M2, S2, N2, M4) from $c\tau_{\text{lag}}$.

2.8. Tidal Current and Significant Wave Height

The present study measures how the detection efficiency varies as a function of vertically averaged tidal currents computed from the finite volume coastal ocean model, FVCOM [16,17,31]. For present purposes, tidal currents and surface elevation were computed and stored at 10 min intervals at site latitudes and longitudes documented in Table 1. Modeled currents do not capture fluctuations associated with turbulent eddies but are otherwise representative of ADCP current measurements in the TED area [32].

Throughout this study, we will use s to denote the signed tidal current speed, so s is positive on the flood tide and negative on the ebb tide. Tidal elevation ℓ and significant wave height were measured north of the TED area ($-64.4040°$, $45.3690°$).

3. Results

Measuring detection efficiency is not trivial in the TED area. Moorings may move, so range r between moorings must be measured throughout the study. Proper account must be taken of signals taking direct and reflected paths. The interpretation of signals transmitted over near-seafloor paths requires an assessment of vertical level for each mooring.

3.1. Transmission between HR2 Receivers: Reflected Signals

Table 2 documents the number X of HR transmissions from one site and the number X_{det} of those that were detected by a neighboring site. The total number N_{total} of detected HR signals was $X_{\text{det}} + N_{d \wedge r}$ because there were $N_{d \wedge r}$ transmissions that were detected after traveling both a direct and reflected path. For calculating the range between sites, it is important that the $N_{d \wedge r}$ reflections are removed. $N_{d \wedge r}$ is typically 5–6% of the detected signals, so failure to remove reflections can cause the estimates of detection efficiency to exceed 1.

Table 2. The number of HR signals transmitted X and detected X_{det} between sites.

Sites	X	X_{det}	Number Removed $N_{d \wedge r}$	Troublesome Number $N_{\sim d \wedge r}$	β	$N_{d \wedge r}/X_{\text{det}}$ $\approx P_s$
$2 \leftrightarrow 3$	621,816	537,521	27,686	4619	0.8644	0.0515
$3 \leftrightarrow 4$	620,704	452,490	30,101	12,349	0.7290	0.0665
$4 \leftrightarrow 5$	1,053,057	932,725	51,033	7021	0.8857	0.0547
$5 \leftrightarrow 6$	1,055,051	567,080	34,185	33,396	0.5375	0.0603

Detected transmissions X_{det} include $N_{\sim d \wedge r}$ reflections that cannot be identified and removed but are troublesome for clock synchronization and calculating distance between HR2 receivers. The number of troublesome reflections that remain in the time series $N_{\sim d \wedge r}$ was calculated using (6), and values in Table 2 are consistent with scaling relationships (4). $N_{\sim d \wedge r}$ is small compared to $N_{d \wedge r}$, except for transmissions between sites 5 and 6. Nevertheless, we expect that β and P_s might vary with environmental conditions, so there may be times when $N_{\sim d \wedge r}$ is a smaller/larger proportion of X_{det} than the averaged values in Table 2 might indicate.

The detection of reflections is expected to depend upon physical factors which vary with respect to time. It is not possible to construct a time series of reflected signals, but it is possible to construct a time series of signals that were detected on both direct and reflected paths at each site. Stratifying this time series with respect to tidal elevation shows that reflections are 2.57 times more commonly detected when tidal elevation is below its 25th percentile than when it is above its 75th percentile. Stratifying this time series with respect to significant wave height shows that reflections are 5.15 times more commonly detected when the significant wave height is below its 25th percentile than when it is above its 75th percentile.

3.2. Vertical Coordinate of the HR2 Receivers

Mooring locations and depths (Table 1) could only be roughly determined at the time of deployment. Times at which an HR2 receiver transmits a self signal HR_{SELF} and then detects the reflection of that signal HR_{SELFr} can be used to determine the subsurface depth of the HR2 receiver. The subsurface depth of the HR2 receivers varies mostly due to the rise and fall of the tide (Figure 2), but at site 2, there is also a step-like depth increase for the latter half of the deployment. At site 4, some signals are reflected from a subsurface object (e.g., a boulder on the seafloor) that is initially about 10 m from the mooring, transitioning to about 12 m from the mooring and then disappearing during the latter part of the deployment. The inset in Figure 2 shows that reflections from the nearby object occur on the flood tide. This indicates horizontal mooring movement and forebodes that bathymetric features can interfere with signal reception.
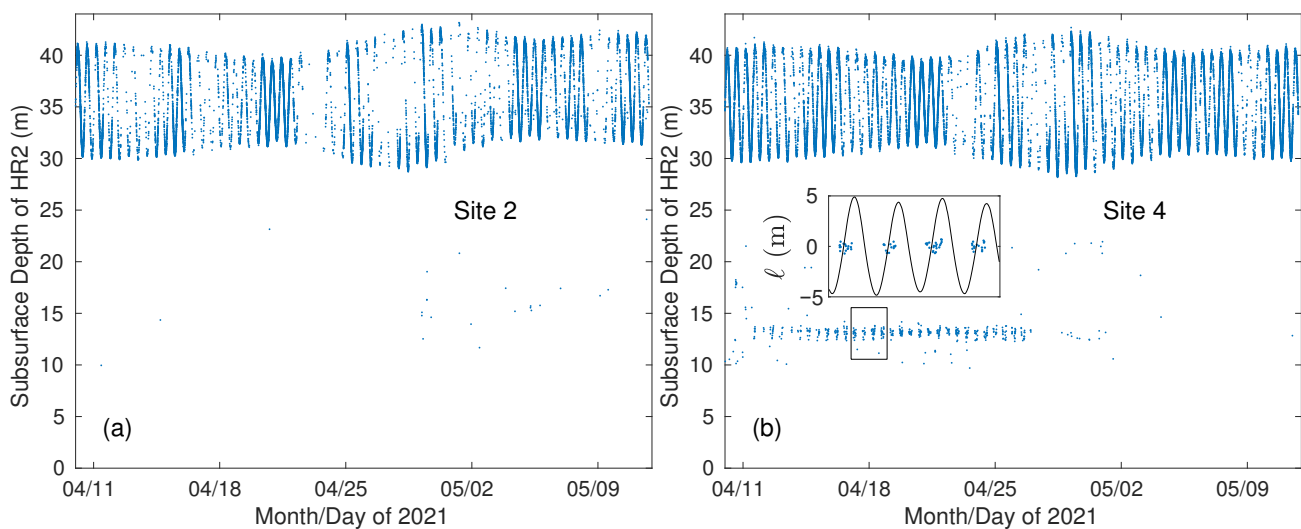
Figure 2. Subsurface depth of the HR2 obtained from HR_{SELF} signals and their reflection from the sea surface. (**a**) Subsurface depth at site 2. (**b**) Subsurface depth at site 4.

Reflections of self signals from the sea surface give gappy time series of the subsurface depth. Reflections that were obviously not from the sea surface were first removed. At each site, a regression fit to tidal harmonics (M2, S2, N2, and M4) was then applied for each day of measurements, so the fitted mean gives daily-averaged subsurface depths (Figure 3). In the latter portion of the deployment period, the mooring at site 2 slipped downwards, whereas the mooring at site 6 dragged slightly upwards. Initially, all HR2 receivers were <0.7 m from the same level, but their levels varied by almost 2 m at the end of the experiment.
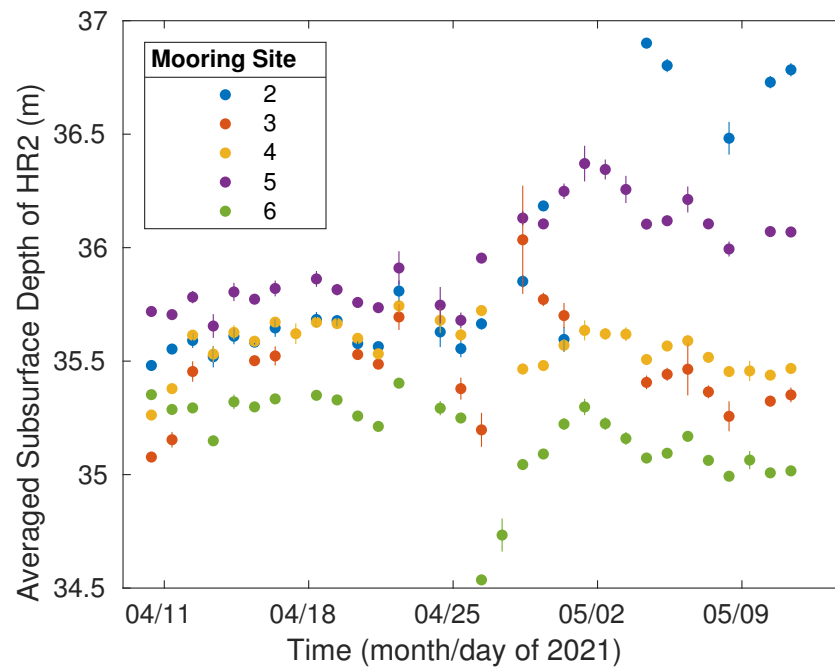
Figure 3. Daily-averaged depths of the HR2 receivers are color coded according to mooring site. Vertical whiskers indicate 95% confidence intervals, which are often too small for the plot to resolve.

3.3. Separation of HR2 Receivers

Begin by eliminating the $N_{d\wedge r}$ HR$_{1r}$ signals. Pattern matching time sequences of transmissions to detections then gives values $\left(t_{2Ri}, t_{1Xi}, t_{1Rj}, t_{2Xj}\right)$ for travel-time Equations (7) and (8). A pair of HR2 receivers can then be synchronized and their separation distance calculated using (9) and (10). An ensemble of many signals can be transmitted and received within a period that is sufficiently short for clock drift and site separation to have negligible change. Within an ensemble, there are relatively few outliers, and they are usually easy to recognize and remove. (Failing to remove the $N_{d\wedge r}$ signals results in many more outliers and makes their removal difficult and tedious.) Averaging each ensemble gave separation ranges.

Figure 4 shows that for the first few days following deployment, there is some small variation in the separation of sites 2,3 and of sites 4,5, but this is of little consequence for measuring detection efficiency. Left insets of Figure 4 show order 1 m changes in separation that are associated with tidal current as though some mooring anchors were dragged slightly back and forth with the tide. These small changes of separation are too large to be attributed to changes in the speed of sound that might be caused by tidal changes in hydrostatic pressure, errors in temperature measurements, or any physically plausible change in salinity.

Major variations in station separation (Figure 4) happened 26–28 April during spring tides (Figure 2) and were timed with the flood tide. This is consistent with the TED area having faster flood currents than ebb currents [16], so overall mooring displacement is most likely towards the east.

Separation between sites 2 and 5 changed little except for briefly moving a little closer together within the period 25 April to 2 May. In that same period, the right inset (Figure 4) shows that transmissions from the HR2 at site 5 are reflected from a nearby object for a time interval that is coincident with sites 2 and 5 being a little closer together. Figure 3 indicates the site 2 mooring settling into deeper water. The most straightforward interpretation is that the movement of site 5 accounts for most of the small change in separation between sites 2 and 5, whereas site 2 shuffled into a local hollow but otherwise was approximately stationary.
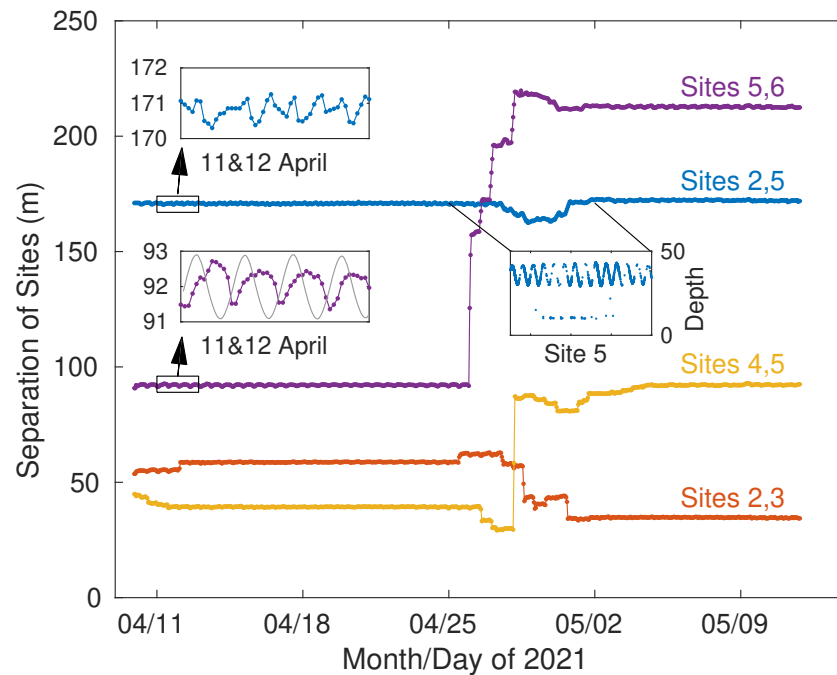
Figure 4. Separations between sites. Left insets show separation changing by about 1 m over the semidiurnal tidal time scale. The lower left inset also plots normalized tidal current (gray). Right inset shows depth at site 5 and also distance to a nearby reflective object.

Given that site 5 moved little, site 6 moved by more than 100 m during 26–28 April 2021. Most likely, sites 3, 4, and 6 all moved to an extent that was consequential for measuring detection range. Nevertheless, the separation ranges shown in Figure 4 are sufficient for estimating the detection efficiency of signals transmitted by one HR2 and received by another, although different ranges apply at different times for the same pair of instruments.

The 240 kg anchor weight was thought sufficient to prevent mooring movement on the volcanic plateau. Movement was greatest at site 6. Figure 5 shows HR2 measurements of the angle that the HR2 at site 6 was tilted from the vertical, which corresponds to SUBS tilt from a streamlined orientation into the current. Such tilt measurements cannot resolve pitch from roll and yaw, but they are indicative of lift and drag forces. When the current speed is less than 2 ms^{-1}, the tilt is mostly in the range 10–15° (red bars in Figure 5), which is consistent with a stable lift-generating SUBS alignment. These low speed tilts occur on both the flood (45%) and ebb (55%) tides. Current speeds greater than 3 ms^{-1} mostly happen (99%) on the flood tide. During fast flood tides, the tilt is distributed over a broad range, consistent with the unstable alignment of the SUBS. In order to visualize the full variation of tilt, the distributions are also plotted on a log-linear scale in Figure 5. Large changes in tilt suggest large forces. The forces that the SUBS applies to the anchor are not just drag and lift; the fluctuating SUBS movement also causes inertial forces due to the mass of the SUBS plus the virtual mass associated with the mass of the seawater that the SUBS displaces [33].

On the flood tide, drifters accelerate to achieve higher speed as they pass over the volcanic plateau of the TED area (Figure 5). On average, the speed increment approaches 0.5 ms^{-1} but individual drifter tracks show a good deal of variability that can be attributed to large-scale turbulent eddies. The flat, hard surface of the volcanic plateau may also make moorings vulnerable to movement. It is unclear whether mooring movement can be expected at sites that are not on the volcanic plateau.
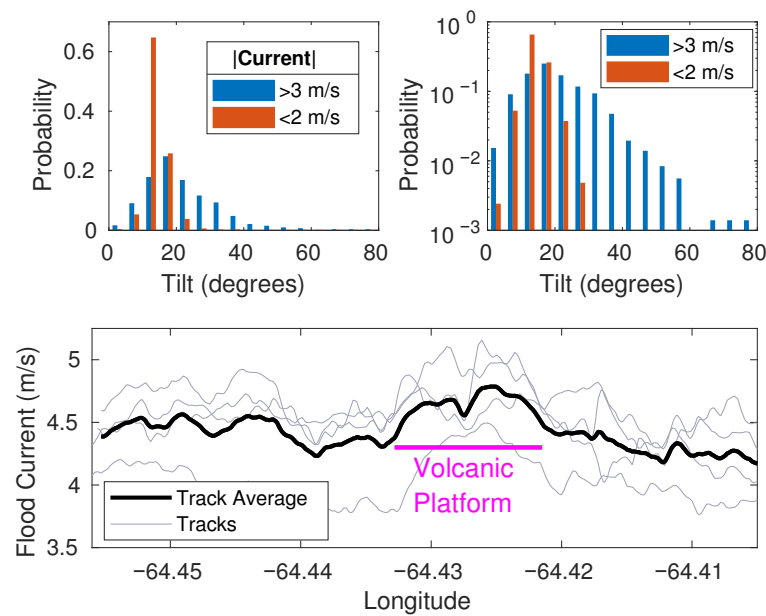
Figure 5. Tilt measured by the HR2 at site 6 (**top**) and current along drifter tracks that passed over the volcanic plateau (**bottom**).

3.4. Separation Ranges from Tags to HR2 Receivers

Ranges from tags (sites 1 and 7) to HR2 receivers were calculated from positions estimated at the time of deployment (second column of Table 3). Ranges from tags to HR2 receivers are only required up until 1832 23 April 2021 when the tags are turned off. During that time, there is little movement of the HR2 moorings at sites 2 through 5 (Figure 4). Temperature measurements were interpolated to the time of each signal to obtain sound speed c and therefore the lag-distance $c\tau_{lag}$. After removing tidal constituents, $c\tau_{lag}$ and subsurface depth $D = 35.5$ m were substituted into (11) to obtain ranges in the third column of Table 3. The standard error in measurements of $c\tau_{lag}$ causes $<0.04\%$ change in the calculation of range r except for the two greatest ranges in Table 3, where the change was $\approx0.6\%$. On the other hand, varying D by ±0.5 m caused $\approx3\%$ change in range. Mooring separations obtained from τ_{lag} are judged to be more reliable than those based upon estimates of the drop position.

Table 3. Ranges from tags to HR2 receivers. GPS ranges are from vessel position when the mooring was dropped overboard.

Sites: Tag,HR2	Drop Range (m)	τ_{lag} Range (m)
1,2	62	73
1,3	139	128
1,4	202	202
1,5	257	236
1,6	337	324
7,2	345	330
7,3	267	272
7,4	204	193
7,5	149	157
7,6	69	66

3.5. Detection Efficiency: Tag to HR2

Separations between HR tags and HR2 receivers were stable while tags operated (Table 3). No record is kept of when each tag transmitted, but on average, each tag is expected to transmit 300 ± 1 times during a 10 min interval. For each 10 min time interval, there is a corresponding signed current speed s obtained from FVCOM. A specific tag–HR2

pair corresponds to a specific range, and detected transmissions are then distributed as a function of s in 0.25 ms^{-1} increments. The ratio of the number of signals detected to the number transmitted gives an estimate of detection efficiency $\rho(s)$ for HR signals between a tag–HR2 pair.

The receiver at site 4 detected the tag at site 1 poorly compared to the tag at site 7 (Figure 6), even though both transmission paths had very similar ranges. The poor reception of signals traveling the 1,4 path might result from the flood tide swinging the moorings so that the signal propagation path becomes blocked by a high spot in the bathymetry. High-resolution bathymetry is available for the study area but although ranges between sites are accurately determined, the positions of the moorings are not. It was not possible, therefore, to test whether or not a particularly high spot existed on or near the 1,4 path. Given that the ultimate goal of such receiver arrays is to detect tagged fish that are usually well clear of the bottom, it was deemed appropriate to neglect results from the 1,4 path.
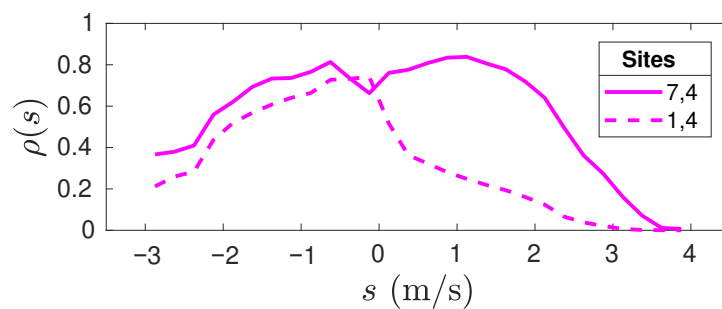
Figure 6. Comparison of detection efficiency for signal propagation from site 1 to 4 (202 m range) and from site 7 to 4 (193 m range).

With two tags each detected by five receivers, there are 10 transmitter–receiver pairs at ranges marked by magenta line ticks on the range axis of Figure 7. Ignoring the 1,4 path, Figure 7 shows contours of detection efficiency $\rho(r, s)$. It appears that the 1,5 and 1,3 paths might also have suffered some diminution of signal detection on the flood tide, less than that seen for the 1,4 path, but similar in form. Detection efficiency drops off rapidly when $|s| > 2$ ms^{-1}. Currents are faster on the flood tide, so estimates of detection efficiency are available for currents in the range $-3 \leq s \leq 4$ ms^{-1}.
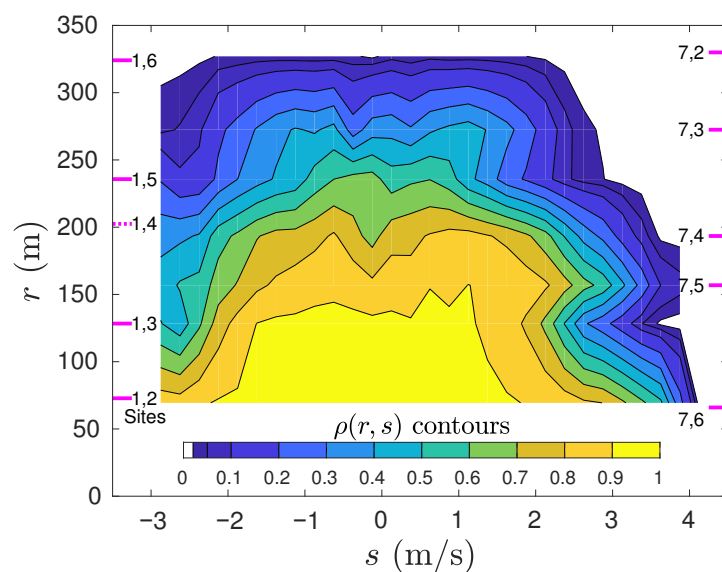
Figure 7. Contours of detection efficiency as a function of current speed (positive flood, negative ebb) and range. Detection efficiency was obtained from HR signals transmitted by the tags and detected by HR2 units. Measurements were obtained at ranges between sites indicated by labeling beside magenta line ticks.

3.6. Detection Efficiency: HR2 to HR2

HR2 moorings afford five receivers and five transmitters that transmit and receive HR signals throughout the study. The experiment was designed to measure two-way signal propagation along 10 transmission paths for a month. Figure 8 shows a time series of detection efficiency ρ_{10} (calculated for 10-minute intervals) for HR signals transmitted between sites 4 and 5. Even for fast currents, $\rho_{10} > 0.38$, while the range is $\approx$40 m. The mooring movement subsequently increases the range to >80 m, and similarly, fast currents cause a substantial reduction in ρ_{10}, although it always remains above 0. Results shown in Figure 8 contribute information near two ranges, and that is how they are used for the calculation of $\rho(r, s)$.
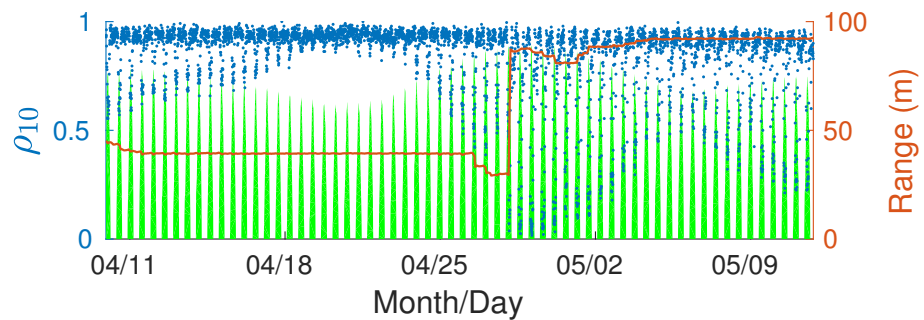
Figure 8. Probability ρ_{10} that HR transmissions between sites 4 and 5 will be detected during each 10 min interval (blue). Green shading shows flood tide normalized by 5 ms^{-1}. Red shows range between the sites.

Figure 4 shows separation for four pairs of sites, one of which is largely stable while the others are quite variable. Considering the time series of separations between all HR2 sites, we identified 15 ranges that accommodated the majority of site-to-site separations to within a small uncertainty (Table 4). These ranges are marked with magenta on the vertical axis of Figure 9. Dotted magenta indicates ranges for which detection efficiency was poor compared with neighboring ranges. Poor detection efficiency may result from the signal path being blocked by bathymetry. Figure 3 shows that site 6 was the most elevated throughout the measurement period, and this corresponds to site 6 featuring in most ranges for which the detection efficiency was relatively high and the signal was deemed not to be blocked (Table 4).

Table 4. Ranges used to calculate detection efficiency.

n	Separation (m)	Mooring Sites	Transmission Characteristic
1	35 ± 2	2,3	blocking
2	39 ± 2	4,5	no blocking
3	59 ± 4	2,3	blocking apparent
4	80 ± 5	3,4	blocking apparent
5	92 ± 5	4,5 & 5,6	no blocking
6	107 ± 4	3,5	blocking
7	115 ± 4	3,5	blocking
8	127 ± 6	4,5	no blocking
9	140 ± 5	2,4	blocking
10	153 ± 5	4,6	no blocking
11	171 ± 5	2,5	blocking
12	210 ± 7	3,6 & 5,6	no blocking
13	249 ± 7	3,6	no blocking
14	263 ± 7	2,6 & a few at 3,6	no blocking
14	280 ± 7	2,6	no blocking
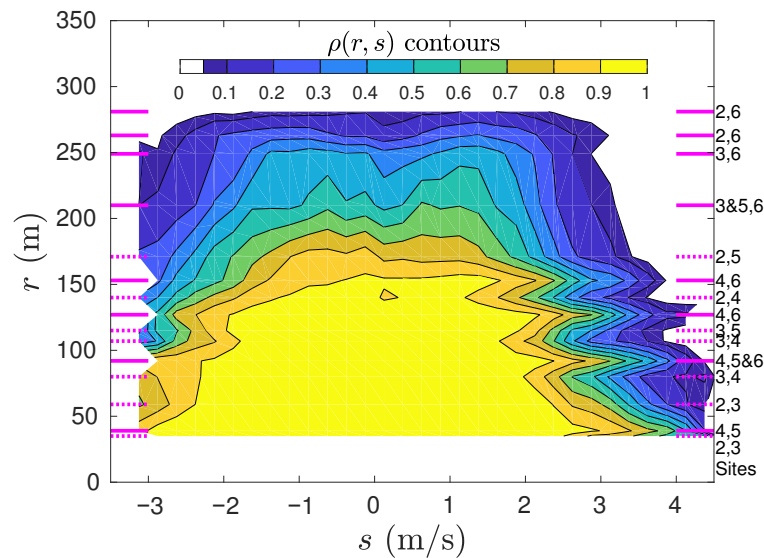
Figure 9. Contours of detection efficiency for HR signals transmitted by one HR2 and detected by another HR2. Ranges measured are indicated in magenta and sites associated with each range are labeled to the right.

It can be shown that poor performance at some ranges cannot be explained by statistical variability. Given the categorical nature of signal detection, the standard error of $\rho(r,s)$ is s.e.$(\rho) = \sqrt{\rho(1-\rho)/N}$, where N is the number of independent measurements used to calculate $\rho(r,s)$. Estimates of $\rho(r,s)$ are obtained from a great many instances and, except for the fastest flood/ebb currents, by averaging over many 10 min intervals. The standard error is too small to explain the variability of $\rho(r,s)$ that is seen in Figure 9. Rather, the variation in $\rho(r,s)$ is more likely associated with physical mechanisms (such as mooring tilt and bathymetric blocking) or errors made while modeling currents. Given this balance of probabilities, it seems that measurements in Figure 9 that are judged to suffer from blocking should be discarded when calculating values for $\rho(r,s)$ that are appropriate for detecting tagged fish that swim well clear of the seafloor.

Our experimental design did not adequately resolve how well signals are detected at ranges less than 40 m. Near the 40 m range, Figure 8 indicates that detection probabilities greater than 0.4 are achievable on the fast flood current during a spring tide. This raises the prospect that, to a reasonable approximation, results shown in Figures 7 and 9 might be made complete if the detection efficiency can be estimated at a very small range.

3.7. Detection Efficiency at Very Small Range

The Innovasea HR2 receiver delivers very few (if any) false detections that correspond to a specified HR tag identity. For example, the tags (IDs 61676 and 61677) at sites 1 and 7 turned off 13.9 days into the present experiment. Before turning off, those tag IDs were detected a total of 2.6 million times by the five HR2 receivers but they were not detected during the subsequent 18.1 days of the experiment.

A different type of false signal was found. The HR2 receiver (serial number 461550) at site 3 transmitted a HR signal with ID 62554 every 25–35 s. That HR2 detected a HR$_{\text{FAKE}}$ signal with ID 25202 a total of 2444 times, and it was detected throughout the duration of the range test. (Innovasea confirmed that they had never manufactured a HR tag with that ID.) Analysis of times between consecutive HR$_{\text{FAKE}}$ transmissions corresponded to an underlying transmission interval in the range 25–35 s as though the time series was a gappy version of signals being transmitted by the HR2 at site 3.

Of the 2444 HR$_{\text{FAKE}}$ signals, 2433 were detected at site 3 with a lag of $(8.42 \pm 0.12) \times 10^{-4}$ s after the HR2 had transmitted its self-signal. That lag corresponds to a transmission distance of 1.250 m. Our physical interpretation is that the HR2 detected a reverberation of its self-signal that was caused by the two flotation spheres housed within the

SUBS. The other 11 times that HR_{FAKE} was detected at site 3, it lagged the self-signal by 0.0490 ± 0.0048 s, which corresponded to detection after being reflected back from the sea surface.

For present purposes, regard the HR_{FAKE} signal as having been transmitted 2444 times from site 3 and detected 2444 times at site 3. At greater range, HR_{FAKE} was detected 503, 341, 267 and 27 times at sites 2, 4, 5 and 6, respectively. Blue bars in Figure 10 show the distribution of current when it is uniformly sampled though the experimental period. The current speed at the times when HR_{FAKE} was detected at sites 2, 4, 5, and 6 had a different distribution (orange bars), which is consistent with the detection at long range being much less likely when the current speed is high. Current speeds at the times that HR_{FAKE} was recorded at site 3 had a distribution (green bars) that was very similar to that for uniform sampling (blue). A fair interpretation is that, for current speeds in the TED area, very nearly all transmitted HR signals would be detected at the 1.25 m range.
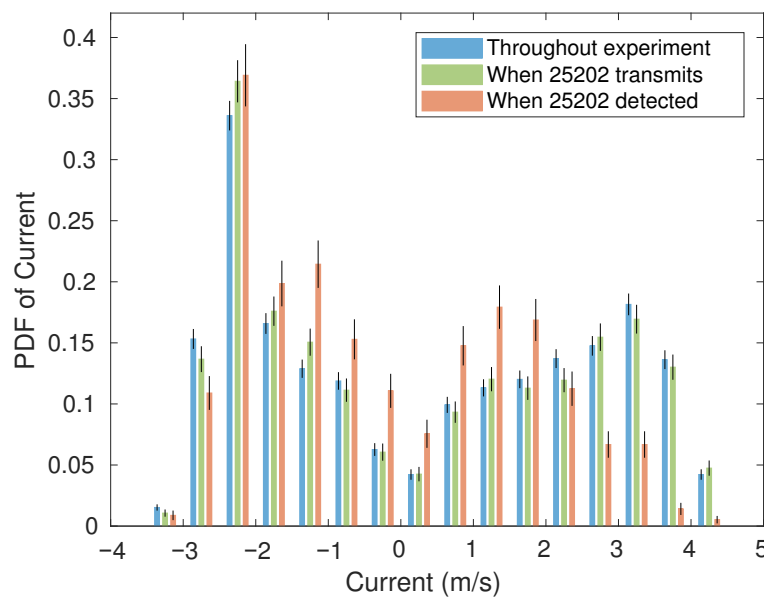
Figure 10. Distribution of current when sampled uniformly (blue), sampled when the HR_{FAKE} signal was detected at 1.25 m range (green), and sampled when HR_{FAKE} was detected at more distant sites (orange). Whiskers on the probability density function indicate $\pm$two standard errors.

3.8. Detection Efficiency and Detection-Positive Interval

The detection efficiency was modeled as a function $\rho(r, s)$. Temporal variation about this averaged formulation is expected because the ambient sound level influences signal detection, but ambient sound is only related to s in a statistically averaged sense. It is, therefore, important to assess how $\rho(r, s)$ might apply to the detection of the presence of a tagged fish during some interval Δt that is sufficiently long so as to span many transmissions and sufficiently brief relative to tidal time scales so as to ensure that the same value of s applies.

Consider a tag that transmits every τ s that is present at a range r from an HR2 receiver when current is s. On average, the probability that a Δt interval will be detection positive is

$$P_{\mathrm{pos}\Delta t} = 1 - ((1 - \rho(r, s))^{\Delta t/\tau}. \tag{12}$$

$P_{\mathrm{pos}\Delta t}$ is thus obtained as 1 minus the probability that none of the $\Delta t/\tau$ transmissions are detected. The calculation depends upon an assumption that the detection of a transmitted signal does not influence the probability that the next transmission is detected.

To test the applicability of (12), consider HR signals transmitted by the tag at site 7 and detected by the HR2 receiver at site 4 (Figure 6). The HR tag transmitted signals every $\tau = 2$ s from a range of $r_{7,4} = 193$ m for 13.86 days. Over that measurement period,

each $\Delta t = 120$ s interval was assessed to be detection positive if one or more signals were detected and otherwise detection negative. Black crosses in Figure 11 show the fraction of detection-positive intervals for each speed bin. Detection efficiency $\rho(r_{7,4}, s)$ for HR signal propagation between these sites can be substituted into (12) to also estimate the fraction of detection-positive $\Delta t = 120$ s intervals (blue circles).
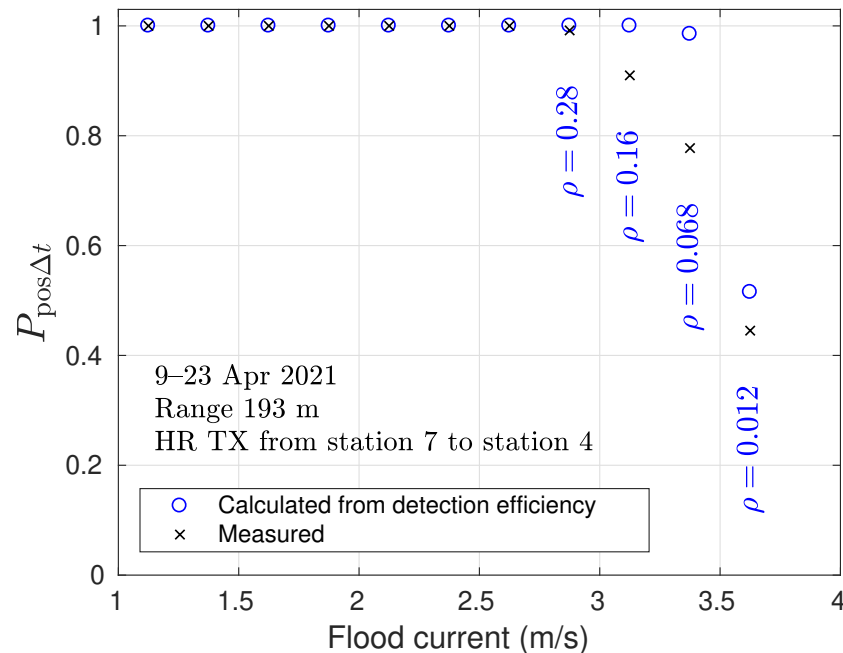

Figure 11. Detection efficiency underestimates the probability of a detection-positive 120 s interval.

At low current speeds, the detection efficiency is high and all intervals are detection positive, as expected. Lower detection efficiency at higher current speeds results in an appreciable fraction of the intervals being detection negative, and measurements show more detection-negative intervals than expected from (12). This demonstrates that the detection of a HR signal is not independent of whether the previous signal was detected. Obviously, if a given number of detected signals have a clumped distribution, then there will be more detection-negative intervals than for a random distribution.

3.9. Detection Efficiency and Area of Effective Detection

Our present interest is to use near-seafloor HR2 receivers to detect tagged fish that are sufficiently clear of the seafloor so that the signal path from fish to moored HR2 receiver is unlikely to be blocked by bathymetric features. Removing these blocked paths (Table 4), and extrapolating to all signals detected at near-zero range, gives the detection efficiency $\rho(r, s)$ as contoured in Figure 12.

If a tagged fish is detected by a HR2, then $\rho(r, s)$ provides a means to estimate the area within which the fish is expected to be located. Surrounding the position of the detecting HR2, an area of effective detection $A(s)$ can be calculated (13) by integrating over the horizontal plane:

$$A(s) = 2\pi \int_0^\infty \rho(r, s) r \, dr \tag{13}$$

A is the area within which the tagged fish are effectively detected in a statistical sense. A might be conceptualized as an effective area within which the probability of detecting a tagged fish is 1 and outside of which the tagged fish would not be detected. Of course, no such sharp transitions exist, so sometimes a tagged fish within A will not be detected and sometimes a tagged fish outside A will be detected.
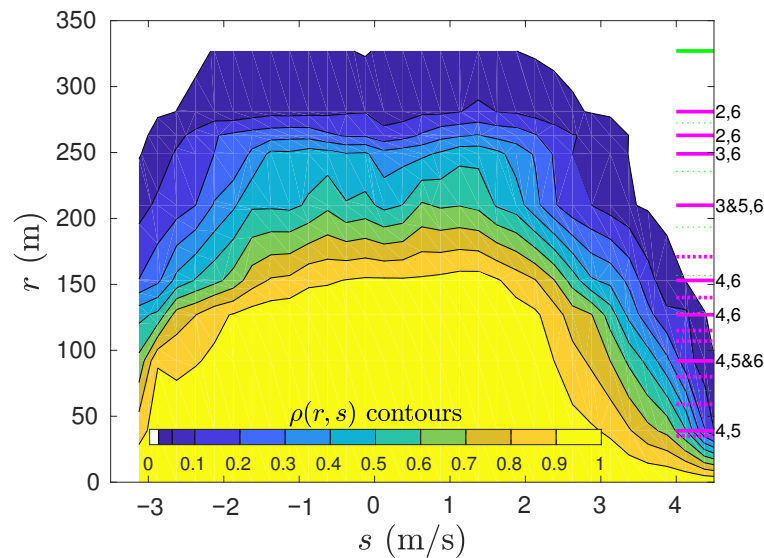
Figure 12. Contours of the detection efficiency that best applies to detecting tagged fish that swim well clear of the seafloor. This detection efficiency is obtained by selecting those HR2-HR2 propagation paths that do not appear to be blocked by variations in seafloor topography (solid magenta lines). Tag–HR2 transmissions were used to add probabilities at the greatest range (green line, top-right corner).

Given tag signals from N_f tagged fish, where those signals are all detected throughout some time period T when the current is s, then an estimate of abundance $\mathcal{F}$ (number of tagged fish per unit area in the horizontal plane) can be obtained

$$\mathcal{F} = \frac{\tau N_f}{TA} \tag{14}$$

where τ is the tag transmission interval. This is the elemental concept that can be used to convert signals detected by a receiver to an estimate of fish abundance.

Corresponding to the idea of an effective area for detecting tags, the range of effective detection is defined by

$$R(s) = \sqrt{\frac{A(s)}{\pi}}. \tag{15}$$

If $\rho(r, s)$ is obtained from those transmission paths that do not appear to be blocked (Figure 12), then $R(s)$ is as plotted by the blue line in Figure 13. Including blocked transmission paths in $\rho(r, s)$ has the effect of diminishing R for fast flood currents (red line) but otherwise causes little change. Considering ρ obtained from tag transmissions (Figure 9), and assuming that all signals are detected at a very close range gives a larger effective range in slow currents (yellow line in Figure 13) but underestimates the effective range in fast flood currents.

Having obtained the effective range, it is possible to describe the concept of the effective detection area $A(s)$ in a more quantitative way than above. Begin by calculating the inner area

$$A_{\text{inner}} = 2\pi \int_0^R \rho(r, s) r \, dr \tag{16}$$

by integrating only out to the effective radius R. The proportion of detected signals that originate within a physical space bounded by $r < R$ (within the effective area) is then given by the ratio A_{inner}/A. For present measurements of detection efficiency, this ratio is about 0.8 when the current is slow. At higher current speeds, we might think of ρ as being less step-like with respect to the range, which increases the likelihood that a detected fish may be outside the effective range.
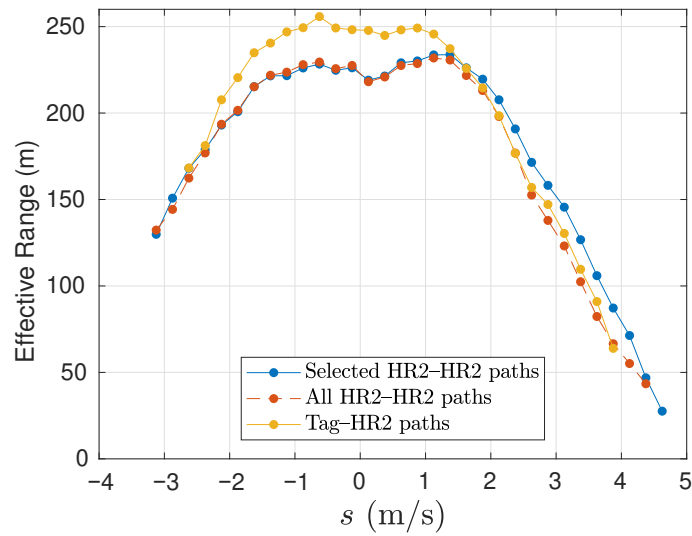
Figure 13. Effective detection range obtained by integrating the probability that a HR signal is detected. Using HR2-to-HR2 transmission paths that do not exhibit obvious blocking (blue), all of the HR2-to-HR2 transmission paths that were measured (red), and tag–HR2 transmission paths (orange).

3.10. Comparison of 170 kHz-HR and 180 kHz-PPM Signals

Tags at sites 1 and 7 transmit more frequently than the HR2 receivers and there was little mooring movement during the period for which tags transmitted. Thus, the detection of tag signals by the HR2 receivers provides the most reliable head-to-head comparison of detection efficiency for HR and PPM signals. Figure 7 shows the detection efficiency for tag HR signals, and the same procedure was used to obtain the detection efficiency for tag PPM signals. The ratio of detection efficiencies (Figure 14) shows that HR signals are better detected than PPM signals, particularly at large range and in fast currents.
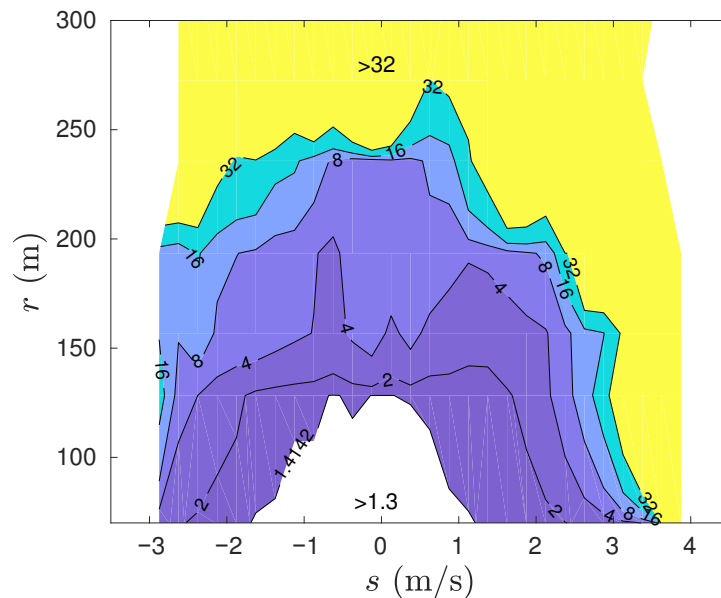
Figure 14. Contours of the ratio of HR detection efficiency to PPM detection efficiency. Contours are on a geometric scale.

4. Discussion

Using tidal MHK turbines [14,15] to harvest kinetic energy [16] may offset some carbon emissions caused by Earth's large human population relying on fossil fuel [34]. To address concern about fish–turbine encounters, acoustically tagged fish were monitored in the Minas Passage since 2010. Most of that work used Innovasea 69 kHz PPM tags [2,4,6], but

poor detection efficiency [12] hinders the reliable calculation of fish–turbine encounters when tidal currents are fast at the TED area in the Minas Passage [35].

The present results show that 170 kHz HR signals are better detected than 180 kHz PPM signals, and this is especially so as the range and current speeds increase. Additionally, the HR signals do not suffer from CPDI [11] and can be transmitted much more frequently than PPM signals. Considering all these factors, HR tags will be more effective than PPM tags for studying fish–turbine encounters in the Minas Passage. Recently, alewives with HR tags were measured making multiple passes through the Minas Passage TED area [3], so the presently obtained detection efficiency raises the prospect for the reliable calculation of the probability of alewife–turbine encounter.

Some illustrative progress on the MHK turbine encounter problem has been made using passive drifters [19]. While the collision probability of drifters with MHK turbines at the TED area is a matter of concern for engineers and scientists, it does not directly translate to the fish–turbine encounter probability because the drifters are usually deployed on quasi-stable tracks that pass through the Minas Passage, whereas fish might have quite different distributions depending on how they utilize their broader habitat [2–4,6]. Whereas a drifter track is well resolved in space and time, the position of an acoustically tagged fish is entirely unknown, except for those rare occasions when it is detected by a receiver. It is obvious when a tagged drifter passes by an array of receivers without being detected, but there is no way to know how many times a tagged fish passes by without being detected.

Detection efficiency measurements expand the utility of detected signals from tagged fish. Given accurate detection efficiency $\rho(r, s)$ and detected signals from tagged individuals belonging to a local population, Equation (14) provides an estimate for abundance, $\mathcal{F}$. If those signals were detected by HR2 receivers at the TED area in the Minas Passage, then $\mathcal{F}$ is an estimate of the number of tagged individuals per unit area. Fish in the water column are expected to approximately move with the water when the current speed is fast [19]. Given the vertical distributions of tagged fish [2,4], it is then straightforward to estimate the flux of tagged fish through a cross-current area that would, at some future time, be swept by the blades of a tidal MHK turbine. The probability that an individual belonging to a local population would encounter such a turbine can then be estimated by prorating according to the number of tagged individuals belonging to that population. Some fish might avoid the site when a MHK turbine is actually installed [36], while others may pass through a MHK turbine without being harmed [37], so the probability of encounter provides an upper limit on probability that an individual belonging to the population of interest may be harmed. Such metrics are directly relevant to population modeling [38], and thence to the objective regulation of MHK turbines and fisheries.

The ability of the HR2 receiver to identify and record HR signals in quick succession show that the probability was typically $P_d \approx 0.94$ that a received pulse followed a direct path as opposed to being reflected from the sea surface. The probability of detecting a PPM signal depends upon the reception of eight direct-path pulses without corruption by a reflected pulse. Making the physically plausible assumption that 69 kHz PPM pulses are reflected similarly to 170 kHz HR pulses, the probability of a PPM signal being corrupted by a reflected pulse is $1 - P_d^8 \approx 0.4$, which is consistent with CPDI [11,12] being caused by pulses reflected from the sea surface. This was not unexpected because seawater has much greater acoustic impedance than air [25], and non-breaking surface waves are characterized by broad troughs and crests with maximum steepness less than 1/7 [39]. Other high-frequency sound pulses were previously observed to reflect from the sea surface with relatively little distortion compared to the highly scattered signals that reflect off the seafloor [26]. Furthermore, the present work demonstrated that the probability of receiving a reflected signal decreases with increasing significant wave height, a result that mechanistically supports an observation by others of low CPDI for an experiment conducted in choppy waters [11].

Careful account must be taken of reflected HR signals in order to ensure that the same signal is not counted twice when measuring the detection efficiency. With respect to signals received from a tagged fish, there is no way to know whether an isolated signal

traveled a direct or reflected path. Arguably, this does not matter for measuring detection efficiency because both instances represent a single detection for a single transmitted signal. While reflected signals may not warrant mention for acoustic localization in very shallow water [9], the present work demonstrates that they matter when the tag is at a greater depth because the source-to-receiver travel time of a reflected signal becomes quite different from that taking the direct path. Sometimes, that difference can be useful for localization [26], but it is usually a hindrance. The present work found that most reflected signals could be identified and removed because they closely followed a signal taking a direct path.

Provided that HR2 moorings are within range of one and other, it may be possible to calibrate ρ for the times that tagged fish are detected. When tagged fish are detected, the concurrent measurement of ρ might refine the estimate of the area of effective detection and thus abundance. Alternatively, when tagged fish are not detected, we can discern whether this might be due to a poorly performing HR2 receiver. A poorly performing HR2 receiver might also be indicated if it detects few reflections of its self signal compared to neighboring receivers. The separation of moorings can also be measured as a test that moorings have remained in place while fish are being monitored. Similarly, it is easy to monitor instrument depth when a HR2 receiver detects a reflection of its own HR_{SELF} signal. Where bathymetry is highly variable—as it is south of the TED area—such depth monitoring might indicate a HR2 mooring has slipped into a crevasse. All these matters are of concern for the accurate interpretation of measurements made in the Minas Passage, where the available technology is pushed right to the edge of its capability.

Available mooring systems only enabled tags and receivers to be placed near the seafloor, whereas tagged fish that we study usually swim well clear of the seafloor when they are in the Minas Passage [2,4,40]. The range test could only measure signal paths that traveled from a near seafloor source to a near seafloor receiver. A 170 kHz sound wave has wavelength $\approx$ 8.7 mm, and so, little energy can be expected to diffract around a much bigger object that obstructs the direct path from the transmitter to the receiver. Ray theory applies, and there is an acoustic shadow zone behind the object [41]. Such blocking is not representative for the detection of tagged fish that swim higher in the water column, so we presently consider it to be a source of error for the measurement of ρ. For that reason, measurements from some signal paths were discarded because comparison with other paths of similar length made it obvious that signals were blocked by obstacles on the seafloor (Table 4). This procedure can remove the most obvious errors, but it cannot ensure that those paths that remained do not, themselves, suffer from some degree of signal blocking, especially when fast currents tilt the mooring line [12]. Given that ρ is of the most interest in fast currents, it is necessary to resolve the possibility of such systematic error in order to calculate probabilities of encounter with confidence.

To confirm that the present measurements of HR detection efficiency apply for a tagged fish, measurements can been made by suspending tags beneath a drifter that passes over a receiver array. It is logistically difficult to use drifting tags to measure ρ for all current speeds and ranges, but quasi-stable trajectories [19] do pass through the Minas Passage when the current is fast and thereby provide a means to test the applicability of present measurements of ρ under conditions of concern. Consider a tagged drifter (or tagged fish) that transmits with interval τ and moves at speed past a fixed HR2 mooring. The number of signals that are expected to be detected $E(N_{det})$ can be calculated by integrating ρ over the path taken by the drifter and multiplying by the number of signals transmitted along the path. Whereas the path of a tagged fish is not known, GPS measurements can accurately give the path of a drifter that carries tags. If our estimates of ρ are accurate, $E(N_{det})$ should be comparable with the number of detections that are observed $Obs(N_{det})$ when the drifter passes by a receiver. Appropriate drifter measurements will be reported shortly [42].

5. Conclusions

1. In fast tidal currents, it is most advantageous for an array of HR2 receivers to be spaced so that each HR2 can detect signals from its neighbors. This enables the time

synchronization of receivers and mooring movement to be quantified. Additionally, it enables detection efficiency to be estimated concurrent with the time that a tagged fish is detected.

2. Measurements of detection efficiency were variable over short intervals, and values were not independent from one interval to the next. Such correlation can influence the number of detection positive intervals. Further work is, therefore, necessary to verify that the present measurements of detection efficiency apply to the detection of tagged fish that quickly pass by receivers [42].

3. Some of the present detection efficiency measurements were discarded because there were indications that bathymetry blocked the near seafloor signal paths. Further testing is required to confirm those indications and verify that the presently obtained detection efficiencies apply to signals from tags that are well clear of the seafloor [42].

4. The concept of an effective detection area is introduced and can be calculated from detection efficiency. The effective detection area enables signals detected from tagged fish to be converted to an estimate of the abundance of tagged fish.

5. Provided that drifter measurements [42] verify the utility of the present estimates of detection efficiency, there is every prospect of using detected signals from tagged fish to calculate fish–turbine encounter probability in the tidal energy demonstration area in the Minas Passage [43]. Encounter probability places an upper bound on the possibility of fish being harmed by MHK turbines and is, therefore, expected to be an important consideration for the regulation of MHK turbines under the *Canadian Environmental Assessment Act*, *Fisheries Act*, and *Species at Risk Act*.

Abbreviations

The following abbreviations are used in this manuscript:

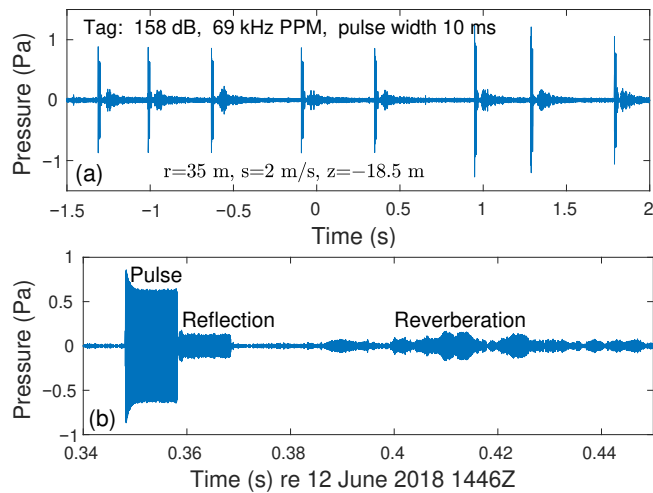|	
FORCE	Fundy Ocean Research Center for Energy
TED	Tidal Energy Demonstration
PPM	Pulse Position Modulation
HR	High Residency
HR2	High-residence receiver
CPDI	Close Proximity Detection Interference
FVCOM	Finite-Volume Coastal Ocean Model
GPS	Global Positioning System
UTC	Coordinated Universal Time
ADCP	Acoustic Doppler Current Profiler

Appendix A

Figure A1. (**a**) Time series of a 69 kHz pulse position modulation signal (PPM) that was measured in the Minas Passage. (**b**) Detail of the fifth pulse showing a reflection from the sea surface and reverberation.
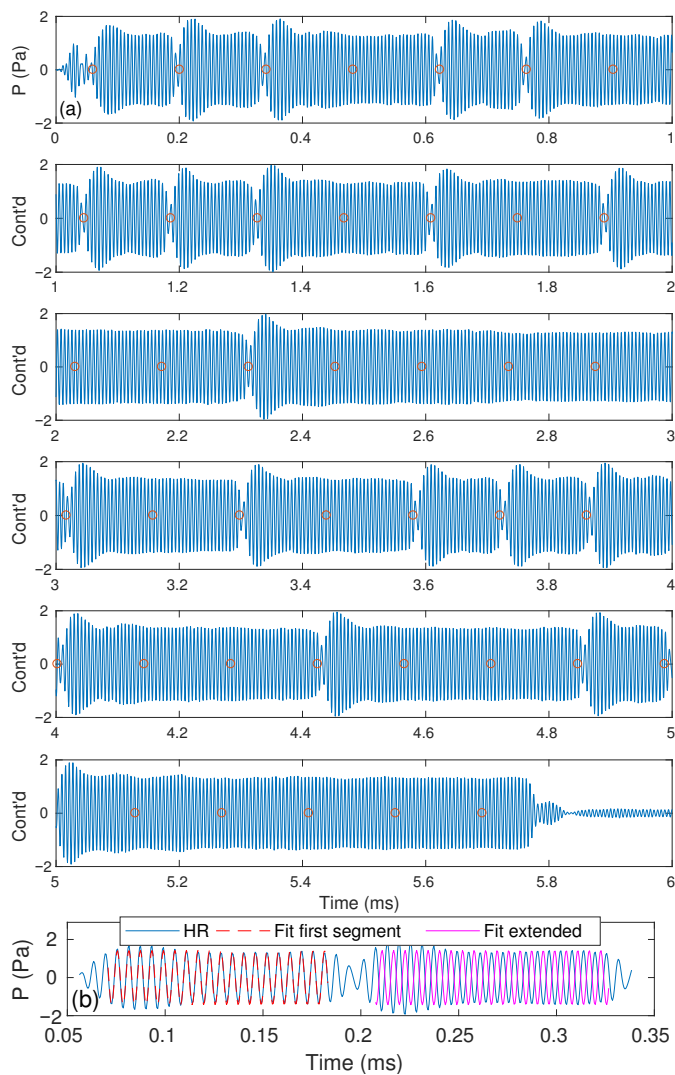

Figure A2. (**a**) Time series of a high-residency (HR) signal measured at close range. Carrier wave frequency is 170 kHz, and signal duration is approximately 5.8 ms. Information is encoded by abrupt phase changes from one segment to the next. (**b**) Detail showing the first phase change in the HR signal.

References

1. Chavarie, L.; Honkanen, H.M.; Newton, M.; Lilly, J.M.; Greetham, H.R.; Adams, C.E. The benefits of merging passive and active tracking approaches: New insights into riverine migration by salmonid smolts. *Freshw. Ecol.* **2022**, *13*, e4045. [CrossRef]
2. Stokesbury, M.J.W.; Logan-Chesney, L.M.; McLean, M.F.; Buhariwalla, F.F.; Redden, A.M.; Beardsall, J.W.; Broome, J.; Dadswell, M.J. Atlantic sturgeon spatial and temporal distribution in Minas Passage, Nova Scotia: A region of future tidal power extraction. *PLoS ONE* **2016**, *11*, e0158387. [CrossRef] [PubMed]
3. Tsitrin, E.; Sanderson, B.G.; McLean, M.F.; Gibson, A.J.F.; Hardie, D.C.; Stokesbury, M.J.W. Migration and apparent survival of postspawning alewife (*Alosa pseudoharengus*) in Minas Basin, Bay of Fundy. *Anim. Biotelem.* **2022**, *10*, 11. [CrossRef]
4. Keyser, F.; Redden, A.M.; Sanderson, B.G. Winter presence and temperature-related diel vertical migration of Striped Bass *Morone saxatilis* in an extreme high flow passage in the inner Bay of Fundy. *Can. J. Fish. Aquat. Sci.* **2016**, *73*, 1777–1786. [CrossRef]
5. Kessel, S.; Hussey, N.; Crawford, R.; Yurkowski, D.; O'Neill, C.; Fisk, A. Distinct patterns of arctic cod (*Boreogadus saida*) presence and absence in a shallow high arctic embayment, revealed across open-water and ice-covered periods through acoustic telemetry. *Polar Biol.* **2009**, *39*, 1057–1068. [CrossRef]
6. Keyser, F.M. Patterns in the Movement and Distribution of Striped Bass (*Morone saxatilis*) in Minas Basin and Minas Passage. Master's Thesis, Acadia University, Department of Biology, Wolfville, NS, Canada, 2015.
7. Martins, E.G.; Gutowsky, L.F.G.; Harrison, P.M.; Mills Flemming, J.E.; Jonsen, I.D.; Zhu, D.Z.; Leake, A.; Patterson, D.A.; Power, M.; Cooke, S.J. Behavioral attributes of turbine entrainment risk for adult resident fish revealed by acoustic telemetry and state-space modeling. *Anim. Biotelem.* **2014**, *2*, 13. Available online: http://www.animalbiotelemetry.com/content/2/1/13 (accessed on 18 April 2022). [CrossRef]
8. McLean, M.F.; Simpfendorfer, C.A.; Heupel, M.R.; Dadswell, M.J.; Stokesbury, M.J.W. Diversity of behavioural patterns displayed by a summer feeding aggregation of Atlantic sturgeon in the intertidal region of Minas Basin, Bay of Fundy, Canada. *Mar. Ecol. Prog. Ser.* **2014**, *496*, 59–69. [CrossRef]
9. Guzzo, M.M.; Van Leeuwen, T.E.; Hollins, J.; Koeck, B.; Newton, M.; Webber, D.M.; Smith, F.I.; Bailey, D.M.; Killen, S.S. Field testing a novel high residence positioning system for monitoring the fine-scale movements of aquatic organisms. *Methods Ecol. Evol.* **2018**, *9*, 1478–1488. [CrossRef]
10. Kessel, S.T.; Cooke, S.T.; Heupel, M.R.; Hussey, N.E.; Simpfendor, C.A.; Vagle, S.; Fisk, A.T. A review of detection range testing in aquatic passive acoustic telemetry studies. *Rev. Fish Biol. Fish.* **2014**, *24*, 199–218. [CrossRef]
11. Kessel, S.T.; Hussey, N.E.; Webber, D.M.; Gruber, S.H.; Young, J.M.; Smale, M.J.; Fisk, A.T. Close proximity detection interference with acoustic telemetry: The importance of considering tag power output in low ambient noise environments. *Anim. Biotelem.* **2015**, *3*, 5. [CrossRef]
12. Sanderson, B.G.; Buhariwalla, C.; Adams, M.; Broome, J.; Stokesbury, M.; Redden, A.M. Quantifying detection range of acoustic tags for probability of fish encountering MHK devices. In Proceedings of the 12th European Wave and Tidal Energy Conference, Cork, Ireland, 27 August–1 September 2017.
13. Krebs, C.J. *Ecology: The Experimental Analysis of Distribution and Abundance*, 6th ed.; Pearson Benjamin Cummings: San Francisco, CA, USA, 2009.
14. Jeffcoate, P.; McDowell, J. Performance of PLAT-I, a floating tidal energy platform for inshore applications. In Proceedings of the 12th European Wave and Tidal Energy Conference, Cork, Ireland, 27 August–1 September 2017.
15. Murray, J. Evolution of a solution for low cost tidal stream energy. *J. Ocean. Technol.* **2021**, *16*, 1–8.
16. Karsten, R.; McMillan, J.; Lickley, M.; Haynes, R. Assessment of tidal current energy in the Minas Passage, Bay of Fundy. *J. Power Energy* **2008**, *222*, 289–297. [CrossRef]
17. Karsten, R. An assessment of the potential of tidal power from Minas Passage, Bay of Fundy, using three-dimensional models. In Proceedings of the ASME 2001 30th International Conference on Ocean, Offshore and Arctic Engineering, OMEA2011-49249, Rotterdam, The Netherlands, 19–24 June 2011.
18. Sanderson, B.G.; Redden, A.M. Perspective on the risk that sediment-laden ice poses to in-stream tidal turbines in Minas Passage, Bay of Fundy. *Int. J. Mar. Energy* **2015**, *10*, 52–69. [CrossRef]
19. Sanderson, B.G.; Stokesbury, M.J.W.; Redden, A.M. Using trajectories through a tidal energy development site in the Bay of Fundy to study interaction of renewable energy with fish. *J. Ocean. Technol.* **2021**, *16*, 50–70.
20. Dadswell, M.J.; Spares, A.D.; Porter, E.; Porter, D. Diversity, abundance and size structure of fishes and invertebrates captured by an intertidal fishing weir at Bramber, Minas Basin, Nove Scotia. *Proc. Nova Scotia Inst. Sci.* **2020**, *50*, 283–318.
21. Redden, A.M.; Stokesbury, M.J.W.; Broome, J.E.; Keyser, F.M.; Gibson, A.J.F.; Halfyard, E.A.; McLean, M.F.; Bradford, R.; Dadswell, M.J.; Sanderson, B.; et al. Acoustic Tracking of Fish Movements in the Minas Passage and FORCE Demonstration Area: Pre-Turbine Baseline Studies (2011–2013). 2014. Available online: https://tethys.pnnl.gov/publications/acoustic-tracking-fish-movements-minas-passage-force-demonstration-area-pre-turbine (accessed on 19 November 2022).
22. Adams, M.; Sanderson, B.G.; Redden, A.M. Comparison of co-deployed drifting passive acoustic monitoring tools at a high flow tidal site: C-pods and icListenHF hydrophones. *J. Ocean Technol.* **2019**, *14*, 61–83. Available online: https://www.thejot.net/article-preview/?show_article_preview=1073 (accessed on 19 August 2019).
23. Tollit, D.; Joy, R.; Wood, J.; Redden, A.; Booth, C.; Boucher, T.; Porskamp, P.; Oldreive, M. Baseline presence of and effects of tidal turbine installation and operations on harbor porpoise in Minas Passage, Bay of Fundy, Canada. *J. Ocean Technol.* **2019**, *14*, 24–48. Available online: https://www.thejot.net/article-preview/?show_article_preview=1071 (accessed on 28 November 2022).

24. Viehman, H.A.; Hasselman, D.J.; Douglas, J.; Boucher, T. The ups and downs of using active acoustic technologies to study fish at tidal energy sites. *Front. Mar. Sci.* **2022**, *9*, 425. [CrossRef]

25. Lighthill, J. *Waves in Fluids*; Cambridge University Press: Cambridge, UK, 1980.

26. Sanderson, B.G.; Adams, M.J.; Redden, A.M. Using reflected clicks to monitor range and depth of Atlantic harbour porpoise. *J. Ocean Technol.* **2019**, *14*, 85–100. Available online: https://www.thejot.net/article-preview/?show_article_preview=1074 (accessed on 19 August 2019).

27. Mackenzie, K.V. Discussion of sea water sound-speed determinations. *J. Acoust. Soc. Am.* **1981**, *70*, 801–806. . [CrossRef]

28. Bousfield, E.L.; Leim, A.H. The fauna of Minas Basin and Minas Channel. *Natl. Mus. Can. Bull.* **1959**, *166*, 1–30.

29. Oceans Ltd. Appendix 5: Currents in Minas Basin. 2010. Available online: https://fundyforce.ca/document-collection/environmental-assessment-2009- (accessed on 18 November 2022).

30. Stewart: Oceanographic Measurements—Salinity, Temperature, Suspended Sediment & Turbidity, Minas Passage Study Site. 2010. Available online: https://fundyforce.ca/document-collection/ (accessed on 18 November 2022).

31. Chen, C.; Beardsley, R.C.; Cowles, G. An Unstructured-Grid, Finite-Volume Coastal Ocean Model (FVCOM) System. *Oceanography* **2006**, *19*, 78–89. [CrossRef]

32. Passage and Minas Basin. 2011. Available online: https://fundyforce.ca/document-collection/assessment-of-the-potential-of-tidal-power-from-minas-passage-and-minas-basin (accessed on 18 November 2022).

33. Lighthill, J. *An Informal Introduction to Theoretical Fluid Mechanics*; Oxford University Press: Oxford, UK, 1986.

34. May, R.M. Ecological science and tomorrow's world. *Philos. Trans. R. Soc. B* **2010**, *365*, 41–47. . [CrossRef] [PubMed]

35. Sanderson, B.G.; Redden, A.M. Use of Fish Tracking Data to Model Striped Bass Turbine Encounter Probability in Minas Passage. 2016. Available online: https://oera.ca/research-portal (accessed on 19 November 2022).

36. Viehman, H.A.; Zydlewski, G.B. Fish interactions with a commercial-scale tidal energy device in the natural environment. *Estuaries Coasts* **2015**, *38* (Suppl. 1), 214–252. [CrossRef]

37. Amaral, S.V.; Bevelhimer, M.S.; Cada, G.F.; Giza, D.J.; Jacobson, P.T.; McMahon, B.J.; Pracheil, B.M. Evaluation of behavior and survival of fish exposed to an axial-flow hydrokinetic turbine. *N. Am. J. Fish. Manag.* **2015**, *35*, 97–113. [CrossRef]

38. Gibson, A.J.F.; Myers, R.A. A statistical, age-structured, life history based, stock assessment model for anadromous alosa. In *Biodiversity and Conservation of Shads Worldwide*; Limburg, K.E., Waldman, J.R., Eds.; American Fisheries Society: Bethesda, MD, USA, 2003; pp. 275–283.

39. LeBlond, P.H.; Mysak, L.A. *Waves in the Ocean*; Elsevier: New York, NY, USA, 1978.

40. Renkawitz, M.D.; Sheehan, T.F.; Goulette, G.S. Swimming depth, behavior, and survival of Atlantic salmon postsmolts in Penobscot Bay, Maine. *Trans. Am. Fish. Soc.* **2012**, *141*, 1219–1229. [CrossRef]

41. Morse, P.M.; Ingard, K.U. *Theoretical Acoustics*; McGraw-Hill: New York, NY, USA, 1968.

42. Sanderson, B.G.; Hasselman, D.J. Using drifters equipped with acoustic tags to verify the utility of detection efficiency measurements for estimating probability of fish-turbine encounter. *J. Mar. Sci. Eng.* 2023, *submitted*.

43. Sanderson, B.G.; Karsten, R.; Solda, C.; Hardie, D.C.; Hasselman, D.J. Probability of Atlantic salmon post-smolts encountering a tidal turbine installation in Minas Passage, Bay of Fundy. *J. Mar. Sci. Eng.* **2023**, *11*, 1095. [CrossRef]

Appendix IV

MDPI

Article

Towards Estimating Probability of Fish–Turbine Encounter: Using Drifters Equipped with Acoustic Tags to Verify the Efficacy of an Array of Acoustic Receivers

Brian G. Sanderson [1,*] , Richard H. Karsten [2] and Daniel J. Hasselman [3,*]

1   Acadia Centre for Estuarine Research, Acadia University, Wolfville, NS B4P 2R6, Canada
2   Department of Mathematics and Statistics, Acadia University, Wolfville, NS B4P 2R6, Canada;
     richard.karsten@acadiau.ca
3   Fundy Ocean Research Center for Energy, Halifax, NS B3J 3N5, Canada
*   Correspondence: bxs@bellaliant.net (B.G.S.); dan.hasselman@fundyforce.ca (D.J.H.);
     Tel.: +1-902-697-2592 (B.G.S.); +1-902-406-1166 (ext. 7) (D.J.H.)

Abstract: An area has been designated for demonstrating the utility of marine hydrokinetic turbines in Minas Passage, Bay of Fundy. Marine renewable energy may be useful for the transition from carbon-based energy sources, but there is concern for the safety of fish that might encounter turbines. Acoustic receivers that detect signals from acoustically tagged fish that pass through the tidal demonstration area and the detection efficiency of tag signals might be used to estimate the likelihood of fish encountering marine hydrokinetic turbines. The method requires that tagged fish passing through the development area will be reliably detected by a receiver array. The present research tests the reliability with which passing tags are detected by suspending tags beneath GPS-tracked drifters. Drifters carrying high residency Innovasea tags that transmitted every 2 s were usually detected by the receiver array even in fast currents during spring tides but pulse-position modulation tags were inadequate. Sometimes very few high residency tag signals were detected when fast tidal currents swept a drifter through the receiver array, so increasing the transmission interval degrades performance at the tidal energy development area. High residency tags suspended close to the sea surface were slightly less likely to be detected if they passed by during calm conditions. Previously measured detection efficiencies were found to slightly overestimate the chances of a high residency tag carried by a drifter being detected as it passed by a receiver. This works elucidates the effectiveness with which acoustically tagged fish are detected in fast, highly turbulent tidal currents and informs the application of detection efficiency measurements to calculate the probability that fish encounter a marine hydrokinetic turbine.

Keywords: acoustic tag; verify; detection efficiency; tagged drifter; tidal energy; MHK turbine; fish–turbine encounter; acoustic telemetry

1. Introduction

There has been, and continues to be, a substantial effort to develop marine renewable energy (MRE) in order to address the effects of climate change and ensure a transition from carbon-based energy sources that is both sustainable and environmentally benign [1]. In Minas Passage, Bay of Fundy, tidal currents can exceed 5 ms^{-1} and that raises the possibility that marine hydrokinetic (MHK) turbines [2,3] might be used to generate electricity from the kinetic energy of the tides, thereby offsetting Canadian carbon emissions [4,5]. An area has been designated and equipped for tidal energy demonstration (TED) adjacent to the northern shore of Minas Passage, Bay of Fundy, Canada (Figure 1). The installation of MHK turbines is subject to assessing and mitigating potential harm to marine animals (*Canadian Environmental Assessment Act*, *Fisheries Act*, and *Species at Risk Act*) [6]. There is particular concern for local populations of various fish species that are found in the

region [7–9]. For example, a local population of striped bass *(Morone saxatilis)* that spawns in the Shubenacadie River [10], Atlantic sturgeon *(Acipenser oxyrhinchus)* from the Saint John River stock [11], and inner Bay of Fundy Atlantic salmon *(Salmo salar)* that were once abundant but are now supported by local hatchery stocking programs [12].

Acoustic telemetry provides a means to tag individuals belonging to a specific population and measure how frequently they pass through the TED area. If an acoustic receiver is placed within the TED area and it detects an acoustically tagged fish, then there is a distribution of positions about the receiver where the fish might be, and the distribution can be estimated if we know the detection efficiency of a signal from the acoustic tag. Measurements of detection efficiency, ρ, enable detections of tagged fish to be converted into an estimate of abundance [13]. When the current is fast, tagged fish move with the water to a first approximation [14], so the flux of tagged fish can be estimated. Thinking of the receiver as a proxy for where an MHK turbine might later be deployed, the flux of tagged fish passing through the area swept by MHK turbine blades is an Eulerian formulation [15] from which we can calculate the probability that an individual fish will encounter a turbine. This probability of encounter is only an upper limit on the probability of harm. A fish that encounters an MHK turbine might avoid dangerous interaction or may even be struck by a turbine blade but not be harmed [16,17], but presently, there is little prospect of measuring avoidance behavior and strike survivability at the TED area in Minas Passage [18].

Detection efficiency, $\rho(r,s)$, has been measured in the TED area as a function of range, r, from tag to receiver and signed current speed, s ($\pm$ on flood/ebb tides) [13]. These measurements were made using Innovasea high residency (HR) tags that were detected by Innovasea HR2 receivers. Both tags and receivers were moored near the seafloor, and there were indications that signal paths were sometimes blocked by variable bathymetry. The present work will more definitively demonstrate signals blocked by variable bathymetry. In Minas Passage, MHK turbines have been deployed, and are expected to be deployed, well clear of the seafloor, and many of the fish species of concern are known to also swim well clear of the seafloor in the TED area [10,11,19]. The present work addresses, therefore, a pressing need to verify the extent to which the previously measured detection efficiency [13] is applicable to the detection of tags that are located higher in the water column.

In order for later work to rigorously estimate the probability of fish–turbine encounter [20], it is necessary to presently verify that the number of signals detected during the time interval in which a tagged fish passes by a receiver will be consistent with the number estimated from detection efficiency that was measured using a tag moored to the seafloor [13]. Such measurements cannot be made using tagged fish because there is no way to know when a tagged fish passed the receiver array without being detected. Based on previously published work [14,20], to a good approximation, in the fast currents of Minas Passage, tagged fish move like drifters. To be representative of a tagged fish, the following work deployed HR tags suspended beneath GPS-tracked drifters in order to verify that they were detected by near-seafloor receivers in a way that was consistent with previously measured detection efficiency [13] and their track. Given that the species of interest can be found at different levels within the water column [10,11,19], each drifter suspends four tags at different subsurface depths.

Two measurement strategies were used. First, short-term drifts (STDs), where the tagged drifter was repeatedly released upstream and collected downstream of HR2 receivers in order to obtain many measurements in the TED area (Section 2.2). Second, long-term drifts (LTDs), where drifters were released onto a quasi-stable trajectory [14] and not recovered until many days later (Section 2.3). The quasi-stable trajectory [14] was chosen to efficiently obtain many measurements over HR2 receivers moored to the south of the TED area.

Conventionally, detection efficiency has been measured using acoustic tags and receivers that are at fixed positions [13,21,22]. Although seldom stated, such measurements give a strictly Eulerian formulation for detection efficiency. Such measurements of detection efficiency are related to the probability of detecting a tagged fish as it passes fixed receivers.

The presently obtained measurements provide a Lagrangian formulation [15] to directly obtain the probability of detecting a moving tag as it drifts by a receiver on a specific track. It should be stressed that the analysis presented below is only of acoustic tags attached to drifters. However, since the ultimate goal is to apply this work to detecting tagged fish moving through Minas Passage (see [14]), the analysis is discussed in terms of its relevance to tagged fish.

2. Materials and Methods

The volcanic plateau of the TED area in Minas Passage (Figure 1) is presently favored for future installations of both gravity-based MHK turbines and also for MHK turbines mounted to a floating platform [2]. The field program was designed to minimize the possibility of equipment, particularly drifters, becoming entangled with a non-operational OpenHydro turbine at the position marked by a circled cross in Figure 1a.
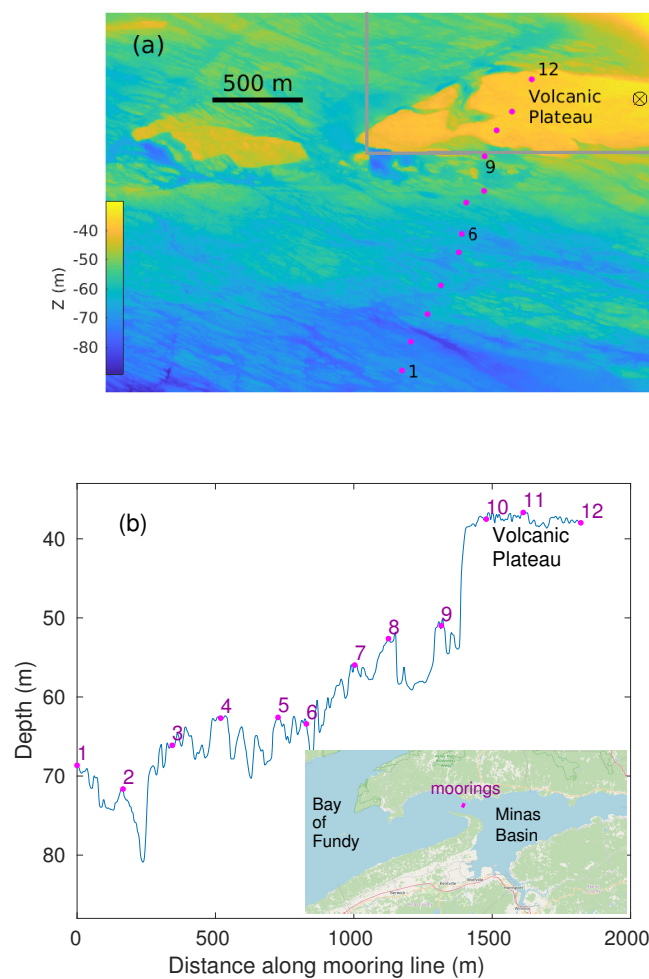

Figure 1. Mooring layout in Minas Passage. (**a**) Plan view shows moorings 1 through 12 and the TED area (gray box). (**b**) Depth profile along the mooring line. Inset shows location of the moorings within Minas Passage, Bay of Fundy.

2.1. Moorings

Twelve mooring sites were chosen so as to deploy an array of acoustic receivers on high ground along a line that was oriented approximately orthogonal to the flood tide (Figure 1). Mooring sites 1–8 monitored tagged drifters that crossed a line to the south of the TED area. Sites 10–12 were on the volcanic plateau, and site 9 was in deeper water off the edge of the plateau. Jointly, sites 9–12 are considered to monitor the TED area. Whereas

the volcanic plateau is relatively flat, the area to its south is characterized by highly variable bathymetry (Figure 1b).

All moorings consisted of a 240 kg chain link that served as an anchor to which a SUBS-Model A2 float (Open Seas Instrumentation Inc., Musquodoboit Harbour, Canada) was tethered by a 3 m riser chain. Each SUBS carried an acoustic release and an HR2 receiver within its streamlined hull and an Innovasea VR2W-69kHz receiver mounted symmetrically behind its tail fin. The HR2 receivers were set to transmit 143 dB HR signals every 25–35 s and record tilt and water temperature every 10 min. At moorings 9–12, a V9 tag was mounted to the top of the SUBS tail fin, and it transmitted a 170 kHz HR signal with a manufacturer-specified transmission interval of 1.8–2.2 s. Actual transmission intervals for the V9 tags were 1.800–2.1750 s with an average of 1.9875 s. V9 tags at moorings 9 and 10 operated throughout the deployment period but the tags at moorings 11 and 12 failed on 16 July 2022 and 1 August 2022, respectively.

Moorings were deployed during 5–6 May 2022. The SUBS at mooring 3 re-surfaced immediately following deployment. The hull of the SUBS was deformed and scuffed, and the attachment for its mooring assembly (anchor and riser chain) had sheared from the fiberglass strong-back that held the acoustic release. The most likely explanation was that the anchor of mooring 3 had fallen into a deep crevasse that was too narrow for the SUBS to follow.

An initial estimate of each mooring deployment position was obtained from the deployment vessel's GPS at the time that the mooring was released overboard from the stern. The estimate of the mooring position had uncertainty due to the vessel's GPS being located 10.4 m forward of the stern and vessel heading being variable and uncertain when the mooring was released. To refine the deployment position, Columbus V990 GPS loggers were placed on each side of the stern deck, and another was used to mark the time at which a mooring was released overboard.

Of the 11 moorings successfully deployed, 10 were recovered on 6 September 2022 with receivers in good working order. The acoustic release at mooring 5 did not respond to the deck unit. On 18 September 2022, the SUBS from mooring 5 washed ashore near Harbourville, Nova Scotia, and was promptly recovered with its chain riser still attached to the acoustic release. The VR2W receiver had broken off the SUBS and was lost, but the HR2 was still attached and its data were successfully downloaded. The last time the HR2 at mooring 5 detected HR signals from neighboring moorings was 13 August 2022 00:55:41, so it must have become detached from its anchor weight at about that time.

HR2 clocks were set relative to UTC shortly before mooring deployment and shortly after mooring recovery when data were downloaded. The clock sets enable linear clock skew to be corrected by Innovasea software as a part of the data download. Over the deployment period for the 11 HR2 receivers that were recovered, linear time offsets ranged from −172 s to 161 s, with a mean of −80 s and a root mean square of 132 s. Provided a pair of HR2 receivers could detect each other's HR transmissions, their separation range was calculated, and their clocks were synchronized to each other [13].

2.2. Short-Term Drifts (STDs)

Short-term drifts (STDs) comprised many (n = 62) brief drifts during spring flood tides in order to determine how well HR tags could be detected as they passed over the array of HR2 receivers deployed in the TED area. A pole float was convenient for quick and easy handling during drifter deployment and recovery.

A Columbus V-990 GPS logger was fixed to the top of the pole float and logged GPS positions every second. Beneath the sea surface, the pole-float drifter was configured with four V9 170 kHz HR tags placed at 3 m, 8 m, 16 m, and 26 m subsurface depths. The V9 tags transmitted an HR signal every 1.8–2.2 s. An HR2 receiver was suspended at 21 m depth with its hydrophone sensor pointing downwards and configured to record temperature and instrument tilt every 60 s. A V16 69 kHz PPM tag was attached at 27 m subsurface and

transmitted every 10 s. A 4.7 kg lead weight was attached 28.5 m subsurface to vertically align equipment within the water column.

The STDs were conducted using a 6 m rigid-hull inflatable boat (RHIB) that was fitted with a 110 hp outboard engine. Experiments were conducted during relatively calm weather (forecast wind either light or up to 5 ms^{-1} and directed with the tidal current) and timed to coincide with large spring tides so tests could be conducted during elevated tidal current speeds. Although the pole-float drifter was not drogue, the fast tides and light winds ensured that drifter movement was a good approximation to that of the top 28 m of the water column. Most measurements were made on and about peak flood tide because these were the conditions for which we had least confidence in the reliability of the previously measured detection efficiency [13].

The operating procedure was to deploy the drifters about 800–1000 m upstream of the moored receivers and begin recovering them after they had drifted 600 m past the receivers. Deployment was swift and easy, so drifters were almost always safely set and the research vessel's engine turned off before the drifter had approached within 500 m of the moorings. Recovery was laborious and time-consuming, which limited how many drift tracks could be achieved in a day. The onset of wind or fog shortened some working days. Drifts were conducted on 13 June (n = 16), 15 June (n = 15), 16 June (n = 6), 17 July (n = 16), and 18 July (n = 9).

The HR2 suspended beneath the STD operated over short time periods, and clock sets gave linear time offsets of −5.5 s over the June experiments and −3.9 s over the July experiments. When signals from the drifting HR2 were detected by moored HR2 receivers, it was possible to synchronize clocks between the moorings and drifter.

2.3. Long-Term Drifts (LTDs)

The long-term drifters were designed so they could be tracked remotely using either a web browser or an application (app) on a smartphone or tablet. Drifters suspended HR tags and were usually deployed so that they would settle onto quasi-stable trajectories that passed over the moored HR2 receivers [14]. When drifters went off track, they could be located using the app and recovered or redeployed using the abovementioned RHIB.

Three long-term drifters were constructed. Each drifter consisted of a surface float, a 1.8 m by 2.45 m window shade drogue centered at a 6.3 m depth, and a long trailing line that held instruments and terminated at a 7 kg steel weight. The surface float was constructed from 38 mm ABS pipe and standard plumbing fittings with flotation fashioned from 50 mm boards of extruded polystyrene foam. Batteries and electronics were assembled on a length of ABS and slid into the ABS pipe.

The electronics package consisted of a Tractive® GPS LTE dog tracker, a Columbus V-990 GPS logger, and a buck converter that supplied 5V DC via USB connectors. Tractive® enabled remote tracking but provided position measurements at irregular intervals, ranging from a few minutes to many hours depending upon the cellular network. Columbus V-990 logged GPS positions every second but had to be physically recovered to download data. The buck converter could provide 5V-USB to instruments from an 8–24 V D-cell stack.

The Columbus GPS logger prematurely stopped logging during some early LTD drifts because an inappropriate USB cable was used to connect with the buck converter. This problem was solved by using the USB cable that was sold with the Columbus GPS logger.

2.4. Tidal Current and Surface Elevation

Using drifters that carry both acoustic tags and GPS loggers has the advantage of providing current information that coincides with the detection of tags by moored receivers. Nevertheless, the detection efficiency that we aimed to test was formulated as a function of current speeds that were calculated using the FVCOM hydrodynamic model [4,13,23]. Tidal currents and sea surface elevation have been simulated for the Bay of Fundy, and the present work utilizes values saved at 10-min intervals at each of the mooring positions.

Modeled tidal elevation was used to obtain the vertical part of tag–receiver separation so that the slant range could be calculated.

3. Results

3.1. STD Tracks and FVCOM Current

A total of 62 drift tracks were made during large spring tides: 37 during June and 25 during July flood tides. Figure 2 shows the portion of each track that was kept for analysis. Six tracks were measured on the 15 June ebb tide, and the remainder were measured during flood tides. Ebb tide tracks are more zonal than flood tracks, consistent with centrifugal effects as the flood tide enters Minas Passage [14]. Except near the turn of the tide, drifter tracks take a fairly straight path across the line of moorings. Smaller-scale variability in the track is probably associated with flow over variable bathymetry (Figure 1) and turbulent "boils", which intensify with tidal current speed.
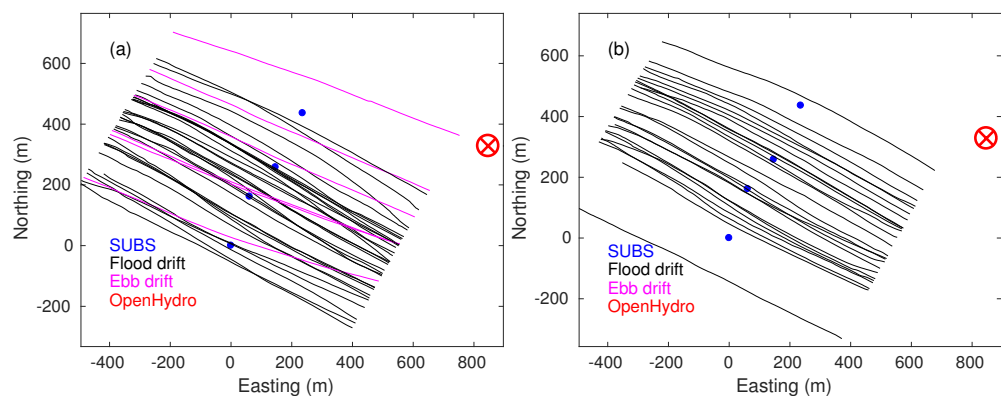

Figure 2. STD tracks. Positions of moorings 9–12 are marked with blue dots. Black lines show flood tracks. Ebb tracks are magenta. Tracks were measured on (**a**) 13, 15, and 16 June 2022 (n = 37) and (**b**) 17 and 18 July 2022 (n = 25).

HR signals are only expected to be detected in the mid portion of the plotted tracks, near where they most closely approach a moored HR2 receiver (Figure 2). With that in mind, each track can be characterized relative to a mooring by the time of closest approach, t_{ca}; the slant range of closest approach, r_{ca}; and signed drifter speed, s_{ca}, at the time of closest approach. Signed drifter speed is defined herein as positive on the flood tide and negative on the ebb tide. Drifter velocity was computed from drifter positions 10 s before and after t_{ca}.

Previously measured detection efficiency [13] was expressed as a function of signed current speed at the position of the detecting mooring, so it is germane to compare drifter current with FVCOM simulated current. For each of the 62 drifts, the signed current speed, s_{FV}, was obtained from FVCOM simulated current at the mooring, m_{ca}, most closely approached and at the time of closest approach. Regressing s_{FV} against the corresponding s_{ca} gives:

$$s_{FV} = as_{ca} + b, \tag{1}$$

where $a = 0.87$ (95%CI 0.84–0.89), $b = 0.14$ ms^{-1} (95%CI 0.04–0.25), and R-square is 0.99. Caution is warranted because few ebb tides were measured, but it is quite clear that drifters move faster than FVCOM simulations would suggest during flood tide in the TED area. FVCOM currents were vertically averaged over the water column and the pole-float drifter extended from about 1.5 m above the sea surface to a depth of about 29 m.

3.2. Mooring Separation, Synchronization, and Depth

Figure 1 plots the estimated deployment positions for moorings and shows the depths at these positions. There is a possibility that moorings may move during the experiment due to drag and lift forces exerted on the SUBS. A change in the separation of moorings

can indicate the extent of mooring movement, as can a change in depth and a change in HR signals reflected from a nearby object [13].

When two HR2 receivers can detect each other's transmissions, then it is straightforward to calculate their separation and synchronize their clocks [13]. Similarly, an HR2 can be treated as an inverted echosounder in order to measure the distance below the sea surface, which must then be detided to find depth [13]. HR2 separation ranges were essentially constant with respect to time for each of the following pairs of moorings: 1–2, 4–5, 5–6, 6–7, and 9–10 (Table 1). Furthermore, HR2 depths at sites 1, 2, 4, 5, 6, 7, 9, and 10 did not substantially change with time, so it is safe to conclude that these moorings did not move to any meaningful extent (except for mooring 5 breaking free on 13 August). Moorings at sites 8, 11, and 12 moved, but the depth changes were not great.

Table 1. Separations between moorings.

Mooring Pair	Separation (m)	Dates (2022)	Depths (m)
1–2	166	7 May–6 September	66.3, 69.2
4–5	209.5	7 May–14 May	59.3, 59.9
4–5	209.4	14 May–13 August	60.0, 59.9
5–6	106	7 May–13 August	59.9, 61.1
6–7	206	7 May–6 September	61.1, 52.8
7–8	123	7 May–14 June	52.8, 49.7
7–8	132	18 June–17 July	52.8, 49.6
7–8	135	19 July–12 August	52.8, 50.4
7–8	137	13 August–6 September	52.8, 50.7
8–9	190	7 May–12 May	50.0, 48.4
8–9	193	14 May–14 June	50.0, 48.4
8–9	200	19 June–17 July	49.6, 48.4
8–9	206	19 July–6 September	50.5, 48.4
9–10	182	7 May–6 September	48.4, 34.8
10–11	133	7 May–15 May	34.8, 34.1
10–11	152	19 May–14 July	34.8, 34.9
10–11	174	17 July–6 September	34.8, 35.7
11–12	211	7 May–15 May	34.1, 34.9
11–12	232	21 May–14 July	34.9, 34.8
11–12	230	17 July–6 September	35.7, 34.9

Pairs of HR2 receivers (sites 9–10, 10–11, and 11–12) were synchronized. Given that all adjacent pairs could be synchronized, it is straightforward to obtain the time corrections that will synchronize HR2 receivers at sites 10, 11, and 12 with the HR2 at site 9 (Figure 3). Usually, the dominant term for the nonlinear time correction is quadratic, so we were surprised to observe an abrupt 1 s jump for the HR2 clock at site 12. Site 12 is nearest to a highly turbulent area associated with Black Rock, a small island close to the northeast corner of the TED area. It is possible that the SUB at site 12 became unstable and crashed into the seafloor, perhaps causing an interruption of the power supply. Alternatively, Innovasea suggested that infrequent 1 s clock jumps were a feature of some early HR2 models, but changes to firmware are thought to have eliminated that problem. Regardless, this clock jump cannot be dismissed as "a bad data point" because all the following estimates of time correction are consistent, and they are all calculated from independent measurements.

The time corrections in Figure 3 are two orders of magnitude smaller than the linear clock skew that Innovasea software automatically corrects for when data are downloaded. Synchronizing an array of HR2 receivers is useful if that array were to be used for localizing the position of a passing tag, but this is not sufficient to relate HR signals detected by moored HR2 receivers to the concurrent position of the STD.
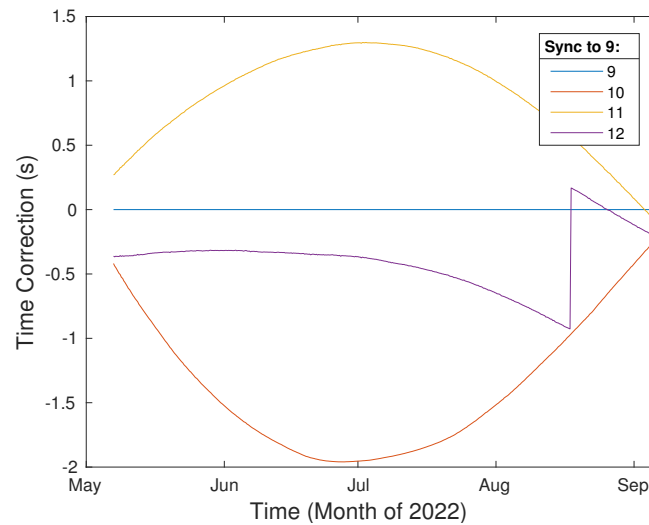
Figure 3. Nonlinear offset to synchronize receivers at stations 9 through 12 to the receiver at station 9.

3.3. Synchronizing Moored HR2 Receivers to the STD

The requirement is to use time as a parametric variable in order to match a detected signal to the concurrent position of a drifter. Drifter positions are synchronized to UTC, so the task is to synchronize the array of HR2 receivers (at moorings 9–12) to UTC. Our method requires an assumption that will turn out to be justified by the outcome.

Short-term drifts were conducted for a few days in June and a few days in July. The HR2 carried by the drifter operated over short periods between clock sets, and the corrections for linear clock skew were only -5.5 s and -3.9 s for the June and July experiments, respectively. Assume for a moment that the uncorrected nonlinear drift would have been much smaller than linear clock skew so that the HR2 suspended beneath the drifter records detected HR signals to within a fraction of a second of UTC. The suspended HR2 detects the HR tag suspended 5 m below it very well. Drifts 11 and 31 occurred within the first pair of time sets (i.e., June experiments), and during these drifts, the HR2 at mooring 9 also detected the suspended tag. The intervals between the tag transmissions are variable, so by lining up the pattern of detection times measured by the HR2 on the drifter with the pattern of detection times measured by the HR2 at mooring 9, we can synchronize the HR2 at mooring 9 to the HR2 suspended by the pole float. In this way, all clocks become synchronized to UTC within a fraction of a second. (Signal time of travel is small enough to be ignored for present purposes). Drifts 54 and 55 can similarly be used to synchronize HR2 receivers for the July experiments.

Table 2 shows how much the HR2 at mooring 9 needed its time advanced in order to match the times of the HR2 attached to the pole float/UTC. The time advance is small compared with the linear clock skew (root mean square, 132 s) over the duration of HR2 moorings, so it was fair to assume that data downloaded from the HR2 suspended on the drifter would have matched UTC to within a fraction of a second. It is noteworthy that Table 2 indicates nonlinear time drift that is common to the four HR2 receivers and that this is large when compared with the differences between receivers (Figure 3). More relevant for our present purpose, not accounting for the time increment in Table 2 would correspond to a 4 ms^{-1} current causing about 60 m error when aligning drifter position with times that signals are detected.

Table 2. Time corrections to add to the HR2 at mooring 9 in order for it to match the HR2 receiver suspended below the pole-float drifter.

Drift Number	Date	Time Correction (s)
11	13 June 2022	16.75
31	15 June 2022	16.45
54	18 July 2022	15.5
55	18 July 2022	15.5

Figure 4 shows HR signals detected at various ranges along drift tracks. Upwards propagating signals travel from the moored tag to the drifting HR2 and downwards signals from the 25 m tag on the drifter to the moored HR2. With a 3.46 ms^{-1} flood current, both upward and downward HR signals are detected over many ranges. When the flood current is 4.92 ms^{-1}, the signals are detected at relatively small ranges (up to 69 m in Figure 4b). Using (1), the corresponding FVCOM speeds would be 3.15 ms^{-1} and 4.42 ms^{-1} for which interpolating from earlier work [13] gives detection efficiencies of 0.75 and 0.09 in a 75 m range, respectively. Consistent with low detection efficiency and reasonably accurate synchronization to UTC, most detected signals are clustered near the range of closest approach in Figure 4b.
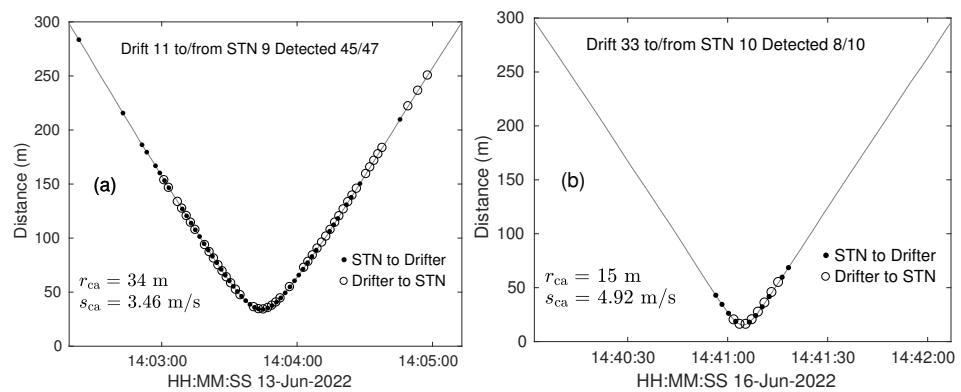

Figure 4. Signals detected as a function of distance and range along STD tracks. (**a**) Many signals are detected at moderately high current speed. (**b**) Fewer signals are detected at very high current speed.

3.4. Number of STD Tracks Detected by the Receiver Array

Of the tagged fish that pass through the TED area, it is of particular interest to know what fractions are expected to be detected by the moored receiver array. This question can be addressed by asking how many of the tagged STD drifts were detected. Given that the STD carried HR tags at four subsurface depths, we can also address the question as to whether or not the swimming depth of a tagged fish matters for signal detection.

STD tracks were always detected when current speed was low, so let us select the 45 fast tracks that had $|s_{ca}| > 3.5$ ms^{-1} for more detailed analysis. For each drift, we counted the number of times, N_{DA}, that each tag was detected by the array of moored HR2 receivers. Thus, for a given tag, we construct an $I = 45$ element vector $\vec{N}_{DA} = (N_{DA1}, N_{DA2}, \cdots, N_{DA45})$ containing the number of times the tag was detected during each of its 45 drifts. Counting the number of drifts for which the array detected a specific tag at least once gives the number, N_{PEDA}, of passing events detected by the array

$$N_{PEDA} = \sum_{i=1}^{I} \min(N_{DAi}, 1), \tag{2}$$

as recorded for each tag in the first row of Table 3. Of the 45 fast drifts that passed the HR2 array, 44 were on the flood tide.

Fewer drifts were detected by a tag nearer the sea surface (Table 3). In part, this may be because the HR2 receivers were on the seafloor, so a tag is a little further away if it is near the sea surface. During spring flood tides, visual observations have been made of tidal eddies that generate localized, breaking surface waves near strong convergence at the edge of the eddy. It is possible that bubbles are entrained well into the water column and that these may make it more difficult for near-bottom receivers to detect near-surface tags. Another mechanism is the possibility that an HR signal taking a direct path might interfere with its reflection from the sea surface. The time lag between direct and reflected paths is

$$\delta t = \frac{1}{c}(\sqrt{H^2 + (D_X + D_R)^2} - \sqrt{H^2 + (D_X - D_R)^2}), \tag{3}$$

where H is the horizontal distance from a transmitter at depth D_X to a receiver at depth D_R. Considering the typical values for the tag closest to the sea surface ($H = 50$, $D_X = 3$, $D_R = 34$) gives a 2.2×10^{-3} s time lag, so the reflection and direct signal will partially overlap in the received signal, given the 6×10^{-3} s duration of an HR signal. HR tags encode identity using a sequence of phase shifts [13], and signals are not recorded as detected unless they have also been identified.

Table 3. Out of the 45 fast ($|s_{ca}| > 3.5$ ms^{-1}) STD passing events, we tabulate the number of passing events (N_{PEDA}) for which a tag at a given depth was detected by the HR2 array.

τ (s)	3 m Tag	8 m Tag	16 m Tag	26 m Tag
2	39	38	42	44
4	36	37	40	42
8	31	34	34	39
16	22	25	26	34
32	14	17	17	21
64	7	10	10	13

Each of the four tags had an average transmission interval of $\tau = 2$ s. If the tags had been programmed for a T s transmission interval, then the number of transmitted signals would be reduced by a factor of τ / T, so the expected number of detected signals, $_eN_{DAi}$, during the ith drift (past the array) would be reduced by the same factor

$$_eN_{DAi} = \frac{\tau}{T}N_{DAi}, \tag{4}$$

and the expected number of detected drifts would be

$$_eN_{PEDA} = \text{nint}\left(\sum_{i=1}^{I} \min(_eN_{DAi}, 1)\right). \tag{5}$$

As the transmission interval is increased, successive rows in Table 3 show that fewer drifts will be detected by the receiver array. With $\tau = 2$ s, about 15% of near-surface tags will not be detected as they drift by in >3.5 ms^{-1} currents but, at greater depth, only 2–6% would not be detected. Thus, the great majority of fish carrying $\tau = 2$ s tags would be detected, and a first-order estimate of the probability of encounter might be achievable and might be prorated for the small fraction that passes by without being detected. Reducing τ is expected to improve performance, but further measurements would be required in order to quantify by how much.

The STD experiments included a 27 m subsurface V16 69 kHz PPM tag that transmitted every 10 s. Due to mistakes in the field, this tag was only turned on for 55 of the 62 drifts. Although the V16 tag was powerful (158 dB), it was only detected for 29 of the 55 tracks, and these tracks were usually slow $1.6 < |s_{ca}| < 4.3$ ms^{-1} (mean 3.3 ms^{-1}). The 69 kHz PPM tag was not detected for 26 fast tracks where current speeds were $4.3 < |s_{ca}| < 5.1$ ms^{-1} (mean 4.6 ms^{-1}). For the two STD tracks with $|s_{ca}| < 2$ ms^{-1}, the 69 kHz PPM tag was

detected by VR2W receivers at 8 and 9 of the 11 mooring locations. The detection of 69 kHz PPM tags at a great range was expected when current speed was low [24], and this strongly contrasts with the poor performance observed in fast currents. Usually, the interval between PPM signals is much larger than 10 s, for fear of interference when more than one tag is present. A transmission interval of 60 s would be more typical, and in this case, it should be expected that only 21 of the 55 passing tracks would have been detected. For measuring the probability of fish–turbine encounter, PPM tags are deemed inadequate in the TED area.

3.5. Comparison of Detection Efficiencies at the TED Area

The present line of moored HR2 receivers and tags can be used to obtain estimates of detection efficiency, which can be compared with those previously reported [13]. Previous measurements were sometimes called into question because there were good physical grounds for the possibility that variable bathymetry blocked signals, even though bathymetry and signal paths could not be sufficiently resolved to determine where the signal was blocked [13].

Figure 1b shows that moorings 8 and 9 are on high ground relative to the path between them. On the other hand, the path from moorings 9 to 10 is most certainly blocked by the edge of the volcanic plateau. To make a comparison between these paths, we consider how the HR tag at mooring 9 is detected by HR2 receivers at moorings 8 and 10. Figure 5a shows that from 19 July to 6 September, the detection efficiency along the 9–8 path was very similar to that previously obtained [13] by eliminating measurements that were thought to be blocked. There was some mooring movement at site 8, but similar results were obtained during other time intervals when separation between moorings 8 and 9 was stable (Table 1). If anything, when currents are slow, the signal detection is more efficient than had previously been measured. On the other hand, the obvious blockage caused by the edge of the volcanic plateau causes detection efficiency to be extremely poor for signals propagating from mooring 9 to mooring 10 (Figure 5b). These results provide a little more confidence in the detection efficiencies obtained by [13] and also indicate that they apply immediately to the south of the TED area.
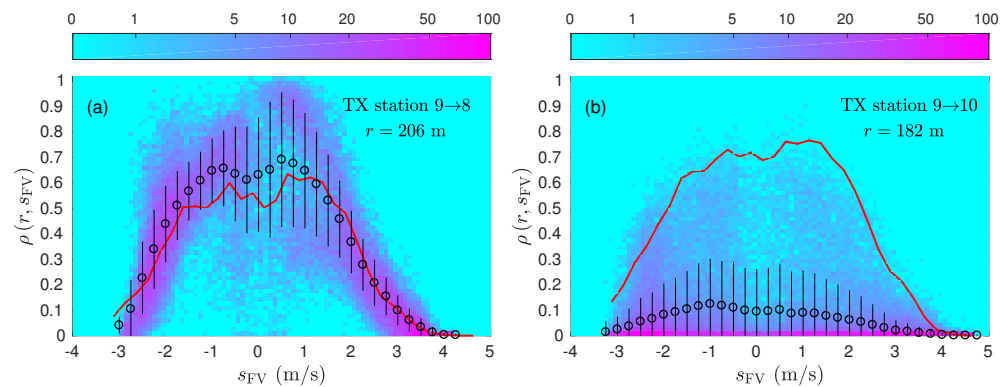

Figure 5. Average detection efficiencies are plotted as functions of s_{FV}, with black circles and lines indicating $\pm$ SD. Signals from the HR tag at mooring 9 are detected by (**a**) the HR2 at mooring 8, (**b**) the HR2 at mooring 10. For corresponding ranges, the red lines show detection efficiencies measured in 2022. The distribution of detection efficiencies calculated from 2 to minute intervals is shown using a logarithmic color scale. The distribution was normalized to a maximum value of 100 per ρ-s_{FV} bin.

The four SUBS used to monitor the TED area (i.e., moorings 9–12) carried an HR tag on the tail fin and an HR2 mounted inside the streamlined hull, so this enabled detection efficiency to be estimated as a function of FVCOM current, s_{FV}, when the range was about 1 m. Detection efficiency varied from 0.997 to 1.000 and, thus, can be considered effectively 1 for all current speeds observed at the TED area. This confirms the previous result [13],

which was based on more tenuous evidence (an HR signal with a fake identity) and a complicated line of reasoning.

3.6. Number of HR Signals Expected to Be Detected during a Passing Event at the TED Area

Define a *passing event* as a tagged drifter (or tagged fish) passing a moored HR2 receiver. For present purposes, passing events of interest result from the drifter (or fish) being advected by fast tidal currents. Tagged drifter measurements enable direct measurement of the number, N_D, of HR signals detected by a specific HR2 receiver during a passing event. In our study, the drifter tracks follow a straight line to a reasonable approximation (Figure 2), so $N_D(r_{ca}, s_{ca}, \tau)$.

We expect that an estimate N_E for N_D could be calculated from detection efficiency [13]. Let the position of the drifter relative to an HR2 be a function of time $(x(t), y(t), z)$, such that range from drifter to HR2 is also a function of time, $r(t) = \sqrt{x^2 + y^2 + z^2}$. Then, the number of HR signals that are expected to be detected during a passing event is found by integrating along the passing track as follows:

$$N_E(r_{ca}, s_{ca}, s_{FV}, \tau) = \frac{1}{\tau} \int \rho(r(t), s_{FV}) dt. \tag{6}$$

A comparison of N_E with N_D requires that the position of the moored HR2 receiver be accurately known. At the TED area, recall that only moorings 9 and 10 did not move (Table 1). For each of the tag-passing events, begin by comparing the number of HR signals detected by the array, N_{DA}, comprising receivers at moorings 9 and 10 with the number expected to be detected, N_{EA}. Summing over the 44 tracks that had $s_{ca} > 3.5$ ms^{-1}, the number of HR signals detected from each tag, $\sum N_{DA}$, it is evident that near-surface tags are detected much less frequently than the deeper tags (Table 4). However, tag depth has only a small effect on the number of signals expected to be detected, $\sum N_{EA}$, by the array. The above calculation of N_E, and thence N_{EA}, does not take into account the possibility of interference due to the signal being reflected from the sea surface. These three facts indicate that interference by reflected HR signals (3) can reduce the chances that a near-surface tag will be detected (e.g., Table 3).

It is notable that the expected number of detected signals is greater than the number actually detected (Table 4). Such overestimation might happen because the range testing [13] obtained few measurements during the fastest currents and because errors in FVCOM modeling can sometimes assign detected signals to fast currents when they were actually detected in slow currents for which detection efficiency is higher. Furthermore, some signal paths to the HR2 at mooring 9 may have been blocked by the edge of the volcanic plateau (Figures 1b and 5b).

Table 4. Comparison of number of signals detected by an array, N_{DA}, with number expected, N_{EA}, at each tag depth. Measurements are from 44 fast flood drifts at the TED area. N_{PEDA} is the number of passing events detected by the array, and N_{PEEA} is the number that was expected to be detected. The rows labeled $_{0.78}N_{PEEA}$ and $_{0.43}N_{PEEA}$ show values of N_{PEEA} obtained when N_{EA} was rescaled by factors of 0.78 and 0.43, respectively.

	2.25 m Tag	9 m Tag	19 m Tag	28 m Tag
$\sum N_{DA}$	127	185	214	270
$\sum N_{EA}$	295	308	325	344
N_{PEDA}	26	28	28	26
N_{PEEA}	33	33	33	33
$_{0.78}N_{PEEA}$	32	32	33	33
$_{0.43}N_{PEEA}$	29	30	31	31

Of the 44 passing events, we can use (2) to determine the number of passing events that were detected by the array (N_{PEDA}), and similarly, the number of passing events that were expected to be detected by the array

$$N_{\text{PEEA}} = \sum_{i=1}^{45} \min(N_{EAi}, 1). \tag{7}$$

Comparing N_{PEDA} with N_{PEEA} (Table 4) shows that fewer tracks were detected than expected. Note that this cannot be accounted for by simply adjusting the values of N_{EA} to reflect the depths of the drifting tags. Rescaling N_{EA} by a factor of 0.78 (consistency with the 28 m tag) did not bring the expected number of detected tracks into alignment with the measured number. Even rescaling N_{EA} by a factor of 0.43 (consistency with the 2.25 m tag) does not sufficiently change the expected number of detected tracks.

In addition to "downward" paths from the drifting tags to the moored HR2 receivers, there were also "upward" paths from the moored tags to the HR2 receiver that was suspended at a 21 m depth (5 m above the lowest tag suspended by the drifter). Let us now consider the upward paths from moorings 9 and 10 along with downward paths from the two lowest tags on the drifter to moorings 9 and 10. Selecting the 44 passing events with $s_{\text{ca}} > 3.5$ ms^{-1}, it is confirmed that N_E generally declines with increasing r_{ca} (Figure 6), although there is a good deal of scatter, some of which might be associated with s_{ca} varying from track to track. Each downward path had a similar upward path.
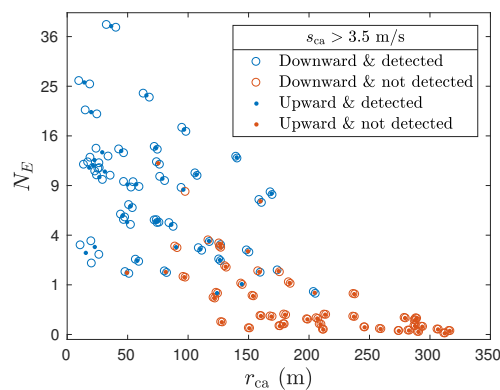

Figure 6. The expected number of detected signals, N_E, declines with increasing slant range of closest approach, r_{ca}. Only the 44 STD tracks with $s_{\text{ca}} > 3.5$ ms^{-1} are included.

Figure 6 stratifies N_E into those for which the corresponding measurement obtained $N_D > 0$ (blue) and those for which $N_D = 0$ (red). HR2 receivers did not detect HR signals when nint(N_E) = 0, but there are a problematic number of occasions when nint(N_E) is considerably greater than 1, and yet, no signals were detected by the HR2 receiver. (The operator nint(x) gives the nearest integer to x). To see the issue more clearly, Figure 7 plots the number of detected signals, N_D, as a function of the number expected nint(N_E). Clearly, sometimes more signals are detected than expected and sometimes fewer. One might expect that sometimes no signals are detected when several are expected, but it is very odd that it never happens that a few signals are detected against an expectation that none are expected. Rescaling N_E so that $\sum N_E = \sum N_D$ (e.g., Table 4) made no difference. This unexpected asymmetry of Figure 7 points to something being wrong about the calculation made using (6).
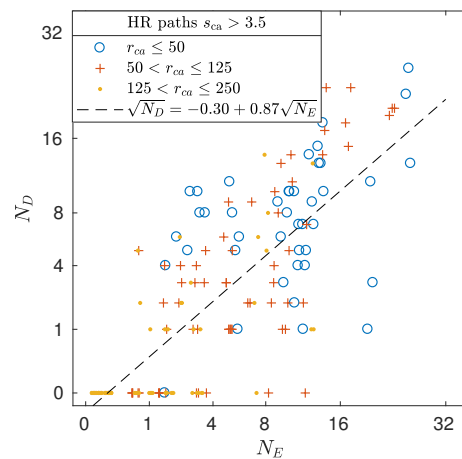
Figure 7. Number of detected signals for STD passing events plotted as a function of the number expected.

Equation (6) uses an empirical functional form $\rho(r, s_{\text{FV}})$ for detection efficiency in the sense that each black circle in Figure 5 represents an average of a cloud of many detection efficiencies calculated from many 2-min time intervals. Rather than plot each 2-min detection efficiency, Figure 5 uses color to represent their distribution on the ρ–s_{FV} plane. Clearly, detection efficiency is a fluctuating variable relative to its long-term average. If s_{FV} accurately resolved the local current, including turbulent eddies, then some portion of the variability in Figure 5 would likely be resolved within the function, $\rho(r, s_{\text{FV}})$, but there would still be variability about $\rho(r, s_{\text{FV}})$ because the local sound level is only related to current speed in a statistical sense. In reality, FVCOM does not perfectly model tidal currents, let alone accurately resolve turbulent eddies.

Representing the fluctuations of detection efficiency as $\rho'(t)$ gives

$$N_E + N_E' = \frac{1}{\tau} \int \rho(r(t), s_{\text{FV}}) + \rho'(t) dt. \tag{8}$$

Both ρ' and N_E' average to zero for a sufficiently large ensemble, but tag signals may only be detected for 30 s (or less) during a passing event (Figure 4). A fluctuation, $\rho'(t)$, cannot be expected to be totally independent of the fluctuation, $\rho'(t - \delta t)$, shortly before. Such correlation has implications for the detection of passing events. Fluctuations in $\rho(r, s_{\text{FV}})$ will not change the total number of signals detected over a large number of passing events, but correlations will distribute these detections differently among passing events. Where correlations cause a drifter track to be detected more often than for uncorrelated fluctuations, it will still be counted as the detection of a single passing event. Where correlations cause a drifter track to be detected fewer times, a passing event might be shifted from being detected to not being detected. Mathematically speaking, if $N_{E,i}$ signals are expected to be detected along the ith drift track, then the calculation of the number of passing events (tracks) that are detected, N_{PED}, involves a highly nonlinear operator

$$N_{\text{PED}} = \text{nint}\left(\sum_i \min(N_{E,i})\right). \tag{9}$$

So, including fluctuations, $N_{E,i}'$, will change the outcome. Thus, $\rho(r, s_{\text{ca}})$ is not sufficient in and of itself to calculate whether or not a passing event is expected to be detected and will tend to overestimate the number of passing events that are detected.

3.7. LTD Tracks and FVCOM Current

LTD tracks mostly pass near the middle of Minas Passage. Figure 8 shows a quasi-steady track (black) that passes repeatedly through the mid-channel of Minas Passage when

tides are running fast. Other quasi-steady trajectories have been identified [14], but they are of less interest to the present project because either they do not enter Minas Passage or they arrive at the study site near the low-water slack tide. Tracks that pass through the TED area have more variable trajectories over subsequent tidal cycles, as shown by the orange trajectory in Figure 8 and as reported for other trajectories [14]. As a result, LTDs are mostly suited for measuring how well passing events are detected to the south of the TED area.
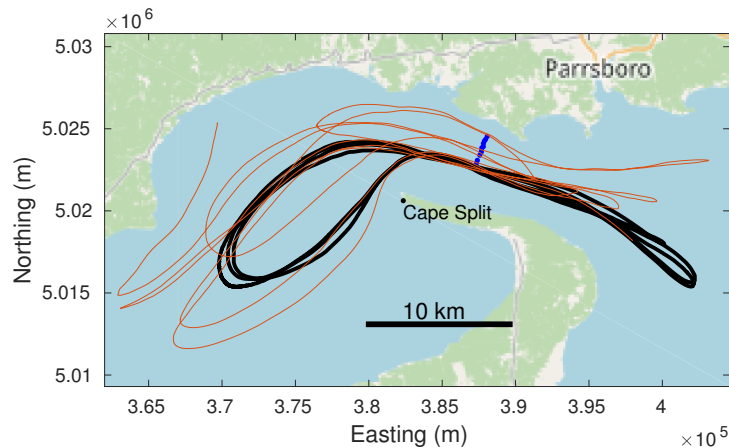
Figure 8. Two LTD tracks. A quasi-steady track (black) frequently passes near the southern end of the line of moored receivers (blue). A highly variable track (orange) sometimes passes through the northern end of the receiver line.

For the present analysis, we will only be concerned with the LTD passing events that crossed an extended line through the array of HR2 receivers. Sometimes, an LTD crossed the line, but GPS position measurements were too infrequent for accurate analysis. Of the remaining LTD passing events, 103 were measured on the flood tide and 114 on the ebb tide (Figure 9). Each LTD carried four tags, and the receiver array detected at least one of those tags for 81 passing events on the flood tide and 57 on the ebb tide. These detected passing events are colored blue in Figure 9. On the flood tide, centrifugal effects associated with inflow around Cape Split [14] tend to cause passing events to be distributed more to the north than during ebb tides (Figure 9).
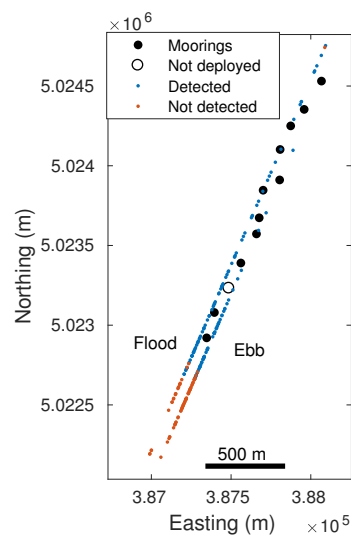

Figure 9. Dots indicate where LTD tracks crossed the mooring line, with flood crossings displaced to the left and ebb crossings displaced to the right. Blue dots indicate passing events that were detected by the array of HR2 receivers and orange dots indicate passing events that were not detected.

Figure 10 compares signed current speeds, s_{ca}, obtained at LTD passing events south of mooring 6 with the corresponding values of s_{FV} obtained from the FVCOM simulation. In the TED area, FVCOM underestimated STD current speed by about 13% (1), whereas in deeper waters to the south, FVCOM underestimates LTD current speed by about 24%. Some of this difference may be attributable to the LTD being drogue at about 6.3 m depth.

The energy-containing turbulent eddies are not resolved by FVCOM but they are a part of the drifter motion so they are expected to appear within the residuals in Figure 10. It is particularly noticeable that residuals show much more scatter about the fitted line on the flood tide than on the ebb tide (Figure 10). On the ebb tide, the mid-channel current is well collimated, whereas on the flood tide, there is substantial cross-channel movement associated with a strongly rotational flow around Cape Split (Figure 8). Turbulence is expected to be less in a collimated flow than in a strongly rotational flow, consistent with the pattern of residuals.
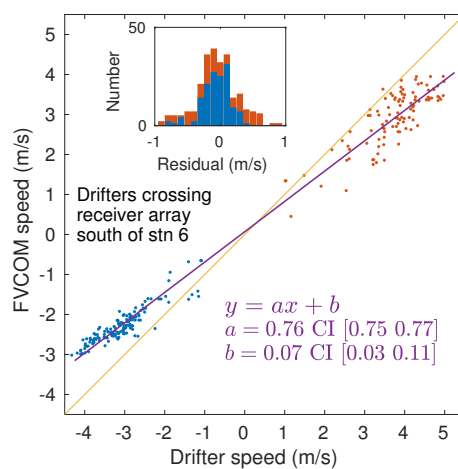

Figure 10. For each crossing that is south of mooring 6, the signed speed of the drifter, s_{ca}, is compared with the value obtained from the FVCOM model. A best-fit linear regression is plotted (purple).

3.8. Number of LTD Passing Events Detected by the Receiver Array

When a tagged fish is detected, we know that it has passed by our receivers, but we have no way to know how many times it passed by *without* the tag being detected. On the other hand, a GPS logger shows when a tagged drifter passed by receivers regardless of whether or not the tag is detected. The blue dots in Figure 9 show 138 LTD tracks had at least one tag detected while passing within (or nearby) the HR2 array.

Of course, each LTD carried four HR tags at different depths, so the 4×138 tag-passing events should be examined before drawing quantitative conclusions about how well a tagged fish might have been detected by such an array. Analysis for this question begins by excluding those passing events that were undetected (orange dots in Figure 9) because these were simply beyond the area over which the array can monitor. It is generally understood that passing events are more likely to be detected when current speed is slow, and it should not be assumed that the detection of passing events on a flood tide will be the same as on an ebb tide. This suggests four categories to investigate: slow flood, slow ebb, fast flood, and fast ebb.

The LTD passed the array 45 times on a fast flood tide, $s_{ca} > 3.5$ ms^{-1}. Counting the number of passing events for which the array detected a specified tag at least once gives the number of detected passing events for that tag, as shown in the top row of Table 5. None of the tags were detected on all 45 passing events, but 92% of the 4×45 tag-passing events were detected, and tags at different depths were detected similarly. Doubling the interval between transmissions (i.e., $\tau = 4$ s) did not change the number of detected passing events. Greater increases in τ reduced the number of detected passing events, and this reduction was always a little more for the near-surface (2.25 m) tag.

Table 5. Out of 45 fast flood-tide ($s_{ca} > 3.5$ ms^{-1}) LTD passing events, we tabulated the number of passing events for which tags at different depths were detected by the HR2 array. Dependence on increasing transmission interval, τ, was calculated.

τ (s)	2.25 m Tag	9 m Tag	19 m Tag	28 m Tag
2	41	42	40	42
4	41	42	40	42
8	40	41	39	40
16	35	39	37	37
32	28	34	34	31
64	18	26	27	21

Each tag was detected during 35 of the 36 slow flood passing events (Table 6). Clearly, if a tag was detected during a passing event, then it was typically detected many times because greatly increasing the interval between transmissions only caused a modest decline in the number of detected passing events. This is generally consistent with Figure 4, which shows many more detected signals for a lower speed passing event than for a faster passing event, even though the faster event more closely approached a moored receiver.

Table 6. Out of 36 slow flood-tide ($0 < s_{ca} \leq 3.5$ ms^{-1}) LTD passing events, we tabulated the number of passing events for which tags at different depths were detected by the HR2 array. Dependence on increasing transmission interval, τ, was calculated.

τ (s)	2.25 m Tag	9 m Tag	19 m Tag	28 m Tag
2	35	35	35	35
4	35	35	35	35
8	34	34	35	34
16	33	33	34	34
32	32	32	33	33
64	28	31	31	31

Ebb tide passing events (Tables 7 and 8) show similar trends to those of the flood tide (Tables 5 and 6). Generally, most tag-passing events were detected, and when compared to the STD passing events, they were also detected relatively well for moderately increased τ. Furthermore, it seems that signals reflected from the sea surface did not disrupt detection of near-surface tags for the LTD, although they did for the STD (Table 3). Many of the LTDs were detected by receivers moored at greater depths than those that detected the STD (Figure 1). All else being equal, (3) shows that the time lag between the direct signal and its reflection will be greater for a receiver at greater depths, but this is partly offset by the top tag being nearer the sea surface during the LTD, and the overall effect is not so great as to avoid interference. Previous work found that reflected signals were more likely to be detected in shallow than in deep water [13], so this might reduce interference for the near-surface tags of the LTD. Reflected signals are also less likely to be detected as significant wave height increases [13], and we note that calm conditions were selected for the STD, whereas LTD spanned a range of weather conditions.

Table 7. Out of 13 fast ebb tide ($s_{ca} < -3.5$ ms^{-1}) LTD passing events, we tabulated the number of passing events for which tags at different depths were detected by the HR2 array. Dependence on increasing transmission interval, τ, was calculated.

τ (s)	2.25 m Tag	9 m Tag	19 m Tag	28 m Tag
2	9	11	12	13
4	9	11	12	13
8	9	10	12	12
16	8	10	11	11
32	8	9	10	9
64	5	7	7	7

Table 8. Out of 44 slow ebb tide ($0 > s_{ca} \geq -3.5$ ms^{-1}) LTD passing events, we tabulated the number of passing events for which tags at different depths were detected by the HR2 array. Dependence on increasing transmission interval, τ, was calculated.

τ (s)	2.25 m Tag	9 m Tag	19 m Tag	28 m Tag
2	38	39	44	39
4	38	39	43	39
8	37	38	40	37
16	34	36	38	36
32	30	33	35	35
64	25	30	31	30

3.9. Number of HR Signals Detected by a Receiver during an LTD Passing Event

In order to use the telemetry measurements to calculate the probability of fish–turbine encounter, we could consider a moored HR2 receiver as a proxy for an MHK turbine and obtain the probability that a tagged fish would pass within a distance of the receiver that is commensurate with the projected frontal area, A_{MHK}, that the blades of an MHK turbine would sweep. Before studying tagged fish in our next paper [20], we presently use tags on drifters to evaluate whether or not a receiver detects a tag as it passes by at some range, r_{ca}, and speed, s_{ca}, at closest approach. HR2 receivers at moorings 1, 2, 4–7, and 9–10 showed no evidence of being moved, and mooring 8 did not move much. Let us, therefore, consider how receivers 1, 2, and 4–10 detected tags at 19 m and 28 m depth on the LTD.

In the TED area, Eulerian measurements of detection efficiency, ρ, did not have flood–ebb symmetry with respect to modeled tidal current, so ρ was represented as a function of signed speed, s_{FV}. The LTD provides an accurate current measurement, s_{ca}, at the time of a passing event, whereas currents from FVCOM simulations differ in various ways (Figure 10). For the LTD measurements, we found that N_D had flood–ebb symmetry with respect to measured currents and could be represented as a function of $|s_{ca}|$. It is unclear how well this symmetry in N_D applies to the TED area because the LTD mostly crossed the mooring line to the south of the TED area.

Given flood/ebb symmetry, Figure 11 groups measurements according to current speed, $|s_{ca}|$, and $\sqrt{N_D}$ is plotted as a function of r_{ca}. For $N_D > 0$, r_{ca} declines linearly with respect to $\sqrt{N_D}$. A best linear fit of $\sqrt{N_D}$ to r_{ca} was obtained for each speed group, as documented in the figure. Having measured a value of N_D from a tag on an LTD that passes by at a time when the current is within one of the plotted speed groups, the fitted equations in Figure 11 enable an estimate of its range of closest approach and the variation about that range. Similarly, evaluating r_{ca} for $N_D = 1/2$ gives a typical minimum range, λ_{LTD}, for the transition from a tag on a passing LTD being detected or not detected. λ is a key metric for calculating the probability of encounter [20].

The LTD measurements can be used to obtain the probability, p_{PED}, that a passing event will be detected by identifying which of the tag-LTD-passing events were detected by an HR2 receiver at r_{ca} and $|s_{ca}|$. Each tag-passing event is marked by a dot in Figure 12, with blue dots indicating a tag-passing event that is detected (i.e., $N_D \geq 1$) and red dots indicating an undetected tag-passing event. For each ($r_{ca}, |s_{ca}|$) bin, p_{PED} is the ratio of the number of blue dots to the number of red and blue dots. Thus, for each range–speed bin, we enumerate the percentage of tag-passing events ($100 \times p_{PED}$) that were detected in each speed-range bin of Figure 12. Repeating this exercise for the tags at 2.25 m and 9 m depth gave a similar result. For all current speeds measured by the LTD, there is an 84–100% chance that an LTD track will be detected, providing it comes within $r_{ca} < 150$ m of a moored HR2 receiver.
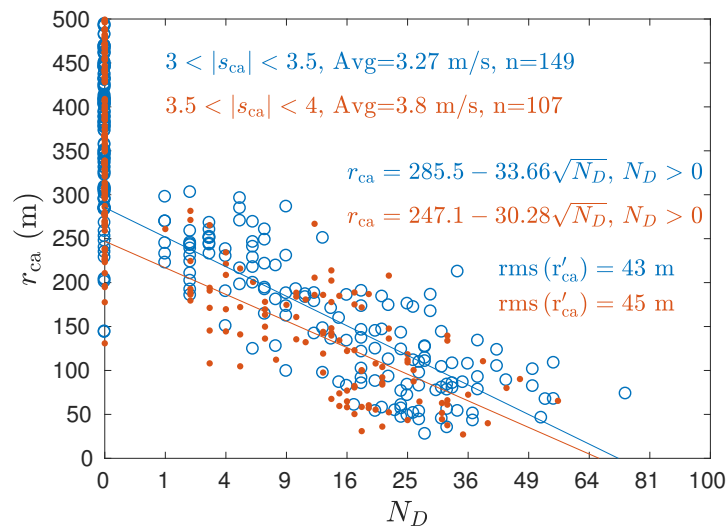
Figure 11. Relating the number of HR signals detected during am LTD passing event, N_D, to the range at closest approach, r_{ca}, for measurements grouped according to the speed at closest approach, $|s_{ca}|$. Each HR tag transmitted every $\tau = 2$ s.
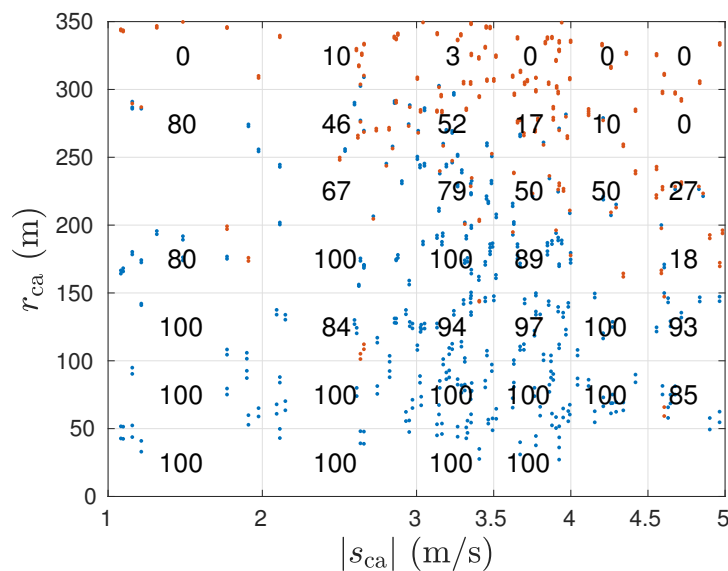

Figure 12. Percentage of tag-passing events that are detected by a moored HR2 receiver as a function of speed, $|s_{ca}|$, and range, r_{ca}, at closest approach. Here, we consider LTD of the two deepest HR tags (19 m and 28 m). Each tag transmitted every $\tau = 2$ s.

Figure 12 was obtained using HR tags that transmit every $\tau = 2$ s. The *i*th dot in Figure 12 represents a passing event for which the number of detected signals, N_{Di}, can be transformed following (4) in order to estimate how well tags are detected when fish carry tags with some larger transmission interval, T. Note that tagged-drifter experiments should use tags with small τ because (4) requires $T \geq \tau$.

3.10. LTD Comparison of HR and 69 kHz PPM

Two of the LTDs suspended a 69 kHz PPM tag (transmission interval 20 to 30 s) that was 0.5 m below the bottom HR tag (i.e., 28.5 m). For these two LTDs, we identified all tracks in which any of the five tags (four HR tags and a PPM tag) were detected. Table 9 compares the number of tracks for which the bottom HR tag was detected with the number of tracks for which the 69 kHz PPM tag was detected. Both tags were well detected at low current speed, with the 69 kHz PPM tag being detected on a few of the tracks where the

distance to a receiver was beyond the range of HR tags (Figure 9). At higher current speeds, the HR tag was much more reliable for detecting passing events.

Table 9. Number of LTD tracks for which the bottom HR and 69 kHz PPM tag were detected. Tracks are categorized according to whether the current is fast or slow on the ebb or flood tide.

# Tracks	HR Tag	PPM Tag	Current (ms^{-1})	Mean Current (ms^{-1})
28	27	28	$0 < s_{ca} < 3.5$	2.84
35	25	29	$0 > s_{ca} > -3.5$	-2.8
35	34	19	$s_{ca} > 3.5$	4.17
11	11	1	$s_{ca} < -3.5$	-3.8

4. Discussion

Using efficient MHK turbines [25] to harvest tidal energy at locations with high power density [4] is a state-of-the-art undertaking, but less intensive use of tidal energy is not a new thing [26]. Humans have exploited the energy of a turning tide ever since they began to use fishing weirs and marine craft [27]. The basic principle of a fishing weir is to collect fish that would otherwise pass by with the tide, and this is a conceptual starting point for quantifying an upper bound on the number of fish that might interact with an operating MHK turbine in Minas Passage.

If one were to replace the MHK turbine with a net that spans the same cross-current area, A_{MHK}, swept by the turbine blades, then the fish caught could be considered to approximate the number of individuals (belonging to captured species) that might pass through the operating turbine. Ecologists have similarly attempted to use active hydroacoustic devices to monitor backscatter from targets in a water volume similar to that which fluxes through A_{MHK}, but it has not proven possible to enumerate individuals or identify species from the backscatter observed in Minas Passage [18]. Optical cameras provide much higher resolution [28], and visibility may be sufficient in Minas Passage for cameras to identify a subset of those fish that an active hydroacoustic device detected upstream as backscatter.

It would be most useful if the above Eulerian methods successfully measured the number of individuals (for some species) that might encounter a MHK turbine, but this would still leave outstanding issues. From a population point of view, what matters is not so much the number that encounters an MHK turbine, but rather the proportion of a local population that encounters an MHK turbine. This proportion is difficult to calculate from catch/backscatter numbers because the local population number is not known for any of the species captured [9]. Furthermore, sometimes two fish belonging to the same species may belong to different populations [11]. Such difficulties can be resolved by using acoustic tags [10,11] to track individuals belonging to a known population, which amounts to measuring in the Lagrangian frame [15]. Tagging studies have been published for striped bass of Shubenacadie River origin [10]; Atlantic sturgeon that mostly originate from the Saint John River, New Brunswick [11]; and alewife of the Gaspereau River stock [29]. Lagrangian methods provide population-specific information that augments the previously discussed Eulerian methods that attempt to count all fish that pass through A_{MHK}.

It was hoped that probabilities of fish–turbine encounters could be calculated from measurements of striped bass [10] and Atlantic sturgeon [11] that carried 69 kHz PPM tags. Such calculations require estimates of detection efficiency in order to transform detected signals into estimates of abundance or a probability distribution of distance from the detecting receiver [13]. Detection range testing in Minas Passage [24] showed poor detection efficiency for 69 kHz PPM tags when current speed was fast. Another study [30] found that sturgeons carrying 69 kHz PPM tags were seldom detected in Minas Passage when the current was fast. The present results confirm that fish carrying 69 kHz PPM tags are unlikely to be detected by the receiver array in fast currents and yet will be detected by many receivers in the array when the current is slow. For estimating the probability of encounter, being detected over too wide an area causes uncertainty and not being detected

biases values low in fast currents for which a fish–turbine encounter is more likely to be harmful.

These shortcomings of PPM tags motivated the use of HR tags to track fish passing through the TED area in Minas Passage. Alewives carrying HR tags were detected at the TED area during a range of flood and ebb current conditions [29], which supports further consideration of HR tags. Detection range measurements [13] show that the HR signals are better detected than PPM signals in fast currents. A single PPM signal extends over an interval >2 s, whereas an HR signal takes only 6 ms, so it is possible to transmit a great many more HR signals, which gives more chances for an HR tag to be detected (6). The present work quantifies how a higher transmission rate makes it more likely that a drifter carrying an HR tag (a proxy for a tagged fish) will be detected by fixed receivers (Table 3).

When a PPM signal is reflected from the sea surface [13], it can cause close proximity detection interference [22] and prevent a nearby PPM tag from being detected. We observe that there are also geometric configurations of tag and receiver for which an HR signal overlaps with its reflection from the sea surface (3), but this only happens for a narrow set of circumstances, mostly when the tag is very near the sea surface and the sea surface is calm (Table 3). Under slightly different geometric circumstances, the reflected signal will not overlap with that taking a direct path, so the HR2 receiver has a second opportunity to detect the one HR transmission. Reflected signals are less likely to be observed, and less likely to cause interference, when the sea surface is rougher ([13], Table 5).

Another concern about both HR and PPM signal propagation was that previous detection range experiments [13,24] placed both receiver and acoustic tags close to the seafloor so that signals might sometimes be blocked by variable bathymetry. These previous experiments could not unambiguously identify where signal paths were blocked. The present mooring layout (Figure 1b) affords one obviously blocked path (mooring 9 to 10) plus a matching clear path (mooring 9 to 8), and the results demonstrate that detection efficiency is profoundly diminished for the blocked signal path (Figure 5). This justifies a decision to reject paths along which signal detection was poor in order to obtain an estimate for the detection efficiency, ρ, that applies to tagged fish that swim well clear of the seafloor [13].

Detection efficiency, ρ, is usually measured in the Eulerian frame, with both acoustic tag and receiver being at fixed coordinates relative to the seafloor [13,21,24]. On the other hand, a tagged fish is naturally described in a Lagrangian frame [15], as defined by its position at some initial time and subsequent trajectory due to movement by tidal current and swimming behavior. To achieve a robust estimate for the probability of fish–turbine encounters, we need to quantify that a fish carrying an HR tag will be detected as it passes over an array of HR2 receivers that monitor the TED area. Equation (6) relates the Eulerian detection efficiency, ρ, [13] to the number of times an HR signal is expected to be detected from a tagged fish (Lagrangian) as it passes a moored receiver. Given that ρ tended to overestimate the number of detection-positive intervals [13], the presently reported experiments were deemed necessary to directly measure how many times a fixed receiver detects a drifting tag as it passes by. Equation (6) was found to overestimate the number of passing trajectories for which there was at least one detected signal, and this overestimation can be attributed to the autocorrelation of variability about the general functional form of ρ. Nevertheless, most of the HR tags that drifters carried through the HR2 receiver array were detected, even during spring flood tides when current speeds were near their greatest extent in the TED area. Sometimes a passing tag was detected only a small number of times, so there was little margin for error. Indeed, the HR tags transmitted every 1.8 to 2.2 s, and if they had transmitted at longer intervals, then more tags would have passed by without being detected. A tagged fish that actively swims in the same sense as the tidal current may be somewhat less likely to be detected than a tagged fish drifting with the current [14].

The issue of tagged fish passing through a receiver array without being detected is also central to studies that use a sequence of receiver arrays to measure migration and

mortality/loss of tagged fish [29,31,32]. When fish are migrating, it is often possible to utilize detections of the tagged fish to roughly estimate detection efficiencies of most receiver arrays along the migration route, except for the last array [29,32]. It is very desirable, therefore, that the last array be designed so that it will detect all migrating fish as they pass by. The above work shows that detection range measurements are useful for obtaining a first estimate of the probability that the migrating fish will be detected by an array, but this estimate will be biased a little high.

A total of four HR2 receivers were used to monitor the TED area during this experiment. Although this was sufficient to detect the majority of HR tags passing by on drifters, the number of signals detected during a passing event was often small when tidal currents were greatest. It would be better to have had more HR2 receivers monitoring the TED area in order to (1) provide some redundancy in case of instrument failure, (2) better ensure that every tagged fish would be detected as it passed by, and (3) increase the possibility of localizing the position of a passing tag when several receivers detect the same HR signal. Localization does not have to be perfect, but it would be very helpful to know if tagged fish passed directly over the TED area or a little to the north or south.

Additionally, it would be advantageous to have a mooring system that enables HR2 receivers to be held sufficiently off the seafloor so as to prevent signals from one HR2 from being blocked before they reached a neighboring HR2. If this could be achieved, then HR detection efficiency could be accurately monitored as a function of time throughout the period when tagged fish are also being monitored. Rather than only relying on a fitted function for detection efficiency, $\rho(r, s_{\mathrm{FV}})$, it would be advantageous to also have a direct measurement of detection efficiency for the minute before and after a tagged fish is actually detected.

5. Conclusions

1. The present work clearly demonstrates that variable bathymetry can block HR signals. It follows that the omission of apparently blocked signal paths was justified in a previous study [13] that measured detection efficiency.
2. Detection efficiency is effectively 1 for HR signals transmitted from a $\approx$1 m range. This applies to all current speeds found in the TED area.
3. There is a reduced probability of HR signal detection when the tag drifts sufficiently near the sea surface for the reflection to interfere with the signal taking a direct path. Under calm conditions, this is expected to degrade the efficacy of HR telemetry for species of fish that swim near the sea surface.
4. The transmission interval between tag signals should be as short as practicable in order to minimize the chances that a drifting tag passes over the receiver array without being detected. With a transmission interval of 2 s, the receiver array at the TED area typically detected more than 90% of the deeper HR tags that drifted by when current speed was greater than 3.5 ms^{-1}.
5. Current speeds from the drifter tracks were larger than those from the FVCOM model.
6. Current speed has flood–ebb symmetry to the south of the TED area, but within the TED area, the flood current is much faster than the ebb.
7. The number of signals detected when LTD tags crossed the receiver array had flood–ebb symmetry with respect to drifter speed, whereas detection efficiency measured at the TED [13] does not have flood–ebb symmetry with respect to the current speed obtained from the FVCOM.
8. In fast currents, the number of signals detected from a tag that drifts by a fixed receiver was found to be slightly overestimated by integrating the Eulerian detection efficiency over the drift track. This effect might be attributed to correlated fluctuations in detection efficiency.
9. Drifter measurements have been used to tabulate the number of signals detected from a passing drifter as a function of current speed and the range of closest approach. This

can be considered a Lagrangian analog to an Eulerian detection efficiency, and subsequent work [20] shows how it is related to the probability of fish–turbine encounters.

10. The presently obtained results demonstrate how the previously measured detection efficiency, $\rho(r, s_{\text{FV}})$, [13] is related to the number of signals detected from a drifting tag when it passes over an array of receivers in the TED area. It, therefore, becomes possible to calculate the probability of fish–turbine encounters when the receiver array detects tagged fish as they pass through the TED area [20].

Author Contributions: Conceptualization, B.G.S. and D.J.H.; methodology, B.G.S. and D.J.H.; software, B.G.S.; validation, B.G.S.; formal analysis, B.G.S. and R.H.K.; investigation, B.G.S. and D.J.H.; resources, D.J.H. and B.G.S.; data curation, B.G.S.; writing—original draft preparation, B.G.S.; writing—review and editing, B.G.S., R.H.K. and D.J.H.; visualization, B.G.S.; supervision, B.G.S. and D.J.H.; project administration, D.J.H. and B.G.S.; funding acquisition, D.J.H. and B.G.S. All authors have read and agreed to the published version of this manuscript.

Institutional Review Board Statement: Not applicable.

Informed Consent Statement: Not applicable.

Data Availability Statement: The data sets analyzed during the current study are available from the corresponding author upon reasonable request.

Conflicts of Interest: The authors declare no conflict of interest. The funders had no role in the design of the study; in the collection, analyses, or interpretation of data; in the writing of the manuscript; or in the decision to publish the results.

Abbreviations

The following abbreviations are used in this manuscript:

FORCE	Fundy Ocean Research Centre for Energy
MHK	Marine Hydrokinetic
TED	Tidal Energy Development
PPM	Pulse-Position Modulation
HR	High Residency
HR2	High Residence Receiver
CI	Confidence Interval
UTC	Coordinated Universal Time
FVCOM	Finite-Volume Coastal Ocean Model
ABS	Acrylonitrile–Butadiene–Styrene
LTE	Long-Term Evolution
DC	Direct Current
USB	Universal Serial Bus
STD	Short-Term Drifts
LTD	Long-Term Drifts
GPS	Global Positioning System

References

1. Copping, A.; Hemery, L. (Eds.) *OES-Environmental 2020 State of the Science Report: Environmental Effects of Marine Renewable Energy Development Around the World*; Report for Ocean Energy Systems (OES); Office of Scientific and Technical Information: Oak Ridge, TN, USA, 2020. [CrossRef]
2. Jeffcoate, P.; McDowell, J. Performance of PLAT-I, a floating tidal energy platform for inshore applications. In Proceedings of the 12th European Wave and Tidal Energy Conference, Cork, Ireland, 27 August–1 September 2017.

3. Murray, J. Evolution of a solution for low cost tidal stream energy. *J. Ocean. Technol.* **2021**, *16*, 1–8.
4. Karsten, R.; McMillan, J.; Lickley, M.; Haynes, R. Assessment of tidal current energy in the Minas Passage, Bay of Fundy. *J. Power Energy* **2008**, *222*, 289–297. [CrossRef]
5. Karsten, R. An assessment of the potential of tidal power from Minas Passage, Bay of Fundy, using three-dimensional models. In Proceedings of the ASME 2001 30th International Conference on Ocean, Offshore and Arctic Engineering, OMEA2011-49249, Rotterdam, The Netherlands, 19–24 June 2011.
6. Bangley, C.W.; Hasselman, D.J.; Flemming, J.M.; Whoriskey, F.G.; Culina, J.; Enders, L.; Bradford, R.G. Modeling the Probability of Overlap Between Marine Fish Distributions and Marine Renewable Energy Infrastructure Using Acoustic Telemetry Data. *Front. Mar. Sci.* **2022**, *9*, 851757. [CrossRef]
7. Dadswell, M.J.; Wehrell, S.A.; Spares, A.D.; Mclean, M.F.; Beardsall, J.W.; Logan-Chesney, L.M.; Nau, G.S.; Ceapa, C.; Redden, A.M.; Stokesbury, M.J. The annual marine feeding aggregation of Atlantic sturgeon Acipenser oxyrinchus in the inner Bay of Fundy: population characteristics and movement. *J. Fish Biol.* **2016**, *89*, 2107–2132. [CrossRef]
8. Dadswell, M.J.; Spares, A.D.; McLean, M.F.; Harris, P.J.; Rulifon, R.A. Long-term effect of a tidal, hydroelectric propeller turbine on the populations of three anadromous fish species. *J. Fish Biol.* **2018**, *93*, 192–206. [CrossRef]
9. Dadswell, M.J.; Spares, A.D.; Porter, E.; Porter, D. Diversity, abundance and size structure of fishes and invertebrates captured by an intertidal fishing weir at Bramber, Minas Basin, Nove Scotia. *Proc. Nova Scotia Inst. Sci.* **2020**, *50*, 283–318.
10. Keyser, F.; Redden, A.M.; Sanderson, B.G. Winter presence and temperature-related diel vertical migration of Striped Bass *Morone saxatilis* in an extreme high flow passage in the inner Bay of Fundy. *Can. J. Fish. Aquat. Sci.* **2016**, *73*, 1777–1786. [CrossRef]
11. Stokesbury, M.J.W.; Logan-Chesney, L.M.; McLean, M.F.; Buhariwalla, F.F.; Redden, A.M.; Beardsall, J.W.; Broome, J.; Dadswell, M.J. Atlantic sturgeon spatial and temporal distribution in Minas Passage, Nova Scotia: A region of future tidal power extraction. *PLoS ONE* **2016**, *11*, e0158387. [CrossRef]
12. DFO. *Recovery Potential Assessment for Inner Bay of Fundy Atlantic Salmon*; DFO Canadian Science Advisory Secretariat Science Advisory Report 2008/050; Centre for Science Advice (CSA), Maritimes Region, Department of Fisheries and Oceans: Dartmouth, NS, Canada, 2008.
13. Sanderson, B.G.; Bangley, C.W.; McGarry, L.P.; Hasselman, D.J. Measuring detection efficiency of 170 kHz high-residency acoustic signals in a fast-flowing tidal passage. *J. Mar. Sci. Eng.* **2023**, *11*, 1172. [CrossRef]
14. Sanderson, B.G.; Stokesbury, M.J.W.; Redden, A.M. Using trajectories through a tidal energy development site in the Bay of Fundy to study interaction of renewable energy with fish. *J. Ocean Technol.* **2021**, *16*, 50–70.
15. Neumann, G.; Pierson, W. *Principles of Physical Oceanography*; Prentice-Hall Inc.: Englewood Cliffs, NJ, USA, 1966; pp. 1–545.
16. Viehman, H.A.; Zydlewski, G.B. Fish Interactions with a Commercial-Scale Tidal Energy Device in the Natural Environment. *Estuaries Coasts* **2015**, *38* (Suppl. S1), S214–S252. [CrossRef]
17. Amaral, S.V.; Bevelhimer, M.S.; Cada, G.F.; Giza, D.J.; Jacobson, P.T.; McMahon, B.J.; Pracheil, B.M. Evaluation of behavior and survival of fish exposed to an axial-flow hydrokinetic turbine. *N. Am. J. Fish. Manag.* **2015**, *35*, 97–113. [CrossRef]
18. Viehman, H.A.; Hasselman, D.J.; Douglas, J.; Boucher, T. The ups and downs of using active acoustic technologies to study fish at tidal energy sites. *Front. Mar. Sci.* **2022**, *9*, 851400. [CrossRef]
19. Renkawitz, M.D.; Sheehan, T.F.; Goulette, G.S. Swimming depth, behavior, and survival of Atlantic salmon postsmolts in Penobscot Bay, Maine. *Trans. Am. Fish. Soc.* **2012**, *141*, 1219–1229. [CrossRef]
20. Sanderson, B.G.; Karsten, R.; Solda, C.; Hardie, D.C.; Hasselman, D.J. Probability of Atlantic salmon post-smolts encountering a tidal turbine installation in Minas Passage, Bay of Fundy. *J. Mar. Sci. Eng.* **2023**, *11*, 1095. [CrossRef]
21. Kessel, S.T.; Cooke, S.T.; Heupel, M.R.; Hussey, N.E.; Simpfendor, C.A.; Vagle, S.; Fisk, A.T. A review of detection range testing in aquatic passive acoustic telemetry studies. *Rev. Fish Biol. Fish.* **2014**, *24*, 199–218. [CrossRef]
22. Kessel, S.T.; Hussey, N.E.; Webber, D.M.; Gruber, S.H.; Young, J.M.; Smale, M.J.; Fisk, A.T. Close proximity detection interference with acoustic telemetry: The importance of considering tag power output in low ambient noise environments. *Anim. Biotelemetry* **2015**, *3*, 5. [CrossRef]
23. Chen, C.; Beardsley, R.C.; Cowles, G. An Unstructured-Grid, Finite-Volume Coastal Ocean Model (FVCOM) System. *Oceanography* **2006**, *19*, 78–89. [CrossRef]
24. Sanderson, B.G.; Buhariwalla, C.; Adams, M.; Broome, J.; Stokesbury, M.; Redden, A.M. Quantifying detection range of acoustic tags for probability of fish encountering MHK devices. In Proceedings of the 12th European Wave and Tidal Energy Conference, Cork, Ireland, 27 August–1 September 2017.
25. Betz, A. *Introduction to the Theory of Flow Machines*; Randall, D.G., Ed.; Pergamon Press: Oxford, UK, 1966.
26. Charlier, R.H.; Menanteay, L. The saga of tide mills. *Renew. Sustain. Energy Rev.* **1997**, *1*, 171–207. [CrossRef]
27. Pederson, L. 7000 years of fishing; stationary fishing structures in the Mesolithic and afterwards. In *Man and Sea in the Mesolithic*; Fisher, A., Ed.; Oxbow Books: Oxford, UK, 1995; pp. 75–86.
28. Hammar, L.; Andersson, S.; Eggertsen, L.; Haglund, J.; Gullstrom, M.; Ehnberg, J.; Molander, S. Hydrokinetic Turbine Effects on Fish Swimming Behaviour. *PLoS ONE* **2013**, *8*, e84141. [CrossRef]
29. Tsitrin, E.; Sanderson, B.G.; McLean, M.F.; Gibson, A.J.F.; Hardie, D.C.; Stokesbury, M.J.W. Migration and apparent survival of postspawning alewife (*Alosa pseudoharengus*) in Minas Basin, Bay of Fundy. *Anim. Biotelemetry* **2022**, *10*, 11. [CrossRef]
30. Lilly, J.; Dadswell, M.J.; Mclean, M.f.; Avery, T.S.; Comolli, P.D.; Stokesbury, M.J.W. Atlantic sturgeon presence in a designated marine hydrokinetic test site prior to turbine deployment: A baseline study. *J. Appl. Ichthyol.* **2021**, *37*, 826–834. [CrossRef]

31. Kocik, J.F.; Hawkes, J.P.; Sheehan, T.F.; Music, P.A.; Beland, K.F. Assessing Estuarine and Coastal Migration and Survival of Wild Atlantic Salmon Smolts from the Narraguagus River, Maine Using Ultrasonic Telemetry. *Am. Fish. Soc. Symp.* **2009**, *69*, 293–310.
32. Halfyard, E.A.; Gibson, A.J.; Ruzzante, D.E.; Stokesbury, M.J.; Whoriskey, F.G. Estuarine survival and migratory behaviour of Atlantic salmon *Salmo salar* smolts. *J. Fish. Biol.* **2012**, *81*, 1626–1645. [CrossRef] [PubMed]

Appendix V

Article

Probability of Atlantic Salmon Post-Smolts Encountering a Tidal Turbine Installation in Minas Passage, Bay of Fundy

Brian G. Sanderson [1,*] , Richard H. Karsten [2], Cameron C. Solda [3], David C. Hardie [4] and Daniel J. Hasselman [5,*]

1   Acadia Centre for Estuarine Research, Acadia University, Wolfville, NS B4P 2R6, Canada
2   Department of Mathematics and Statistics, Acadia University, Wolfville, NS B4P 2R6, Canada;
    richard.karsten@acadiau.ca
3   Department of Biology, Acadia University, Wolfville, NS B4P 2R6, Canada; cameronsolda@acadiau.ca
4   Department of Fisheries and Ocean, Dartmouth, NS B2Y 4A2, Canada; david.hardie@dfo-mpo.gc.ca
5   Fundy Ocean Research Center for Energy, Halifax, NS B3J 3N5, Canada
*   Correspondence: bxs@bellaliant.net (B.G.S.); dan.hasselman@fundyforce.ca (D.J.H.);
    Tel.: +1-902-697-2592 (B.G.S.); +1-902-406-1166 (ext. 7) (D.J.H.)

Abstract: Tidal stream energy is a renewable energy resource that might be developed to offset carbon emissions. A tidal energy demonstration (TED) area has been designated in Minas Passage, Bay of Fundy, for testing and installing marine hydrokinetic (MHK) turbines. Regulations require quantification of the potential for MHK turbine installations to harm local populations of marine animals. Here, we use acoustic telemetry to quantify the probability that post-smolt inner Bay of Fundy salmon encounter a turbine installation at the TED area. Previous work has quantified the detection efficiency of Innovasea HR acoustic tags as a function of the current speed and range from a moored HR2 receiver and also demonstrated that drifters carrying HR tags will be effectively detected when the drifter track crosses the array of HR2 receivers in Minas Passage. Salmon smolts were tagged and released in Gaspereau and Stewiacke Rivers, Nova Scotia, in order that the HR2 receiver array could monitor seaward migration of the post-smolts through Minas Passage and particularly through the TED area. Presently, we formulate and apply a method by which tag signals detected by the HR2 array can be used to estimate the expected number of times that a post-smolt would encounter a single near-surface MHK turbine installation during its seaward migration.

Keywords: fish; MHK turbine; probability of encounter; tidal energy; Atlantic salmon; smolt; acoustic telemetry

1. Introduction

A large human population that depends on energy-dense fossil fuels [1] causes environmental changes [2]. Large amounts of renewable energy might be harvested from the tides of Canada's Bay of Fundy [3] to offset the use of fossil fuels. It is hoped that ecosystem disruption can be reduced by obtaining energy from renewable resources. Historically, however, exploitation of renewable energy has not been ecologically benign. In Europe, the spread of watermill technology from the early Middle Ages to early modern times has been associated with the dramatic decline of Atlantic salmon (*Salmo salar*) populations [4]. More recently, measurements showed 39% mortality for 0.136 m juvenile striped bass (*Morone saxatilis*) immediately after passing through a low-head turbine [5]. On the other hand, very little mortality was observed for a low-head turbine that was specially designed for fish safety [6]. At Anapolis Royal, Bay of Fundy, fish mortality has been associated with the 20 MW reaction turbine that relied upon a tidal barrage to create a pressure head [7].

Marine hydrokinetic (MHK) turbines harvest kinetic energy of ocean currents rather than relying on a pressure head. Without a pressure head, a turbine must have a larger diameter to produce the same amount of power, but fish-damaging pressure forces (and shear stress) may be reduced, depending upon turbine design. A tidal barrage directs

much of the flow through a turbine, whereas MHK turbines often obstruct only a small proportion of the tidal flow and a flood or ebb tide might see many fish pass by without encountering a turbine.

A 1.6 km × 1 km tidal energy demonstration (TED) area has been designated for deploying MHK turbines in Minas Passage where the current can exceed 5 m s^{-1} [8,9]. Three gravity-base MHK turbines (up to 2 MW) have been tested at the TED area, but their interactions with fish remain unquantified. Given that Minas Passage is approximately 5 km wide, it is fair to say that most fish would not encounter a turbine during an ebb or flood tide. Quasi-stable drifter tracks pass repeatedly back and forth through Minas Passage but most of those tracks pass to the south of the TED area and, therefore, have low probability of encountering a MHK turbine installation [10]. Other drifter tracks through the TED area have been observed to subsequently disperse elsewhere [9,10], which indicates that, should an individual fish encounter a MHK turbine, then that experience would not be repeated for many of the following tidal cycles.

Quantifying whatever harm a MHK turbine may or may not do to a fish population begins with the probability of an individual encountering the turbine. A definition for probability of a fish encountering a MHK turbine is a precondition for unambiguous calculation from practicable measurements.

Definition 1. *Probability of encounter is the probability that—at some location, during some time interval $t_0 \leq t \leq t_0 + T$—a fish that belongs to a distinguishable population will pass through the area A_{MHK} that would be swept by the blades of a MHK turbine without the turbine actually being deployed at that position at that time.*

The probability of encounter can only be considered to be an upper limit on the probability of harm. If a MHK turbine is present, then there is always a possibility that an individual will simply avoid swimming through A_{MHK}. An idealized turbine operating at the Betz limit [11] diverts about 30% of the incoming flow around A_{MHK}, so an individual might sometimes avoid the turbine by passively drifting with the flow. In clear tropical waters with comparatively weak currents, video observations showed large fish avoiding a small MHK turbine, whereas smaller fish sometimes passed through the turbine but evaded the blades [12]. At higher latitude, video footage showed fish aggregating near a MHK turbine at slack-water high-tide [13] but that analysis subsampled observations to an extent that neither fish-turbine encounter nor avoidance behaviour could be estimated when the tidal current was faster. Studies in an open channel flume showed both avoidance behaviour and salmon evading turbine blades [14]. Echosounder transects [15,16] and analysis of images taken by acoustic cameras [17] both indicated avoidance behaviour by fish upstream from a MHK turbine in ≈2 m s^{-1} tidal currents at Cobscook Bay. At a high latitude MHK turbine site, echosounder measurements showed fish aggregation near slack water and an indication of avoidance behaviour when the tidal current was faster [18]. Such measurements of avoidance and blade evasion have not been successfully achieved in the more challenging conditions at Minas Passage [19].

Previous measurements and analysis [10] indicate that fast tidal currents dominate fish movement in Minas Passage, so given the abundance (number of individuals per unit horizontal area) and distribution of a population of interest, then it is straightforward to estimate the probability of an encounter from the tidal flux through A_{MHK}. In practice, abundance has not been accurately quantified for any population found in Minas Passage [17,19]. Nevertheless, the following work will show how the probability of encounter can be estimated from a different method which uses acoustic telemetry to detect acoustically tagged individuals as they pass by acoustic receivers in the TED area.

Early efforts implanted Innovasea 69 kHz pulse position modulation (PPM) tags in the body cavities of striped bass belonging to a local population that spawns in the Shubenacadie River, Nova Scotia [20]. Similarly, 69 kHz PPM tags were implanted in Atlantic sturgeon (*Acipenser oxyrhinchus*) that were mostly from the Saint John River, New Brunswick,

population stock [21]. While these measurements were useful for demonstrating swimming depth and presence near the TED area [20–22], range detection measurements [23] indicated that presence would often be undetected when the tidal current was fast. Undetected presence was unambiguously demonstrated when an array of receivers in the TED area often failed to detect a passing drifter that carried a 69 kHz PPM tag when currents were fast and yet many receivers in the array concurrently detected the tag signals when currents were slow [9]. Drifters also carried 170 kHz High Residency (HR) tags that did enable passing drift tracks to be reliably detected in fast tidal currents [9]. In 2019, post-spawn alewives (*Alosa pseudoharengus*) in Gaspereau River, Nova Scotia, were implanted with HR tags and were detected during their seaward migration through Minas Passage [24].

Three gravity-base MHK turbines have been installed at the TED area but now only one remains and it is in a non-operational state. MHK turbines may also be installed on floating platforms [25,26]. Such near surface turbines raise concerns for the safety of Atlantic salmon because they swim near the sea surface [27,28]. Canada's *Species At Risk Act (SARA)* lists inner Bay of Fundy Atlantic salmon as endangered and the Department of Fisheries and Oceans (DFO) operates a hatchery stocking program [29] that presently makes a significant contribution to the population by releasing unfed fry at freshwater locations that provide suitable habitat.

In the following work, we estimate the probability that individual post-smolts would encounter MHK turbines at the TED area in Minas Passage. Specifically, HR acoustic tags were implanted within the body cavities of smolts as they migrated down river and an array of HR2 receivers was installed to detect them as they passed through Minas Passage. By considering a moored HR2 receiver as a proxy for some yet-to-be installed MHK turbines and utilizing results from our studies of detection efficiency [9,30], it is possible to estimate the probability of a fish–turbine encounter when a tagged post-smolt is detected passing through the TED area.

2. Materials and Methods

As an outline, the method is to deploy an array of moored HR2 receivers within and nearby the TED area in order to detect post-smolts that were tagged earlier during their seaward migrations from Gaspereau River and the Stewiacke River (Figure 1). Previous work has quantified the detection efficiency of HR2 receivers that were deployed within the TED area in 2021 [30]. Here, we detect tagged post-smolts as they pass by receivers and develop a method to convert that information into a probability of an encounter at and near the TED area.
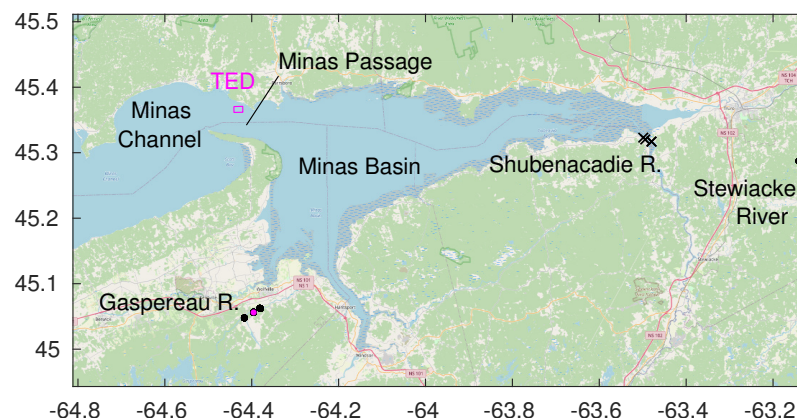

Figure 1. Locations in Minas Passage and neighbouring waters. Black dots show where 2019 smolts were released in Gaspereau River and Stewiacke River. Stewiacke River is a tributary to Shubenacadie River which connects to Minas Basin. Magenta dot shows release site for smolts tagged in 2022. Black crosses show positions of VR2W-180 kHz receivers moored near the mouth of Shubenacadie River.

2.1. Receiver Arrays

In 2019, the Fundy Ocean Research Centre for Energy (FORCE) moored four HR2 receivers in Minas Passage at positions marked S2, W1, W2, and D1 (Figure 2). Each mooring used SUBS-Model A2 (Open Seas Instrumentation Inc., Musquodoboit Harbour, Canada) with an acoustic release that was tethered to a 240 kg steel weight by a 3 m riser. Innovasea HR2 and VR2W-69 kHz receivers were attached just forward of the tail fin of each SUBS. The volcanic plateau within the TED area is favoured for MHK turbines and only the D1 mooring was deployed at that site but moorings W1 and W2 are also judged as useful because they are aligned with the tidal flow over the volcanic plateau. Mooring S2 provides a comparison for locations nearer the middle of Minas Passage. The FORCE moorings are primary to the present study but peripheral use will be made of Innovasea receivers that were deployed by other organizations (Ocean Tracking Network, Acadia University, Department of Fisheries and Oceans) at other locations in Minas Passage, Minas Basin, and the Gaspereau River [24].

In 2022, FORCE deployed 11 SUBS at mooring sites (Figure 2) that were generally aligned orthogonal to the tidal current with most positions selected to place receivers on local high ground where the available high-resolution bathymetry indicated relatively low local variation. Again, a SUBS-Model A2 was used with an acoustic release and a 3 m riser from a 240 kg weight. In 2022, the HR2 receiver was housed mostly within the SUBS with its hydrophone sensor protruding above the hull of the SUBS and the VR2W-69kHz receiver was mounted directly behind the tail fin. The 2022 receiver array has previously been used for further range testing and for confirming that receivers will detect tags carried beneath drifters that pass over the array [9]. HR2 receivers at sites 9 to 12 monitor trajectories over that part of the volcanic plateau where MHK turbines are most likely to be deployed in the future, whereas sites 1, 2, and 4 to 8 enable comparison to the south. Mooring 3 failed [9].
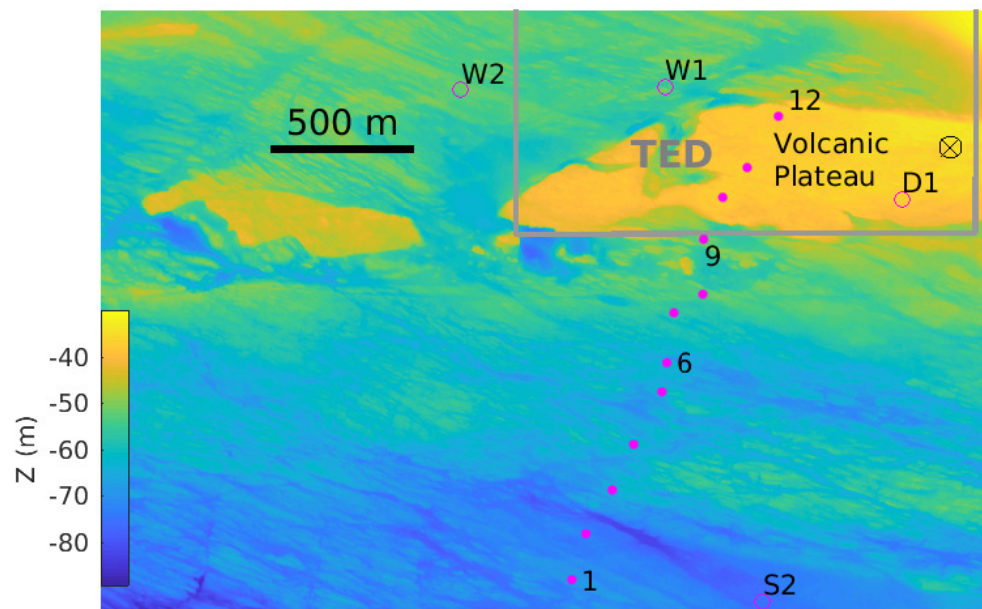

Figure 2. Mooring locations in Minas Passage. HR2 receivers were moored at sites S2, W1, W2, and D1 (magenta circles) in 2019. HR2 receivers were moored at sites 1−2 and 4−12 in 2022 (magenta dots).

2.2. Tagging Smolts

Tagging conducted during 2019 was registered under DFO Scientific License to Fish license # 330657 and salmon surgical procedures were performed under Acadia University Animal Care Committee protocol #07-18.

Smolts were captured during their down-river migration. Innovasea V5 HR tags were surgically implanted and after a recovery period the smolts were released to continue their

migration. Tags were programmed to transmit a 170 kHz, 143 dB high residency (HR) signal every 1.8 s to 2.2 s and a 180 kHz pulse position modulation (PPM) signal every 25 s to 35 s.

From 7 to 18 May 2019, 87 smolts from the Gaspereau River were captured and tagged near the bypass dam (Figure 1, [24]) where the DFO hatchery program has a fish trap. Tagged smolts were released upstream of the bypass dam, in the pool at the foot of the bypass dam, and 2 km further downstream in the Gaspereau River. From 20 May to 12 June 2019, 57 smolts were captured, tagged and released in the Stewiacke River (Figure 1).

In 2022, smolt capture was conducted under a scientific sampling permit issued to D Hardie and surgical procedures were approved under the Acadia University Animal Care Committee protocol #08-22. Smolts were captured in the DFO trap at the bypass dam during their migration down the Gaspereau River. There were 25 smolts tagged and they were all released into the pool below the bypass dam. Tagging and releases were performed in three groups: 9 smolts on 9 May, 8 on 10 May, and 8 on 11 May.

2.3. Detection Efficiency and Tidal Current

Definition 2. *Detection efficiency ρ is the probability that a signal transmitted by a tag will be detected by a nearby receiver.*

Measurements of detection efficiency have been made at the TED site in Minas Passage for both HR signals and 180 kHz PPM signals [9,30]. Detection efficiency declines with increasing range from transmitting tag to receiver and also declines with increased tidal current speed. The HR signals are more efficiently detected than PPM signals and also have the advantage of being able to be transmitted more frequently. Frequent transmission is of paramount importance for detecting a tagged fish as it passes by because even in fast currents there will be brief intervals when ambient noise levels are lower than typical and a signal can be detected [9]. Detection efficiency can be related to the area that is effectively monitored [30] and will similarly play a central role in the following calculation of probability of fish–turbine encounters.

2.4. Tidal Current

The detection efficiency $\rho(r, s)$ has been measured as a function of range r from tag to receiver and vertically averaged flood/ebb tidal current speed s at the site of the HR2 receiver [30]. Tidal current speed is designated s positive on the flood tide and negative on the ebb. It was not usually possible for us to directly measure tidal current speed so values of s were downloaded from a FVCOM simulation [3,8,31].

The FVCOM current speed s is always used for the calculation of detection efficiency because ρ was empirically parameterized as a function of s [30]. For some other purposes it will be more appropriate to use drifter speed s_d, which [9] has empirically related to s

$$s_d = \begin{cases} (s - 0.14)/0.87 & \text{Within the TED area} \\ (s - 0.07)/0.76 & \text{South of the TED area.} \end{cases} \tag{1}$$

2.5. Detecting Passing Events

Small fish, such as post-smolts and alewife, are substantially moved past moored receivers by the fast tidal currents in Minas Passage [10,24]. A passing event is presently understood to be the time when a sequence of closely spaced HR signals are detected from a tagged post-smolt that is passing a line of receivers. The relationship between detection efficiency ρ and detection of a passing event has been quantified in detail using tags that are carried by GPS-tracked drifters [9]. Sometimes the same passing event was recorded by more than one mooring and in such instances we consider the smolt to have passed by the mooring station that detected the most signals. Thus, for a flood tide (or an ebb tide) there can be at most one passing event for any particular post-smolt and this preserves the statistical independence of all passing events.

To estimate the probability of encounter, we consider that the receiver that detects the passing event is replaced by a hypothetical turbine that has the same x, y coordinates but with a z coordinate representative of the type of turbine that is of interest. The Lagrangian coordinate applies most naturally to the trajectory of a post-smolt, as it would for most moving animals. There are two Lagrangian methods that might be used to convert a set of passing events to an estimate of probability of encounter.

1. Measure the distance of closest approach of each passing tagged fish to the receiver (proxy turbine) and identify those that were close enough to cross the area A_{MHK} that would be swept by turbine blades. Two measurement methods might be used.

    (a) The number of signals that are detected during a passing event will typically be larger if the smolt passes closer to the receiver. Drifter studies demonstrate much variability in the measured number of detections relative to the expected number [9].

    (b) Use many closely spaced HR2 receivers to localize the track of each tagged fish as it passes by. Measurements of detection efficiency [30] indicated an impractical number of receivers would be required.

2. Another approach is to consider that a detected passing event might have been on any one of a set of all paths that passed the receiver/turbine. This approach builds on an assumption of statistical similarity for paths that cross within a scale comparable to the effective range of detection [9]. This was the approach that was previously used to calculate the probability that drifters would collide with a turbine installation in Minas Passage [10]. Presently, we build upon this approach.

2.6. Calculation of Probability of Encounter

The measured detection efficiency for a HR signal ρ is a function of range r and current speed s [9]. Here, $r = \sqrt{x^2 + y^2 + z^2}$ is the slant range from a near-surface tagged post smolt to a HR2 receiver at the origin of the horizontal plane $x = 0, y = 0$ but at depth z relative to the post-smolt. Without loss of generality, we consider a coordinate system so that the ensemble of possible post-smolt trajectories travel in the x-direction so that their y coordinate becomes the horizontal distance of the closest approach of the tagged post-smolt to the moored HR2 receiver that detected the passing event. Figure 3 lays out the situation with two mathematically convenient symmetries. The first symmetry is that $r(x, y, z) = r(x, -y, z)$, so we only need to perform the calculation on the positive y half-plane. The second symmetry is that ρ will be the same for a tag on the smolt and receiver at the origin as for a receiver on the smolt and a tag at the origin.

Consider an encounter with one side of a turbine installation that has total width W oriented across-current and centered on the origin in Figure 3. A presently planned turbine installation consists of six near-surface turbines that have been estimated to span an effective width of $W = 38$ m [10,25,26]. Post smolts swim near the sea surface [28], so to a first approximation we consider that they are within the depth range spanned by the blades of the turbines. To the extent that this approximation does not apply for some specific turbine installation, a correction factor can be estimated and applied after the following.

Consider a tagged smolt at position x, y, z relative to the HR2 receiver that detects a passing event. The HR2 receiver can be considered to be a proxy for a turbine installation at the same position except for the HR2 being a distance z below both the turbine installation and the post-smolt that might encounter it. Thus, the range from post-smolt to HR2 is $r = \sqrt{x^2 + y^2 + z^2}$ and we write $\rho(r, s) = \rho(x, y | z, s)$ to represent the detection efficiency along tracks that share the same values for z and s. Figure 3 uses color to show detection efficiency on the half-plane.
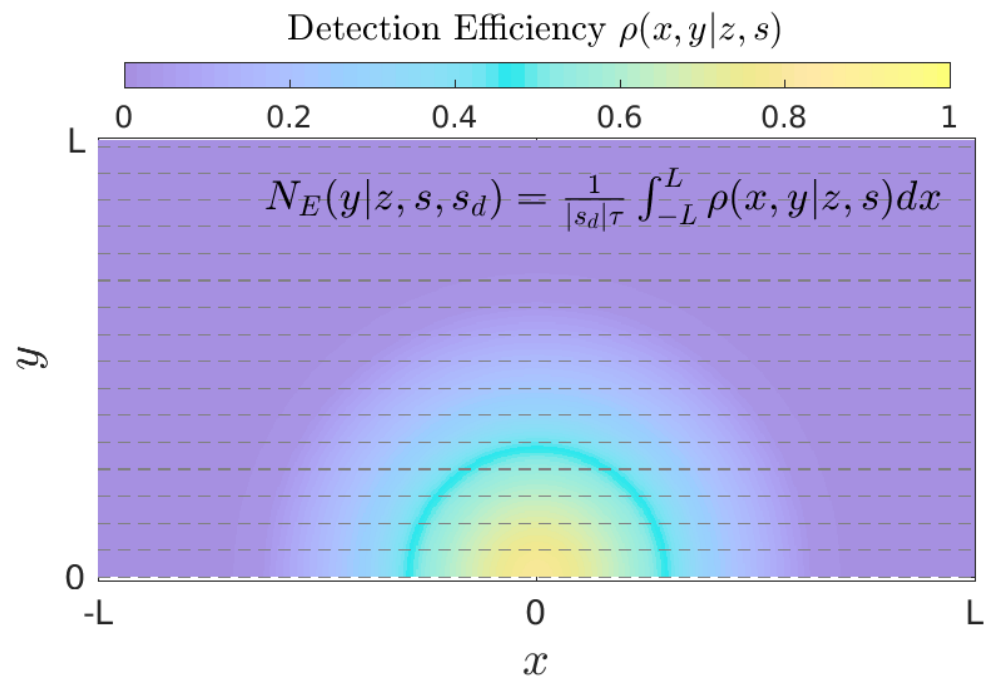
Figure 3. Plan view of an ensemble of smolt tracks (dotted lines in the $x-$direction) that pass within a distance y of a receiver/turbine that is located at the origin. The color scale shows probability of detecting a transmitted signal depending upon the position of a smolt.

Tracks with larger y are less likely to be detected. Following [9], the number of signals expected to be detected along the length of a track is

$$N_E(y|z,s,s_d) = \frac{1}{|s_d|\tau} \int_{-L}^{L} \rho(x,y|z,s)dx \tag{2}$$

where τ is the time scale between signals transmitted by the tag and $L = 350$ m is the range beyond which ρ is effectively zero. The calculation of travel distance $|s_d|\tau$ between HR signals uses drift speed s_d (1). Equation (2) identifies the expected number of times that a tag would be detected if it passed by an HR2 receiver along a track with closest approach y. N_E is a real number≥ 0. The expected probability that at least one signal will be detected along that track with closest approach y is

$$p_E(y,|z,s,s_d) = \min(N_E(y|z,s,s_d),1). \tag{3}$$

Tracks passing close to the turbine (small y) would have $N_E \gg 1$ and, therefore, $p_E = 1$, because at least one signal would be detected. Tracks passing further away from the turbine (larger y) have $1 > N_E \geq 0$ and $p_E = N_E$ (i.e., the expected number of detected signals is the probability of detecting a signal). Given (3), the expected probability of encounter would be

$$^E\mathcal{P}(z,s) = \frac{\int_0^{W/2} p_E(y|z,s)dy}{\int_0^L p_E(y|z,s)dy} \tag{4}$$

where we note that $^E\lambda = \int_0^L p_E(y|z,s)dy$ can be considered to be half the cross-current width over which passing tags are expected to be detected.

Experiments using tags suspended beneath GPS-tracked drifters compared measured values for the number of detected signals N_D (integers≥ 0) against the expected number N_E (real numbers≥ 0) (see Figure 7 of [9]) and a linear regression gave

$$\sqrt{N_D} = -0.30 + 0.87\sqrt{N_E} \tag{5}$$

Given (5) and the physical requirement that the number of signals must be ≥ 0, it seems that an improved estimate for the expected number of signals detected along a track would be

$$\mathcal{N}(y|z, s, s_d) = \left[\max\left(-0.30 + 0.87\sqrt{N_E}, 0\right)\right]^2 \tag{6}$$

and the probability of the track with closest approach y being detected would be

$$p(y, |z, s, s_d) = \min(\mathcal{N}(y|z, s, s_d), 1) \tag{7}$$

in which case a better estimate of the probability of encounter $\mathcal{P}$ might be calculated as the ratio of two cross current scales,

$$\mathcal{P}(z, s, s_d) \quad = \quad \frac{\int_0^{W/2} p(y|z, s, s_d)dy}{\lambda} \tag{8}$$

$$\lambda(z, s, s_d) \quad = \quad \int_0^L p(y|z, s, s_d)dy, \tag{9}$$

the numerator of (8) being the effective half-width of the turbine installation and the denominator, λ, being the effective half-width of all passing tracks that might be detected.

$\mathcal{P}$ is backed by the more thorough set of measurements, relying on both empirical estimation of ρ and empirical testing of how ρ relates to detecting tags carried by GPS-tracked drifters as they pass by a receiver with a measured distance of closest approach. $^E\mathcal{P}$ is only backed by Eulerian measurements of ρ but is easier to obtain from an experimental point of view. It will be of interest to compare $^E\mathcal{P}$ with $\mathcal{P}$ in view of the possibility of improving results by obtaining more drifter measurements in future.

3. Results

In 2022, the FORCE array spanned much more of the width of Minas Passage than did the 2019 FORCE array (Figure 2). It is, therefore, expected that in 2019 a tagged post-smolt was less likely to be detected during its migration through Minas Passage than in 2022. On the other hand, more smolts were tagged in 2019.

3.1. Presence of Tagged Post-Smolts in Minas Passage

In 2022, there were 11 HR2 receivers in the FORCE array at Minas Passage (Figure 2) and they detected 22 of the 25 smolts that were tagged in Gaspereau River. One additional post-smolt was detected by the Ocean Tracking Network (OTN) array that is also in Minas Passage and less than 2 km east of the FORCE array. The OTN array is only relevant to the present objective in so much as it confirms that at least 23 tagged post-smolts arrived at Minas Passage. The same two post-smolts that were not detected in Minas Passage were also the only smolts not detected by receivers in the tidal section of Gaspereau River. Receivers between the release location and tidal Gaspereau detected 24 tagged smolts. Applying the appropriate analysis—Equation (3) of [24]—the most probable estimate is that $N_{\mathrm{MP}} = 23$ tagged post-smolts migrated into Minas Basin and they all reached Minas Passage. There was no apparent mortality for that part of the migration from the mouth of Gaspereau River to Minas Passage [27].

In 2019, the FORCE array had only four HR2 receivers that spanned a small portion of the Minas Passage cross-section (Figure 2) [24]. Those receivers detected 43 of the 87 smolts tagged in Gaspereau River and 29 of the 57 smolts tagged in Stewiacke River.

Many receivers were deployed in Minas Basin and Gaspereau River in 2019 and these have been used to study migration of alewives [24]. The same receivers and methods also enable examination of the migration of post-smolts that were tagged in Gaspereau River to the extent that this is relevant for the encounter problem. Of the 61 post-smolts detected beyond the mouth of Gaspereau River in 2019, all were detected by the receiver array at the mouth of Gaspereau River. Thus, the efficiency of that receiver array for detecting passing post-smolts was $\eta = 1$. A total of 71 smolts were detected by the receiver array

at the mouth of Gaspereau River, corresponding to 16 being lost within the Gaspereau River. Assuming no losses from the mouth of Gaspereau River to Minas Passage (i.e., as for 2022 measurements), then $N_{MP} = 71$ tagged post-smolts were expected to have reached Minas Passage.

In 2019, a total of 57 smolts were tagged and released in the Stewiacke River. The Stewiacke River runs into Shubenacadie River. Figure 1 shows 4 VR2W-180kHz receivers at the mouth of Shubenacadie River, which detected 26 smolts. A total of 33 post-smolts were detected by receivers in Minas Passage and Minas Basin at locations beyond the mouth of the Shubenacadie and 22 of those were also detected by receivers at the mouth of the Shubenacadie River. It follows that the receiver array at the mouth had detection efficiency $\eta = 22/33$ (67%) and given that a total of 26 smolts were detected passing the mouth it is expected that $26/\eta = 39$ smolts passed the mouth of Shubenacadie River. Thus, we expect that $57 - 39 = 18$ smolts were lost within the Stewiacke and Shubenacadie Rivers. As before, assuming no mortality in Minas Basin, as many as $N_{MP} = 39$ tagged post-smolts were expected to have reached Minas Passage.

3.2. Post-Smolt Motion in Minas Passage, Passing Events

In 2022, a HR2 receiver was suspended beneath a GPS-tracked drifter that moved with the currents through Minas Passage and neighbouring waters [9]. On three occasions, the HR2 detected signals from a tagged post-smolt that remained sufficiently close to the drifter to continue to be detected over 3–4 km track segments (red lines in Figure 4). Furthermore, the moored HR2 receivers detected the passing post-smolts at much later times when the drifter had moved by more than 10 km but was still relatively nearby the moored receiver when it detected the tagged post-smolt (Figure 4). Signals detected by receivers on and nearby the drifter demonstrate that post-smolts in Minas Passage are substantially displaced by/with the tidal currents/waters.
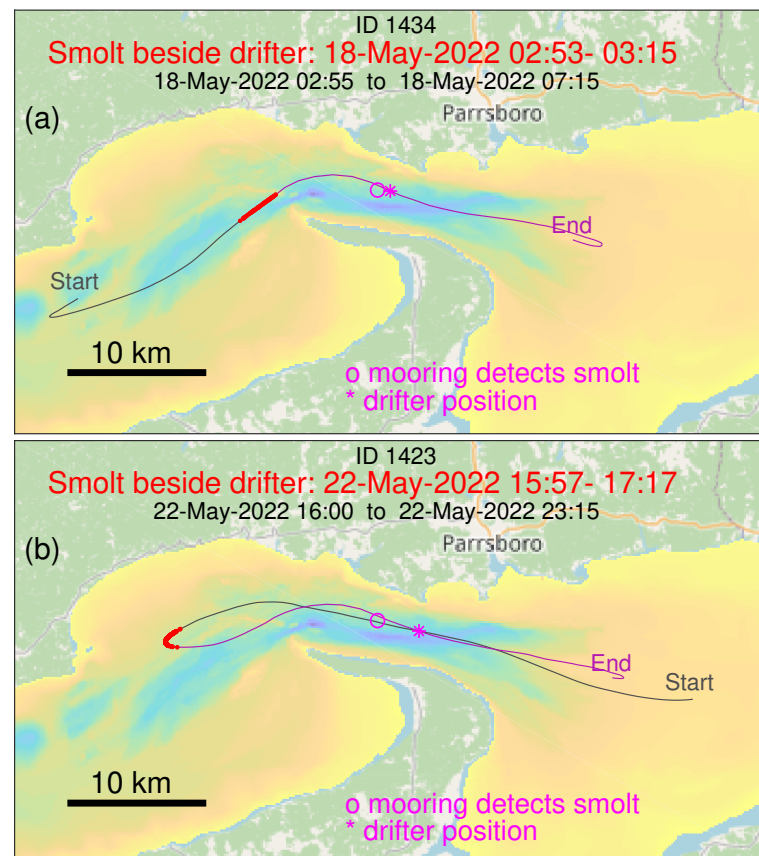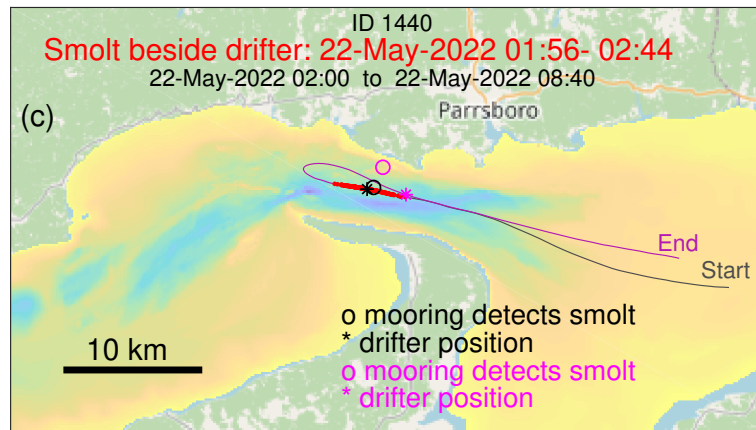

Figure 4. *Cont.*

Figure 4. The black line shows a portion of the track of a drifter that has a HR2 receiver suspended beneath it. Red shows where the drifter was when its HR2 detected HR signals from a tagged post-smolt that was nearby. Subsequently, the tagged post-smolt was detected by a moored HR2 receiver (magenta circle) when the drifter was at a nearby position (magenta asterisk). (**a**) Detected on flood. (**b**) Detected low tide and flood. (**c**) Detected late ebb and early flood.

The duration of a passing event is defined as the time elapsed from first to the last HR signal detected during the passing event. Figure 5 shows the duration of each passing event measured by the FORCE line of 11 HR2 receivers that were deployed in 2022. It takes much less time for the tagged post-smolt to pass the receiver line when tidal current is fast. This is consistent with fast currents advecting post-smolts more quickly past receivers and reducing effective detection range [30].
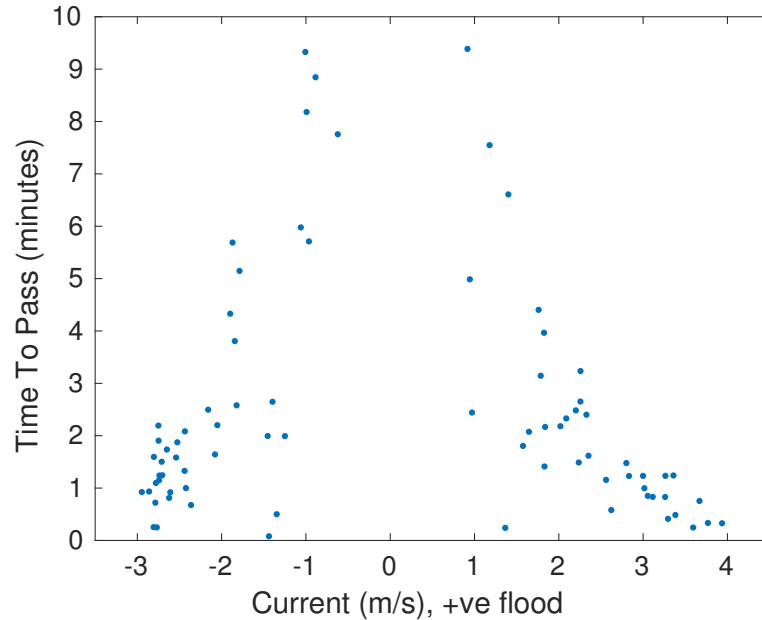

Figure 5. Duration of 2022 passing events diminishes with increasing current speed.

Given the fast tidal currents in Minas Passage, it is hardly surprising that post-smolts can be swept back and forth many times during their seaward migration. Figure 6 documents the number of passing events that the 2022 FORCE array measured for each smolt tagged in 2022. While two of the smolts never reached Minas Passage and another was only detected by the OTN line, other post-smolts were detected for up to eight passing events. Multiple passing events increases the likelihood of post-smolt-turbine interaction during migration, as has also been suggested for alewives [24] and striped bass [20].

The bars of Figure 6 are labelled with the days (elapsed since tagging) that span passing events recorded for each post-smolt. The time from tagging to first detected passing event ranged from 3 to 12 days (mean 8) and the time to last detected passing event ranged from 5 to 13 days (mean 10). The most passing events were measured for post-smolt 7, which had 8 passing events detected over a 6-day time span. Clearly, passing events were not detected on each flood-ebb tide, in part because the receiver array does not span the entire passage, but also because we should not think of post-smolts moving back and forth through Minas Passage with each successive ebb and flood tide because although some drifter trajectories exhibit such behaviour, others do not [9,10].
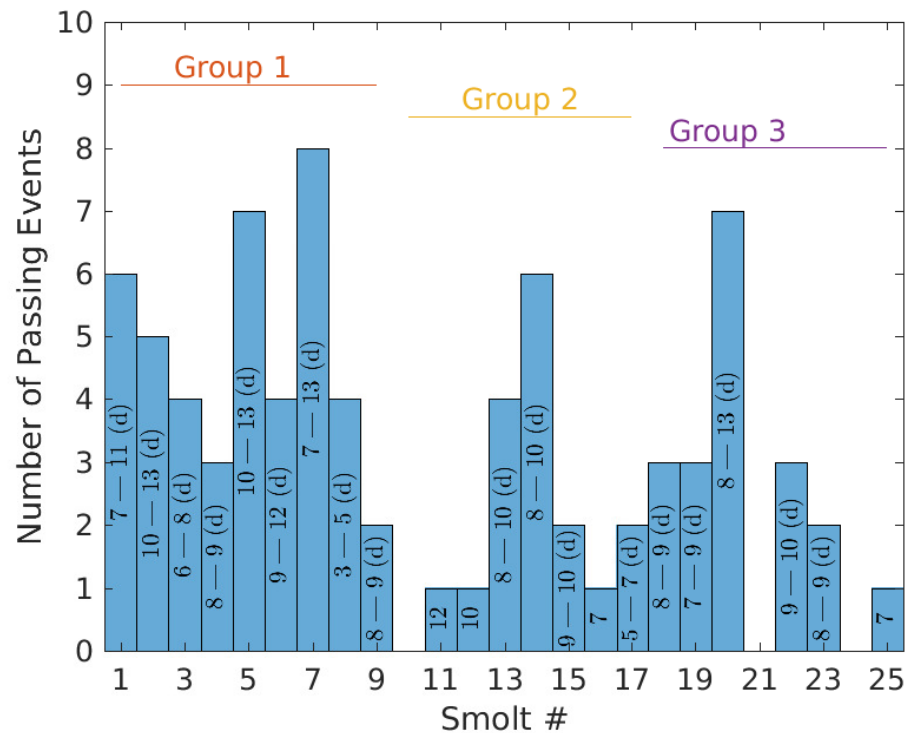
Figure 6. Post-smolts can cross the Minas Passage receiver array multiple times during their 2022 outbound migration.

3.3. Probabilities of Encounter for Post-Smolts in Minas Passage

Equation (9) obtains the half cross-current width scale λ for detection of a passing tag from p. Values for p have been obtained above from Eulerian measurements [30] of detection efficiency ρ and these give values for λ, as plotted by the blue circles in Figure 7. Values of λ rapidly diminish at large current speeds but $\lambda > W/2$ for all the current speeds for which λ was calculated. Values of p can be directly measured from tagged drifters that pass nearby a moored receivers (e.g., Figure 12 in [9]) and the red asterisks in Figure 7 show estimates of λ obtained from those measurements. Drifter measurements poorly resolved p with respect to range and current speed and the drifter tracks were mostly south of the TED area. Nevertheless, the two measurement methods show a broadly similar magnitude and trend for λ. Drifter measurements directly measure N_D as a function of the distance of the closest approach to the HR2 receiver (e.g., Figure 11 in [9]) and the fitted functions in that figure give the values of λ that are plotted with black dots in Figure 7. This final method seems to be the most straightforward way to obtain λ from drifter tracks.
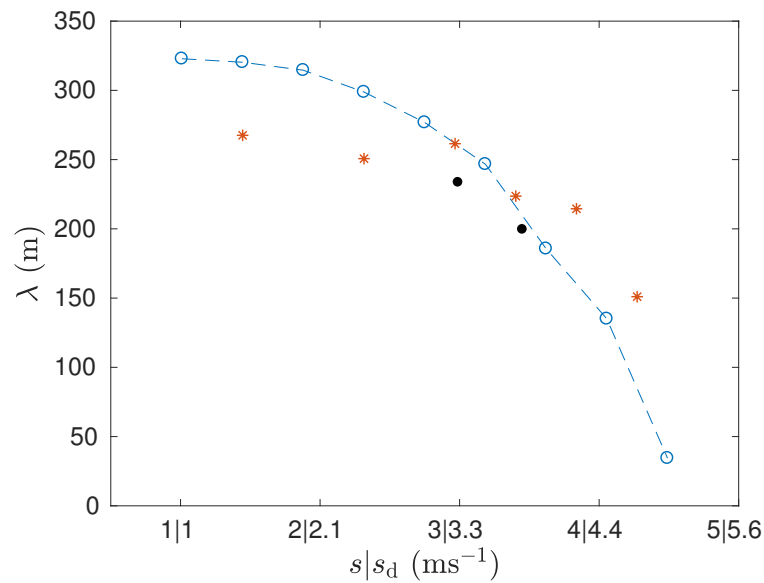
Figure 7. The half cross-current width scale for tag detection is a function of current speed. Blue circles show values obtained from Eulerian measurements of detection efficiency. Red asterisks show estimates obtained from Lagrangian measurements of p.

The trend for λ to decline with current speed (Figure 7) fundamentally defines the utility of our method for estimating the probability of encounter. As the current speed increases, the decline in λ shows that an individual HR2 receiver (proxy MHK turbine) will detect fewer tagged fish as they pass by, but λ appears in the denominator of (8), so this is offset by each detected passing event giving a higher value for $\mathcal{P}$. This compensating tendency will break down when λ becomes so small that limitations in the measurement of ρ also prevent λ from being numerically resolved. Figure 7 indicates that that limitation might start to apply for $s_d \approx 5 \text{ ms}^{-1}$, but that is a somewhat tentative number because the calculation of λ then depends on values for ρ that are interpolated between measurements made at ranges of about 1 m and 40 m [9]. In addition, range tests must have a long duration to obtain a large sample size for such fast tidal currents.

A passing event $E_{n,j,k}$ is characterized by the identity number n of the post-smolt, the station number j of the HR2 that best detected the passing post-smolt, and the time k at which the post-smolt passed by. With respect to obtaining estimates of probability of encounter, the time and station number serve to obtain signed current speed s that applies to a passing event. Equation (8) can be used to calculate a probability of encounter $\mathcal{P}_{n,j,k}$ for each passing event, as illustrated in Table 1 for seven smolts tagged in 2022 and detected at stations j and times k when the drift current speed was s_d. Without a correction for correlated ρ fluctuations, the probabilities of encounter ${}^E\mathcal{P}_{n,j,k}$ (4) tend to be about 6% smaller than $\mathcal{P}_{n,j,k}$.

Table 1 lays out the sequence of passing events for individual post-smolts in 2022. It is notable that successive passing events of a mid-passage station ($j = 1$ or 2) were common, whereas successive passing events of a station in the TED area were rare. The one occasion when a post-smolt ($n = 5$) passed Station 12 on both a flood tide and the immediately following ebb tide was preceded by five passing events at mid-passage and other offshore sites. These observations of post-smolts are consistent with drifter tracks that have quasi-stable trajectories through mid-passage but not, apparently, through the TED area [10].

Table 1. Probability $\mathcal{P}$ that each passing event would result in an encounter with a turbine installation at the position of the receiver that detected the passing event. These results are for the passing events for post-smolts 1–7, which were tagged in Gaspereau River in 2022.

$\mathcal{P}_{n,j,k}$	$^{E}\mathcal{P}_{n,j,k}$	smolt$_n$	stn$_j$	s_d (ms^{-1})	time$_k$
0.0608	0.0595	1	1	−1.91	17-May 10:33
0.0597	0.0597	1	2	0.06	18-May 18:24
0.0649	0.0613	1	1	2.86	19-May 02:07
0.1333	0.1075	1	12	4.36	19-May 16:33
0.0755	0.0678	1	9	3.42	20-May 06:05
0.0727	0.0662	1	5	−3.71	20-May 09:36
0.0607	0.0595	2	1	−1.76	20-May 13:00
0.0799	0.0689	2	8	4.08	20-May 15:53
0.0691	0.0634	2	12	−3.19	21-May 11:08
0.0713	0.0652	2	4	−3.61	21-May 23:38
0.0614	0.0597	2	7	2.26	22-May 08:39
0.0597	0.0586	3	12	−1.75	16-May 09:12
0.0643	0.0599	3	4	−2.55	16-May 21:29
0.0747	0.0672	3	4	−3.84	17-May 07:09
0.0671	0.0624	3	6	3.09	17-May 16:42
0.0739	0.0669	4	1	−3.78	17-May 20:48
0.1140	0.0955	4	2	4.68	18-May 03:58
0.0872	0.0762	4	2	−4.13	18-May 08:54
0.0618	0.0601	5	6	2.32	20-May 07:09
0.0719	0.0665	5	2	3.53	20-May 19:12
0.0757	0.0678	5	2	−3.85	20-May 22:47
0.0817	0.0699	5	4	4.09	21-May 06:06
0.0650	0.0606	5	1	−2.85	21-May 12:43
0.0777	0.0680	5	12	3.52	22-May 05:10
0.0636	0.0596	5	12	−2.64	22-May 12:49
0.0608	0.0595	6	1	−1.88	19-May 12:09
0.0676	0.0621	6	10	−3.06	20-May 11:16
0.0695	0.0641	6	2	3.27	20-May 19:21
0.4116	0.2615	6	1	5.86	21-May 04:54
0.0603	0.0594	7	1	−1.37	16-May 22:28
0.0604	0.0595	7	1	1.73	16-May 23:56
0.0610	0.0595	7	1	−1.99	17-May 10:29
0.0591	0.0587	7	9	−0.92	19-May 00:08
0.0606	0.0596	7	2	1.76	19-May 01:32
0.0699	0.0651	7	9	3.09	20-May 15:40
0.0587	0.0585	7	11	0.73	21-May 20:46
0.0647	0.0603	7	7	−2.82	21-May 22:26

Presently, the probabilities of an encounter are not discounted for the possibility that a post-smolt might swim above or below the levels swept by the blades of a near-surface turbine installation. This adjustment is best left until such time as more engineering details are available for a specific MHK turbine installation. It is generally understood that post-smolts swim near the surface [28].

The n'th post-smolt makes K passing events with each passing event having some probability of encounter with a turbine installation at some station location j (Table 1). From those probabilities, we can calculate the expected number of times that the n'th post-smolt will encounter a turbine installation in the TED area during a time interval required for the tagged post-smolt to complete its seaward migration through Minas Passage. The expected number of times $\mathcal{E}_{n,\text{TED}}$ that post-smolt n will encounter a single turbine installation within the TED area can be estimated using

$$\mathcal{E}_{n,\text{TED}} = \frac{1}{4} \sum_{k=1}^{K} \mathcal{P}_{n,9 \leq j \leq 12,k} \tag{10}$$

where the sum term is over those K passing events of four HR2 receivers within the TED area ($9 \leq j \leq 12$). Thus, the factor of $1/4$ normalizes to the expected number of times that post-smolt n would encounter a single turbine installation within the TED area. Although (10) is written to calculate $\mathcal{E}_{n,\mathrm{TED}}$ from $\mathcal{P}_{n,j,k}$, it equally applies to calculate ${}^E\mathcal{E}_{n,\mathrm{TED}}$ from values of ${}^E\mathcal{P}_{n,j,k}$. Similarly, selecting stations $1 \leq j \leq 2$ and normalizing by $1/2$ gives a mid-passage value $\mathcal{E}_{n,\mathrm{mid-passage}}$.

Averaging over all 23 post-smolts that reached Minas Passage in 2022 gives an estimate for the average number of times $\overline{\mathcal{E}}_{\mathrm{TED}}$ that a post-smolt might be expected to encounter a single turbine installation within the TED area

$$\overline{\mathcal{E}}_{\mathrm{TED}} = \frac{1}{23} \sum_{n=1}^{23} \mathcal{E}_{n,\mathrm{TED}}. \tag{11}$$

Figure 8 shows $\mathcal{E}_{n,\mathrm{TED}}$ for each tagged post-smolt that was estimated to have reached Minas Passage in the years 2019 and 2022. Note, for easy visualization we have renumbered the post-smolts in order of descending values of $\mathcal{E}_{n,\mathrm{TED}}$. There are many zero values for $\mathcal{E}_{n,\mathrm{TED}}$ because, of the N_{MP} post-smolts that were estimated to reach Minas Passage, only N_{TED} passed through the TED area (Table 2). Of those post-smolts that were detected within the TED area ($\mathcal{E}_{n,\mathrm{TED}} > 0$), values for $\mathcal{E}_n$ tended to be highest for 2019 post-smolts that were tagged in the Stewiacke River and lowest for 2022 post-smolts that were tagged in the Gaspereau River. High values of $\mathcal{E}_n$ for the post-smolts tagged in the Stewiacke River are, at least in part, associated with a relatively large ratio of the number E_{TED} of passing events that they make through the TED area relative to the number N_{TED} of post-smolts that passed through the TED area (Table 2).
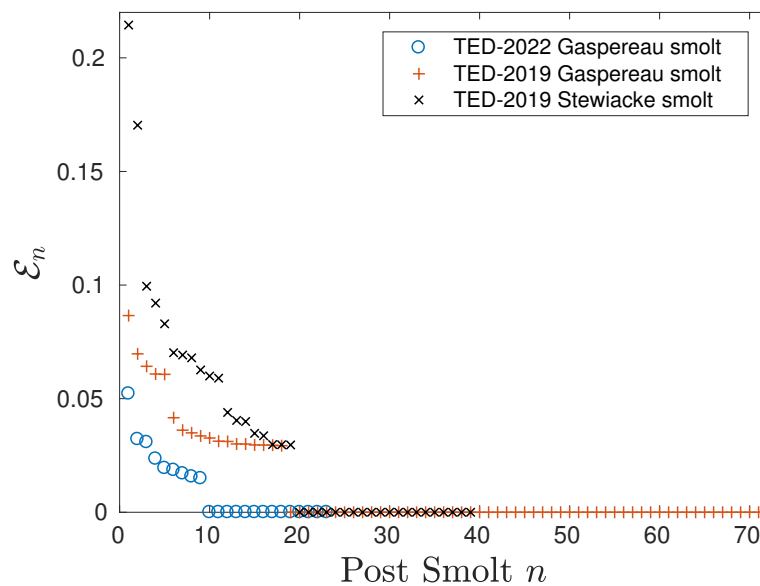

Figure 8. Expected number of encounters that each post-smolt would make with a single turbine installation at the TED area.

Table 2 indicates no meaningful difference between the 2019 and 2022 measurements of the average number of encounters $\overline{\mathcal{E}}_{\mathrm{TED}}$ for post-smolts that came from the Gaspereau River. On the other hand, $\overline{\mathcal{E}}_{\mathrm{TED}}$ is substantially greater for 2019 post-smolts from the Stewiacke River. These values are sensitive to the ratio of E_{TED} to N_{MP}. In 2022, the value of N_{MP} was confirmed in two ways. First, from measurements of tagged smolts travelling through the Gaspereau River, and second, by the extensive arrays (OTN and FORCE) of HR2 receivers in Minas Passage. In 2019, there were relatively few HR2 receivers deployed in Minas Passage, so estimates of the number of tagged post-smolts reaching Minas Passage N_{MP} are more open to question.

Table 2. Relating the expected number of encounters to the number of post-smolts detected in Minas Passage N_{MP} and at the TED area N_{TED}.

Post Smolts	N_{MP}	N_{TED}	E_{TED}	$\overline{\mathcal{E}}_{\text{TED}}(\mathcal{E}_{n,\text{TED}} > 0)$	$\overline{\mathcal{E}}_{\text{TED}}$
2022 Gaspereau	23	9	11	0.025 ± 0.004	0.010 ± 0.003
2019 Gaspereau	71	18	22	0.042 ± 0.004	0.011 ± 0.002
2019 Stewiacke	39	19	38	0.070 ± 0.011	0.034 ± 0.008

The 29 Stewiacke post-smolts that FORCE Minas Passage receivers detected in 2019 averaged 7.8 passing events each. This was considerably higher than the average of 3.0 passing events for the 43 Gaspereau post-smolts that were detected by the same receivers in Minas Passage. Taking values of N_{MP} at face value, Table 2 indicates that post-smolts from the Stewiacke River were more likely to migrate through the northern side of Minas Passage (i.e., through the TED area) than post-smolts from the Gaspereau River. This apparent difference is based on measurements made in a single year, so the result is tentative. Nevertheless, there might be a physical explanation for this difference. There is evidence for a clockwise gyre in the southern arm of Minas Basin [32,33]. Smolts migrating from Gaspereau River might be transported by this gyre, which would tend to put them on trajectories that would be more likely to pass through the mid or southern half of Minas Passage.

It might be argued that post-smolt encounters with turbines are benign at a sufficiently small current speed. Discarding $\mathcal{P}_{n,j,k}(|s_d| < 1)$ leaves an expected number of encounters applicable to an assumption that harm can only result if $|s_d| \geq 1$ m/s. Successive rows in Table 3 show how the number of harmful encounters drops as the threshold current is increased. The threshold current for harm is expected to depend upon the specific design of the turbines. For example, in order to approach the Betz limit the turbine blades typically have a tip speed much greater than the current speed [34] and harm becomes more likely for strike speeds above 5 m/s [35].

Table 3. Expected number of times that a smolt would encounter a single turbine installation during its seaward migration from the Gaspereau and Stewiacke Rivers.

2022 Gaspereau River		2019 Gaspereau River		2019 Stewiacke River		$|s_d|$
$\overline{\mathcal{E}}_{\text{TED}}$	$\overline{\mathcal{E}}_{\text{mid-passage}}$	$\overline{\mathcal{E}}_{\text{TED}}$	$\overline{\mathcal{E}}_{\text{S2}}$	$\overline{\mathcal{E}}_{\text{TED}}$	$\overline{\mathcal{E}}_{\text{S2}}$	(ms^{-1})
0.0098 ± 0.0030	0.075 ± 0.031	0.0110 ± 0.0024	0.014 ± 0.004	0.034 ± 0.0078	0.075 ± 0.017	≥ 0
0.0091 ± 0.0028	0.073 ± 0.031	0.0087 ± 0.0022	0.014 ± 0.004	0.032 ± 0.0078	0.072 ± 0.017	≥ 1
0.0091 ± 0.0028	0.072 ± 0.031	0.0082 ± 0.0022	0.013 ± 0.004	0.03 ± 0.0079	0.063 ± 0.016	≥ 1.5
0.0085 ± 0.0029	0.069 ± 0.032	0.0074 ± 0.0021	0.011 ± 0.004	0.026 ± 0.0071	0.058 ± 0.015	≥ 2
0.0078 ± 0.0029	0.067 ± 0.031	0.0070 ± 0.0020	0.008 ± 0.004	0.024 ± 0.0064	0.044 ± 0.013	≥ 2.5

Table 3 also compares the expected number of encounters with a turbine installation within the TED area (Figure 2) with an installation near mid-passage (Station 1 or 2 in 2022 and Station S2 in 2019). The number of encounters is greater for a turbine installation near the middle of Minas Passage than within the TED area. This is consistent with previous qualitative observations of tagged striped bass being detected more frequently to the south of the TED area than within the TED area [20]. There are two physical mechanisms that might be related to this result. First, the water column having been more stretched in the vertical (more horizontal convergence) as it passed into those deeper waters to the south of the TED area [36]. Such a convergence would concentrate animals that maintain their vertical component of position near the sea surface. Second, there is a quasi-stable drifter trajectory through mid-passage [10] so that post-smolts that get on that trajectory might pass many times back and forth with the tide.

4. Discussion

Fish mortality caused by a low-head turbine can sometimes be estimated by recovering all fish after they passed through the turbine [5,6]. It seems improbable that such straightforward and comprehensive methodology could be adapted to obtain mortality caused by a MHK turbine in the TED area in Minas Passage. A harm reduction premise of a MHK turbine is to enable free passage around the turbine, which makes recovering all fish that pass through the turbine an ill-defined objective unless their detailed trajectories are first accurately determined.

It seems more feasible to break the fish-turbine interaction problem into sequential parts, at least some of which may be tractable for measurement. First, identify whether local populations of interest are found at a TED area [20,21,24], in which case they might be said to have *co-occurrence* with MHK turbines. Estimation of the probability of encounter $\mathcal{P}$ might be considered a next step towards estimating percentage harm or mortality for a population.

We have defined the probability of encounter and calculated and measured it in a way that is consistent with modelling a local population. Elsewhere [15,37], metrics that were called "probability of encounter" are different in kind from those that we have defined and calculated. The metrics obtained by [15,37] are of interest in their own right but they cannot be compared to what we have carried out.

The present calculations of the probability of encounter are based upon a 500 kW near-surface installation of 6 MHK turbines set side-by-side in the FORCE TED area [10,25,26]. It is generally understood that post-smolts swim near the surface [28] so the probability of encounter takes no account of the possibility that some fish might swim at levels different from those swept by the turbine blades. Some measurements of post-smolt swimming depth have been made in Minas Passage [27] but it is presently unclear whether these will be sufficient for a robust calculation of the overlap of swimming depth with some specific turbine installation. More measurements of post-smolt swimming depth may be required. Swimming depth can be a key factor for the probability of encounter in the TED area, so a near-surface turbine is expected to have little overlap with striped bass [20] and a near-seafloor turbine to have little overlap with post-smolts.

A given post-smolt may pass through the TED area more than once during its seaward migration so we have summed over probabilities of encounter and normalized in order to estimate an average number of encounters $\overline{\mathcal{E}}_{\mathrm{TED}}$ that a post-smolt would be expected to make with a turbine installation within the TED area. If every encounter was fatal at current speeds greater than $1\,\mathrm{ms}^{-1}$, then that single turbine installation would cause approximately a 0.9% loss in the out-migrating population of post-smolts from the Gaspereau River and about a 3% loss of post-smolts from the Stewiacke River. Loses during the downriver migration were much higher (32% for the Stewiacke River in 2019, 18% for the Gaspereau River in 2019, and 8% for the Gaspereau River in 2022), although some of those losses may be a result of tagging effects and large downriver losses should not be thought to be inevitable [38]. It has been estimated that the average at-sea mortality of immature salmon was 97% for the 1990–2003 time period [29], so 0.9% or 3% out-migration losses caused by turbine installation would only add 0.027% or 0.09% to the 97% at-sea mortality. On the other hand, at-sea losses of immature salmon have not always been so high [29] and if the causes for those losses were identified and corrected then encounters of post-smolts with the turbine installation may be deemed more problematic. In this sense, the management of MHK turbine installations is fundamentally entangled with the management of fish populations in general.

Measuring the expected number of encounters $\overline{\mathcal{E}}_{\mathrm{TED}}$ requires an accurate estimate of the number N_{MP} of tagged post-smolts that reach Minas Passage. The 2022 array of HR2 receivers reliably detected tags passing through the central and northern portion of Minas Passage but did not extend sufficiently to the south to monitor all passing events [9]. Nevertheless, the 2022 array was sufficient to accurately determine N_{MP} because most post-smolts make multiple passes through the passage so the odds were improved that

at least one pass was through that part of the passage that was monitored. Larger fish may move more independently of the tidal currents and so it would be desirable for the receiver array to extend all the way across Minas Passage. The limited extent of the 2019 array makes corresponding estimates of N_{MP} less certain. A relatively large value of $\overline{\mathcal{E}}_{\mathrm{TED}}$ must still stand for the post-smolts that were tagged in the Stewiacke River because the largest possible value for N_{MP} would be 57, which is only sufficient to diminish $\overline{\mathcal{E}}_{\mathrm{TED}}$ from 0.032 to 0.022. On the other hand, the 2019 post-smolts from the Gaspereau River had a logically smallest value for N_{MP} of 43 (the number detected in Minas Passage), which would increase $\overline{\mathcal{E}}_{\mathrm{TED}}$ to 0.014. It is unlikely that both extremes of N_{MP} would apply, so it seems that in 2019 $\overline{\mathcal{E}}_{\mathrm{TED}}$ was larger for post-smolts from the Stewiacke River than for those from the the Gaspereau River. The proximate reason is that 2019 Stewiacke post-smolts made more passes through the TED area. More fundamentally this might indicate some difference in post-smolt trajectories to Minas Passage depending upon whether they began at the mouth of the Schubenacadie River or the mouth of the Gaspereau River. Further work is required to elucidate whether such differences are repeated and, if so, why?

The tip speed of a MHK turbine blade must be much faster than the current speed in order for the turbine to efficiently extract tidal energy [11,34]. Nevertheless, the current speed at which turbine blades become dangerous is unknown for specific turbines and operational procedures that might apply for future installations in Minas Passage. $\overline{\mathcal{E}}_{\mathrm{TED}}$ was, therefore, estimated for a range of critical current speeds, s_d from 0 to 2.5 ms^{-1}. $\overline{\mathcal{E}}_{\mathrm{TED}}$ typically declined by about 30% over that current range (Table 3).

Probability of encounter was estimated using a method that does not actually have a turbine installation in place. This was performed deliberately because where a turbine is installed it might influence fish behaviour, either by causing them to aggregate at the installation near slack tide [13,18] or to avoid the installation during fast currents [15–18]. A turbine operating near the Betz limit [11] will divert approximately one third of the approaching flow around the turbine, so if fish simply follow the flow then it should be expected that one third of them will avoid the turbine. Flume tank studies [14] showed salmon passing above the downwards sweeping blade, consistent with following deflected flow. It is expected that near surface MHK turbines that operate near the Betz limit would generate vibrational energy which fish might detect and respond to, perhaps by avoiding the area swept by turbine blades. This possibility has not been measured within the TED area in Minas Passage.

Presently, we have calculated the probability of encounter $\mathcal{P}$ from an ensemble averaged estimate of detection efficiency $\rho(r, s)$ with a small empirical correction (5) for fluctuations about the typical value at a given range r and modelled current speed s. In principle, signal detection is more fundamentally related to ambient noise level than modelled current or some other environmental variable. This raises the prospect of more directly estimating detection efficiency by directly measuring ambient levels at the 170 kHz frequency of HR signals and, perhaps, obtaining estimates of probability of encounter that are more specific to time and place.

The calculation of λ becomes uncertain in very fast currents (Figure 7) because very few measurements of ρ were obtained when $s > 4$ ms^{-1} [30]. Targeted range-test experiments to augment existing values for ρ should be carried out in the TED area during the largest spring tides with separations of tags and receivers to resolve ranges <50 m. Better mooring technology should be used to keep HR2 receivers sufficiently clear of the seafloor so signal paths are not blocked [30]. Based upon the present work, we recommend using tagged drifters to better quantify how well ρ relates to the detection of tagged fish as they pass the HR2 array [9]. Tagged drifters should also be used to obtain independent estimates of p and λ [9], and thereby enable independent spot checks of p and λ obtained from ρ. In the difficult field conditions encountered in Minas Passage, it is important to have multiple lines of evidence that confirm results.

In conclusion, we have measured the probabilities that post-smolts would encounter a turbine installation in the TED area in Minas Passage and have provided some context

for interpreting those probabilities. The probability that post-smolts will be harmed is expected to be lower than their probability of encounter because some might avoid the turbine or not suffer harm even though they pass through the area swept by turbine blades. It is hoped that the work will be useful for guiding future studies and, in the interim, be useful for assessing the merit of installing MHK turbines in the TED area relative to the ecological harm that they might inadvertently cause.

Abbreviations

The following abbreviations are used in this manuscript:

FORCE	Fundy Ocean Research Centre for Energy
DFO	Department of Fisheries and Oceans, Canada
OTN	Ocean Tracking Network, Canada
MHK	Marine hydrokinetic
TED	Tidal Energy Demonstration
PPM	Pulse position modulation
HR	High residency
HR2	High residence receiver
FVCOM	Finite-Volume Coastal Ocean Model
GPS	Global Positioning System

References

1. Price, D. Energy and human evolution. *Popul. Environ.* **1995**, *16*, 301–319. [CrossRef]
2. May, R.M. Ecological science and tomorrow's world. *Philosphical Trans. R. Soc. B* **2010**, *365*, 41–47. [CrossRef] [PubMed]
3. Karsten, R.; McMillan, J.; Lickley, M.; Haynes, R. Assessment of tidal current energy in the Minas Passage, Bay of Fundy. *J. Power Energy* **2008**, *222*, 289–297. [CrossRef]
4. Lenders, H.J.R.; Chamuleau, T.P.M.; Hendriks, A.J.; Lauwerier, R.C.G.M.; Leuven, R.S.E.W.; Verberk, W.C.E.P. Historical rise of waterpower initiated the collapse of salmon stocks. *Sci. Rep.* **2016**, *6*, 29269. [CrossRef] [PubMed]
5. DuBois, R.B.; Gloss, S.P. Mortality of juvenile shad and striped bass passed through Ossberger crossflow turbines at a small-scale hydroelectric site. *N. Am. J. Fish. Manag.* **1993**, *13*, 178–185. [CrossRef]
6. Watson, S.M.; Schneider, A.D.; Gardner, L.C.; Apell, B.R.; Thompson, P.C.; Cadman, G.B.; Gagnon, I.F.; Frese, C.R.; Wechsler, J.F. Juvenile alewife passage through a compact hydropower turbine designed for fish safety. *N. Am. J. Fish. Manag.* **2023** , *43*, 465–475. [CrossRef]

7. Dadswell, M.J.; Rulifson, R.A. Macrotidal estuaries: A region of collision between migratory marine animals and tidal power development. *Biol. J. Linn. Soc.* **1994**, *51*, 93–113. [CrossRef]

8. Karsten, R. An assessment of the potential of tidal power from Minas Passage, Bay of Fundy, using three-dimensional models. In Proceedings of the ASME 2001 30th International Conference on Ocean, Offshore and Arctic Engineering, OMEA2011-49249, Rotterdam, The Netherlands, 19–24 June 2011.

9. Sanderson, B.G.; Karsten, R.; Hasselman, D.J. Using drifters equipped with acoustic tags to verify the utility of detection efficiency measurements for estimating probability of fish-turbine encounter. *J. Mar. Sci. Eng.* 2023, *submitted*.

10. Sanderson, B.G.; Stokesbury, M.J.W.; Redden, A.M. 2021. Using trajectories through a tidal energy development site in the Bay of Fundy to study interaction of renewable energy with local fish. *J. Ocean. Technol.* **2021**, *16*, 50–70.

11. Betz, A. *Introduction to the Theory of Flow Machines*; Randall, D.G., Translator; Pergamon Press: Oxford, UK, 1966.

12. Hammar, L.; Andersson, S.; Eggertsen, L.; Haglund, J.; Gullstrom, M.; Ehnberg, J.; Molander, S. Hydrokinetic Turbine Effects on Fish Swimming Behaviour. *PLoS ONE* **2013**, *8*, e84141. [CrossRef]

13. Broadhurst, M.; Barr, S.; Orme, D. In-Situ Ecological Interactions with a Deployed Tidal Energy Device; An Observational Pilot Study. *Ocean. Coast. Manag.* **2014**, *99*, 31–38. [CrossRef]

14. Castro-Santos, T.; Haro, A. Survival and behavioral effects of exposure to a hydrokinetic turbine on juvenile Atlantic salmon and adult American Shad. *Estuaries Coasts* **2015**, *38* (Suppl. S1), 203–214. [CrossRef]

15. Shen, H.; Zydlewski, G.; Viehman, H.; Staines, G. Estimating the probability of fish encountering a marine hydrokinetic device. *Renew. Energy* **2016**, *97*, 746–756. [CrossRef]

16. Grippo, M.; Zydlewski, G.; Shen, H.; Goodwin, R.A. Behavioral responses of fish to a current-based hydrokinetic turbine under mutliple operational conditions. *Environ. Monit. Assess.* **2020**, *192*, 645. [CrossRef]

17. Viehman, H.A.; Zydlewski, G.B. Fish Interactions with a Commercial-Scale Tidal Energy Device in the Natural Environment. *Estuaries Coasts* **2015**, *38* (Suppl S1), S241–S252. [CrossRef]

18. Fraser, S.; Williamson, B.J.; Nikora, V.; Scott, B.E. Fish distributions in a tidal channel indicate the behavioural impact of a marine renewable energy installation. *Energy Rep.* **2018**, *4*, 65–69. [CrossRef]

19. Viehman, H.A.; Hasselman, D.J.; Douglas, J.; Boucher, T. The ups and downs of using active acoustic technologies to study fish at tidal energy sites. *Front. Mar. Sci.* **2022**, *9* , 1–16. [CrossRef]

20. Keyser, F.; Redden, A.M.; Sanderson, B.G. Winter presence and temperature-related diel vertical migration of Striped Bass *Morone saxatilis* in an extreme high flow passage in the inner Bay of Fundy. *Can. J. Fish. Aquat. Sci.* **2016**, *73*, 1777–1786. [CrossRef]

21. Stokesbury, M.J.W.; Logan-Chesney, L.M.; McLean, M.F.; Buhariwalla, F.F.; Redden, A.M.; Beardsall, J.W.; Broome, J.; Dadswell, M.J. Atlantic sturgeon spatial and temporal distribution in Minas Passage, Nova Scotia: A region of future tidal power extraction. *PLoS ONE* **2016**, *11*, e0158387. [CrossRef]

22. Lilly, J.; Dadswell, M.J.; McLean, M.f.; Avery, T.S.; Comolli, P.D.; Stokesbury, M.J.W. Atlantic sturgeon presence in a designated marine hydrokinetic test site prior to turbine deployment: A baseline study. *J. Appl. Ichthyol.* **2021**, *37*, 826–834. [CrossRef]

23. Sanderson, B.G.; Buhariwalla, C.; Adams, M.; Broome, J.; Stokesbury, M.; Redden, A.M. Quantifying detection range of acoustic tags for probability of fish encountering MHK devices. In Proceedings of the 12th European Wave and Tidal Energy Conference, Cork, Ireland, 27 August–1 September 2017.

24. Tsitrin, E.; Sanderson, B.G.; McLean, M.F.; Gibson, A.J.F.; Hardie, D.C.; Stokesbury, M.J.W. Migration and apparent survival of postspawning alewife (Alosa pseudoharengus) in Minas Basin, Bay of Fundy. *Anim. Biotelemetry* **2022**, *10*, 11. [CrossRef]

25. Davie, E. Tidal Energy Companies Join Forces for Bay of Fundy Project. CBC News. 2019. Available online: www.cbc.ca/news/canada/nova-scotia/sustainable-marine-energy-minas-tidal-lp-bay-of-fundy-tidal-power-1.5304276 (accessed on 1 March 2023).

26. Jeffcoate, P.; McDowell, J. Performance of PLAT-I, a floating tidal energy platform for inshore applications. In Proceedings of the 12th European Wave and Tidal Energy Conference, Cork, Ireland, 27 August–1 September 2017.

27. Solda, C. Migration Ecology of Inner Bay of Fundy Atlantic Salmon (*Salmo Salar*) Smolt, and the Relationship between Improvements in Tagging Technology and Surgical Procedures and Estimates of Post Surgery Survival. Master's Thesis, Acadia University, Wolfville, NS, Canada, 2023. *in preparation*.

28. Renkawitz, M.D.; Sheehan, T.F.; Goulette, G.S. Swimming depth, behavior, and survival of Atlantic salmon postsmolts in Penobscot Bay, Maine. *Trans. Am. Fish. Soc.* **2012**, *141*, 1219–1229. [CrossRef]

29. DFO. Recovery Potential Assessment for Inner Bay of Fundy Atlantic Salmon. DFO Canadian Science Advisory Secretariat Science Advisory Report 2008/050. 2008. Available online: https://waves-vagues.dfo-mpo.gc.ca/library-bibliotheque/335147.pdf (accessed on 1 March 2023).

30. Sanderson, B.G.; Bangley, C.W.; McGarry, L.P.; Hasselman, D.J. Measuring detection efficiency of 170 kHz high-residency acoustic signals in a fast-flowing tidal passage. *J. Mar. Sci. Eng.* 2023, *submitted*.

31. Chen, C.; Beardsley, R.C.; Cowles, G. An unstructured-grid, finite-volume coastal ocean model (FVCOM) system. *Oceanography* **2006**, *19*, 78–89. [CrossRef]

32. Greenberg, D.A. Modelling the mean barotropic circulation in the Bay of Fundy and Gulf of Maine. *J. Phys. Oceanogr.* **1983**, *13*, 886–904. [CrossRef]

33. Tee, K.T. Tide induced residual motion—verification of a numerical model. *J. Phys. Oceanogr.* **1977**, *7*, 396–402. [CrossRef]

34. Bahaj, A.S. Marine current energy conversion: The dawn of a new era in electricity production. *Phil. Trans. R. Soc. A* **2013**, *317*, 20120500. [CrossRef]

35. Amaral, S.V.; Bevelhimer, M.S.; Cada, G.F.; Giza, D.J.; Jacobson, P.T.; McMahon, B.J.; Pracheil, B.M. Evaluation of Behavior and Survival of Fish Exposed to an Axial-Flow Hydrokinetic Turbine. *N. Am. J. Fish. Manag.* **2015**, *35*, 97–113. [CrossRef]

36. Okubo, A. Horizontal dispersion of floatable particles in the vicinity of velocity singularities such as convergences. *Deep.-Sea Res.* **1970**, *17*, 445–454. [CrossRef]

37. Viehman, H.; Boucher, T.; Redden, A.M. Winter and summer differences in probability of fish encounter (spatial overlap) with MHK devices. In Proceedings of the 12th European Wave and Tidal Energy Conference, Cork, Ireland, 27 August–1 September 2017.

38. Newton, M.; Barry, J.; Dodd, J.A.; Lucas, M.C.; Boylan, P.; Adams, C.E. A test of the cumulative effect of river weirs on downstream migration success, speed and mortality of Atlantic salmon (*Salmo salar*) smolts: An empirical study. *Ecol. Freshwat. Fish* **2018**, *28*, 176–186. [CrossRef]

Appendix VI

'Scaling up' our understanding of environmental effects of marine renewable energy development from single devices to large-scale commercial arrays

Daniel J. Hasselman [a,*], Lenaïg G. Hemery [b], Andrea E. Copping [c], Elizabeth A. Fulton [d,e], Jennifer Fox [f], Andrew B. Gill [g], Brian Polagye [h]

[a] *Fundy Ocean Research Center for Energy, Halifax, NS, Canada*
[b] *Pacific Northwest National Laboratory, Coastal Sciences Division, Sequim, WA, USA*
[c] *Pacific Northwest National Laboratory, Coastal Sciences Division, Seattle, WA, USA*
[d] *CSIRO Environment, Hobart, TAS, Australia*
[e] *Centre for Marine Socioecology, University Tasmania, Hobart, TAS, Australia*
[f] *Aquatera Ltd., Stromness, Orkney, UK*
[g] *The Centre for Environment, Fisheries and Aquaculture Science, Lowestoft, Suffolk, UK*
[h] *Department of Mechanical Engineering, University of Washington, Seattle, WA, USA*

HIGHLIGHTS

- Marine renewable energy (MRE) growth is needed to help address impacts of climate change.
- MRE growth is impeded by uncertainty about how environmental effects manifest for arrays.
- We adapt and apply cumulative environmental effects terminology to stressors to conceptualize how effects 'scale up'.
- Environmental effects of a stressor may be dominant, additive, antagonistic or synergistic.
- How effects manifest is dependent on various factors (e.g., environmental heterogeneity, array location and configuration).

GRAPHICAL ABSTRACT
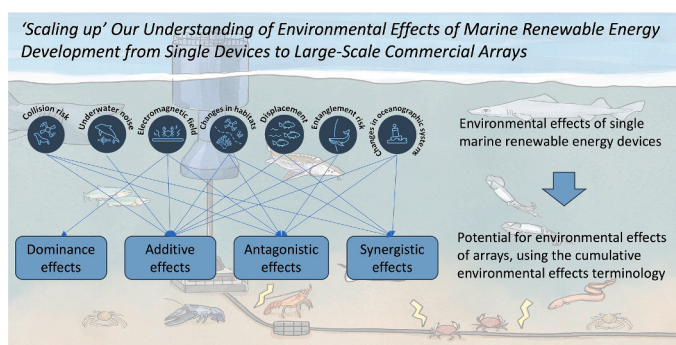
ARTICLE INFO

Editor: Martin Drews

ABSTRACT

Global expansion of marine renewable energy (MRE) technologies is needed to help address the impacts of climate change, to ensure a sustainable transition from carbon-based energy sources, and to meet national energy security needs using locally-generated electricity. However, the MRE sector has yet to realize its full potential due to the limited scale of device deployments (i.e., single devices or small demonstration-scale arrays), and is hampered by various factors including uncertainty about environmental effects and how the magnitude of these effects scale with an increasing number of devices. This paper seeks to expand our understanding of the environmental effects of MRE arrays using existing frameworks and through the adaptation and application of

* Corresponding author.
  E-mail address: dan.hasselman@fundyforce.ca (D.J. Hasselman).

Environmental monitoring
Marine ecosystems

cumulative environmental effects terminology to key stressor-receptor interactions. This approach facilitates the development of generalized concepts for the scaling of environmental effects for key stressor-receptor interactions, identifying high priority risks and revealing knowledge gaps that require investigation to aid expansion of the MRE sector. Results suggest that effects of collision risk for an array may be additive, antagonistic, or synergistic, but are likely dependent on array location and configuration. Effects of underwater noise are likely additive as additional devices are deployed in an array, while the effects of electromagnetic fields may be dominant, additive, or antagonistic. Changes to benthic habitats are likely additive, but may be dependent on array configuration and could be antagonistic or synergistic at the ecosystem scale. Effects of displacement, entanglement, and changes to oceanographic systems for arrays are less certain because little information is available about effects at the current scale of MRE development.

1. Introduction

Persistent development and global adoption of renewable energy systems, including marine renewable energy (MRE) technologies (e.g., tidal stream and riverine turbines, wave energy converters), is a crucial component in addressing the impacts of climate change (IPCC, 2019, 2022; IRENA, 2020), ensuring a sustainable transition from carbon-based energy sources, and for meeting national energy security needs using locally-generated electricity (e.g., European Commission, 2022). Globally, the amount of potentially harvestable tidal stream power is estimated to be 1200 TWh yr^{-1}, while that for wave power is estimated to be 29,500 TWh yr^{-1}; sufficient to meet current global electricity demand (Mørk et al., 2010; IRENA, 2020). However, the share of MRE in global electricity generation has remained low at approximately 1 TWh yr^{-1} since 2015 (IPCC, 2022); falling well short of its potential due to the relatively small number of MRE devices deployed to date (i.e., single devices, small demonstration-scale arrays). To meaningfully contribute to addressing the impacts of climate change, the scale of device deployments must increase to large-scale commercial arrays (hereafter 'arrays') for ensuring a sustainable transition from carbon-based energy sources (Vennell, 2012; Malki et al., 2014).

Numerous obstacles to MRE expansion exist (e.g., high capital cost of technology development, lack of infrastructure for device deployment/ maintenance, etc.), including difficulty obtaining regulatory approvals due to uncertain environmental effects (hereafter 'effects') of arrays (Neill et al., 2012; Kempener and Neumann, 2014a, 2014b; Copping et al., 2016). The limited scale of deployments to date has generated a paucity of post-installation data on effects that has generated uncertainty about their impacts on marine animals and habitats, and confounds our ability to differentiate between unknown (but perceived) and realized risks of MRE development for marine ecosystems (Copping et al., 2016; Copping and Hemery, 2020). A long-established framework for assessing the effects of MRE development focuses on understanding the interactions between 'stressors' (i.e., those parts of a device or system that may cause harm) and 'receptors' (i.e., those components of the ecosystem that may elicit some response to the stressor) (Boehlert et al., 2008; Boehlert and Gill, 2010; Copping and Hemery, 2020). Seven stressor-receptor interactions have been collectively recognized by regulators, stakeholders, developers, and researchers as key concerns post-installation (Copping and Hemery, 2020), and include:

- Collision risk for marine animals with tidal turbine blades or other device components,
- Effects of underwater noise on marine animal behavior and health from device operation,
- Effects of electromagnetic fields (EMFs) on marine species from cables and energized devices,
- Changes in benthic and pelagic habitats from anchors, foundations, and mooring lines,
- Displacement (i.e., attraction, avoidance, or exclusion) of marine animal populations from arrays of devices,
- Risk of entanglement of marine animals in mooring lines of floating devices, and

- Changes in oceanographic systems (e.g., water circulation, changes in wave heights, and sediment transport) from device operation and effects of energy removal from the system.

Our understanding of effects for these stressor-receptor interactions continues to improve for single devices and small pre-commercial arrays (Copping and Hemery, 2020; Copping et al., 2021; Gillespie et al., 2021). However, remaining uncertainties complicate the task of predicting how marine animals, habitats, and ecosystems will be impacted by arrays, and it is not realistic to assume that effects would scale linearly with the number of operational devices (Copping et al., 2016; Zhang et al., 2022). Effects of arrays are likely to be complex and nuanced, site specific and dependent on array configuration, cumulative in some form, and have potential for non-linear environmental responses. Thus, establishing generalized concepts for how effects may manifest with the development of arrays provides a foundation from which hypotheses can be formulated and tested to refine predictions and improve our understanding of the potential risks of 'scaling up'.

Informed development of such generalized concepts requires a multitiered approach incorporating modeling, experiments in controlled laboratory conditions and field settings, and the collection of empirical data to support (or refute) predictions and experimental results. This paper focuses on the development of generalized concepts for the seven stressor-receptor interactions, so that a robust scientific approach for developing and testing hypotheses can be applied to increase our knowledge of effects for arrays. This information is crucial for understanding risks and developing effective mitigation measures (as necessary) and is needed to facilitate the deployment of MRE technologies at scales that can make meaningful contributions for climate change, energy system transition and security. A brief overview of MRE technologies that are likely to comprise large-scale commercial arrays, and some of the previous work that has been conducted in support of establishing arrays is provided in the Appendix.

2. Methods

2.1. Defining 'large-scale commercial array'

No consistent definition exists in the literature about how many devices constitute a 'large-scale commercial array'. For the purposes of this study, we define this as 10–30 devices. We do not consider power generation capacity (e.g., megawatts of rated generation) in this definition, but rather the number of individual devices (wave energy converters, turbine rotors) that independently contribute to increasing the magnitude of effects for a given stressor. Under this definition, MRE technologies with multiple converters/rotors may be classified as arrays (albeit, typically small) and have intrinsic value for in situ testing of hypotheses and empirical data collection about how effects scale up.

2.2. Framework for understanding the scaling of environmental effects

In consultation with Ocean Energy Systems-Environmental (OES-E) analysts from around the world (experts in the environmental effects of MRE devices), we developed and applied a structured approach (i.e.,

multi-step framework outlined below; Fig. 1) for evaluating each of the seven stressor-receptor interactions, and conceptualizing how effects may scale up for arrays:

1. **Describe the stressor-receptor interaction.** Device deployment and operation can trigger various effects; the goal of this step was to describe the interaction.
2. **Summarize existing knowledge.** Existing knowledge about effects of the interaction for single MRE devices was summarized based on available literature (e.g., Copping and Hemery, 2020) and relevant surrogate industries.
3. **Define the nature of scaling up and identify any caveats that could influence how effects might manifest.** Generalized concepts about how effects of the interaction might scale up were developed using terminology adapted from the cumulative environmental effects literature (see below) and considering knowledge gaps that could influence our understanding.
4. **Identify the research required to improve our understanding of effects for arrays.** The most beneficial research (e.g., modeling exercises, laboratory trials, field studies) for testing the generalized concepts to increase our knowledge of how effects of the interaction scale were identified.

2.3. Environmental effects terminology for MRE arrays

Terminology does not exist to describe how effects of stressor-receptor interactions may scale with an increasing number of devices. While the cumulative environmental effects literature provides an informative framework for developing such nomenclature, that terminology is not easily or directly transferable because much of that research focuses on describing the nature of interactions *between*

different stressors (e.g., habitat loss, invasive species, climate change, etc.) (Folt et al., 1999; Halpern et al., 2008; Carrier-Belleau et al., 2021). Here, we are specifically interested in understanding how the effects of the *same* stressor changes with the number of devices, and have adapted cumulative effects terminology for that purpose. Earlier work associated with Environmental Impact Assessments does consider different activities (e.g., construction, operation, decommissioning) of a single development or the implications of multiple developments of a similar type within a general region. The latter, in particular, is relevant but typically relies on expert opinion, and does not have the desired rigor around the terminology that we seek to establish. However, we can take lessons from prior discourse on cumulative effects from an ecotoxicological perspective that has its foundations in human health (Suter et al., 2003). There are some parallels in the experience of the U.S. Environmental Protection Agency (2002) in going from considering a single exposure to increasing (intensifying) exposure from a single source, to exposure from multiple concurrent pathways that are useful in this context.

To help illustrate how effects may scale up, let us denote an individual device by D_i. As the number of devices increases (i.e., D_1, D_2, …, D_i…, D_n), the effects for a stressor may be characterized by comparatively simple additive or more complex non-linear (e.g., multiplicative) effects due to synergistic and antagonistic interactions (Coors and De Meester, 2008). We outline several scenarios to describe these effects below, and provide definitions for this terminology in an associated glossary (Table 1).

2.3.1. Scenario 1 – dominance effects

Albeit unlikely, for some stressors the effect may not scale with the number of devices (Fig. 2; Folt et al., 1999; Halpern et al., 2008; Côté et al., 2016; Carrier-Belleau et al., 2021), and the effect from one device may overwhelm the effect from other devices in an array.
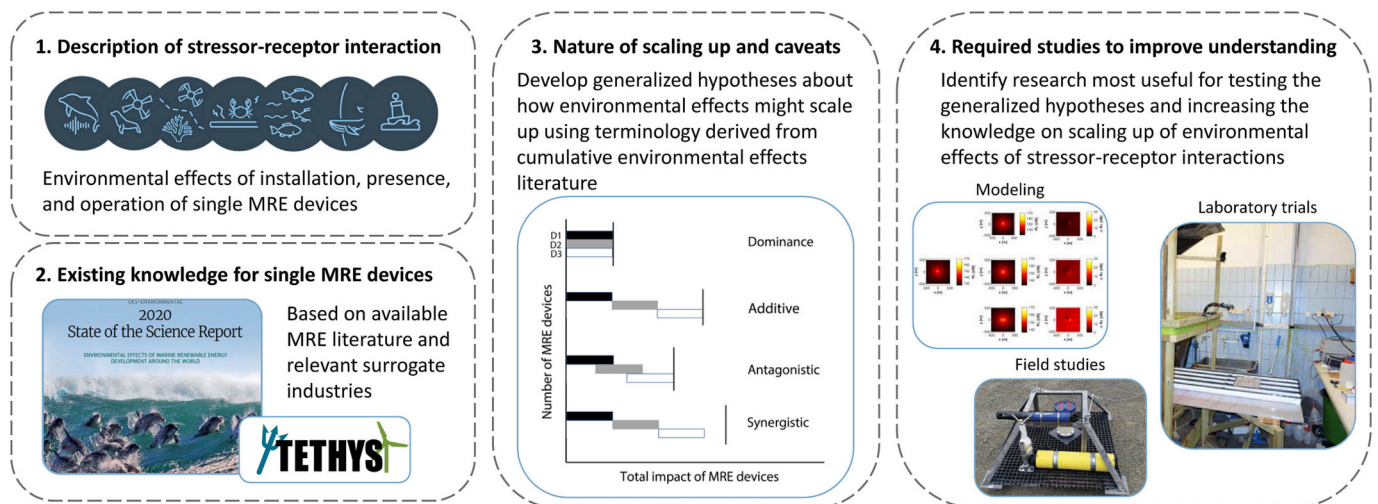

Fig. 1. Graphical representation of the multi-step framework developed for assessing each stressor-receptor interaction (icons from left to right: underwater noise, collision risk, changes in habitat, electromagnetic fields, displacement, entanglement, and changes to oceanographic systems) and conceptualizing how environmental effects may scale up from single marine renewable energy (MRE) devices to large-scale commercial arrays.

Table 1
Glossary of cumulative environmental effects terminology as applied to MRE arrays (derived from Folt et al., 1999; Halpern et al., 2008; Côté et al., 2016; Carrier-Belleau et al., 2021).

| Term	Description
Dominance effects	The environmental effect from the first device (or its associated infrastructure) overwhelms the effect from additional devices added to an array so that only the signature/footprint of the first device/infrastructure can be detected.
Additive effects	The cumulative environmental effect for a stressor equals the sum of the individual effects for each device in an array.
Antagonistic effects	The cumulative environmental effect for a stressor with an increasing number of devices in an array is diminished relative to additive expectations; possibly due to interactions between the actions of individual devices.
Synergistic effects	The cumulative environmental effect for a stressor with an increasing number of devices in an array is amplified relative to additive expectations; possibly due to interactions between the actions of individual devices.
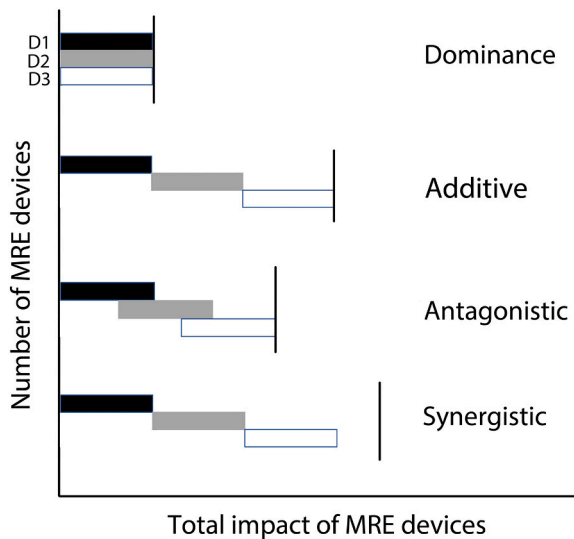
Fig. 2. Conceptual schematic for how environmental effects of a single stressor may scale with an increasing number of marine renewable energy (MRE) devices. Color bars represent the number of MRE devices (i.e., D1, D2, D3) and solid vertical lines represent the total environmental effect of the MRE devices for a given stressor. Conceptual design follows that outlined from the cumulative environmental effects literature (Halpern et al., 2008; Côté et al., 2016).

Quantitatively, this would be expressed as $D_{TOT} = \max (D_1, D_2, D_n)$. This could manifest if the installation of base infrastructure for devices was the dominant effect (e.g., common array infrastructure such as a power export cable to shore), and there was no increased footprint associated with additional devices.

2.3.2. Scenario 2 – additive effects

Additive effects are equal to the algebraic sum of the effect of a stressor for each device ($D_{TOT} = D_1 + D_2 + \ldots + D_i + \ldots + D_n$) (Fig. 2; Folt et al., 1999; Halpern et al., 2008; Côté et al., 2016). This could manifest with biofouling organisms independently colonizing all devices in an array, or with mobile organisms using all devices interchangeably as artificial reefs.

2.3.3. Scenario 3 – antagonistic effects

Under this scenario, the effect is equal to the sum of the effects for each additional device, but adjusted by some proportion that describes a diminished effect as the number of devices increases ($D_{TOT} = s_1D_1 + s_2D_2 + \ldots + s_nD_n$; where the individual s_i terms may all be identical or may vary with the device and where $s_i < 1$ (Fig. 2; Folt et al., 1999; Halpern et al., 2008; Côté et al., 2016). Where it is clear that the diminished effect is due to interactions between the actions of devices, this may also be represented as ($D_{TOT} = (D_1 + D_2 + \ldots + D_n) - (D_1 \times D_2 \times \ldots \times D_n)$). This scenario may arise for collision risk with tidal stream turbines, where the risk of collision for animals with each device may be equal, but they exhibit avoidance or evasion behaviors to prevent being struck by turbines (e.g., Gillespie et al., 2021); thereby decreasing the risk of collision as they navigate through (or past) an array.

2.3.4. Scenario 4 – synergistic effects

Synergistic effects can also originate from a scalar on the individual effects of a device or from multiplicative interactions, but in this case the effect from multiple devices exceeds the sum of the effects from individual devices (Fig. 2; Folt et al., 1999; Côté et al., 2016). This can be represented as either ($D_{TOT} = s_1D_1 + s_2D_2 + \ldots + s_nD_n$) where $s_i > 1$, or ($D_{TOT} = (D_1 + D_2 + \ldots + D_n) + (D_1 \times D_2 \times \ldots \times D_n)$) or simply ($D_{TOT} = D_1 \times D_2 \times \ldots \times D_n$), with the exact representation depending on the pathway of action. This scenario may be observed for displacement; while the presence of a single device may trigger some slight avoidance

Table 2
Summary of hypotheses for how environmental effects of seven key stressor-receptor interactions may scale up with the deployment of marine renewable energy (MRE) large-scale commercial arrays.

| Stressor-receptor interaction	Environmental effects				Notes
	Dominance	Additive	Antagonistic	Synergistic	
Collision risk		✓	✓	✓	Dependent on array layout, configuration (e.g., 'in parallel' vs. 'in series'), MRE technology type, site location, species' ability to detect device and avoid/evade collisions
Underwater noise		✓	✓		Area over which sound will be elevated will increase with array size; elevation in received levels will increase non-linearly
Electromagnetic fields	✓	✓	✓		EMFs increase linearly with additional electrical current; effects may be influenced by spatial arrangement of subsea cables
Changes to habitat		✓	✓	✓	Complex effects that may vary across spatiotemporal scales, with array geometry, and equivalency of effects for individual devices within an array
Displacement		✓	✓	✓	Effects observed at some threshold number of devices; no single threshold applicable across species or MRE device type
Risk of entanglement		✓	✓		Risk increases with number of MRE devices, but dependent on scale and configuration of mooring lines/cables, depth at MRE site, and animal behavior/movement
Changes to oceanographic systems		✓	✓		Effects observed at some threshold number of devices; dependent on MRE technology, number of devices, array configuration, and site specific hydrodynamics
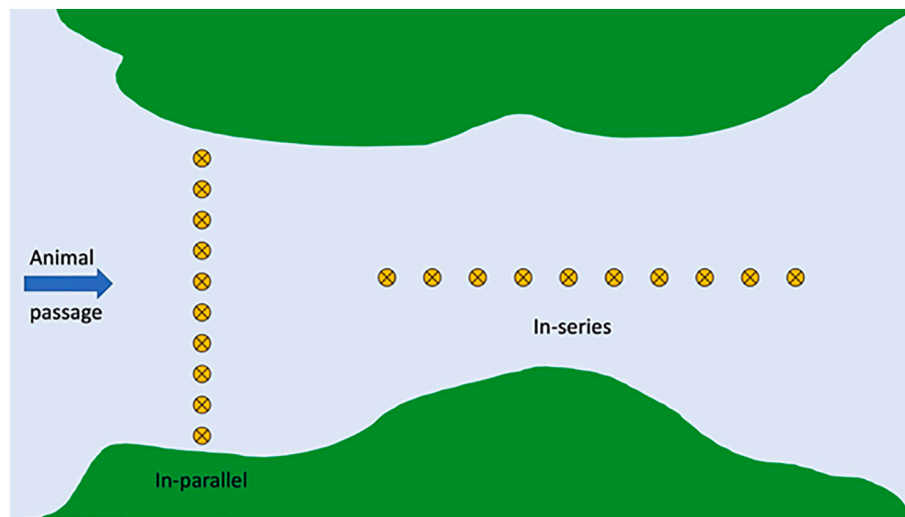
Fig. 3. Hypothetical 'in-parallel' and 'in-series' tidal turbine array configurations (redrawn from Wilson et al., 2006) relevant for considering the environmental effects of collision risk.

behavior with an animal swimming around the device, the presence of an array may result in complete exclusion from an area, particularly if the array spans a natural constriction in available habitat (e.g., tidal channels).

3. Results

Throughout this section, it is important to recognize that the scaling up of effects will be influenced by environmental heterogeneity, the characteristics of the environment that devices are deployed in (i.e., physical habitat, biological constituents), and the spatial arrangement of the array, among other factors. While understanding the effects of arrays requires a means for evaluating interactive effects among stressors and their cumulative impacts on marine ecosystems, that is beyond the scope of this paper.

3.1. Collision risk

3.1.1. Description

Collisions between animals and devices are thought to be the greatest risk of ocean current, river, and tidal stream turbine operations (Copping and Hemery, 2020). Collision risk describes the likelihood that animals might be harmed by coming into contact with moving parts of devices (Wilson et al., 2006), and applies most directly to components with a high velocity relative to the movement of water, such as turbine blades, tidal kites, or oscillating foils (Scottish Natural Heritage, 2016; Sparling et al., 2020a). Wave energy converters have no such components and are not thought to present much potential for collision risk (Copping et al., 2016; Greaves et al., 2016).

3.1.2. Existing knowledge

Collisions between marine animals and devices has been the focus of much research around single devices (Sparling et al., 2020a), and are expected to occur infrequently (Copping and Hemery, 2020). A recent synthesis of international research revealed no observations of collisions for marine mammals or seabirds (Sparling et al., 2020a), and the limited number of interactions with fish have not resulted in obvious harm (Matzner et al., 2017); although recent evidence suggests that fish passing through river turbines may become disoriented (Courtney et al., 2022). While it can be difficult to directly observe collisions in the field (Copping et al., 2021), mounting evidence suggests that when marine animals can detect turbines, they exhibit avoidance or evasion behaviors (Wilson et al., 2006; ABP Marine Environmental Research Ltd., 2010) to

prevent being struck (Viehman and Zydlewski, 2015; Fraser et al., 2018; Joy et al., 2018; Williamson et al., 2019; Gillespie et al., 2021; Onoufriou et al., 2021; Palmer et al., 2021). Laboratory-based studies (i.e., flume tests) support field observations that fish can exhibit avoidance and evasion behaviors under controlled conditions with relatively low flow (<2.5 ms^{-1}) (Castro-Santos and Haro, 2013; Amaral et al., 2015; Müller et al., 2023). However, the extent to which free-swimming fish can detect devices and exhibit avoidance and evasion in environments dominated by greater flow rates is generally unknown (Shen et al., 2016), but will be influenced by their size and swimming ability (Zhang et al., 2017) and the size and rotational speed of the device.

3.1.3. Nature of scaling and caveats

Considerable uncertainty remains about collision risk with single devices, and this limits what can be determined for arrays. Results to date suggest that collisions may manifest as additive, antagonistic, or synergistic effects (Table 2), but this may depend on the configuration and location of the array. Additive or perhaps synergistic effects may result if an array is configured to optimize energy extraction and is installed across an important migratory corridor (i.e., 'in-parallel'; Wilson et al., 2006) with no alternative routes for animals to access important resources (e.g., foraging grounds, spawning habitats, etc.) (Fig. 3). Under this scenario, migratory animals would need to navigate through the array and may have an elevated risk of collision as they attempt to access resources. Additive effects could also arise under this scenario if the animals exhibit avoidance and/or evasion behaviors to prevent collisions. Antagonistic effects could manifest if the array is configured 'in series' (Wilson et al., 2006) so that much of the migratory corridor remains unobstructed and animals have ample space to navigate around the array (Fig. 3).

How effects of collisions manifest for arrays may be site specific and technology specific (e.g., floating vs. bottom-mounted devices) and dependent on a variety of additional factors, including the physical habitat characteristics of the environment and the species under consideration, including their capacity to exhibit evasion and avoidance.

3.1.4. Research required to understand scaling effects

A better understanding of collision risk for marine animals with single devices is required to advance our understanding of the potential effects of arrays. In the absence of arrays for in situ assessments, modeling approaches and simulation studies provide some insight into understanding how effects may scale up (Table 3). Species distribution

Table 3

Generalized concepts, associated hypotheses, and research required to understand how environmental effects scale up for key stressors.

Stressor-receptor interaction	Conceptualized environmental effect(s) of arrays	Associated hypotheses	Research required
Collision risk	Additive, antagonistic, or synergistic	• How effects manifest is largely dependent on array layout/configuration (i.e., 'in parallel' vs. 'in series'). • Relevant factors are MRE technology type, habitat characteristics of deployment location, and species' capacity for avoidance and evasion.	• Additional in situ observations of marine animal interactions with single turbines are needed to determine number and effect of potential collisions. • Numerical models and simulations using realistic array layouts and configurations are needed to determine encounter rate, collision risk, and effects on populations. • Future collision risk modeling and simulations should incorporate avoidance and evasion behavior.
Underwater noise	Additive	• The elevation in received levels will be low but will increase logarithmically and level off after an initially rapid increase.	• Robust in situ characterization of received levels for a variety of MRE technologies using standardized protocols with comparison to known levels of disturbance. • Characterization of pertinent environmental parameters for meaningful interpretation of received levels. • Development of new, or modification of existing, underwater acoustic propagation models to predict received levels for arrays.
Electromagnetic fields	Dominance, additive, or antagonistic	• Effects will increase linearly with additional electrical current but will be dependent on array cable layout.	• Development of robust sensors for in situ measurement. • Systematic measurement over a range of power outputs where devices connect to shore-based facilities. • Controlled laboratory- and field-based studies of behavioral responses for EMF sensitive species to validate model predictions.
Changes to habitat	Additive, antagonistic, or synergistic	• Effects will vary across spatial and temporal scales, and with array configuration/layout and habitat characteristics (e.g., sediment type).	• Consistent collection of high-quality baseline habitat data prior to device deployment. • Incorporation of empirical data and development of habitat suitability models and ecosystem-wide models for simulating effects of arrays.
Displacement	Additive or synergistic	• Effects will become manifest at a threshold number of devices that induces sufficient levels of underwater noise, EMF, habitat changes, etc. to cause avoidance, exclusion, or attraction relative to array. • No single threshold number of devices is applicable across species or device type.	• A commonly accepted definition of displacement is required. • Models that simulate animal movement and migration in the vicinity of array are needed to predict effects of displacement. • Model validation using empirical observations are needed to determine deviations from normal movement pathways and migratory routes.
Risk of entanglement	Additive or antagonistic	• Effect will increase with number of deployed floating devices and associated mooring lines and draped power cables.	• Models and simulations are required to understand how effect increases with array size. • Empirical observational data (e.g., acoustic telemetry, imaging sonars, underwater video) for susceptible species required to validate model predictions.
Changes to oceanographic systems	Additive, antagonistic, or synergistic	• Effects will become manifest at a threshold number of devices. • Magnitude of effects will depend on MRE technology type, hydrodynamic conditions, and array size/layout/configuration.	• Improvements to numerical and physical hydrodynamic models are required, with particular focus on accurate resource characterization, site-specific bathymetry and hydrodynamics, and using realistic energy extraction modules (devices and their operation). • Empirical data for standard oceanographic variables to validate model predictions, with focus towards quantifying variability and uncertainty once arrays are deployed.

models derived from acoustic telemetry studies that draw linkages between species presence and physical environmental variables (e.g., turbulence and flow characteristics, water temperature, etc.) provide a means to predict the likelihood of species distributions overlapping with proposed MRE installations (Bangley et al., 2022) and can help quantify encounter rate and collision risk (Sanderson et al., 2023a, 2023b, 2023c). Incorporating studies of avoidance behavior into this framework and expansion to collision risk models, perhaps using a numerical Agent-Based Model (Rossington and Benson, 2020), a Eulerian-Lagrangian-Agent Method (ELAM) (Grippo et al., 2017), or fault tree analysis used in probabilistic risk assessments (Hammar et al., 2015), may further elucidate how site-specific effects of collisions scale up with an increasing number of devices (Table 3).

3.2. Underwater noise

3.2.1. Description

Animals use sound in the marine environment for a variety of biological functions, including communication, navigation, intraspecific and interspecific interactions, foraging and predation, and to avoid predation. Underwater noise generated during device installation may disrupt animal behavior, induce stress, and if sufficiently high in intensity (e.g., pile driving), may result in a range of physical injuries including a temporary or permanent reduction in hearing ability (Copping et al., 2013; Copping and Hemery, 2020; Hawkins and Popper, 2017; Southall et al., 2019), and in extreme cases barotrauma or death (Polagye and Bassett, 2020). Because of this, regulatory thresholds have been established in the United States for underwater noise effects on

marine mammals (NMFS, 2018), and guidance has been provided for fish (Hawkins et al., 2020). While the simplicity of such thresholds is attractive, ongoing research (e.g., Southall et al., 2021) aims to improve the understanding of behavioral effects, which have more nuanced drivers than the onset of hearing loss. Operational noise identified to date has been primarily associated with the device power take-off system (e.g., generator, power electronics), cable strumming, moorings, and maintenance activities (e.g., vessel traffic).

3.2.2. Existing knowledge

Operational noise measurements from tidal turbines and wave energy converters in France, Portugal, Spain, the United Kingdom, and the United States have not been associated with effects on marine life (Copping et al., 2020). While evidence suggests that operational noise is unlikely to cause acoustic injury to marine animals, behavioral responses are possible (Polagye and Bassett, 2020), and it has been shown that harbour seals (*Phoca vitulina*) avoid sounds from operational devices (Hastie et al., 2018), and harbour porpoise (*Phocoena phocoena*) activity was significantly reduced compared to baseline levels (Tollit et al., 2019). Because operational noise is generally low intensity (Polagye and Bassett, 2020), establishing a causal link between MRE operational noise and consequences to marine animals is challenging. Indeed, extrapolation of noise levels to effects on animals can be difficult because the undisturbed behavioral ecology of many marine animals is poorly characterized (De Dominicis et al., 2017), and because effects may be confounded by variation in the probability and severity of behavioral responses across taxonomic groups, among individuals across situational contexts, and across the temporal and spatial scales
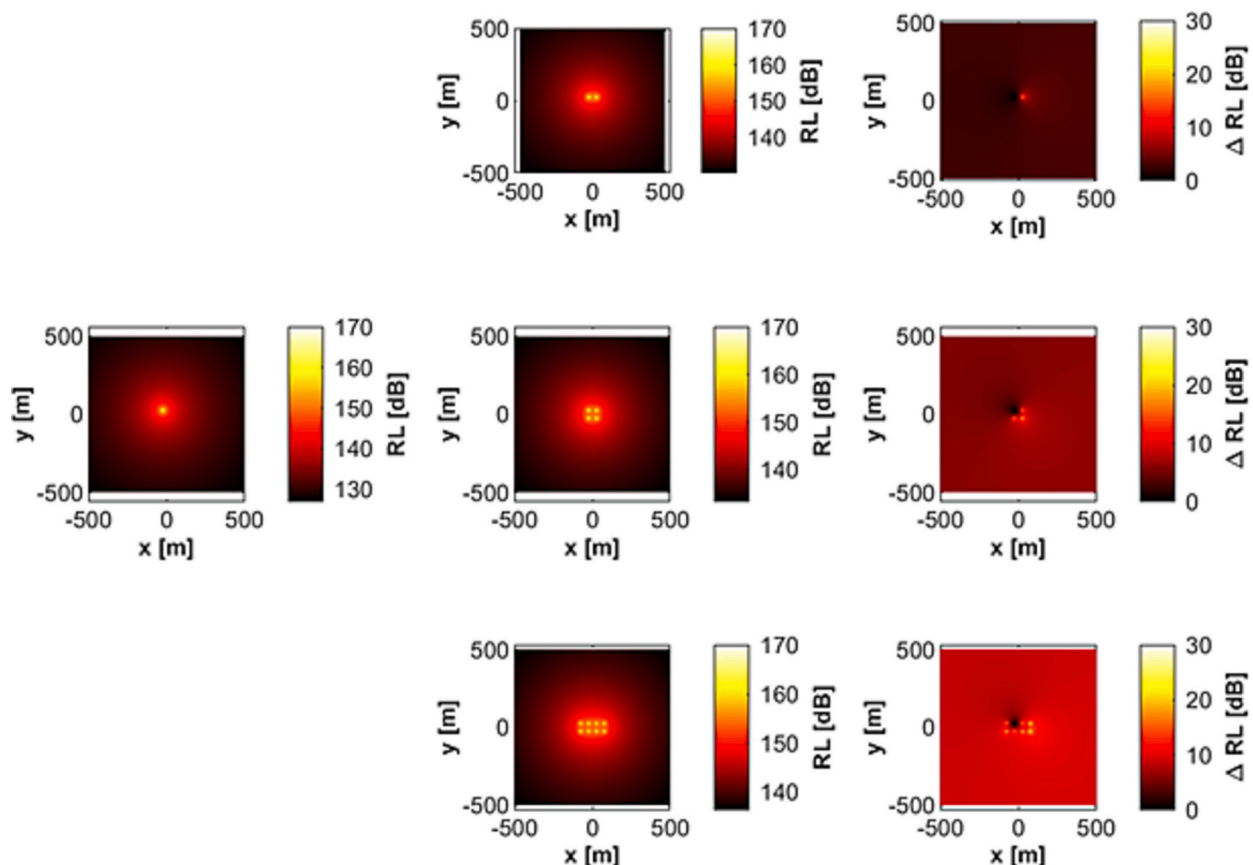

Fig. 4. Changes in far-field received levels (RL) as the number of MRE devices increases from two (top row) to four (middle row) to eight (bottom row), using as case study a source level of 170 dB, transmission loss coefficient of 15, 50 m spacing between devices, incoherent summation in pressure-squared space for the wave component of sound propagation. Left column is the spatial variation in RL for a single device (constant), the middle column is the map of RL for multiple devices, and the right column is the difference from the baseline case of a single marine renewable energy device. Note that the color bar range is different for the right column.

over which exposure can occur (Southall et al., 2021).

Sound propagates both as a pressure wave and as particle motion. There is greater scientific knowledge about the pressure wave portion of underwater noise, which affects marine mammals, than the particle motion component, which is more likely to affect fish and invertebrates (Nedelec et al., 2016; Popper and Hawkins, 2018; Copping et al., 2021). However, the distinction between wave and particle motion is only complicated at close range to a sound source (Popper and Hawkins, 2018); at greater range, a plane wave approximation is reasonable, and sound pressure (the propagating wave) and particle velocity are related by a simple algebraic expression.

3.2.3. Nature of scaling and caveats

The squared pressure for the wave portion of underwater noise is expected to scale in an additive manner with an increasing number of devices (Fig. 4; Table 2); however, the sound from adjacent devices will likely be incoherent due to variations in the tidal currents or wave fields. The area over which sound will be elevated from baseline levels is expected to scale with array size; although the maximum levels within the array are not expected to be significantly affected. Environmental conditions (e.g., bathymetry), array geometry, and technology type will influence how noise propagates within and around an array (e.g., Harding et al., 2023). While underwater noise from an array is expected to exceed baseline conditions at a greater range than for single devices, the elevation in received levels will be low; although greater at lower frequencies than at higher frequencies (Felis et al., 2021) (Fig. 4). As the number of devices increases, the elevation in received levels around an array is expected to increase logarithmically, leveling off after an initial rapid increase.

Several robust numerical acoustic propagation models exist (e.g., parabolic equation models) that can include the effects of environmental variables (e.g., bathymetry, seabed composition, sound speed profile). However, these attributes need to be thoroughly characterized in a MRE development area for the models to be meaningful (Madrid et al., 2021; Felis et al., 2021). Field data collected at MRE sites should adhere to the IEC 62600-40 technical specifications (International Electrotechnical Commission, 2019) to validate the models. Running these models will require intensive computational resources, and the requisite information about sound speed profiles and seabed composition can be difficult to collect, particularly at tidal energy sites where currents often result in a 'cobble pavement' that inhibits study of the seabed.

3.2.4. Research required to understand scaling effects

Gaps remain around acoustic characteristics of sound sources, the spatial and temporal resolution of acoustic data, incorporation of uncertainty in simulations, calibration of parameters and validation of results that need to be addressed (Madrid et al., 2021). To properly characterize the acoustic output of devices, we need in situ measurements of the underwater noise generated by multiple types of wave energy converter and tidal turbines in various environments using standardized protocols like the IEC 62600-40 technical specification (International Electrotechnical Commission, 2019) (Table 3). This protocol requires measurements at multiple ranges and operating conditions to build a more complete temporal-spatial knowledge base, as well as assess source directionality. To interpret these measurements through modeling, it would be beneficial to systematically collect additional environmental parameters such as bathymetry, seabed composition, and water column properties (e.g., temperature, salinity). However, we note that such data collection was explicitly excluded from the IEC 62600-40 specification to avoid imposing unreasonably high economic costs on early stage projects. That being said, with robust environmental data collected around single devices we could then develop or modify underwater acoustic propagation models to determine received levels within and around arrays (Harding et al., 2023). Even with significant uncertainty, the outputs from such models would be helpful in identifying relevant hydrophone deployment locations for in situ acoustic monitoring. In addition, through cooperation with MRE technology developers, it may be possible to systematically shut down turbines within an array during an acoustic survey, thereby isolating the effects of individual turbines from the array footprint and testing hypotheses about received sound levels.

Additionally, understanding how marine animals react to the frequency and sound level of underwater noise from devices is needed (ORJIP, 2022). While information about animal response to underwater noise could be generated through controlled laboratory studies, the most meaningful empirical data will be acquired around operational devices, and through relating noise levels to marine animal behavior at varying distances from a device. In addition, playback studies in representative environments (e.g., Hastie et al., 2018) can help to disentangle acoustic effects from other factors (e.g., prey aggregation). While some knowledge can be gained from single devices, greater uncertainty remains about how fish and marine mammals may respond to the noise emitted by arrays, which are likely to exceed ambient noise at greater ranges. For devices with novel components or larger size than those previously characterized, it will be important to examine the acoustic output to determine potential levels of harm and, if necessary, pursue mitigation measures.

3.3. Electromagnetic fields

3.3.1. Description

Electromagnetic fields (EMFs) are naturally present throughout the world's oceans from the background magnetic field of the Earth and also from atmospheric and solar influences. All species live within these natural fields and some animals have evolved the ability to sense and respond to them. EMFs are also generated by subsea power cables (inter-array and power export cables) that are needed to transmit power from MRE devices to shore. These sources may modify natural EMFs and can influence animal behavior (Gill et al., 2014; Hutchison et al., 2020) or have effects on species physiology, development, and growth (Woodruff et al., 2012) and biochemical processes (Kuz'mina et al., 2015); reviewed by Gill and Desender (2020). Power export cables that transmit the combined energy from multiple devices in an array have higher EMF levels resulting in greater spatial extent of EMFs; thereby, increasing the likelihood of encounter with EMF that may affect animals. While subsea cables between bottom-mounted devices will be placed on the seafloor, subsea cables between floating devices may be suspended in the water column; the location and orientation of the cable may result in different organisms coming into contact with emitted EMFs.

3.3.2. Existing knowledge

EMF research has primarily focused on single species responses for power cables from surrogate industries (e.g., offshore wind), or has involved laboratory-based experiments (Gill and Desender, 2020). Marine animals known to be receptive to EMFs include elasmobranchs (e.g., sharks and rays) and several other fish species, mammals, sea turtles, and some invertebrates (e.g., several molluscs and crustaceans) (Taormina et al., 2018). There is consensus among MRE researchers, developers, and regulators that EMFs traveling through cables from single or small numbers of devices will have relatively low EMF intensities and therefore of very localized extent, resulting in low potential for encounter with animals, and therefore pose a low risk to sensitive marine species (Copping et al., 2020).

Modeling studies have deduced levels of EMFs from energized cables, but none shed light on the potential effects on marine animals, and are only speculative about effects on behavior (Hutchison et al., 2021). Numerical models show that EMFs decrease with distance from the cable core (known as 'r', with the decay being $1/r$ or $1/r^2$, or exponential depending on the cable characteristics and geometries (Hutchison et al., 2021; Chainho and Bald, 2021)) which represents depending on whether power is direct current (HVDC) or alternating current (HVAC) (Normandeau Associates et al., 2011; Hutchison et al., 2021. In situ

measurements have shown that the EMFs can be present over several 10s of metres as the overall EMF environment is complex, and influenced by the power system, ambient magnetic fields (such as the geomagnetic field) and water movements (Hutchison et al., 2020, 2021). While burying cables under 1–2 m of sediment is often possible in areas with soft substrate and will reduce animal exposure to the strongest EMFs near the cable surface, the sediment layer does not alter the magnetic field (Taormina et al., 2018). Cable burial is not possible on hard bottom and, although cable protections (e.g., concrete mattresses or rock dumps) can provide some distance between a cable and most mobile EMF-receptive species, they also create new habitat for shelter-seeking animals like crustaceans, increasing their risk of EMF exposure (Albert et al., 2020).

3.3.3. Nature of scaling and caveats

The effects of EMFs for arrays are likely to be additive if cables are 10s of metres apart so that they do not interact (Fig. 2; Table 2). Basic physics shows that magnetic fields increase linearly as electrical current in a cable increases; this would occur with the additional power generation from multiple devices in an array, given a fixed transmission voltage. The layout of inter-array cables may also have additive effects, as each additional cable generates its own magnetic field. However, depending on the proximity and orientation of these cables relative to each other (e.g., 180°), the magnetic fields from separate cables could overlap, combine or cancel each other out (dominance or antagonistic effects).

Theoretical models of the intensity of EMF emitted from cables are available, but have rarely been verified or validated at scales that are relevant to the marine environment and EMF-sensitive animal (Madrid et al., 2021). Most EMF models have focused on deployments of bipole HVDC, or HVAC 3-conductor cables which are typically twisted around each other, which will lower emissions compared to the basic HVAC model (Grear et al., 2022).

It is possible that some magnetic field emissions are more biologically relevant than others. EMF-receptive species can respond to very low intensity changes (i.e., nT to µT for magnetic fields, nV/m to uV/m for electric fields) but the emission range at which these species may respond (such as attraction or avoidance) to artificial EMFs remains unknown and challenging to identify (Albert et al., 2020; Hutchison et al., 2020).

3.3.4. Research required to understand scaling effects

Accurately measuring in situ EMF emissions has been challenging and the development of robust sensors are needed for additional data acquisition from the marine environment (Gill and Desender, 2020; Hutchison et al., 2020), and for understanding how the effects of EMFs for arrays scale up (Table 3). Indeed, systematic measurements of EMFs are required where devices are connected to shore, particularly at test sites with multiple berths and power export cables. In the absence of arrays, such measurements could be gathered from existing high-capacity subsea power cables used in surrogate industries (e.g., offshore wind). Further, controlled laboratory and field-based studies using underwater imagery combined with fine-scale acoustic telemetry for EMF-sensitive species could enable observations of behavioral changes in the presence of EMFs (Table 3). Other effects and determination of thresholds to responses could be assisted by specific controlled studies as well.

3.4. Changes to habitat

3.4.1. Description

MRE systems (i.e., the device and supporting infrastructure – foundations and anchors, mooring lines and cables) will interact with benthic and pelagic habitats (Hemery, 2020) and may alter where animals live and how common they are in particular locations. Changes to habitats can result from the installation, operation, and/or decommissioning of MRE systems. Installations may lead to alteration, loss or creation of benthic and pelagic habitats, can lead to the inadvertent introduction of non-native species, and may cause potential changes to animal behavior or ecosystem function (Copping et al., 2016; Hemery, 2020).

3.4.2. Existing knowledge

The effects of MRE on benthic and pelagic habitats are similar to those of infrastructure involved in other well-studied marine industries (e.g., offshore wind turbines, oil and gas rigs, navigation and observation buoys, platforms, docks, and piers). However, unlike most other marine industries, MRE devices rarely span the entire water column to provide a continuum between intertidal and subtidal habitats.

Several studies of individually deployed devices have shown rapid recovery of the seafloor from the disturbance caused by device (O'Carroll et al., 2017) and cable installations (Taormina et al., 2018). While arrays have yet to be deployed, 21 "ecological foundations" were installed off the coast of Sweden in 2007 to study the effects of wave energy converter gravity-based foundations on the benthic environment. Soon after installation, a greater abundance of fish and invertebrates was observed on and around the foundations than at control sites (Langhamer and Wilhelmsson, 2009). The greater abundance persisted throughout the 12 year study, although with inter-annual variation in all taxa and years; successional increases in abundance and species richness were observed over the course of the study (Bender et al., 2020). Similar results have been observed elsewhere (Muxika et al., 2020, 2022).

Modeling studies suggest that i) species with pelagic larval dispersal may benefit from the presence of arrays to cross dispersal barriers (Adams et al., 2014), ii) increases in biomass at lower trophic levels due to the greater artificial reef effect of arrays will contribute to increasing biomass for higher trophic levels (Alexander et al., 2016), iii) effects on habitat suitability will differ for different species and array designs (du Feu et al., 2019), and iv) changes in biogeochemistry and primary productivity are not expected from array operations (Van Der Molen et al., 2016). The knowledge gained from these studies, combined with existing information from analogous offshore industries, can be leveraged to understand how effects of habitat changes will scale up with arrays; particularly with respect to the relatively small footprint of MRE foundations, anchors, cables, and mooring lines.

3.4.3. Nature of scaling and caveats

Changes to habitat is a complex stressor-receptor interaction with differing effects at varying spatiotemporal scales and different expectations about how effects may scale with an increasing number of devices. For changes like alterations to sedimentation patterns due to seabed scour and/or cable installation, seafloor area loss due to installation of foundations or cables, or artificial reef effects and biofouling biomass increases associated with new habitat creation, the scaling of effects is expected to be additive, with each device or associated structure in an array producing relatively similar levels of effects. However, scaling of the seabed scouring effect may depend on array geometry (e.g., spacing of anchors or foundations) and sediment type, and may be antagonistic in some cases (Fig. 2; Table 2). Moreover, each device within an array may not result in the same level of effect for facilitating larval dispersal of non-native species, or contributing to the overall changes to the local food web or reserve effect, due to the location of the device within the array (i.e., antagonistic or synergistic effects). Uncertainties remain about the spatial scales of these ecosystem-wide effects and their potential cumulative impacts, and there is an absence of empirical data to implement models (especially for less-studied species and habitats) and a lack of standardized methods for data collection.

3.4.4. Research required to understand scaling effects

Additional research is needed to identify the habitat changes that are most likely at MRE sites. Collecting robust and consistent baseline data prior to device deployments will provide empirical data for modeling

studies (e.g., habitat suitability models or ecosystem-wide models) that simulate the presence and operation of MRE arrays (Buenau et al., 2022) (Table 3). However, validation data will not be available until arrays are installed. Moreover, ecosystem-wide models need specific types of biological data (e.g., diet, growth rate, mortality rate) that are rarely (if ever) required by licensing authorities to be collected during baseline and monitoring surveys at MRE project sites. Comprehensive literature reviews will be needed to gather such data from foundational research studies; in the absence of such information, empirical data will need to be collected and included in models.

3.5. Displacement

3.5.1. Description

Displacement of aquatic animals due to the presence and/or operation of devices can be defined as the result of mechanisms (i.e., avoidance, exclusion, or attraction) that cause animals to depart from, or not enter into, their preferred or critical habitats, or to move into areas that are new to them (Hemery et al. *in review*). These mechanisms are triggered by a receptor's response to stressor(s), with a range of potential consequences from effects on individuals to populations.

3.5.2. Existing knowledge

Displacement of marine animals around single devices has not been thoroughly investigated and it is not expected to be observed at the current scale of the industry; it is likely to only become observable once arrays are installed (Buenau et al., 2022; Copping et al., 2021). Stressors likely to trigger displacement are the physical presence of devices, underwater noise, EMF, changes to habitat (including formation of artificial reefs), movement of devices, and hydrodynamic changes (Sparling et al., 2020b). Various marine animals are susceptible to displacement because of their lifestyle and biological attributes (e.g., maneuverability around devices): large whales, small cetaceans, pinnipeds, sirenians, sea turtles, seabirds, pelagic sharks and large fish, benthic sharks and rays, demersal fish, mobile invertebrates, and sessile invertebrates.

3.5.3. Nature of scaling and caveats

With little information available from single devices (e.g., Palmer et al., 2021), we anticipate that displacement will be observed at some threshold number of devices. This threshold may be device- and environment-specific, with no single threshold being broadly applicable across species or device types. Even though we may come to understand how some of the triggering stressors will scale up from single devices to arrays, there is nothing to indicate how the environmental effects of displacement will change with the number of MRE devices; they may be additive or synergistic (Fig. 2; Table 2). Although it seems intuitive that the effects of displacement will scale with the physical increase in area covered by an array, this hypothesis needs to be tested.

3.5.4. Research required to understand scaling effects

A commonly accepted definition of displacement is required to advance targeted research. With that definition established, and prior to the deployment of arrays, some information could be gleaned from agent-based models to demonstrate movement of animals in the vicinity of simulated arrays and the likely changes resulting from their presence (Table 3). These modeling exercises will need to consider the driving forces of attraction, avoidance, and exclusion. Both long distance migratory animals and those engaged in localized movements should be considered in models, including various life stages (e.g., pelagic larvae of benthic organisms) and animals with different maneuverability capacity around devices. Once arrays are installed, validation of model predictions using empirical data from field observations will be needed to ensure that the movements are as anticipated (Table 3). This could be conducted using acoustic and/or satellite telemetry, unmanned aerial vehicles (drones), passive acoustic monitoring, or other observational methods.

3.6. Risk of entanglement

3.6.1. Description

Floating and mid-water devices are attached to the seabed using anchors and mooring lines that allow them to maintain their position in the water column or on the sea surface. In an array, cables are often used to transport power from multiple devices to a single power export cable on the seabed. The potential for these lines and cables to become a hazard for marine animals that may become entangled or entrapped in them increases with the number of devices in an array.

3.6.2. Existing knowledge

Marine animals most at risk of entanglement are large cetaceans and sharks because of their size and behavior; however, smaller marine mammals, sea turtles, seabirds, and some large fish may also be at risk (Benjamins et al., 2014; Garavelli, 2020). The likelihood of entanglement in mooring lines and cables is a function of the line or cable configuration and scale, water depth at the MRE site, and animal size and behavior. The likely consequences of marine animal encounters with mooring lines and power cables (e.g., risk of injury or death) remains largely unknown, but parallels can be drawn from studies of entanglement with fishing gear (Garavelli, 2020). However, unlike lost or abandoned fishing gear, device mooring lines and cables do not have sufficient slack to form a loop, and there are no loose ends on lines or cables that pose such a risk. While the risk from single devices is perceived to be quite low, it may increase with the deployment of arrays.

3.6.3. Nature of scaling and caveats

While the presence of many mooring lines and intra-array cables in an array could create an increased risk of entanglement, this has not been shown for surrogate industries (e.g., nearshore or offshore aquaculture pens) (DeCew et al., 2012; Clement, 2013). We hypothesize that the effects will increase with the number and length of lines/cables in an additive or antagonistic manner (Fig. 2; Table 2). However, this will need to be tested using data collected from field observations and using numerical models. Currently, there is no empirical data about interactions of marine animals with MRE mooring lines and cables, and knowledge of animal usage, areas of occupancy, and behavior around MRE infrastructure is absent. Although simulation models of entanglement are being developed for large cetaceans with fishing gear (Howle et al., 2019), these would need to be adapted to the specific case of devices and deployment locations to be applicable.

3.6.4. Research required to understand scaling effects

There is an absence of empirical data for understanding the effects of entanglement, and it is not generally understood how much room species need to safely navigate through the series of mooring lines and cables required to support devices. This may be both species and site dependent. Prior to the deployment of arrays, baseline data about the spatial and temporal distribution of marine animals in the planned deployment area is needed to understand what species may be susceptible to entanglement. Thereafter, information from agent-based models and computer simulations that demonstrate animal movement in the vicinity of an array could be used to estimate the probability of an animal's path intersecting with mooring lines and cables (Table 3). This work should focus on species that are deemed to be at greatest risk from entanglement (e.g., large marine mammals, sea turtles). Once arrays are installed, validation of model predictions using empirical data from field observations will be needed to ensure that animal movements and probability of encounter estimates are accurate. This could be conducted using acoustic tags, imaging sonars mounted at various locations in the array, and underwater optical video.

3.7. Changes to oceanographic systems

3.7.1. Description

Tides, waves, currents, and water circulation comprise the oceanographic processes that control the marine environment by determining the concentrations of dissolved gases and nutrients, transporting sediment, and supporting habitats and water quality that maintain marine organism health and ecosystem function. The presence of devices and the extraction of energy from tidal currents and waves may alter these processes at varying spatial scales, reducing the amount of energy available in marine systems, potentially affecting water circulation (Hasegawa et al., 2011) and wave heights, and may impact marine chemical and biological processes with ecosystem-level effects. Depending on the location, scale of energy extraction, and local hydrodynamic processes, changes to water column and hydrography may be felt over large geographic areas (Frid et al., 2012).

3.7.2. Existing knowledge

Marine energy extraction may impact hydrodynamic features that are important for marine animal distribution (Jones et al., 2014; Mcilvenny et al., 2021; Bangley et al., 2022), predator-prey interactions (Lieber et al., 2021; Couto et al., 2022), and may influence sedimentation patterns and coastal erosion processes (Neill et al., 2012). However, the effects of energy extraction by single devices on circulation patterns and wave height are too small to be measured against the natural variability inherent in dynamic marine environments. While numerical models predict physical changes to current speed and wave amplitude from MRE extraction, these changes are only likely to become observable with the installation of arrays (e.g., de Santiago et al., 2020; Santiago et al., 2023). These changes and their subsequent effects on chemical and biological processes are likely to be site specific, but trends may be identified that apply across marine environments, differing MRE technology types, and specific groups of organisms (Whiting and Chang, 2020).

3.7.3. Nature of scaling and caveats

With no information available on the effects of single MRE devices on water circulation and wave height, we must rely on hydrodynamic models that use realistic simulations of devices for identifying the potential effects of arrays. Changes to oceanographic systems will become observable at some threshold number of devices, but this is highly dependent on the MRE technology, the number of devices in the array and their spatial arrangement, and site-specific hydrodynamic conditions. We anticipate that the effects of an array may be additive (Fairley et al., 2015), increasing with the physical area occupied by the array, or perhaps antagonistic or synergistic (Fig. 2; Table 2).

3.7.4. Research required to understand scaling effects

To understand the effects of arrays on oceanographic systems, numerical and physical models of systems must continue to be improved. Particular focus should be paid to accurate resource characterization, site-specific bathymetry and hydrodynamics, and the use of simulations that incorporate realistic devices and their operation (Table 3). Once arrays are installed, these models need to be validated using standard oceanographic measurements (i.e., temperature, salinity, conductivity, current measurements, wave height and period) with a focus on quantifying variability and uncertainty (Madrid et al., 2021).

4. Discussion and future directions

The generalized concepts established herein provide a basis for developing testable hypotheses so that a robust scientific approach can be used to increase our understanding of effects of arrays; thereby, improving our ability to delineate between unknown and realized risks of MRE development, identify critical knowledge gaps, and facilitate expansion of the MRE sector. A variety of factors (e.g., environmental heterogeneity, physical habitat characteristics, biological constituents of the environment, spatial arrangement of an array, etc.) will influence how effects of various interactions scale with an increasing number of devices. Beyond the potential for non-linear effects, it is important to consider that neither ecosystem components nor stressors exist in isolation, and associations between stressor-receptor interactions may result in magnified effects at larger spatiotemporal scales as the MRE sector expands (Raoux et al., 2021).

We have identified the need for simulation and modeling studies for several stressor-receptor interactions to help advance our understanding of environmental effects around large-scale commercial MRE arrays (Table 3). It is equally important to gather empirical data using standardized (where applicable) and appropriate methods to validate (or refute) model predictions and improve our capacity to understand how environmental effects of devices scale up. Future modeling exercises should consider realistic array configurations that will be limited by the physical constraints of the environment (e.g., geography, water depth, hydrodynamic complexities, channel width, bathymetric constraints, etc.) rather than the hypothetical configurations that have previously been used for understanding wake characteristics to maximize efficient energy extraction (Bryden et al., 2007; Myers and Bahaj, 2005; Turnock et al., 2011) (Appendix).

In this paper, we have defined large-scale commercial arrays based on the number of individual devices that independently contribute to increasing the magnitude of environmental effects for a given stressor-receptor interaction. Thus, MRE technologies with multiple converters/rotors can be considered as arrays (albeit, typically small) and have inherent value for in situ testing of some of the hypotheses developed herein and for collection of required empirical data; advancing our understanding about how environmental effects 'scale up' and informing decisions about commercial scale development of the MRE sector.

While the generalities of the effects for some stressors (e.g., underwater noise, EMF) may be transferable across some MRE sites, the specifics about how the magnitude of these effects scale up may not be, and could manifest as dominance, additive, antagonistic, or synergistic effects depending on the location. It is therefore important to recognize that the effects observed for an array in one location are not necessarily indicative of the effects of an array in a different area, and will need to be investigated using standardized methodologies.

As larger arrays are deployed in the ocean, there will be a need to assess the effects in the context of other anthropogenic activities. Using methods from the advancing field of cumulative effects assessment (Stelzenmüller et al., 2020), the pressures of devices and arrays on marine environments can be placed in context. At the same time, it will be important to assess the cumulative effects of the stressor-receptor interactions described in this paper. The framework proposed here, derived from cumulative environmental effects literature, may hold clues for determining the overall effect of a device or array on a group of animals or area of the ocean, from the sum of the stressors applied.

The greatest impediment to resolving the effects of MRE development on marine animals, habitats, and ecosystems remains the lack of empirical data collected around single devices and arrays after installation. The absence of available and consistent data will become more acute as the industry deploys arrays, particularly at scales that will provide substantial electricity to national grids. A system is needed to ensure that data are collected every time a demonstration, pilot, or commercial MRE project is deployed. While project and device developers are responsible for collecting data to satisfy regulatory requirements, much of the data needed to ensure that the design and

operation of MRE systems cause minimal damage and change to the marine environment must be the purview of a wider public interest. Governments and stakeholders supporting the deployment of MRE projects must facilitate funding for independent data collection using consistent and comparable methods to decrease the uncertainty inherent in the interactions described in this paper. This could be achieved by following the research actions advocated herein to validate the generalized concepts and test the associated hypotheses for each stressor-receptor interaction (Table 3). Devices are deployed at dedicated test sites to assess their survivability, power production potential, and pathway to commercialization. These are ideal locations for creating robust coordinated environmental monitoring programs, and can provide important empirical data for assessing some of the generalized concepts developed herein, but they require a stable source and suitable level of funding to conduct the required work. Consistent data collection over time will yield the data required to confidently put aside low risk aspects of MRE development, identify the functional limits of data collection to avoid expensive studies that are unlikely to yield actionable information, and to focus on those interactions that may cause elevated risks to the marine environment and its constituents.

CRediT authorship contribution statement

Daniel J. Hasselman: Conceptualization, Investigation, Methodology, Visualization, Writing - Original draft preparation, Writing - Reviewing and editing
Lenaïg G. Hemery: Conceptualization, Investigation, Methodology, Visualization, Writing - Original draft preparation, Writing - Reviewing and editing
Andrea E. Copping: Conceptualization, Funding acquisition, Resources, Writing - Original draft preparation, Writing - Reviewing and editing
Elizabeth A. Fulton: Writing - Original draft preparation, Writing - Reviewing and editing
Jennifer Fox: Methodology
Andrew B. Gill: Writing - Reviewing and editing
Brian Polagye: Writing - Reviewing and editing

Declaration of competing interest

The authors declare no conflict of interest. The project funders had no role in the design of the study, in the synthesis of the available information, in the writing of the manuscript, or in the decision to publish the study.

Data availability

No data was used for the research described in the article.

Acknowledgements

Appendix A

A.1. MRE technologies

Understanding environmental effects for MRE arrays requires knowledge of the technologies that may form the basis of large-scale commercial developments. While >40 ocean current and tidal stream turbine technologies were developed between 2006 and 2013, a convergence towards horizontal-axis turbines has been observed (Kempener and Neumann, 2014b; IRENA, 2020). Like the dominant wind turbine design, horizontal-axis turbines typically have 2–3 blades that are radially attached to a horizontal shaft that is connected to a powertrain system. Wave energy development has not witnessed a similar convergence on specific technologies, and over 50 different designs have been developed for generating electricity (Lewis et al., 2011). The most likely technologies for commercialization include i) point absorbers consisting of floating or submerged buoys that use the relative movement of the buoy to generate electricity, ii) oscillating water columns that use passing waves to compress air in a semi-submerged structure and drive an air turbine, and iii) oscillating water surge converters that use the surge motion of waves to capture energy via an oscillating flap (Kempener and Neumann, 2014a; IRENA, 2020).

A.2. Prior considerations with MRE arrays

Although consideration has been given to the effects of MRE arrays on seawater circulation patterns (Ahmadian et al., 2012; Bryden et al., 2007; De Dominicis et al., 2017; Zhang et al., 2022) and sediment dynamics (Neill et al., 2012; Robins et al., 2014; Fairley et al., 2015; Martin-Short et al., 2015; Auguste et al., 2022), the primary focus has been on optimizing device spacing to reduce detrimental wake interactions and maximize energy extraction and device efficiency (Stallard et al., 2013; Funke et al., 2016). This has been explored through laboratory experiments (Myers and Bahaj, 2012) and computer simulations (Wang and Müller, 2012; Malki et al., 2014; Karsten et al., 2013; Zhang et al., 2022) that typically use hypothetical rectilinear and staggered grid array configurations (Turnock et al., 2011). However, actual device deployments are limited by a variety of factors (e.g., geography, water depth, hydrodynamics, channel width, bathymetry) that directly influence array layout design (Bryden et al., 2007; Myers and Bahaj, 2005; Turnock et al., 2011). Consequently, large-scale commercial arrays will manifest as highly optimized geometric configurations (Malki et al., 2014; Myers and Bahaj, 2012) composed of clusters of devices vs. the generic/hypothetical layouts used in simulations. This reality of array configuration is important to consider for understanding how environmental effects for different stressors may scale up.

References

ABP Marine Environmental Research Ltd, 2010. Collision Risk of Fish With Wave and Tidal Devices. Southampton, Hampshire (Available from https://www.gov.wales/sites/default/files/publications/2019-07/marine-renewable-energy-strategic-framework-risk-to-fish.pdf).

Adams, T.P., Miller, R.G., Aleynik, D., Burrows, M.T., 2014. Offshore marine renewable energy devices as stepping stones across biogeographical boundaries. J. Appl. Ecol. 51 (2), 330–338. https://doi.org/10.1111/1365-2664.12207.

Ahmadian, R., Falconer, R., Bockelmann-Evans, B., 2012. Far-field modelling of the hydro-environmental impact of tidal stream turbines. In: Renew. Energy, 38(1). Elsevier Ltd., pp. 107–116. https://doi.org/10.1016/j.renene.2011.07.005

Albert, L., Deschamps, F., Jolivet, A., Olivier, F., Chauvaud, L., Chauvaud, S., 2020. A current synthesis on the effects of electric and magnetic fields emitted by submarine power cables on invertebrates. Mar. Environ. Res. 159 (November 2019), 104958 https://doi.org/10.1016/j.marenvres.2020.104958.

Alexander, K.A., Meyjes, S.A., Heymans, J.J., 2016. Spatial ecosystem modelling of marine renewable energy installations: gauging the utility of Ecospace. In: Ecol. Modell, 331. Elsevier B.V., pp. 115–128. https://doi.org/10.1016/j.ecolmodel.2016.01.016

Amaral, S.V., Bevelhimer, M.S., Čada, G.F., Giza, D.J., Jacobson, P.T., McMahon, B.J., Pracheil, B.M., 2015. Evaluation of behavior and survival of fish exposed to an axial-

flow hydrokinetic turbine. North Am. J. Fish. Manag. 35 (1), 97–113. https://doi.org/10.1080/02755947.2014.982333.

Auguste, C., Nader, J.R., Marsh, P., Penesis, I., Cossu, R., 2022. Modelling the influence of Tidal Energy Converters on sediment dynamics in Banks Strait, Tasmania. In: Renew. Energy, 188. Elsevier Ltd., pp. 1105–1119. https://doi.org/10.1016/j.renene.2022.02.077

Bangley, C.W., Hasselman, D.J., Flemming, J.M., Whoriskey, F.G., Culina, J., Enders, L., Bradford, R.G., 2022. Modeling the probability of overlap between marine fish distributions and marine renewable energy infrastructure using acoustic telemetry data. Front. Mar. Sci. 9 (July), 1–13. https://doi.org/10.3389/fmars.2022.851757.

Bender, A., Langhamer, O., Sundberg, J., 2020. Colonisation by wave power foundations by mobile mega- and macrofauna – a 12 year study. In: Mar. Environ. Res, 161 (February). Elsevier Ltd., 105053 https://doi.org/10.1016/j.marenvres.2020.105053

Benjamins, S., Hamois, V., Smith, H.C.M., Johanning, L., Greenhill, L., Carter, C., Wilson, B., 2014. Understanding the potential for marine megafauna entanglement risk from marine renewable energy developments. In: Scottish Nat. Herit. Comm. Rep. No. 791, 7, p. 95 (Available from http://www.snh.gov.uk/publications-data-and-research/publications/search-the-catalogue/publication-detail/?id=2174).

Boehlert, G., Gill, A., 2010. Environmental and ecological effects of ocean renewable energy development – a current synthesis. Oceanography 23 (2), 68–81. https://doi.org/10.5670/oceanog.2010.46.

Boehlert, G.W., McMurray, G.R., Tortocici, C.E., 2008. Ecological effects of wave energy development in the Pacific Northwest. In: NOAA Technical Memorandum NMFS-F/SPO-92 (Available from http://hdl.handle.net/1957/9426).

Bryden, I.G., Couch, S.J., Owen, A., Melville, G., 2007. Tidal current resource assessment. Proc. Inst. Mech. Eng. A J. Power Energy 221 (2), 125–135. https://doi.org/10.1243/09576509JPE238.

Buenau, K.E., Garavelli, L.J., Hemery, L.G., Medina, G.G., 2022. A review of modeling approaches for understanding and monitoring the environmental effects of marine renewable energy. J. Mar. Sci. Eng. 10 (94) https://doi.org/10.3390/jmse10010094. Available from.

Carrier-Belleau, C., Drolet, D., McKindsey, C.W., Archambault, P., 2021. Environmental stressors, complex interactions and marine benthic communities' responses. In: Sci. Rep, 11(1). Nature Publishing Group, UK, pp. 1–14. https://doi.org/10.1038/s41598-021-83533-1.

Castro-Santos, T., Haro, A., 2013. Survival and behavioral effects of exposure to a hydrokinetic turbine on juvenile Atlantic salmon and adult American shad. Estuar. Coasts 38 (1), 203–214. https://doi.org/10.1007/s12237-013-9680-6.

Chainho, P., Bald, J., 2021. Deliverable 3.1 (EMF Modelling). Corporate Deliverable of the WESE Project Funded by the European Commission. Agreement Number EASME/EMFF/2017/1.2.1.1/02/s12.787640. https://doi.org/10.13140/RG.2.2.22464.87049.

Clement, O., 2013. Effects on marine mammals. In: Sagar, P. (Ed.), Literature Review of Ecological Effects of Aquaculture. Ministry for Primary Industries, Cawthron Institute & National Institute for Water and Atmospheric Research Ltd, New Zealand, pp. 4.1–4.19.

Coors, A., De Meester, L., 2008. Synergistic antagonistic and additive effects of multiple stressors-predation threat parasitism and pesticide exposure in Daphnia magna. J. Appl. Ecol. 45, 1820–1828. https://doi.org/10.1111/j.1365-2664.2008.01566.x.

Copping, A.E., Hemery, L.G., 2020. OES-Environmental 2020 State of the Science Report: Environmental Effects of Marine Renewable Energy Development Around the World. Report for Ocean Energy Systems (OES). In: State Sci. Rep. https://doi.org/10.2172/1632878.

Copping, A.E., Hanna, L., Whiting, J., Geerlofs, S., Grear, M., Blake, K., Coffey, A., Massaua, M., Brown-Saracino, J., Battey, H., 2013. Environmental Effects of Marine Energy Development Around the World: Annex IV Final Report.

Copping, A.E., Sather, N.K., Hanna, L., Whiting, J., Zydlewski, G.B., Staines, G., Gill, G., Hutchison, I., O'Hagan, A.M., Simas, T., Bald, J., Sparling, C., Wood, J., Madsen, E., 2016. Annex IV 2016 State of the Science Report: Environmental Effects of Marine Renewable Energy Development Around the World. https://doi.org/10.1097/JNN.0b013e3182829024.

Copping, A.E., Freeman, M.C., Gorton, A.M., Hemery, L.G., 2020. Risk retirement — decreasing uncertainty and informing consenting processes for marine renewable energy development. J. Mar. Sci. Eng. 8 (3), 172. https://doi.org/10.3390/jmse8030172.

Copping, A.E., Hemery, L.G., Viehman, H., Seitz, A.C., Staines, G.J., Hasselman, D.J., 2021. Are fish in danger? A review of environmental effects of marine renewable energy on fishes. In: Biol. Conserv, 262. Elsevier Ltd., 109297 https://doi.org/10.1016/j.biocon.2021.109297

Côté, I.M., Darling, E.S., Brown, C.J., 2016. Interactions among ecosystem stressors and their importance in conservation. Proc. R. Soc. B Biol. Sci. 283 (1824), 20152592. https://doi.org/10.1098/rspb.2015.2592.

Courtney, M.B., Flanigan, A.J., Building, O.N., Hostetter, M., Seitz, A.C., 2022. Characterizing sockeye salmon smolt interactions with a hydrokinetic turbine in the Kvichak River, Alaska. North Am. J. Fish. Manag. 42, 1054–1065. https://doi.org/10.1002/nafm.10806.

Couto, A., Williamson, B.J., Cornulier, T., Fernandes, P.G., Fraser, S., Chapman, J.D., Davies, I.M., Scott, B.E., 2022. Tidal streams, fish and seabirds: understanding the linkages between mobile predators, prey and hydrodynamics. Ecosphere (November 2021), 1–15. https://doi.org/10.1002/ecs2.4080.

De Dominicis, M., O'Hara Murray, R., Wolf, J., 2017. Multi-scale ocean response to a large tidal stream turbine array. In: Renew. Energy, 114. Elsevier Ltd., pp. 1160–1179. https://doi.org/10.1016/j.renene.2017.07.058

de Santiago, I., Moura, T., Chambel, J., Liria, P., Bald, J., 2020. Deliverable 3.3 Marine Dynamics Modelling. Corporate Deliverable of the WESE Project Funded by the European Commission. Agreement Number EASME/EMFF/2017/1.2.1.1/02/s12.787640. https://doi.org/10.13140/RG.2.2.24981.45283.

DeCew, J., Celikkol, B., Baldwin, K., Chambers, M., Irish, J., Robinson Swift, M., Tsukrov, I., 2012. Assessment of a mooring system for offshore aquaculture. World Aquac. 43 (3), 32–36.

du Feu, R.J., Funke, S.W., Kramer, S.C., Hill, J., Piggott, M.D., 2019. The trade-off between tidal-turbine array yield and environmental impact: a habitat suitability modelling approach. In: Renew. Energy, 143. Elsevier Ltd., pp. 390–403. https://doi.org/10.1016/j.renene.2019.04.141

European Commission, 2022. REPowerEU: Joint European action for more affordable, secure and sustainable energy. https://commission.europa.eu/strategy-and-policy/priorities-2019-2024/european-green-deal/repowereu-affordable-secure-and-sustainable-energy-europe_en.

Fairley, I., Masters, I., Karunarathna, H., 2015. The cumulative impact of tidal stream turbine arrays on sediment transport in the Pentland Firth. In: Renew. Energy, 80. Elsevier Ltd., pp. 755–769. https://doi.org/10.1016/j.renene.2015.03.004

Felis, I., Madrid, E., Bald, J., 2021. Deliverable 3.2 (Acoustic Modelling). Corporate Deliverable of the WESE Project Funded by the European Commission. Agreement number EASME/EMFF/2017/1.2.1.1/02/S12.787640. https://doi.org/10.13140/RG.2.2.11559.68001.

Folt, C.L., Chen, C.Y., Moore, M.V., Burnaford, J., 1999. Synergism and antagonism among multiple stressors. Limnol. Oceanogr. 3 (2), 864–877. https://doi.org/10.1002/ece3.1465.

Fraser, S., Williamson, B.J., Nikora, V., Scott, B.E., 2018. Fish distributions in a tidal channel indicate the behavioural impact of a marine renewable energy installation. In: Energy Reports, 4. Elsevier Ltd., pp. 65–69. https://doi.org/10.1016/j.egyr.2018.01.008

Frid, C., Andonegi, E., Depestele, J., Judd, A., Rihan, D., Rogers, S.I., Kenchington, E., 2012. The environmental interactions of tidal and wave energy generation devices. In: Environ. Impact Assess. Rev., 32(1) Elsevier B.V., pp. 133–139. https://doi.org/10.1016/j.eiar.2011.06.002

Funke, S.W., Kramer, S.C., Piggott, M.D., 2016. Design optimisation and resource assessment for tidal-stream renewable energy farms using a new continuous turbine approach. In: Renew. Energy, 99. Elsevier Ltd., pp. 1046–1061. https://doi.org/10.1016/j.renene.2016.07.039

Garavelli, L., 2020. Encounters of marine animals with marine renewable energy device mooring systems and subsea cables. In: Copping, A.E., Hemery, L.G. (Eds.), OES-Environmental 2020 State Sci. Rep. Environ. Eff. Mar. Renew. Energy Dev. Around World, pp. 147–153.

Gill, A.B., Desender, M., 2020. Risk to animals from electro-magnetic fields emitted by electric cables and marine renewable energy devices. In: OES-Environmental 2020 State of the Science Report: Environmental Effects of Marine Renewable Energy Development Around the World. Report for Ocean Energy Systems (OES), pp. 86–110. https://doi.org/10.2172/1633088.

Gill, A.B., Gloyne-Philips, I., Kimber, J., Sigray, P., 2014. Marine renewable energy, electromagnetic (EM) fields and EM-sensitive animals. In: Shields, M.A., Payne, A.I.L. (Eds.), Marine Renewable Energy Technology and Environmental Interactions. Springer Netherlands, Dordrecht, pp. 61–79.

Gillespie, D., Hastie, G., Palmer, L., Macaulay, J., Sparling, C., 2021. Harbour porpoises exhibit localized evasion of a tidal turbine. Aquat. Conserv. Freshw. Ecosyst. 31 (9), 2459–2468. https://doi.org/10.1002/aqc.3660.

Grear, M.E., McVey, J.R., Cotter, E.D., Williams, N.G., Cavagnaro, R.J., 2022. Quantifying background magnetic fields at marine energy sites: challenges and recommendations. J. Mar. Sci. Eng. 10 (5), 687. https://doi.org/10.3390/jmse10050687.

Greaves, D., Conley, D., Magagna, D., Aires, E., Chambel, J., Witt, M., Embling, C.B., Godley, B.J., Bicknell, A.W.J., Saulnier, J., Simas, T., Marie, A., Hagan, O., Callaghan, J.O., Holmes, B., Sundberg, J., Torre-enciso, Y., Marina, D., 2016. Environmental Impact Assessment: gathering experiences from wave energy test centres in Europe. In: Int. J. Mar. Energy, 14. Elsevier Ltd., pp. 68–79. https://doi.org/10.1016/j.ijome.2016.02.003

Grippo, M., Shen, H., Zydlewski, G., Rao, S., Goodwin, A., 2017. Behavioral Responses of Fish to a Current-based Hydrokinetic Turbine Under Multiple Operational Conditions: Final Report (Available from). https://doi.org/10.1007/s10661-020-08596-5.

Halpern, B.S., Mcleod, K.L., Rosenberg, A.A., Crowder, L.B., 2008. Managing for cumulative impacts in ecosystem-based management through ocean zoning. Ocean Coast. Manag. 51, 203–211. https://doi.org/10.1016/j.ocecoaman.2007.08.002.

Hammar, L., Eggertsen, L., Andersson, S., Ehnberg, J., Arvidsson, R., Gullström, M., Molander, S., 2015. A probabilistic model for hydrokinetic turbine collision risks: exploring impacts on fish. PLoS One 10 (3), 1–25. https://doi.org/10.1371/journal.pone.0117756.

Harding, J.L., Preston, L.A., Johnson, E., Roberts, J.D., Jones, C.A., Raghukumar, K., Hafla, E., 2023. Modeling the acoustic noise from a wave energy converter farm and its impact on marine mammals at the PacWave South site, offshore Newport Oregon. Renew. Energy 209, 677–688. https://doi.org/10.1016/j.renene.2023.04.014.

Hasegawa, D., Sheng, J., Greenberg, D.A., Thompson, K.R., 2011. Far-field effects of tidal energy extraction in the Minas Passage on tidal circulation in the Bay of Fundy and Gulf of Maine using a nested-grid coastal circulation model. Ocean Dyn. 61 (11), 1845–1868. https://doi.org/10.1007/s10236-011-0481-9.

Hastie, G.D., Russell, D.J.F., Lepper, P., Elliott, J., Wilson, B., Benjamins, S., Thompson, D., 2018. Harbour seals avoid tidal turbine noise: implications for collision risk. J. Appl. Ecol. 55 (2), 684–693. https://doi.org/10.1111/1365-2664.12981.

Hawkins, A.D., Popper, A.N., 2017. A sound approach to assessing the impact of underwater noise on marine fishes and invertebrates. ICES J. Mar. Sci. 74 (3), 635–651. https://doi.org/10.1093/icesjms/fsw205.

Hawkins, A.D., Johnson, C., Popper, A.N., 2020. How to set sound exposure criteria for fishes. J. Acoust. Soc. Am. 147 (3), 1762–1777. https://doi.org/10.1121/10.0000907.

Hemery, L.G., 2020. Changes in benthic and pelagic habitats caused by marine renewable energy devices. In: C.A.E, Hemery, L.G. (Eds.), OES-Environmental 2020 State of the Science Report: Environmental Effects of Marine Renewable Energy Development Around the World. Report for Ocean Energy Systems (OES), pp. 105–125.

Howle, L.E., Kraus, S.D., Werner, T.B., Nowacek, D.P., 2019. Simulation of the entanglement of a North Atlantic right whale (*Eubalaena glacialis*) with fixed fishing gear. Mar. Mamm. Sci. 35 (3), 760–778. https://doi.org/10.1111/mms.12562.

Hutchison, Z.L., Gill, A.B., Sigray, P., He, H., King, J.W., 2020. Anthropogenic electromagnetic fields (EMF) influence the behaviour of bottom-dwelling marine species. Sci. Rep. 10 (1), 1–15.

Hutchison, Z.L., Gill, A.B., Sigray, P., He, H., King, J.W., 2021. A modelling evaluation of electromagnetic fields emitted by buried subsea power cables and encountered by marine animals: considerations for marine renewable energy development. Renew. Energy 177, 72–81. https://doi.org/10.1016/j.renene.2021.05.041.

International Electrotechnical Commission, 2019. Marine Energy - Wave, Tidal and Other Water Current Converters - Part 40: Acoustic Characterization of Marine Energy Converter.

IPCC, 2019. Special report on the ocean and cryosphere in a changing climate. In: The Ocean and Cryosphere in a Changing Climate. https://doi.org/10.1017/9781009157964 (Cambridge UK and New York, NY, USA).

IPCC, 2022. Climate change 2022: mitigation of climate change. In: Shukla, J.M.P.R., Skea, J., Slade, R., Al Khourdajie, A., van Diemen, R., McCollum, D., Pathak, M., Some, S., Vyas, P., Fradera, R., Belkacemi, M., Hasija, A., Lisboa, G., Luz, S. (Eds.), Contribution of Working Group III to the Sixth Assessment Report of the Intergovernmental Panel on Climate Change. Cambridge University Press, Cambridge, UK and New York, NY, USA. https://doi.org/10.1017/9781009157926.

IRENA, 2020. Innovation Outlook - Ocean Energy Technologies. Abu Dhabi (Available from https://www.irena.org/-/media/Files/IRENA/Agency/Publication/2020/Dec/IRENA_Innovation_Outlook_Ocean_Energy_2020.pdf).

Jones, A.R., Hosegood, P., Wynn, R.B., De Boer, M.N., Butler-Cowdry, S., Embling, C.B., 2014. Fine-scale hydrodynamics influence the spatio-temporal distribution of harbour porpoises at a coastal hotspot. In: Prog. Oceanogr, 128. Elsevier Ltd., pp. 30–48. https://doi.org/10.1016/j.pocean.2014.08.002

Joy, R., Wood, J.D., Sparling, C.E., Tollit, D.J., Copping, A.E., McConnell, B.J., 2018. Empirical measures of harbor seal behavior and avoidance of an operational tidal turbine. In: Mar. Pollut. Bull, 136. Elsevier, pp. 92–106. https://doi.org/10.1016/j.marpolbul.2018.08.052.

Karsten, R., Swan, A., Culina, J., 2013. Assessment of arrays of in-stream tidal turbines in the Bay of Fundy. Philos. Trans. R. Soc. A Math. Phys. Eng. Sci. 371 (1985), 20120189. https://doi.org/10.1098/rsta.2012.0189.

Kempener, R., Neumann, F., 2014a. Wave energy technology brief. In: IRENA Ocean Energy Technology Brief 4 (Available from https://www.irena.org/-/media/Files/IRENA/Agency/Publication/2014/Wave-Energy_V4_web.pdf).

Kempener, R., Neumann, F., 2014b. Tidal energy technology brief. In: IRENA Ocean Energy Technology Brief 3 (Available from https://www.irena.org/-/media/Files/IRENA/Agency/Publication/2014/Tidal_Energy_V4_WEB.pdf.).

Kuz'mina, V.V., Ushakova, N.V., Krylov, V.V., 2015. The effect of magnetic fields on the activity of proteinases and glycosidases in the intestine of the crucian carp *Carassius carassius*. Biol. Bull. 42 (1), 61–66. https://doi.org/10.1134/S1062359015010070.

Langhamer, O., Wilhelmsson, D., 2009. Colonisation of fish and crabs of wave energy foundations and the effects of manufactured holes - a field experiment. In: Mar. Environ. Res, 68(4). Elsevier Ltd., pp. 151–157. https://doi.org/10.1016/j.marenvres.2009.06.003

Lewis, A., Estefen, S., Huckerby, J., Musial, W., Pontes, T., Torres-Martinez, J., 2011. Ocean energy. In: Edenhofer, O., Pichs-Madruga, R., Sokona, Y., Seyboth, K., Matschoss, P., Kadner, S., Zwickel, T., Eickmeier, P., Hansen, G., Schlomer, S., von Stechow, C. (Eds.), IPCC Special Report on Energy Sources and Climate Change Mitigtion. Cambridge University Press, Cambridge, UK and New York, NY, USA, pp. 497–534.

Lieber, L., Langrock, R., Nimmo-Smith, A., 2021. A bird's eye view on turbulence: seabird foraging associations with evolving surface flow features. Proc. R. Soc. B 28, 20210592. https://doi.org/10.1098/rspb.2021.0592.

Madrid, E., de Santiago, I., Moura, T., Chainho, P., 2021. Deliverable 3.4 (Synthesis of Knowledge Acquired and Gap Analysis). Corporate Deliverable of the WESE Project Funded by the European Commission. Agreement Number EASME/EMFF/2017/1.2.1.1/02/s12.787640. https://doi.org/10.13140/RG.2.2.34034.58568.

Malki, R., Masters, I., Williams, A.J., Nick Croft, T., 2014. Planning tidal stream turbine array layouts using a coupled blade element momentum - computational fluid dynamics model. In: Renew. Energy, 63. Elsevier Ltd., pp. 46–54. https://doi.org/10.1016/j.renene.2013.08.039

Martin-Short, R., Hill, J., Kramer, S.C., Avdis, A., Allison, P.A., Piggott, M.D., 2015. Tidal resource extraction in the Pentland Firth, UK: potential impacts on flow regime and sediment transport in the Inner Sound of Stroma. In: Renew. Energy, 76. Elsevier Ltd., pp. 596–607. https://doi.org/10.1016/j.renene.2014.11.079

Matzner, S., Trostle, C., Staines, G., Hull, R., Avila, A., Harker-Klimes, G.E.L., 2017. Triton: Igiugig fish video analysis project report. Available from. https://tethys.pnnl.gov/sites/default/files/publications/Triton-Igiugig-Report.pdf.

Mcilvenny, J., Youngson, A., Williamson, B.J., Gauld, N.R., Goddijn-Murphy, L., Del Villar-Guerra, D., 2021. Combining acoustic tracking and hydrodynamic modelling to study migratory behaviour of Atlantic salmon (Salmo salar) smolts on entry into high-energy coastal waters. In: ICES J. Mar. Sci, 78(7). Oxford University Press, pp. 2409–2419. https://doi.org/10.1093/icesjms/fsab111.

Mørk, G., Barstow, S., Kabuth, A., Pontes, M.T., 2010. Assessing the Global Wave Energy Potential. In: Proceedings of the ASME 2010 29th International Conference on Ocean, Offshore, and Arctic Engineering, June 6–11, 2010, Shanghai, China.

Müller, S., Muhawenimana, V., Sonnino-Sorisio, G., Wilson, C.A.M.E., Cable, J., Ouro, P., 2023. Fish response to the presence of hydrokinetic turbines as a sustainable energy solution. Sci. Rep. 13, 7459. https://doi.org/10.1038/s41598-023-33000-w.

Muxika, I., Vinagre, P., Bald, J., 2020. Deliverable 2.4 (Monitoring of Seafloor Integrity). Corporate Deliverable of the WESE Project Funded by the European Commission. Agreement Number EASME/EMFF/2017/1.2.1.1/02/s12.787640. https://doi.org/10.13140/RG.2.2.22464.87049.

Muxika, I., Vinagre, P.A., Le Bourhis, E., Vallarin, E., Tanguy, F., Niclot, C., Bald, J., 2022. Deliverable 2.4 (Monitoring of the Seabed Integrity). Corporate Deliverable of the SafeWAVE Project Co-funded by the European Climate, Infrastructure and Environment Executive Agency (CINEA), Call for Proposals EMFF-2019-1.2.1.1 - Environmental Monitoring of Ocean Energy Devices. https://doi.org/10.13140/RG.2.2.16170.90561/3.

Myers, L., Bahaj, A.S., 2005. Simulated electrical power potential harnessed by marine current turbine arrays in the Alderney Race. Renew. Energy 30 (11), 1713–1731. https://doi.org/10.1016/j.renene.2005.02.008.

Myers, L.E., Bahaj, A.S., 2012. An experimental investigation simulating flow effects in first generation marine current energy converter arrays. In: Renew. Energy, 37(1). Elsevier Ltd., pp. 28–36. https://doi.org/10.1016/j.renene.2011.03.043

National Marine Fisheries Service (NMFS), 2018. 2018 Revisions to: Technical Guidance for Assessing the Effects of Anthropogenic Sound on Marine Mammal Hearing (Version 2.0): Underwater Thresholds for Onset of Permanent and Temporary Threshold Shifts. U.S. Dept. of Commer., NOAA. NOAA Technical Memorandum NMFS-OPR-59 (167 pp.).

Nedelec, S.L., Campbell, J., Radford, A.N., Simpson, S.D., Merchant, N.D., 2016. Particle motion: the missing link in underwater acoustic ecology. Methods Ecol. Evol. 7, 836–842. https://doi.org/10.1111/2041-210X.12544.

Neill, S.P., Jordan, J.R., Couch, S.J., 2012. Impact of tidal energy converter (TEC) arrays on the dynamics of headland sand banks. In: Renew. Energy, 37(1). Elsevier Ltd., pp. 387–397. https://doi.org/10.1016/j.renene.2011.07.003

Normandeau Associates, Exponent, Tricas, T., Gill, A., 2011. Effects of EMF From Undersea Power Cables on Elasmobranchs and Other Marine Species. Camarillo, CA (Available from https://www.boem.gov/sites/default/files/environmental-stewardship/Environmental-Studies/Pacific-Region/Studies/2011-09-EMF-Effects.pdf).

O'Carroll, J.P.J., Kennedy, R.M., Savidge, G., 2017. Identifying relevant scales of variability for monitoring epifaunal reef communities at a tidal energy extraction site. In: Ecol. Indic, 73. Elsevier Ltd., pp. 388–397. https://doi.org/10.1016/j.ecolind.2016.10.005

Onoufriou, J., Russell, D.J.F., Thompson, D., Moss, S.E., Hastie, G.D., 2021. Quantifying the effects of tidal turbine array operations on the distribution of marine mammals: implications for collision risk. In: Renew. Energy, 180. Elsevier Ltd., pp. 157–165. https://doi.org/10.1016/j.renene.2021.08.052

ORJIP, 2022. ORJIP Ocean Energy Information Note: Underwater Noise. Available from. https://tethys.pnnl.gov/publications/orjip-ocean-energy-information-note-underwater-noise.

Palmer, L., Gillespie, D., MacAulay, J.D.J., Sparling, C.E., Russell, D.J., Hastie, G.D., 2021. Harbour porpoise (*Phocoena phocoena*) presence is reduced during tidal turbine operation. Aquat. Conserv. Mar. Freshwat. Ecosyst. 31 (12), 3543–3553. https://doi.org/10.1002/aqc.3737.

Polagye, B., Bassett, C., 2020. Risk to marine animals from underwater noise generated by marine renewable energy devices. In: Copping, A.E., Hemery, L.G. (Eds.), OES-Environmental 2020 State of the Science Report: Environmental Effects of Marine Renewable Energy Development Around the World. Report for Ocean Energy Systems (OES), pp. 67–85. https://doi.org/10.2172/1633082.

Popper, A.N., Hawkins, A.D., 2018. The importance of particle motion to fishes and invertebrates. J. Acoust. Soc. Am. 143 (1), 470–488. https://doi.org/10.1121/1.5021594.

Raoux, A., Robin, I., Pezy, J., Bennis, A., Dauvin, J., 2021. Multi-disciplinary and multi-scale assessment of marine renewable energy structure in a tidal system. J. Energy Power Technol. 3 (1), 1–16. https://doi.org/10.21926/jept.2101012.

Robins, P.E., Neill, S.P., Lewis, M.J., 2014. Impact of tidal-stream arrays in relation to the natural variability of sedimentary processes. In: Renew. Energy, 72. Elsevier Ltd., pp. 311–321. https://doi.org/10.1016/j.renene.2014.07.037

Rossington, K., Benson, T., 2020. An agent-based model to predict fish collisions with tidal stream turbines. Renew. Energy 151, 1220–1229. https://doi.org/10.1016/j.renene.2019.11.127.

Sanderson, B.G., Bangley, C.W., McGarry, L.P., Hasselman, D.J., 2023a. Measuring detection efficiency of high-residency acoustic signals for estimating probability of fish-turbine encounter in a fast-flowing tidal passage. J. Mar. Sci. Eng. 11 (6), 1172. https://doi.org/10.3390/jmse11061172.

Sanderson, B.G., Karsten, R.H., Hasselman, D.J., 2023b. Towards estimating probability of fish-turbine encounter: using drifters equipped with acoustic tags to verify efficacy of an array of acoustic receivers. J. Mar. Sci. Eng. 11 (x), xxxx. https://doi.org/10.3390/jmse11xxxxxx.

Sanderson, B.G., Karsten, R.H., Solda, C.C., Hardie, D.C., Hasselman, D.J., 2023c. Probability of Atlantic salmon post-smolts encountering a tidal turbine installation in Minas Passage, Bay of Fundy. J. Mar. Sci. Eng. 11 (5), 1095. https://doi.org/10.3390/jmse11051095.

Santiago, I., Liria, P., Garnier, R., Bald, J., Leitão, J.C., Ribeiro, J., 2023. Deliverable 3.3 Marine Dynamics Modelling. Corporate Deliverable of the SafeWAVE Project Co-funded by the European Climate, Infrastructure and Environment Executive Agency (CINEA), Call for Proposals EMFF-2019-1.2.1.1 - Environmental Monitoring of Ocean Energy Devices. https://doi.org/10.13140/RG.2.2.36716.74886.

Scottish Natural Heritage, 2016. Assessing collision risk between underwater turbines and marine wildlife. Available from. https://tethys.pnnl.gov/sites/default/files/publications/scottish-natural-heritage-report.pdf.

Shen, H., Zydlewski, G.B., Viehman, H.A., Staines, G., 2016. Estimating the probability of fish encountering a marine hydrokinetic device. In: Renew. Energy, 97. Elsevier Ltd., pp. 746–756. https://doi.org/10.1016/j.renene.2016.06.026

Southall, B.L., Finneran, J.J., Reichmuth, C., Nachtigall, P.E., Ketten, D.R., Bowles, A.E., Ellison, W.T., Nowacek, D.P., Tyack, P.L., 2019. Marine mammal noise exposure criteria: updated scientific recommendations for residual hearing effects. Aquat. Mamm. 45 (2), 125–232. https://doi.org/10.1578/AM.45.2.2019.125.

Southall, B.L., Nowacek, D.P., Bowles, A.E., Senigaglia, V., Bejder, L., Tyack, P.L., 2021. Marine mammal noise exposure criteria: assessing the severity of marine mammal behavioral responses to human noise. Aquat. Mamm. 47 (5), 421–464. https://doi.org/10.1578/am.47.5.2021.421.

Sparling, C.E., Seitz, A.C., Masden, E., Smith, K., 2020a. Collision risk for animals around turbines. In: Copping, A.E., Hemery, L.G. (Eds.), OES-Environmental 2020 State of the Science Report: Environmental Effects of Marine Renewable Energy Development Around the World. https://doi.org/10.2172/1632281.

Sparling, C.E., Hague, E., Sinclair, R., Booth, C., 2020b. Improving understanding of the potential effects and consequences of displacement of marine mammals by wave and tidal stream arrays and development of a suitable assessment framework. In: Marine Biodiversity Impact Evidence Group, Project No: C7759E (67 pp.).

Stallard, T., Collings, R., Feng, T., Whelan, J., Oqd, B.B.S., 2013. Interactions between tidal turbine wakes: experimental study of a group of three-bladed rotors. Philos. Trans. R. Soc. A Math. Phys. Eng. Sci. 371, 20120159.

Stelzenmüller, V., Coll, M., Cormier, R., Mazaris, A., Pascual, M., Loiseau, C., Claudet, J., Katsanevakis, S., Gissi, E., Evagelopoulos, A., Rumes, B., Degraer, S., Ojaveer, H., Moller, T., Gimenez, J., Piroddi, C., Markantonatou, V., Dimitriadis, C., 2020. Operationalizing risk-based cumulative effect assessments in the marine environment. Sci. Total Environ. 724, 138118 https://doi.org/10.1016/j.scitotenv.2020.138118.

Suter, G.W., Norton, S.B., Barnthouse, L.W., 2003. The evolution of frameworks for ecological risk assessment from the red book ancestor. Hum. Ecol. Risk. Assess. 9 (5), 1349–1360. https://doi.org/10.1080/10807030390240391.

Taormina, B., Bald, J., Want, A., Thouzeau, G., Lejart, M., Desroy, N., Carlier, A., 2018. A review of potential impacts of submarine power cables on the marine environment: knowledge gaps, recommendations and future directions. In: Renew. Sustain. Energy Rev., 96(July) Elsevier Ltd., pp. 380–391. https://doi.org/10.1016/j.rser.2018.07.026

Tollit, D.J., Joy, R., Wood, J., Redden, A.M., Booth, C., Boucher, T., Porskamp, P., Oldreive, M., 2019. Baseline presence of and effects of tidal turbine installation and operations on harbour porpoise in Minas Passage, Bay of Fundy, Canada. J. Ocean Technol. 14 (Special Edition), 24–48 (Available from https://www.thejot.net/article-preview/?show_article_preview=1071).

Turnock, S.R., Phillips, A.B., Banks, J., Nicholls-Lee, R., 2011. Modelling tidal current turbine wakes using a coupled RANS-BEMT approach as a tool for analysing power capture of arrays of turbines. In: Ocean Eng., 38(11–12) Elsevier, pp. 1300–1307. https://doi.org/10.1016/j.oceaneng.2011.05.018.

U.S. Environmental Protection Agency, 2002. Guidance on cumulative risk assessment of pesticide chemicals that have a common mechanism of toxicity. Available from. https://www.epa.gov/sites/production/files/2015-07/documents/guidance_on_common_mechanism.pdf.

Van Der Molen, J., Ruardij, P., Greenwood, N., 2016. Potential environmental impact of tidal energy extraction in the Pentland Firth at large spatial scales: results of a biogeochemical model. Biogeosciences 13 (8), 2593–2609. https://doi.org/10.5194/bg-13-2593-2016.

Vennell, R., 2012. The energetics of large tidal turbine arrays. In: Renew. Energy, 48. Elsevier Ltd., pp. 210–219. https://doi.org/10.1016/j.renene.2012.04.018

Viehman, H.A., Zydlewski, G.B., 2015. Fish interactions with a commercial-scale tidal energy device in the natural environment. Estuar. Coasts 38 (Suppl. 1), S241–S252. https://doi.org/10.1007/s12237-014-9767-8.

Wang, J., Müller, N., 2012. Performance prediction of array arrangement on ducted Composite Material Marine Current Turbines (CMMCTs). Ocean Eng. 41, 21–26. https://doi.org/10.1016/j.oceaneng.2011.12.023.

Whiting, J., Chang, G., 2020. Changes in oceanographic systems associated with marine renewable energy devices. In: Report for Ocean Energy Systems (OES), pp. 0–324.

Williamson, B., Fraser, S., Williamson, L., Nikora, V., Scott, B., 2019. Predictable changes in fish school characteristics due to a tidal turbine support structure. In: Renew. Energy, 141. Elsevier Ltd., pp. 1092–1102. https://doi.org/10.1016/j.renene.2019.04.065

Wilson, B., Batty, R.S., Daunt, F., Carter, C., 2006. Collision risks between marine renewable energy devices and mammals, fish and diving birds. In: Report to the Scottish Executive Association of Marine Science, Oban, Scotland (Oban, Scotland. Available from http://nora.nerc.ac.uk/504110/1/N504110CR.pdf).

Woodruff, D., Schultz, I., Marshall, K., Ward, J., Cullinan, V., 2012. Effects of Electromagnetic Fields on Fish and Invertebrates Task 2.1.3: Effects on Aquatic Organisms Fiscal Year 2011 Progress Report. Report No. PNNL-20813. Report by Pacific Northwest National Laboratory for U.S. Department of Energy, Washington DC.

Zhang, J., Kitazawa, D., Taya, S., Mizukami, Y., 2017. Impact assessment of marine current turbines on fish behavior using an experimental approach based on the similarity law. In: J. Mar. Sci. Technol, 22(2). Springer Japan, pp. 219–230. https://doi.org/10.1007/s00773-016-0405-y.

Zhang, J., Zhang, C., Angeloudis, A., Kramer, S.C., He, R., Piggott, M.D., 2022. Interactions between tidal stream turbine arrays and their hydrodynamic impact around Zhoushan Island, China. In: Ocean Eng, 246(January). Elsevier Ltd., 110431 https://doi.org/10.1016/j.oceaneng.2021.110431

Appendix VII

Review

A Probabilistic Methodology for Determining Collision Risk of Marine Animals with Tidal Energy Turbines

Andrea E. Copping [1,2,*], Daniel J. Hasselman [3], Charles W. Bangley [3,4], Joel Culina [3] and Max Carcas [5]

[1] Coastal Sciences Division, Pacific Northwest National Laboratory, Seattle, WA 98109, USA
[2] School of Marine and Environmental Affairs, University of Washington, Seattle, WA 98195, USA
[3] Fundy Ocean Research Center for Energy, Dartmouth, NS B3J 3N5, Canada; dan.hasselman@fundyforce.ca (D.J.H.); charles.bangley@dal.ca (C.W.B.); joel.culina@fundyforce.ca (J.C.)
[4] Department of Mathematics and Statistics, Dalhousie University, Halifax, NS B3H 4R2, Canada
[5] Caelulum Ltd., Strathearn Road, Edinburgh EH9 2AH, UK; m.carcas+j@caelulum.com
* Correspondence: andrea.copping@pnnl.gov

Abstract: Commercial development of tidal stream energy is hampered by technical and financial challenges, and impeded by uncertainty about potential environmental effects that drive environmental risk assessments and permitting (consenting) processes. The effect of greatest concern for operational tidal stream energy devices is the potential for marine animals to collide with turbine blades, resulting in injury or death. Due to the turbulent and often turbid waters that frequently characterize tidal turbine sites, there is an absence of empirical evidence about collisions with marine animals. This paucity of observations often leads to risk-averse permitting decisions that further restrict the deployment of tidal energy devices that are needed to collect this evidence. This paper relies on the framework of stressors and receptors that is widely used in marine energy studies and outlines a stepwise probabilistic methodology that applies existing knowledge to further elucidate the risk to marine animals from operational tidal turbines. A case study using striped bass from the Bay of Fundy, Canada, accompanies the methodology, to partially demonstrate its application.

1. Introduction

The global expansion of marine renewable energy (MRE) devices (e.g., tidal stream and riverine turbines, wave energy converters, and others.) is an integral part of an overall strategy to address the impacts of climate change [1–3], ensure a sustainable transition towards renewable energy sources [4,5], and meet national energy security needs using locally generated electricity [6]. As an emerging industrial sector, MRE development to date has been limited to the deployment of single devices, pilot projects, and small demonstration-scale arrays [7]. The establishment of large-scale commercial arrays is essential for meeting climate change and energy security goals, but is hindered by a variety of factors, including difficulties in obtaining regulatory approvals due to uncertainty about the environmental effects on marine ecosystems and their constituents [8–11]. This uncertainty stems from a paucity of post-installation environmental monitoring data for single MRE devices and demonstration-scale arrays that confounds our ability to differentiate between unknown (but perceived) and realized risks for marine ecosystems stemming from MRE development [12].

A framework for assessing the environmental effects of MRE technologies focuses on understanding the interactions between 'stressors' (i.e., those parts of an MRE device or system that may cause harm) and 'receptors' (i.e., those components of the ecosystem that may elicit some response to the stressor) [12–14]. For tidal stream energy technologies, the risk of collisions between marine animals (particularly marine mammals, diving sea

birds, fish, and sea turtles) and the moving parts of devices (e.g., turbine blades and rotors, or dynamic technologies like tidal kites or oscillating blades; [15,16]) are generally unknown, but are considered to be the greatest potential risk of turbine operations [12]. As such, collision risk (i.e., the likelihood that animals might be harmed by coming into contact with the moving parts of MRE devices [17]) has been the subject of much research (reviewed in [16]), including modelling exercises (e.g., [18–20]), experiments conducted under controlled laboratory conditions (e.g., [21–23]), and in situ studies around various operational turbine technologies (e.g., [24–26]). Collectively, this body of knowledge provides substantive evidence to suggest that when marine animals can detect operational tidal turbines, they can exhibit avoidance or evasion behaviors [17,27] and take measures to prevent being struck by turbine blades [28–33]. Indeed, collisions between marine animals and tidal turbines are expected to occur infrequently [12]. However, the paucity of empirical collision data from post-installation monitoring programs, or analogues from other marine industries, has hampered the coalescing of evidence needed by various regulatory agencies to permit the expansion of some tidal energy projects beyond single devices and small demonstration-scale arrays.

Despite the availability of adaptive, risk-based approaches to MRE project permitting (e.g., 'Survey-Deploy-Monitor' [34,35]), the absence of conclusive empirical evidence about the probability of collisions and their consequences has led to risk-averse permitting decisions for tidal energy projects in some jurisdictions [36,37]. These decisions inadvertently restrict the deployment of tidal energy devices in locations and at scales that are required to collect the very evidence about collision risk that is being sought. This paradox may in turn limit expansion of the MRE sector and hamper global efforts to address the impacts of climate change, ensure a sustainable transition of our energy systems, and provide national energy security.

In the absence of conclusive empirical collision risk data, expansion of the MRE sector still requires a means by which to assess the risk of collisions a priori to facilitate project permitting and support sector growth. Assessing the risk to a marine animal of approaching an operational turbine, being struck by a turbine blade and suffering a critical injury or mortality is determined by the probability of the event occurring and the consequences of the event (e.g., [38]). This risk can be envisaged as a sequence of dependent events, each with an associated probability of occurring, that must coincide for collision risk to be realized [39]. The purpose of this study is to describe the process of collision risk for tidal turbines from a risk management perspective, and expand on the work of Copping et al. [39] to advance a conceptual, probability-based framework for quantifying the associated likelihoods for the sequence of events inherent to collision risk. To that end, we first outline the sequence of events that comprise this framework, and then demonstrate its application (to the extent currently possible) using striped bass (*Morone saxatilis*) in the Minas Passage, Bay of Fundy, Canada.

2. Materials and Methods

This paper addresses the development and application of a conceptual probabilistic framework for the collision risk of marine animals, particularly marine mammals and fish, and demonstrates the initial steps in the framework using a case study.

2.1. Conceptual Probabilistic Framework

We conceptualize collision risk as a series of seven sequential events (i.e., steps) that must each occur for a marine animal to approach an operational turbine, be struck by a turbine blade, and be harmed (i.e., suffer a critical injury or mortality) (Figure 1). Descriptions of these seven events are outlined in the Results section. Each of these events has an associated probability of occurring, and the likelihood of harm is ultimately a product of these dependent probabilities. Consequently, if any of the probabilities in this sequence of events is small (near-zero) or zero, then the overall probability of harm is similarly low and unlikely.
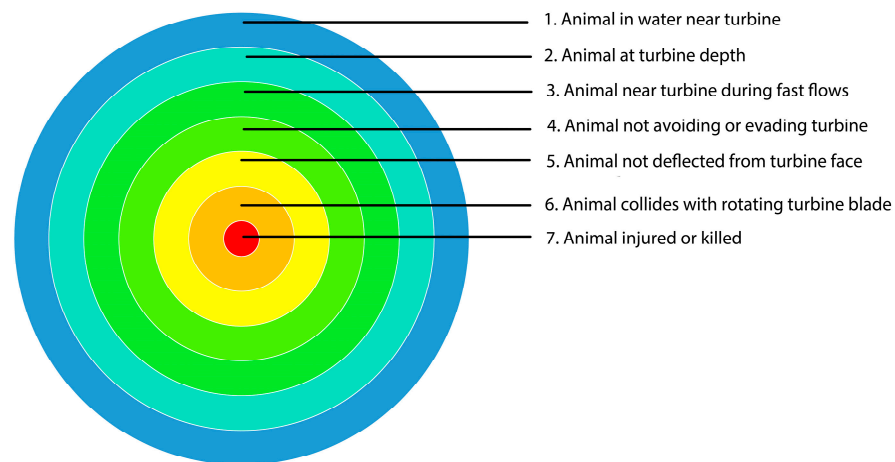
1. Animal in water near turbine
2. Animal at turbine depth
3. Animal near turbine during fast flows
4. Animal not avoiding or evading turbine
5. Animal not deflected from turbine face
6. Animal collides with rotating turbine blade
7. Animal injured or killed

Figure 1. Conceptual probabilistic framework for quantifying the likelihood of collision risk for marine animals and operational tidal energy turbines. The framework outlines a series of sequential steps that must take place, each with an associated probability, for a marine animal to approach an operational turbine, be struck by a turbine blade and be harmed (i.e., suffer a critical injury or mortality). Adapted from Copping et al. [39].

Evidence that supports a risk assessment for each of the seven events was acquired through a search of the literature that included peer-reviewed articles in scientific journals (Web of Science and Tethys knowledge base—a database devoted to compiling information about the environmental effects of MRE—https://tethys.pnnl.gov accessed 1 May 2023) as well as the additional grey literature found on Tethys [40] to contextualize the probability of each event occurring. Although the peer-reviewed scientific literature was the primary base of evidence, the MRE industry is still in the early stages of development, and some key findings are documented in environmental monitoring reports and permitting/consenting documents that are not available in the peer-reviewed literature or found in associated databases. While the value of the non-peer-reviewed reports cannot be weighed as heavily as those in the scientific literature, each has been scrutinized by governmental bodies as evidence to support regulatory processes. We reference these materials judiciously.

2.2. Case Study

We demonstrate an application for a subset of the proposed framework (i.e., steps 1–3; see below) using striped bass (*Morone saxatilis*) in the Minas Passage, Bay of Fundy, Canada, based on the work of Bangley et al. [41]. Bangley et al. [41] used a combination of acoustic tag detection data (2017–2020) for adult striped bass (i.e., >60 cm fork length) from the Shubenacadie River, Nova Scotia, and associated environmental variables at specific locations in the Minas Passage to develop species distribution models and predictive spatiotemporal maps (i.e., 150 m × 150 m grid cells) to determine the presence probabilities of striped bass by season and tidal stage. The species' vertical distribution throughout the water column was incorporated into the approach using data from depth sensors included for a subset of the acoustic tags; we include additional depth distribution data from tagged individuals detected during 2009–2013 to more fully account for the species' vertical distribution in the Minas Passage. Because the detection probability for acoustic tags in tidal channels can be impacted by local hydrodynamics [42], the modeled presence probability of striped bass used here is adjusted using a scaling function adapted from MacKenzie et al. [43] that weights acoustic tag detections during hydrodynamic conditions that are associated with poor detection efficiency [44].

Although the results of this demonstration are specific to adult striped bass from the Shubenacadie River, these factors do not preclude the value of Bangley et al. [41] for demonstrating an application of the framework developed herein. Indeed, the results of Bangley et al. [41] are particularly relevant for understanding the probabilities associated

with the presence of striped bass in the vicinity of an operational turbine (step 1), their presence at the depth of the turbine rotor (step 2), and their presence at tidal flow rates greater than the 'cut in' speed of a turbine (step 3). The probabilities associated with steps 4–7 in the framework are not available from Bangley et al. [41], but may be inferred (conservatively) from other studies on collision risk for striped bass in controlled laboratory conditions (e.g., [22,45]), modelling studies for fish based on computational fluid dynamics and finite element analysis (e.g., [46]), and other relevant sources.

Bangley et al. [41] identified the late ebb tidal stage during October as the period of the greatest presence probability of striped bass in the Minas Passage. To demonstrate a conservative application of the framework, we selected the 150 m × 150 m grid cell with the highest predicted scaled presence probability of striped bass under these conditions as the site where a tidal stream turbine might be deployed (Figure 2). The hypothetical tidal stream device can be described as: a floating horizontal-axis technology with a single rotor at 8 m depth, three blades each with a length of 2 m (rotor diameter 4 m), and a rotor swept area of 12.56 m^2. These measurements allow us to establish a vertical depth of encounter with the turbine blades between 6 and 10 m depth. The turbine would operate from a cut-in speed of 1.0 m/s, up to a speed of 5.0 m/s, with a rotational speed of 65 rpm at a tidal velocity of 3.0 m/s. Following the hierarchy of collision risk proposed in this paper, the probability of species presence within the turbine vicinity (step 1) was measured as the scaled presence probability from the species distribution model, the probability of presence at the turbine depth (step 2) was measured as the proportion of depth sensor measurements falling within the depth of encounter, and the probability of presence between the cut-in and cut-out speeds (step 3) was measured as the proportion of hourly presence records within that current speed range.
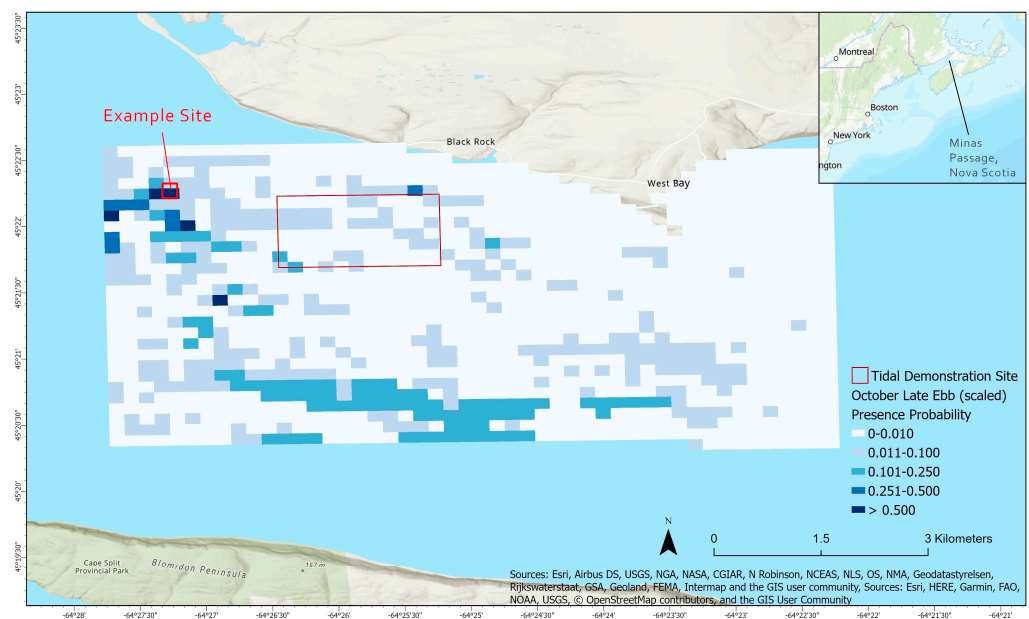

Figure 2. Grid cells (150 m × 150 m) are mapped for the probable presence of striped bass in the Minas Passage, predicted using average environmental conditions during a late ebb tide stage in October. The Fundy Ocean Research Center for Energy tidal demonstration site is delineated by the large red rectangle, while the example site used for the case study (longitude −64.45447, latitude 45.37068) is highlighted to the left.

3. Results

Descriptions for each of the seven events outlined in Figure 1 are provided below. To increase understanding of the likelihood of each event occurring, we identify the factors that need to be considered in determining the risk of each event and synthesize the existing relevant literature. We then examine the framework as it applies to the striped bass case

study. Throughout this section, it is important to recognize that collision risk is most likely to be assessed for a species of interest—those of conservation concern that are afforded legal protection in various jurisdictions, species of commercial or recreational value, or those of cultural relevance. The amount and suitability of available data that can be used in the framework for assessing collision risk will vary by species and may need to be supplemented with additional data collection. Ideally, in situ data collection would be conducted multiple times throughout the year, allowing for variation in species presence, life history, and behavior to be incorporated into the risk assessment. The probability of occurrence of each event should be considered individually; however, few quantitative probabilities are available in the literature for each step in the framework. Our results focus on providing a description of the elements that would drive an estimate of the probability at each ring made from the existing literature.

3.1. Probability of Being Present in the Water Column and in Vicinity of the Turbine

An animal must be present around an operational turbine for a collision to occur. An assessment of which marine animals are present in the waters near a tidal turbine and understanding their spatial and temporal distributions (e.g., resident or migratory species, areas of occupancy, frequency of presence), prior to device installation, is the first component required to estimate the risk of collision. This information can be determined through the development of species distribution models [47] that can link species presence in tidal channels with habitat variables and environmental heterogeneity (e.g., [41,48–50]). Although the spatiotemporal distribution for each species must be assessed separately, existing information may be available from prior monitoring activities to assist in this effort. Species that are resident to an area where tidal turbine installations are planned may be at higher risk of collision, due to their increased spatial and temporal overlap with devices (i.e., increased exposure), than migratory species that may only move through the area occasionally. Species presence and collision risk may also vary by life history stage, with spatiotemporal distributions of juveniles differing from adult animals (e.g., Atlantic salmon (*Salmo salar*) post-smolts vs. kelts); [51,52] and may also vary by population [53].

Assessments of the presence, abundance, and movement of animals are the most common types of data collected in association with marine energy monitoring and are a vital part of an analysis of potential collision risk. This information is gathered using a variety of methods and monitoring instruments, depending on the site conditions and the species of interest. Marine mammals are most often assessed as individuals or pods. Their presence is commonly observed using passive acoustics for vocalizing cetaceans [54,55], active acoustics such as imaging sonars [56–58], underwater optical cameras (still or video) [59,60], and observations made from vessels, aircraft, or land [61]. Fish are commonly assessed as individuals or schools (depending on the species) using various active acoustic instruments like single beam or split beam echosounders [62–64], multibeam acoustic cameras [32,65,66] and multibeam imaging sonars [26,67], acoustic telemetry [41,42,68], and with underwater optical cameras [25,69]. Other marine animals such as sea turtles and diving sea birds may be assessed in conjunction with marine mammal surveys, or from other dedicated monitoring campaigns [70] using some of the approaches mentioned above.

3.2. Probability of Being Present at the Depth of the Turbine Rotor

Animals must be present at the depth of the swept area of an operating turbine for a collision to occur. The amount of time that an animal is present at the depth of the turbine swept area, and therefore its exposure to collision risk, will vary by species, life history, and behavior. For marine mammals, species depth distributions may vary widely over a relatively short period of time. For instance, if marine mammals are transiting through an area to reach important resources (e.g., foraging or breeding habitats) they may primarily be located in the upper portions of the water column ('cruising' or 'porpoising'; [71,72]), and may not be found in the swept area of bottom-mounted devices. However, if foraging for food, marine mammals may make frequent transits between the mid-water column

or seafloor and the surface (to breathe) over protracted periods of time (e.g., [30,73,74]), exhibiting a bimodal depth distribution pattern [75], and may be exposed to risk for both bottom-mounted and surface deployed technologies. The depth distribution of fish species is dependent on life stage, life history and behavior (e.g., species that utilize the entire water column, demersal species that tend to be oriented towards benthic habitats, or pelagic species that tend to be found higher in the water column), and may be influenced by diel migrations (i.e., deeper during the day, shallower at night) and the confounding effects of water temperature and tidal stage [76–79].

Data about species depth distributions are often more challenging to collect than data about their spatial (in the horizontal plane) and temporal distributions. Often the presence of animals is deduced from population estimates at a site and from the assumed depth distribution throughout the water column [28,80]. Marine mammals may be tagged with D-tags that record the depths of dives and allow for estimates of depth distributions at a site (e.g., [73]), but these studies are relatively rare as permission to tag marine mammals is often difficult to acquire [81,82]. Individual fish may be tagged using acoustic tags equipped with depth sensors that record species depth distributions (e.g., [41,83]) that are detected by lines of acoustic receivers [84,85]. The depth distribution of fish populations can also be determined directly with the use of multiple opening nets such as MOCNESS (Multiple Opening/Closing Net and Environmental Sensing System) or bongo nets that can be operated in the water column by remotely opening and closing at specific depths to ascertain which fish or portion of a population are caught at various depth strata [86]. However, nets are seldom employed for monitoring in tidal channels because of the inherent difficulties with successfully utilizing this sampling equipment in areas that are frequently characterized by complex and turbulent hydrodynamics (e.g., [87,88]). Active acoustic (i.e., echosounder) surveys may target different depths, allowing for some estimation of fish biomass at specific depths [89], but correctly delineating species is difficult without ground truthing acoustic targets using accompanying trawl surveys that can be difficult to conduct in these environments [87]. Moreover, tidal channels and their complex hydrodynamics can entrain air in the water column that can obfuscate the use of this approach for collecting accurate depth distribution data [90].

Most commonly, the depth distribution of marine animals is extrapolated from small numbers of behavioral studies that tag or follow specific individuals, but seldom in locations of interest for tidal energy development [30]. The depth distributions of fish are often assumed from associations with physical features and processes such as tidal stage, season, and diel movement [91]. Additionally, fish and other marine animal depth distributions may be determined with the use of underwater optical cameras deployed at a depth around tidal turbines; however, these surveys are still relatively rare, difficult to carry out in turbid waters, and are generally insufficient to determine species depth distributions [92].

3.3. Probability of Being Present at Flow Rates Greater Than the 'Cut in' Speed of the Turbine

Tidal turbines are designed to begin rotating when the flow rate reaches a speed at which power generation becomes viable; often referred to as the 'cut in' speed of the device. The cut in speed will vary with the particular turbine design, but for turbines that can generate utility scale energy, is unlikely to be less than 1.0–1.5 m/s [93,94]. If marine animals are present in the immediate vicinity of the device, or within the turbine swept area, they are not at risk of collision when tidal flows are less than the cut in speed of the turbine. Once a turbine begins to rotate, the rotational speed will be proportional to the speed of the tidal flow, increasing the tip speed of the blade with increasing flow rates. At low flow rates leading up to and just past the cut in speed, the rotational speed of the turbine blades will be low and less risky to marine animals than at the greater flow rates that are optimal for power generation.

Underwater video has captured a phenomenon that shows fish present around the turbine rotor, nacelle, and blades during low flow conditions, but leaving the camera field of view as flow rates increase [95–97]; possibly descending to the seafloor where they can use

the boundary layer, substrate coupling strategies, and rheotaxis to hold station and prevent downstream displacement [98], and associated flow refugia to conserve energy [99]. These species may be at lower risk of collision than those that may be transiting through a tidal channel during seasonal migrations and using selective tidal stream transport to conserve energy [100–102]. Similar evidence shows the presence of marine mammals around tidal turbines at slack tide, followed by avoidance of the rotor area as tidal currents increase and the turbine blades rotate [103].

Information about the movement of species through a tidal channel can be acquired using acoustic telemetry and strategically deployed lines of acoustic receivers that are appropriately spaced [42,53] to account for variation in acoustic signal detection with current speed.

3.4. Probability of Not Exhibiting Avoidance or Evasion Behavior

Behavioral studies of marine animals do not report collisions with underwater objects, with the exception of large masses such as ships that can move at relatively high speed (e.g., [104]). There are few studies that focus on marine animals in close proximity to marine energy devices, partly due to the difficulty of observing interactions in fast flowing, often turbid, waters. Based on observations of marine mammals and fish in their natural habitats, it is likely that they will sense the presence of a turbine underwater at some distance and avoid the obstacle, or may approach out of curiosity and evade the moving parts at closer ranges [30,31].

Marine animals have developed a suite of sensory systems that permit them to accurately perceive their environments and respond appropriately to stimuli by exhibiting a range of behaviors. This includes the ability to detect operational turbines and exhibit avoidance and evasion behaviors to prevent being struck by turbine blades at varying distances from a device that may span up to 100 m or more (e.g., [29,32,62,105]). Despite these intrinsic abilities, there is some potential for collision with a turbine blade to occur under adverse environmental conditions (i.e., turbid, noisy, and turbulent fast-flowing tidal currents) that may prevent detection of the device or where the reaction time between device detection and expression of behaviors to prevent a collision is insufficient.

Empirical in situ evidence for avoidance and evasion behavior has been observed for marine mammals (e.g., [29,105]) and fish (e.g., [26,32,62]), and there is some evidence that diving seabirds avoid areas with fast tidal currents [106]. Numerous laboratory-based studies provide empirical observations of avoidance and evasion by fish in controlled settings, which consistently show similar responses for a variety of species under differing flow regimes, up to approx. 2.5 m/s (e.g., [107–109]).

While fish have been observed to avoid or evade an operational turbine, some have been observed to pass through the rotor swept area [25,110]. Flume studies and a small number of field studies show that fish that pass through a rotating turbine may become disoriented but do not appear to suffer harm [22,24,25,66]. The relative size of the turbine, the design and solidity of the rotor swept area, and the species present near an operational device, are all likely to affect the ability of marine animals to detect and avoid or evade the rotating blades.

The limited observations available cannot be used to definitively determine that fish and other marine animals will always avoid a rotating turbine, or emerge unscathed, but the preponderance of evidence suggests that the sensory capabilities of marine animals are likely to alert them to the presence of a hazard and allow greater than 90% survival [111–113].

3.5. Probability of Not Being Deflected by the Pressure Generated by the Turbine

A turbine that operates near the Betz limit (or the limit of energy extraction) diverts about one-third of the upstream flow, which, since avoidance and evasion is separately considered, provides a purely physics-based discounting factor on overall collision risk [114,115]. This blocking effect can be generalized to turbine arrays to determine the

fraction of incoming flow, and hence passively moving marine life, that will bypass the array. There are two scales of flow diversion: at the array scale, a fraction of flow is diverted as though the array is a single, large turbine, and at the turbine scale, involving interactions among neighboring turbines [116]. Optimizing a multi-row turbine farm for power extraction requires a staggered arrangement (as is common in wind farms) such that flow bypassing one row is met by turbines in the subsequent row [117]. This may be at odds with minimizing collision risk, and both factors should be considered in turbine placement [118]. For small marine organisms such as plankton, including larval fish and invertebrates, and perhaps some small fish, which effectively act as tracers, the probability of not bypassing the turbine/turbine array can be applied with a high degree of certainty towards evaluating collision risk. Larger marine animals, which are apt to travel across streamlines and even against the flow, would not be nearly as predictable, and may be subject to increased risk of collision.

3.6. Probability of a Physical Strike with a Turbine Blade

Should a marine animal enter the rotor swept area of a tidal turbine, the probability of collision with a rotor blade will depend on several factors. Most turbine swept areas are not highly solid, such that the animal may traverse the turbine swept area without experiencing a collision. The rotational speed of the turbine, the particular part of the blade closest to the animal (as the tip of a blade moves much faster than positions closer to the turbine hub), the rotor diameter, and the size and length and swimming speed of the marine animal [119] will affect the likelihood of a collision.

Tip speed is an important parameter in determining marine animal survival after a collision. The rotational speed of a turbine is not a determining factor as larger turbines rotate at a speed proportionally slower than smaller turbines, while the tip speed remains the same [120] at a specific tidal flow speed.

Studies of fish swimming in high flow indicate that they swim into the flow (i.e., exhibit rheotaxis) at most times, at speeds where they can maintain or gain on the current [121,122], and swim only occasionally with current flows, at lower speeds [123,124]. Marine mammals also most commonly swim into the current although some seals have been shown to ride tidal current in pursuit of prey [30]. This behavior suggests that fish and marine mammals may most commonly approach a turbine so they can see and detect its presence and will only occasionally be "overtaken" by a turbine and inadvertently pass through the rotor swept area.

3.7. Probability That Collision Results in Harm (i.e., Critical Injury or Mortality)

If a marine animal were to enter the rotor swept area of a tidal turbine and collide with a blade, the consequences of such a collision could be a minor recoverable injury, immediate mortality, or a critical injury that results in permanent disability or death at a later time (i.e., latent mortality). There has never been an observation of a marine mammal struck by a turbine, and while there is video evidence of fish coming very close to a turbine [66], no harm has been observed. There are few studies that provide definitive information on what the consequences of a strike from a tidal turbine might be, although studies of equivalent forces on marine mammal tissue have shown that damage to skin, blubber, and muscle are likely recoverable from a typical tidal blade strike [39,119]. While no equivalent tests have been carried out for fish, Hecker and Amaral [125] show that survival rate after being struck depends on two variables: strike velocity and the ratio of fish length to blade thickness. Simulations indicate that the speed of the turbine is the factor most likely to determine the impact to the fish [46].

3.8. Case Study Results

Based on species distribution model results from Bangley et al. [41], the scaled probability of striped bass presence at the example site is 0.812 during the late ebb tide stage in October. The proportion of depth sensor measurements falling within the depth of

encounter is 0.350. The proportion of striped bass hourly presence records occurring during ebb tide in October at current velocities between the cut-in and cut-out speeds is 0.729. This gives an overall probability of encounter with the turbine through the first three steps of collision risk framework of 0.207 (0.812 × 0.350 × 0.729) during the late ebb tide stage in October (Figure 3).
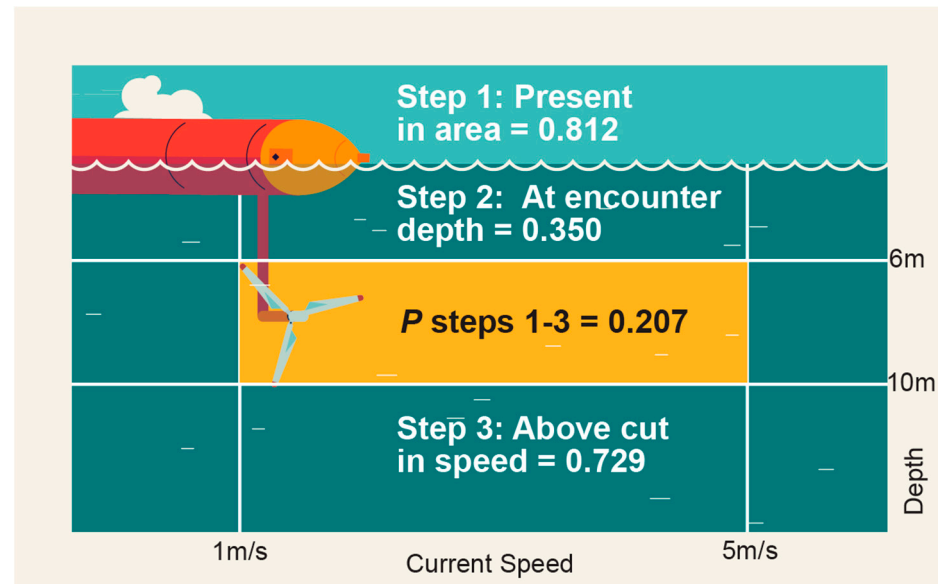

Figure 3. Probability (*P*) based on case study data from striped bass acoustic tag detections of each of the first three collision risk steps. Each step occurs independently (steps 1–3). The central probability (P steps 1–3) indicates the combined probability of all three steps occurring at once. Illustration by Stephanie King.

These results suggest that approximately one out of five adult striped bass of Shubenacadie River origin passing through the Minas Passage will fulfill the first three steps of collision risk. This means that these fish may simultaneously occur (1) in the general vicinity of the turbine, (2) at the depth range of the swept area of the device, and (3) at current velocities under which the turbine is operational. As described above, estimation of the probability of the further steps of collision risk will require data beyond those available to this study.

There are no results available from the case study that apply to the subsequent steps (4–7) in the collision risk assessment framework. The data collection methods needed to address these steps are under development with multiple research groups worldwide working to develop and deploy instrumentation that will collect appropriate data.

4. Discussion

Understanding the mechanics and the spatiotemporal distribution of a marine animal in relation to a rotating tidal turbine is essential for estimating the probability of a collision occurring. Similarly, understanding the forces that may cause an animal to collide with a turbine blade, and the resistance of the tissues, organs, and bones of a marine animal will lead to an assessment of the consequences of collisions. Together, the probability of occurrence and potential consequences can provide a first order estimate for the risk of collision. The assessment framework outlined in this paper steps through the circumstances that must come into play in order to estimate the outcome of a collision. By examining each step in the process that must take place to result in a deleterious outcome, it is possible to get a sense of the risk that might be incurred by a marine animal in the presence of an operational turbine. If any one of the steps in the framework presents a near zero probability of occurrence, the overall probability, and therefore the risk, must be considered near zero as well. Conversely, if collision risk is assessed as considerably greater than

'near zero', then this methodology allows for the identification of the best step at which to apply mitigation measures. Although the peer-reviewed literature does not often provide specific probabilities for the various events in the proposed framework, a general indication about the likelihood for a specific event occurring may be gleaned, and the general shape of a reaction curve determined from Monte Carlo simulations may provide valuable insight [126]. Conducting such simulations is beyond the scope of this paper but warrants further consideration in subsequent work. Early estimates of the probability of collision are being determined [127]. There is an ongoing need for additional research and monitoring around operational tidal turbines to elucidate the risk of collision. It is important to ensure that each step in the sequential approach to collision risk is considered as monitoring programs and data collection efforts are designed.

It is important to note that, while the steps in the framework presented here involve the potential risk for individual marine animals, it is the potential effect on populations that is of greatest concern. The ability to use outcomes of risk to individual animals to assess population-level risk is a commonly used technique by fisheries and wildlife regulators. Each of the events (steps) presented in Figure 1 represents a conditional probability that could lead to a collision for an individual animal. The resulting probability of a collision, and the potential consequences of such a collision (step 7) for an individual animal, must be used to inform population models that assess whether an adverse impact on a population is likely.

The first three steps in the framework presented here are driven by the presence of animals in time and space that might overlap with rotating turbine blades (presence of animals in the channel; presence of animals at the operating depth of the turbine; presence of animals when flows are above the cut-in speed of the device). The overlap of animals with the turbines in these three steps will require gathering data for any species that might be at risk at a project site, with the characteristics of the site taken into consideration, as illustrated by the case study on striped bass. At this point in the risk profile, animals might choose to be present in the area of a turbine, or they might be present as a necessary part of a migratory pathway, a movement corridor, or taking advantage of an essential habitat for feeding, reproduction, rearing, or avoiding predators. The knowledge base to determine risks for the initial three steps in the framework will continue to be built through data collection from the required monitoring programs around demonstration-, pilot-, and commercial-scale tidal deployments. The risk to species of concern should be examined for any prospective tidal project site and for a specific type of turbine; often these assessments can be satisfied with stock assessments for fish of commercial or conservation concern, or population assessments for marine mammals under conservation regulations. Once the presence of the species of concern is understood, further assessments may not be necessary at those locations. Underwater passive acoustic monitoring systems can be deployed to detect and locate vocalizing marine mammals, while a range of active acoustic instruments like single-beam or split-beam echosounders, multibeam acoustic cameras and multibeam imaging sonars and acoustic cameras can all be used to assess the location of marine animals. Underwater video is often very useful in identifying species but collects large amounts of data for analysis and may be prone to failure [66].

The next step in the process (avoiding or taking evasive action) is dependent on the ability of the animal to detect the operating turbine and its ability to maneuver and swim away from the moving parts of the device. Without detailed behavioral studies of marine animals in the vicinity of a turbine, it is difficult to determine at what distance, and under what environmental conditions (extent of turbidity, ambient noise level, tidal flow rate) each species might detect and avoid a turbine, or whether they will approach until forced to evade the blades just prior to collision. Laboratory and flume studies indicate that most fish will evade a turbine blade if possible, with virtually all fish surviving close encounters with turbines and/or traversing the rotor swept area alive. Understanding the behavioral aspects of marine animals around turbines is the most costly and least understood research area in the chain of risk (step 4). While some behaviors can be extrapolated from other

structures in the ocean, there are no direct surrogates. However, marine animals do not generally collide with objects underwater and have the ability to detect new objects in their environment. Behavioral studies around turbines are likely to continue but due to high costs, safety concerns for researchers working in proximity to high tidal flows, and the degree of variability of behaviors among individuals and within populations, these studies are unlikely to reach consensus about how animals interact with turbines. Behavioral studies may use a combination of boat- and remote-based observers, underwater active acoustics, and underwater video. All these techniques are expensive, potentially cause safety concerns in fast flowing tidal waters, and produce vast amounts of data that are often hard to interpret.

For those marine animals that do not avoid or take evasive action near a turbine, the hydrodynamic forces generated at the face of the rotor area may deflect the animal (step 5), decreasing the probability of a collision occurring. The hydrodynamic forces generated from the blades and rotor assembly are likely to deflect only small fish and planktonic organisms like larval fish and eggs, while larger nektonic organisms will be capable of swimming against the forces. These forces are small, particularly in comparison to those from conventional hydropower turbines, and can be calculated using numerical models. Focused research studies on these interactions would help to determine the threshold size of fish that might be subject to the deflection forces at the face of a turbine.

If a marine animal reaches the face of a turbine and continues through the rotor swept area (step 6), there is a probability that the animal may be stuck by a rotating blade. Species with greater body lengths will be more at risk of collision, although many of these larger species also have greater swimming speeds allowing them to clear the rotor swept area before encountering a blade, which may mitigate the probability of an adverse outcome. Numerical models can predict the potential risk to a fish or marine mammal of a collision with a blade, while crossing through the rotor swept area. These models could be validated using continuous underwater video focused on the face of the turbine. This methodology is expensive and prone to failure and is most applicable in clear, relatively shallow waters during daylight hours. More turbid water, greater depths, and the dark portions of the day will require artificial illumination which may change the behavior of some marine animals, and potentially attract additional species that might not otherwise be at risk of collision. Excessively turbid waters make underwater video recordings challenging.

The consequences of a collision between a marine animal and a turbine blade are the least well-defined aspect of the framework (step 7). The only studies of comparable forces to blade collisions on marine animal tissue have been for a small number of marine mammal species. Evidence for the deleterious effects of fish colliding with a rotating turbine are not comparable to the much higher velocity conventional hydropower turbines, nor are propeller strikes from ships of the same nature and severity of what can be expected from tidal turbines [128]. Further studies of additional marine animal tissues are needed, particularly for fish that are considered at risk, to determine if a collision with a tidal blade is likely to cause serious injury or death [46].

The assessment of risk for a marine animal colliding with a tidal turbine must consider the behavior of the particular species at the location in question. Animal behavior is complex and difficult to assess, particularly in the fast-moving and often murky waters where tidal power is sited. This paper attempts to assess a reasonable, if conservative, estimate of collision risk, largely without taking the avoidance and evasion behavior of marine animals into account. The assessment framework outlined in this paper will provide an additional margin of safety for marine animals as well as providing a simple means for tidal developers to progress with confidence.

5. Conclusions

There are significant challenges to developing and operating tidal turbines that range from technical engineering questions, financing options, to the uncertainty of potential harm to marine animals from the devices deployed in the ocean. The risk of marine animals

colliding with rotating turbine blades continues to be the most daunting challenge for the permitting/consenting and licensing of tidal energy around the world. The study of collision risk to marine animals continues to be a high priority within the marine energy community, as it continues to slow and hinder deployments, which, in turn, limits the information available on the interaction. Device and project developers, researchers, regulators and scientific advisers, and other stakeholders need to collaborate to define and implement the most appropriate studies and monitoring programs to better understand the risks, and to ensure that knowledge gained is shared and applied appropriately in deploying and monitoring tidal turbines.

Providing a simple means to apply the accumulated knowledge of collision risk for device and project developers, with sufficient scientific evidence to convince regulators and stakeholders, could be an important step towards normalizing the deployment of tidal turbines and further expanding the knowledge base of its potential effects. The authors have put forward this assessment framework as a pathway to thinking about the risk of collision with a tidal turbine and considering the possibility of an encounter causing definitive and serious harm to marine animals. This methodology suggests that the potential risk to a marine mammal or fish from a tidal turbine is likely small and seeks to clarify the steps that must be taken to collect the necessary data required to validate this supposition.

References

1. Intergovernmental Panel on Climate Change (IPCC). *The Ocean and Cryosphere in a Changing Climate: Special Report of the Intergovernmental Panel on Climate Change*, 1st ed.; Cambridge University Press: Cambridge, UK, 2022; ISBN 978-1-00-915796-4.
2. Intergovernmental Panel on Climate Change (IPCC) (Ed.) *Climate Change 2022—Mitigation of Climate Change: Working Group III Contribution to the Sixth Assessment Report of the Intergovernmental Panel on Climate Change*, 1st ed.; Cambridge University Press: Cambridge, UK, 2023; ISBN 978-1-00-915792-6.
3. IRENA. *Innovation Outlook: Ocean Energy Technologies*; IRENA: Abu Dhabi, United Arab Emirates, 2020; p. 112.
4. Malki, R.; Masters, I.; Williams, A.J.; Nick Croft, T. Planning Tidal Stream Turbine Array Layouts Using a Coupled Blade Element Momentum—Computational Fluid Dynamics Model. *Renew. Energy* **2014**, *63*, 46–54. [CrossRef]
5. Vennell, R. The Energetics of Large Tidal Turbine Arrays. *Renew. Energy* **2012**, *48*, 210–219. [CrossRef]
6. European Commission. *REPowerEU: Joint European Action for More Affordable, Secure and Sustainable Energy*; European Commission: Brussels, Belgium, 2022.
7. Coles, D.; Angeloudis, A.; Greaves, D.; Hastie, G.; Lewis, M.; Mackie, L.; McNaughton, J.; Miles, J.; Neill, S.; Piggott, M.; et al. A Review of the UK and British Channel Islands Practical Tidal Stream Energy Resource. *Proc. R. Soc. A* **2021**, *477*, 20210469. [CrossRef]

8.   Copping, A.E.; Sather, N.; Hanna, L.; Whiting, J.M.; Zydlewski, G.; Staines, G.; Gill, A.; Hutchison, I.; O'Hagan, A.M.; Simas, T.; et al. *Annex IV 2016 State of the Science Report: Environmental Effects of Marine Renewable Energy Development Around the World*; Annex IV, Ocean Energy Systems: Seattle, WA, USA, 2016; p. 224.

9.   Kempener, R.; Neumann, F. *Tidal Energy Technology Brief*; IRENA: Abu Dhabi, United Arab Emirates, 2014.

10.   Kempener, R.; Neumann, F. *Wave Energy Technology Brief*; IRENA: Abu Dhabi, United Arab Emirates, 2014.

11.   Neill, S.P.; Jordan, J.R.; Couch, S.J. Impact of Tidal Energy Converter (TEC) Arrays on the Dynamics of Headland Sand Banks. *Renew. Energy* **2012**, *37*, 387–397. [CrossRef]

12.   Copping, A.; Hemery, L. *OES-Environmental 2020 State of the Science Report: Environmental Effects of Marine Renewable Energy Development around the World. Report for Ocean Energy Systems (OES)*; U.S. Department of Energy Office of Scientific and Technical Information: Seattle, WA, USA, 2020.

13.   Boehlert, G.; McMurray, G.; Tortorici, C.; Klure, J.; Meyer, J. *Ecological Effects of Wave Energy Development in the Pacific Northwest*; National Oceanic and Atmospheric Administration: Corvallis, OR, USA, 2008; p. 174.

14.   Boehlert, G.; Gill, A. Environmental and Ecological Effects of Ocean Renewable Energy Development—A Current Synthesis. *Oceanography* **2010**, *23*, 68–81. [CrossRef]

15.   Scottish Natural Heritage. *Assessing Collision Risk between Underwater Turbines and Marine Wildlife*; Scottish Natural Heritage: Edinburgh, UK, 2016; p. 96.

16.   Sparling, C.; Seitz, A.; Masden, E.; Smith, K. *2020 State of the Science Report, Chapter 3: Collision Risk for Animals around Turbines*; Pacific Northwest National Laboratory (PNNL): Seattle, WA, USA, 2020.

17.   Wilson, B.; Batty, R.S.; Daunt, F.; Carter, C. *Collision Risks between Marine Renewable Energy Devices and Mammals, Fish and Diving Birds*; Report to the Scottish Executive by the Scottish Association for Marine Science: Oban, Scotland, 2006; p. 105.

18.   Hammar, L.; Eggertsen, L.; Andersson, S.; Ehnberg, J.; Arvidsson, R.; Gullström, M.; Molander, S. A Probabilistic Model for Hydrokinetic Turbine Collision Risks: Exploring Impacts on Fish. *PLoS ONE* **2015**, *10*, e0117756. [CrossRef] [PubMed]

19.   Horne, N.; Culloch, R.M.; Schmitt, P.; Lieber, L.; Wilson, B.; Dale, A.C.; Houghton, J.D.R.; Kregting, L.T. Collision Risk Modelling for Tidal Energy Devices: A Flexible Simulation-Based Approach. *J. Environ. Manag.* **2021**, *278*, 111484. [CrossRef]

20.   Brown, E.; Sulaeman, S.; Quispe-Abad, R.; Müller, N.; Moran, E. Safe Passage for Fish: The Case for in-Stream Turbines. *Renew. Sustain. Energy Rev.* **2023**, *173*, 113034. [CrossRef]

21.   Castro-Santos, T.; Haro, A. Survival and Behavioral Effects of Exposure to a Hydrokinetic Turbine on Juvenile Atlantic Salmon and Adult American Shad. *Estuaries Coasts* **2015**, *38*, 203–214. [CrossRef]

22.   Amaral, S.V.; Bevelhimer, M.S.; Čada, G.F.; Giza, D.J.; Jacobson, P.T.; McMahon, B.J.; Pracheil, B.M. Evaluation of Behavior and Survival of Fish Exposed to an Axial-Flow Hydrokinetic Turbine. *N. Am. J. Fish. Manag.* **2015**, *35*, 97–113. [CrossRef]

23.   Müller, S.; Muhawenimana, V.; Sonnino-Sorisio, G.; Wilson, C.A.M.E.; Cable, J.; Ouro, P. Fish Response to the Presence of Hydrokinetic Turbines as a Sustainable Energy Solution. *Sci. Rep.* **2023**, *13*, 7459. [CrossRef]

24.   Bevelhimer, M.; Scherelis, C.; Colby, J.; Adonizio, M.A. Hydroacoustic Assessment of Behavioral Responses by Fish Passing Near an Operating Tidal Turbine in the East River, New York. *Trans. Am. Fish. Soc.* **2017**, *146*, 1028–1042. [CrossRef]

25.   Courtney, M.B.; Flanigan, A.J.; Hostetter, M.; Seitz, A.C. Characterizing Sockeye Salmon Smolt Interactions with a Hydrokinetic Turbine in the Kvichak River, Alaska. *North Am. J. Fish. Manag.* **2022**, *42*, 1054–1065. [CrossRef]

26.   Bender, A.; Langhamer, O.; Francisco, F.; Forslund, J.; Hammar, L.; Sundberg, J.; Molander, S. Imaging-Sonar Observations of Salmonid Interactions with a Vertical Axis Instream Turbine. *River Res. Appl.* **2023**, *39*, 1578–1589. [CrossRef]

27.   Pearson, J.; Roberts, C.; Scott, C.; Hull, S. *Collision Risk of Fish with Wave and Tidal Devices*; ABP Marine Environmental Research Ltd.: Southampton, UK, 2010; p. 106.

28.   Fraser, S.; Williamson, B.J.; Nikora, V.; Scott, B.E. Fish Distributions in a Tidal Channel Indicate the Behavioural Impact of a Marine Renewable Energy Installation. *Energy Rep.* **2018**, *4*, 65–69. [CrossRef]

29.   Gillespie, D.; Palmer, L.; Macaulay, J.; Sparling, C.; Hastie, G. Harbour Porpoises Exhibit Localized Evasion of a Tidal Turbine. *Aquat. Conserv.* **2021**, *31*, 2459–2468. [CrossRef]

30.   Joy, R.; Wood, J.D.; Sparling, C.E.; Tollit, D.J.; Copping, A.E.; McConnell, B.J. Empirical Measures of Harbor Seal Behavior and Avoidance of an Operational Tidal Turbine. *Mar. Pollut. Bull.* **2018**, *136*, 92–106. [CrossRef]

31.   Onoufriou, J.; Russell, D.J.F.; Thompson, D.; Moss, S.E.; Hastie, G.D. Quantifying the Effects of Tidal Turbine Array Operations on the Distribution of Marine Mammals: Implications for Collision Risk. *Renew. Energy* **2021**, *180*, 157–165. [CrossRef]

32.   Viehman, H.A.; Zydlewski, G.B. Fish Interactions with a Commercial-Scale Tidal Energy Device in the Natural Environment. *Estuaries Coasts* **2015**, *38*, 241–252. [CrossRef]

33.   Williamson, B.; Fraser, S.; Williamson, L.; Nikora, V.; Scott, B. Predictable Changes in Fish School Characteristics Due to a Tidal Turbine Support Structure. *Renew. Energy* **2019**, *141*, 1092–1102. [CrossRef]

34.   Marine Scotland. *Survey, Deploy and Monitor Licensing Policy Guidance*; Marine Scotland and Scottish Government: Edinburgh, UK, 2012; p. 12.

35.   Simas, T.; O'Hagan, A.M.; O'Callaghan, J.; Hamawi, S.; Magagna, D.; Bailey, I.; Greaves, D.; Saulnier, J.-B.; Marina, D.; Bald, J.; et al. Review of Consenting Processes for Ocean Energy in Selected European Union Member States. *Int. J. Mar. Energy* **2015**, *9*, 41–59. [CrossRef]

36.   Apolonia, M.; Fofack-Garcia, R.; Noble, D.R.; Hodges, J.; Correia da Fonseca, F.X. Legal and Political Barriers and Enablers to the Deployment of Marine Renewable Energy. *Energies* **2021**, *14*, 4896. [CrossRef]

37. Salvador, S.; Ribeiro, M.C. Socio-economic, Legal, and Political Context of Offshore Renewable Energies. *WIREs Energy Environ.* **2023**, *12*, e462. [CrossRef]

38. Stelzenmüller, V.; Coll, M.; Mazaris, A.D.; Giakoumi, S.; Katsanevakis, S.; Portman, M.E.; Degen, R.; Mackelworth, P.; Gimpel, A.; Albano, P.G.; et al. A Risk-Based Approach to Cumulative Effect Assessments for Marine Management. *Sci. Total Environ.* **2018**, *612*, 1132–1140. [CrossRef]

39. Copping, A.; Grear, M.; Jepsen, R.; Chartrand, C.; Gorton, A. Understanding the Potential Risk to Marine Mammals from Collision with Tidal Turbines. *Int. J. Mar. Energy* **2017**, *19*, 110–123. [CrossRef]

40. Whiting, J.; Copping, A.; Freeman, M.; Woodbury, A. Tethys Knowledge Management System: Working to Advance the Marine Renewable Energy Industry. *Int. J. Mar. Energy* **2019**, *2*, 29–38. [CrossRef]

41. Bangley, C.W.; Hasselman, D.J.; Flemming, J.M.; Whoriskey, F.G.; Culina, J.; Enders, L.; Bradford, R.G. Modeling the Probability of Overlap between Marine Fish Distributions and Marine Renewable Energy Infrastructure Using Acoustic Telemetry Data. *Front. Mar. Sci.* **2022**, *9*, 851757. [CrossRef]

42. Sanderson, B.G.; Bangley, C.W.; McGarry, L.P.; Hasselman, D.J. Measuring Detection Efficiency of High-Residency Acoustic Signals for Estimating Probability of Fish–Turbine Encounter in a Fast-Flowing Tidal Passage. *J. Mar. Sci. Eng.* **2023**, *11*, 1172. [CrossRef]

43. MacKenzie, D.I.; Nichols, J.D.; Lachman, G.B.; Droege, S.; Andrew Royle, J.; Langtimm, C.A. Estimating Site Occupancy Rates When Detection Probabilities Are Less than One. *Ecology* **2002**, *83*, 2248–2255. [CrossRef]

44. Long, M.; Jordaan, A.; Castro-Santos, T. Environmental Factors Influencing Detection Efficiency of an Acoustic Telemetry Array and Consequences for Data Interpretation. *Anim. Biotelemetry* **2023**, *11*, 18. [CrossRef]

45. Bevelhimer, M.S.; Pracheil, B.M.; Fortner, A.M.; Saylor, R.; Deck, K.L. Mortality and Injury Assessment for Three Species of Fish Exposed to Simulated Turbine Blade Strike. *Can. J. Fish. Aquat. Sci.* **2019**, *76*, 2350–2363. [CrossRef]

46. Blumara Corporation. *Finite Element Analysis to Assess Fish Mortality from Interactions with Tidal Turbine Blades*; Offshore Energy Research Association of Nova Scotia: Halifax, NS, Canada, 2018; p. 29.

47. Elith, J.; Leathwick, J.R. Species Distribution Models: Ecological Explanation and Prediction Across Space and Time. *Annu. Rev. Ecol. Evol. Syst.* **2009**, *40*, 677–697. [CrossRef]

48. Benjamins, S.; Van Geel, N.; Hastie, G.; Elliott, J.; Wilson, B. Harbour Porpoise Distribution Can Vary at Small Spatiotemporal Scales in Energetic Habitats. *Deep Sea Res. Part II Top. Stud. Oceanogr.* **2017**, *141*, 191–202. [CrossRef]

49. Lieber, L.; Nimmo-Smith, W.A.M.; Waggitt, J.J.; Kregting, L. Fine-Scale Hydrodynamic Metrics Underlying Predator Occupancy Patterns in Tidal Stream Environments. *Ecol. Indic.* **2018**, *94*, 397–408. [CrossRef]

50. Waggitt, J.J.; Robbins, A.M.C.; Wade, H.M.; Masden, E.A.; Furness, R.W.; Jackson, A.C.; Scott, B.E. Comparative Studies Reveal Variability in the Use of Tidal Stream Environments by Seabirds. *Mar. Policy* **2017**, *81*, 143–152. [CrossRef]

51. McLean, M.; Sanderson, B.; Lilly, J.; Tsitrin, E.; Stokesbury, M. *Quantifying Fish-Turbine Interactions Using VEMCO's New High Residency Acoustic Electronic Tagging Technology*; Offshore Energy Research Association of Nova Scotia: Halifax, NS, Canada, 2019; p. 126.

52. Stokesbury, M.; McLean, M. *Survival, Distribution and Environmental Preferences of Atlantic Salmon Smolts. Final Report—Annex C*; Offshore Energy Research Association of Nova Scotia: Halifax, NS, Canada, 2020; p. 42.

53. Sanderson, B.G.; Karsten, R.H.; Hasselman, D.J. Towards Estimating Probability of Fish–Turbine Encounter: Using Drifters Equipped with Acoustic Tags to Verify the Efficacy of an Array of Acoustic Receivers. *JMSE* **2023**, *11*, 1592. [CrossRef]

54. Gillespie, D.; Palmer, L.; Macaulay, J.; Sparling, C.; Hastie, G. Passive Acoustic Methods for Tracking the 3D Movements of Small Cetaceans around Marine Structures. *PLoS ONE* **2020**, *15*, e0229058. [CrossRef]

55. Porskamp, P.; Redden, A.M.; Broome, J.E.; Sanderson, B.; Wood, J. *Assessing Marine Mammal Presence in and near the FORCE Lease Area during Winter and Early Spring—Addressing Baseline Data Gaps and Sensor Performance*; Offshore Energy Research Association and the Fundy Ocean Research Center for Energy: Halifax, NS, Canada, 2015; p. 35.

56. Hastie, G.D.; Wu, G.-M.; Moss, S.; Jepp, P.; MacAulay, J.; Lee, A.; Sparling, C.E.; Evers, C.; Gillespie, D. Automated Detection and Tracking of Marine Mammals: A Novel Sonar Tool for Monitoring Effects of Marine Industry. *Aquat. Conserv. Mar. Freshw. Ecosyst.* **2019**, *29*, 119–130. [CrossRef]

57. Parsons, M.J.G.; Fenny, E.; Lucke, K.; Osterrieder, S.; Jenkins, G.; Saunders, B.J.; Jepp, P.; Parnum, I.M. Imaging Marine Fauna with a Tritech Gemini 720i Sonar. *Acoust. Aust.* **2017**, *45*, 41–49. [CrossRef]

58. Sparling, C.; Lonergan, M.; McConnell, B. Harbour Seals (*Phoca vitulina*) around an Operational Tidal Turbine in Strangford Narrows: No Barrier Effect but Small Changes in Transit Behaviour. *Aquat. Conserv. Mar. Freshw. Ecosyst.* **2018**, *28*, 194–204. [CrossRef]

59. Hutchison, I.; Tait, C.; Sheehy, J.; Morgan, P. *Review of Underwater Video Data Collected around Operating Tidal Stream Turbines*; NatureScot: Perth, Scotland, UK, 2020.

60. Smith, K. *Shetland Tidal Array Subsea Video Monitoring Report: Subsea Video Monitoring*; NOVA Innovation: Edinburgh, UK, 2021; p. 76.

61. Hodgson, J.C.; Mott, R.; Baylis, S.M.; Pham, T.T.; Wotherspoon, S.; Kilpatrick, A.D.; Raja Segaran, R.; Reid, I.; Terauds, A.; Koh, L.P. Drones Count Wildlife More Accurately and Precisely than Humans. *Methods Ecol. Evol.* **2018**, *9*, 1160–1167. [CrossRef]

62. Shen, H.; Zydlewski, G.B.; Viehman, H.A.; Staines, G. Estimating the Probability of Fish Encountering a Marine Hydrokinetic Device. *Renew. Energy* **2016**, *97*, 746–756. [CrossRef]

63. Staines, G.; Zydlewski, G.B.; Viehman, H.A.; Kocik, R. Applying Two Active Acoustic Technologies to Document Presence of Large Marine Animal Targets at a Marine Renewable Energy Site. *J. Mar. Sci. Eng.* **2020**, *8*, 704. [CrossRef]

64. Melvin, G.D.; Cochrane, N.A. Multibeam Acoustic Detection of Fish and Water Column Targets at High-Flow Sites. *Estuaries Coasts* **2015**, *38*, 227–240. [CrossRef]

65. Staines, G.J.; Mueller, R.P.; Seitz, A.C.; Evans, M.D.; O'Byrne, P.W.; Wosnik, M. Capabilities of an Acoustic Camera to Inform Fish Collision Risk with Current Energy Converter Turbines. *JMSE* **2022**, *10*, 483. [CrossRef]

66. Cotter, E.; Staines, G. Observing Fish Interactions with Marine Energy Turbines Using Acoustic Cameras. *Fish. Fish.* **2023**, *24*, 1020–1033. [CrossRef]

67. Francisco, F.; Sundberg, J. Detection of Visual Signatures of Marine Mammals and Fish within Marine Renewable Energy Farms Using Multibeam Imaging Sonar. *JMSE* **2019**, *7*, 22. [CrossRef]

68. Tsitrin, E.; Sanderson, B.G.; McLean, M.F.; Gibson, A.J.F.; Hardie, D.C.; Stokesbury, M.J.W. Migration and Apparent Survival of Post-Spawning Alewife (*Alosa pseudoharengus*) in Minas Basin, Bay of Fundy. *Anim. Biotelemetry* **2022**, *10*, 11. [CrossRef]

69. Hemery, L.G.; Mackereth, K.F.; Gunn, C.M.; Pablo, E.B. Use of a 360-Degree Underwater Camera to Characterize Artificial Reef and Fish Aggregating Effects around Marine Energy Devices. *JMSE* **2022**, *10*, 555. [CrossRef]

70. Polagye, B.; Joslin, J.; Murphy, P.; Cotter, E.; Scott, M.; Gibbs, P.; Bassett, C.; Stewart, A. Adaptable Monitoring Package Development and Deployment: Lessons Learned for Integrated Instrumentation at Marine Energy Sites. *JMSE* **2020**, *8*, 553. [CrossRef]

71. Au, D.; Weihs, D. At High Speeds Dolphins Save Energy by Leaping. *Nature* **1980**, *284*, 548–550. [CrossRef]

72. McCann, D.L.; Bell, P.S. Observations and Tracking of Killer Whales (*Orcinus orca*) with Shore-Based X-Band Marine Radar at a Marine Energy Test Site. *Mar. Mam. Sci.* **2017**, *33*, 904–912. [CrossRef]

73. Linnenschmidt, M.; Teilmann, J.; Akamatsu, T.; Dietz, R.; Miller, L.A. Biosonar, Dive, and Foraging Activity of Satellite Tracked Harbor Porpoises (*Phocoena phocoena*). *Mar. Mam. Sci.* **2013**, *29*, E77–E97. [CrossRef]

74. Westgate, A.J.; Head, A.J.; Berggren, P.; Koopman, H.N.; Gaskin, D.E. Diving Behaviour of Harbour Porpoises, *Phocoena phocoena*. *Can. J. Fish. Aquat. Sci.* **1995**, *52*, 1064–1073. [CrossRef]

75. MacAulay, J.D.J.; Gordon, J.C.D.; Gillespie, D.M.; Malinka, C.E.; Johnson, M.; Northridge, S.P. Tracking Harbor Porpoises in Tidal Rapids: A Low Cost Autonomous Platform to Track the Movement of Harbor Porpoises in Tidal Rapids. NERC. 2015. Available online: http://www.smru.st-and.ac.uk/documents/nerc/NERC_MRE_KEP_Tracking_Harbour_Porpoises_in_Tidal_Rapids.pdf (accessed on 20 September 2023).

76. Keyser, F.M.; Broome, J.E.; Bradford, R.G.; Sanderson, B.; Redden, A.M. Winter Presence and Temperature-Related Diel Vertical Migration of Striped Bass (*Morone saxatilis*) in an Extreme High-Flow Passage in the Inner Bay of Fundy. *Can. J. Fish. Aquat. Sci.* **2016**, *73*, 1777–1786. [CrossRef]

77. Scherelis, C.; Penesis, I.; Hemer, M.A.; Cossu, R.; Wright, J.T.; Guihen, D. Investigating Biophysical Linkages at Tidal Energy Candidate Sites: A Case Study for Combining Environmental Assessment and Resource Characterisation. *Renew. Energy* **2020**, *159*, 399–413. [CrossRef]

78. Whitton, T.A.; Jackson, S.E.; Hiddink, J.G.; Scoulding, B.; Bowers, D.; Powell, B.; D'Urban Jackson, T.; Gimenez, L.; Davies, A.G. Vertical Migrations of Fish Schools Determine Overlap with a Mobile Tidal Stream Marine Renewable Energy Device. *J. Appl. Ecol.* **2020**, *57*, 729–741. [CrossRef]

79. Viehman, H.; Boucher, T.; Redden, A. Winter and Summer Differences in Probability of Fish Encounter (Spatial Overlap) with MHK Devices. *Int. Mar. Energy J.* **2018**, *1*, 9–18. [CrossRef]

80. Isaksson, N.; Cleasby, I.R.; Owen, E.; Williamson, B.J.; Houghton, J.D.R.; Wilson, J.; Masden, E.A. The Use of Animal-Borne Biologging and Telemetry Data to Quantify Spatial Overlap of Wildlife with Marine Renewables. *J. Mar. Sci. Eng.* **2021**, *9*, 263. [CrossRef]

81. Laplanche, C.; Marques, T.A.; Thomas, L. Tracking Marine Mammals in 3D Using Electronic Tag Data. *Methods Ecol. Evol.* **2015**, *6*, 987–996. [CrossRef]

82. Papastavrou, V.; Ryan, C. Ethical Standards for Research on Marine Mammals. *Res. Ethics* **2023**, *19*, 390–408. [CrossRef]

83. Langård, L.; Skaret, G.; Jensen, K.; Johannessen, A.; Slotte, A.; Nøttestad, L.; Fernö, A. Tracking Individual Herring within a Semi-Enclosed Coastal Marine Ecosystem: 3-Dimensional Dynamics from Pre- to Post-Spawning. *Mar. Ecol. Prog. Ser.* **2015**, *518*, 267–279. [CrossRef]

84. Deng, Z.D.; Weiland, M.A.; Fu, T.; Seim, T.A.; LaMarche, B.L.; Choi, E.Y.; Carlson, T.J.; Eppard, M.B. A Cabled Acoustic Telemetry System for Detecting and Tracking Juvenile Salmon: Part 2. Three-Dimensional Tracking and Passage Outcomes. *Sensors* **2011**, *11*, 5661–5676. [CrossRef] [PubMed]

85. McMichael, G.A.; Eppard, M.B.; Carlson, T.J.; Carter, J.A.; Ebberts, B.D.; Brown, R.S.; Weiland, M.; Ploskey, G.R.; Harnish, R.A.; Deng, Z.D. The Juvenile Salmon Acoustic Telemetry System: A New Tool. *Fisheries* **2010**, *35*, 9–22. [CrossRef]

86. Kubečka, J.; Godø, O.R.; Hickley, P.; Prchalová, M.; Říha, M.; Rudstam, L.; Welcomme, R. Fish Sampling with Active Methods. *Fish. Res.* **2012**, *123–124*, 1–3. [CrossRef]

87. CEF Consultants Ltd. *Report on a Workshop on Fish Behaviour in Response to Seismic Sound Held in Halifax, Nova Scotia, Canada March 28–31, 2011*; Environmental Studies Research Funds: Ottawa, ON, Canada, 2011; p. 109.

88. Brylinski, M. *Results of a Study to Evaluate the Feasibility of Using a Drifted Gill Net to Survey Fish Species Present in the Minas Passage, Bay of Fundy*; Acadia Centre for Estuarine Research: Wolfville, NS, Canada, 2010; p. 4.

89. Urmy, S.S.; Horne, J.K. Multi-Scale Responses of Scattering Layers to Environmental Variability in Monterey Bay, California. *Deep Sea Res. Part I Oceanogr. Res. Pap.* **2016**, *113*, 22–32. [CrossRef]

90. Viehman, H.A.; Hasselman, D.J.; Douglas, J.; Boucher, T. The Ups and Downs of Using Active Acoustic Technologies to Study Fish at Tidal Energy Sites. *Front. Mar. Sci.* **2022**, *9*, 851400. [CrossRef]

91. Staines, G.; Zydlewski, G.; Viehman, H. Changes in Relative Fish Density around a Deployed Tidal Turbine during On-Water Activities. *Sustainability* **2019**, *11*, 6262. [CrossRef]

92. Gillespie, D.; Oswald, M.; Hastie, G.; Sparling, C. Marine Mammal HiCUP: A High Current Underwater Platform for the Long-Term Monitoring of Fine-Scale Marine Mammal Behavior Around Tidal Turbines. *Front. Mar. Sci.* **2022**, *9*, 850446. [CrossRef]

93. Ouro, P.; Dené, P.; Garcia-Novo, P.; Stallard, T.; Kyozuda, Y.; Stansby, P. Power Density Capacity of Tidal Stream Turbine Arrays with Horizontal and Vertical Axis Turbines. *J. Ocean Eng. Mar. Energy* **2023**, *9*, 203–218. [CrossRef]

94. Lewis, M.; O'Hara Murray, R.; Fredriksson, S.; Maskell, J.; De Fockert, A.; Neill, S.P.; Robins, P.E. A Standardised Tidal-Stream Power Curve, Optimised for the Global Resource. *Renew. Energy* **2021**, *170*, 1308–1323. [CrossRef]

95. Xu, W.; Matzner, S. Underwater Fish Detection Using Deep Learning for Water Power Applications. In Proceedings of the 2018 International Conference on Computational Science and Computational Intelligence (CSCI), Las Vegas, NV, USA, 12–14 December 2018.

96. Williamson, B.J.; Blondel, P.; Armstrong, E.; Bell, P.S.; Hall, C.; Waggitt, J.J. Scott A Self-Contained Subsea Platform for Acoustic Monitoring of the Environment Around Marine Renewable Energy Devices–Field Deployments at Wave and Tidal Energy Sites in Orkney, Scotland. *IEEE J. Ocean. Eng.* **2016**, *41*, 67–81. [CrossRef]

97. Broadhurst, M.; Barr, S.; Orme, C.D.L. In-Situ Ecological Interactions with a Deployed Tidal Energy Device; an Observational Pilot Study. *Ocean Coast. Manag.* **2014**, *99*, 31–38. [CrossRef]

98. Coombs, S.; Bak-Coleman, J.; Montgomery, J. Rheotaxis Revisited: A Multi-Behavioral and Multisensory Perspective on How Fish Orient to Flow. *J. Exp. Biol.* **2020**, *223*, jeb223008. [CrossRef] [PubMed]

99. Webb, P.W. Entrainment by River Chub Nocomis Micropogon and Smallmouth Bass Micropterus Dolomieu on Cylinders. *J. Exp. Biol.* **1998**, *201 Pt 16*, 2403–2412. [CrossRef]

100. Parker, S.J.; McCleave, J.D. Selective Tidal Stream Transport by American Eels during Homing Movements and Estuarine Migration. *J. Mar. Biol. Assoc. UK* **1997**, *77*, 871–889. [CrossRef]

101. Gibson, R.N. Go with the Flow: Tidal Migration in Marine Animals. *Hydrobiologia* **2003**, *503*, 153–161. [CrossRef]

102. Benjamins, S.; Dale, A.; Hastie, G.; Waggitt, J.; Lea, M.-A.; Scott, B.; Wilson, B. Confusion Reigns? A Review of Marine Megafauna Interactions with Tidal-Stream Environments. In *Oceanography and Marine Biology*; Hughes, R., Hughes, D., Smith, I., Dale, A., Eds.; Oceanography and Marine Biology—An Annual Review; University of Aberdeen: Aberdeen, UK, 2015; pp. 1–54. ISBN 978-1-4987-0545-5.

103. Palmer, L.; Gillespie, D.; MacAulay, J.D.J.; Sparling, C.E.; Russell, D.J.F.; Hastie, G.D. Harbour Porpoise (*Phocoena phocoena*) Presence Is Reduced during Tidal Turbine Operation. *Aquat. Conserv. Mar. Freshw. Ecosyst.* **2021**, *31*, 3543–3553. [CrossRef]

104. Davies, K.T.A.; Brillant, S.W. Mass Human-Caused Mortality Spurs Federal Action to Protect Endangered North Atlantic Right Whales in Canada. *Mar. Policy* **2019**, *104*, 157–162. [CrossRef]

105. Hastie, G.D.; Russell, D.J.F.; Lepper, P.; Elliott, J.; Wilson, B.; Benjamins, S.; Thompson, D. Harbour Seals Avoid Tidal Turbine Noise: Implications for Collision Risk. *J. Appl. Ecol.* **2018**, *55*, 684–693. [CrossRef]

106. Fraser, S.; Waggitt, J.J. Practical Approaches for Providing Empirical Data on Seabird Behavior and Prey Assemblages in Tidal Channels. *Front. Mar. Sci.* **2022**, *9*, 851476. [CrossRef]

107. Yoshida, T.; Zhou, J.; Park, S.; Muto, H.; Kitazawa, D. Use of a Model Turbine to Investigate the High Striking Risk of Fish with Tidal and Oceanic Current Turbine Blades under Slow Rotational Speed. *Sustain. Energy Technol. Assess.* **2020**, *37*, 100634. [CrossRef]

108. Yoshida, T.; Furuichi, D.; Williamson, B.J.; Zhou, J.; Dong, S.; Li, Q.; Kitazawa, D. Experimental Study of Fish Behavior near a Tidal Turbine Model under Dark Conditions. *J. Mar. Sci. Technol.* **2022**, *27*, 541–548. [CrossRef]

109. Hammar, L.; Andersson, S.; Eggertsen, L.; Haglund, J.; Gullström, M.; Ehnberg, J.; Molander, S. Hydrokinetic Turbine Effects on Fish Swimming Behaviour. *PLoS ONE* **2013**, *8*, e84141. [CrossRef] [PubMed]

110. Viehman, H.A.; Zydlewski, G.B.; McCleave, J.D.; Staines, G.J. Using Hydroacoustics to Understand Fish Presence and Vertical Distribution in a Tidally Dynamic Region Targeted for Energy Extraction. *Estuaries Coasts* **2015**, *38*, 215–226. [CrossRef]

111. Jacobson, P.; Amaral, S.V.; Castro-Santos, T.; Giza, D.J.; Haro, A.; Perkins, N.; Pioppi, N. *Environmental Effects of Hydrokinetic Turbines on Fish: Desktop and Laboratory Flume Studies*; Electric Power Research Institute (EPRI): Palo Alto, CA, USA, 2012.

112. Schweizer, P.; Cada, G.; Bevelhimer, M. *Laboratory Experiments on the Effects of Blade Strike from Hydrokinetic Energy Technologies on Larval and Juvenile Freshwater Fishes*; Oak Ridge National Laboratory (ORNL): Oak Ridge, TN, USA, 2012.

113. Bevelhimer, M.; Colby, J.; Adonizio, M.; Tomichek, C.; Scherelis, C. *Informing a Tidal Turbine Strike Probability Model through Characterization of Fish Behavioral Response Using Multibeam Sonar Output*; Oak Ridge National Laboratory (ORNL): Oak Ridge, TN, USA, 2016.

114. Betz, A. *Introduction to the Theory of Flow Machines*, 1st ed.; Pergamon Press: London, UK, 1966; ISBN 978-1-4831-8090-8.

115. Garrett, C.; Cummins, P. The Efficiency of a Turbine in a Tidal Channel. *J. Fluid. Mech.* **2007**, *588*, 243–251. [CrossRef]

116. Nishino, T.; Willden, R.H.J. Two-Scale Dynamics of Flow Past a Partial Cross-Stream Array of Tidal Turbines. *J. Fluid. Mech.* **2013**, *730*, 220–244. [CrossRef]

117. Draper, S.; Nishino, T. Centred and Staggered Arrangements of Tidal Turbines. *J. Fluid. Mech.* **2014**, *739*, 72–93. [CrossRef]

118. Du Feu, R.J.; Funke, S.W.; Kramer, S.C.; Hill, J.; Piggott, M.D. The Trade-off between Tidal-Turbine Array Yield and Environmental Impact: A Habitat Suitability Modelling Approach. *Renew. Energy* **2019**, *143*, 390–403. [CrossRef]

119. Copping, A.E.; Grear, M.E. Applying a Simple Model for Estimating the Likelihood of Collision of Marine Mammals with Tidal Turbines. *Int. Mar. Energy J.* **2018**, *1*, 27–33. [CrossRef]

120. Manwell, J.F.; McGowan, J.G.; Rogers, A.L. *Wind Energy Explained: Theory, Design and Application*, 2nd ed.; Wiley: Chichester, UK, 2009; ISBN 978-0-470-01500-1.

121. Remen, M.; Solstorm, F.; Bui, S.; Klebert, P.; Vågseth, T.; Solstorm, D.; Hvas, M.; Oppedal, F. Critical Swimming Speed in Groups of Atlantic Salmon Salmo Salar. *Aquacult. Environ. Interact.* **2016**, *8*, 659–664. [CrossRef]

122. Johansson, D.; Laursen, F.; Fernö, A.; Fosseidengen, J.E.; Klebert, P.; Stien, L.H.; Vågseth, T.; Oppedal, F. The Interaction between Water Currents and Salmon Swimming Behaviour in Sea Cages. *PLoS ONE* **2014**, *9*, e97635. [CrossRef] [PubMed]

123. Viehman, H.A.; Zydlewski, G.B. Multi-Scale Temporal Patterns in Fish Presence in a High-Velocity Tidal Channel. *PLoS ONE* **2017**, *12*, e0176405. [CrossRef]

124. Liao, J.C. A Review of Fish Swimming Mechanics and Behaviour in Altered Flows. *Phil. Trans. R. Soc. B* **2007**, *362*, 1973–1993. [CrossRef]

125. Hecker, G.E.; Amaral, S.V. *Turbine Blade Shape Favorable for Fish Survival*; Electric Power Research Institute: Palo Alto, CA, USA, 2008; p. 94.

126. Lane, D. A Framework for Risk Analysis in Fisheries Decision-Making. *ICES J. Mar. Sci.* **1998**, *55*, 1–13. [CrossRef]

127. Peraza, J.; Horne, J. A Conditional Probabilistic Encounter-Impact Model for Fish-Turbine Interactions. In Proceedings of the European Wave and Tidal Energy Conference, Bilbao, Spain, 3–7 September 2023; Volume 15. [CrossRef]

128. Copping, A.E.; Hemery, L.G.; Overhus, D.M.; Garavelli, L.; Freeman, M.C.; Whiting, J.M.; Gorton, A.M.; Farr, H.K.; Rose, D.J.; Tugade, L.G. Potential Environmental Effects of Marine Renewable Energy Development—The State of the Science. *J. Mar. Sci. Eng.* **2020**, *8*, 879. [CrossRef]